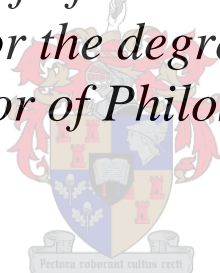


The dynamics of new self-assembled porous materials

by

Varvara I. Nikolayenko

*Submitted in partial fulfilment of the requirements
for the degree
Doctor of Philosophy*



at

Stellenbosch University

Department of Chemistry and Polymer Science
Faculty of Science

Supervisor: Prof. L. J. Barbour

Date: December 2015

DECLARATION

By submitting this thesis electronically, I declare that the entirety of the work contained therein is my own, original work, that I am the owner of the copyright thereof (unless to the extent explicitly stated otherwise) and that I have not previously in its entirety or in part submitted it for obtaining any qualification.

Signature

Name in full

_____/_____/_____
Date

Copyright © 2015 Stellenbosch University
All rights reserved

ABSTRACT

The principal goal of this study was to prepare a wide selection of crystalline second- and third-generation metal-organic materials in order to investigate guest sequestration and storage capabilities, as well as guest exchange and sorption-induced dynamics in the solid state.

Chapters I and II contain a review of the relevant literature, as well as a description of the experimental techniques employed in this work. Chapter III describes the diversity of metal-organic frameworks (MOFs) obtained from a small selection of pyridyl-functionalised ligands (varying in length and rigidity) combined with a series of carboxylic acids (also varying in length and rigidity) in the presence of one of four transition metals. Twenty one different MOFs varying in metal coordination mode, degree of interpenetration, solvent-accessible space and guest were obtained. Four of these MOFs undergo single-crystal to single-crystal (SC-SC) transformations, including activation, gas sorption and solvent exchange.

Chapter IV focuses on two isostructural MOFs. The monochromic zinc-containing framework undergoes SC-SC guest exchange, indicating a mild preference for *para*-xylene, while gas sorption experiments revealed a clear preference for carbon dioxide. The pleochroic crystals of the cobalt analogue showed no xylene selectivity, but gas sorption experiments revealed preferential selectivity toward methane carbon dioxide and ethane. Crystallisation from solutions containing both metals (and the same ligands) resulted in the formation of trichroic solid solutions, the colour of which could be fine-tuned by varying the ratio of the two metals. To complete the study, a homoepitaxial crystal was grown.

Chapter V focuses on a modified version of the ligand described in Chapter IV, with electron-withdrawing fluorine atoms located on the central phenyl ring. Use of this ligand resulted in characterisation of a twofold interpenetrated porous framework, differing from that described in the previous chapter. Activation, as well as guest exchange, elicited “crank-handle” conformational changes in the ligand. Sorption experiments showed the material to be selective for carbon dioxide over several linear alkanes. Reaction using the hydrochloride salt of this ligand yielded a novel interdigitated MOF. Substitution of cadmium for zinc in the reaction gave a third non-interpenetrated framework where the ligand has undergone [2 + 2] cycloaddition and is present in the *anti* conformation.

SC-SC activation as well as guest exchange experiments revealed this framework to be less flexible than its zinc counterpart. Exposure of the activated material to carbon dioxide indicated substantial uptake of carbon dioxide. A mixture of the DMF and DMSO produced two additional isoskeletal structures differing in paddlewheel construction, ligand conformation and, as a result, in the solvent-accessible void space.

Chapter VI describes the response of five MOFs based on diarylethene ligands to light. The structural changes underlying the colour change differ in each case. The first framework is a porous twofold interpenetrated MOF that undergoes change in colour and shape upon UV irradiation. When the same crystal was exposed to white light, the parameters revert back to those of the original form. The activated form of a second fourfold interpenetrated highly porous MOF showed an affinity for carbon dioxide, as well as a change in colour upon irradiation. Incorporation of a more flexible ligand gave a twofold interpenetrated porous material that showed low temperature activation but could not be evacuated without loss of crystallinity. UV irradiation induced a colour change but no structural change. The fourth framework is a twofold interpenetrated structure that collapses to a seemingly non-porous form upon removal of the solvent. UV irradiation of this material results in ring-closure of the diarylethene ligand, along with a colour change. Remarkably, all these processes occur in a SC-SC fashion. This is the first example of photo-induced ring closure of a diarylethene molecule incorporated into a MOF. The fifth framework exhibits a high degree of interpenetration (fourfold) but unlike all previous examples, irradiation with UV light induced no visible colour change and no structural change.

OPSOMMING

Die doel van hierdie studie was om 'n wye verskeidenheid kristallyne tweede- en derde-geslag metaal-organiese materiale voor te berei, om gas sekwestrasie, stoor vermoëns, sowel as gas uitruiling en sorpsie geïnduseerde dinamika in die vaste toestand te bestudeer.

Hoofstukke I en II bevat 'n oorsig van die relevante literatuur en 'n beskrywing van die eksperimentele tegnieke in hierdie werk. Hoofstuk III beskryf die verskeidenheid metaal-organiese raamwerke (MOFs) wat gesintetiseer is vanuit 'n klein seleksie piridiel gefunksionaliseerde ligande (met verskillende lengte en rigiditeit) gekombineer met 'n reeks karboksielsure (ook met verskillende lengte en rigiditeit) in die teenwoordigheid van een van vier oorgangsmetale. Een en twintig verskillende MOFs met verskillende metaal koördinasie modusse, graad van interpenetrasie, oplosmiddel toeganklike ruimte en gaste was gesintetiseer. Vier van hierdie MOFs toon enkel-kristal tot enkel-kristal (SC-SC) transformasies, insluitend aktivering, gas sorpsie en die uitruil van hulle oplosmiddel.

Hoofstuk IV fokus op twee isostrukturele MOFs. Die monokromiese sink-bevattende raamwerk ondergaan SC-SC gas uitruiling, wat dui op 'n matige voorkeur vir *para*-xileen, terwyl gas sorpsie eksperimente 'n duidelike voorkeur vir koolstofdiksied toon. Die pleokroïede kristalle van die kobalt analoog toon geen selektiwiteit teenoor xileen nie, terwyl gas sorpsie eksperimente 'n voorkeur teenoor metaan etaan en koolstofdiksied vertoon. Kristallasie van oplossings wat beide metale bevat (asook dieselfde ligande) lei tot die vorming van trikroïede vaste oplossings, en die kleur hiervan kan verander word deur die verhouding van die twee metale te wissel. Om die studie te voltooi, is 'n homoepitaksiale kristal gegroei.

Hoofstuk V fokus op 'n aangepaste weergawe van die ligand wat in Hoofstuk IV beskryf is, met elektron-onttrekkende fluooratome wat op die sentrale fenielering geleë is. Gebruik van hierdie ligand het gelei tot die karakterisering van 'n tweevoud geïnterpenetreerde poreuse raamwerk, wat verskil van dit wat in die vorige hoofstuk beskryf is. Aktivering, sowel as gas uitruiling, lok slinger konformasie veranderings in die ligand uit. Sorpsie eksperimente toon aan dat die materiaal koolstofdiksied bo 'n paar lineêre alkane verkies. Reaksie met die chloriedsout van hierdie ligand het 'n nuwe MOF opgelewer.

Vervanging van kadmium met sink in die reaksie lewer 'n derde nie-geïnterpenetreerde raamwerk op, waar die ligand [2 + 2] siklo-addisie ondergaan het en in die anti-konformasie teenwoordig is.

SC-SC aktivering, sowel as gas uitruilingseksperimente, het getoon dat hierdie raamwerk minder buigsaam as sy sink eweknie is. Blootstelling van die geaktiveerde materiaal aan koolstofdioksied dui op 'n verstommende opname van koolstofdioksied. Die byvoeging van DMSO tot die DMF oplossing het tot die vorming van nog twee isoskeletale strukture gelei, wat verskil in hul spaanwiel konstruksie, ligand konformasie en, as gevolg hiervan, ook in hul oplosmiddel-toeganklike leë ruimte.

Hoofstuk VI beskryf die reaksie van vyf MOFs gebaseer op diarieleteen ligande met lig. Die kleurveranderinge en onderliggende strukturele veranderinge verskil van kristal tot kristal. Die eerste raamwerk is 'n poreuse tweeledig geïnterpenetreerde MOF, wat 'n dramatiese kleur- en vormverandering tydens UV-bestraling ondergaan. Wanneer dieselfde kristal aan wit lig blootgestel word, keer die selgrense terug na dié van die oorspronklike vorm. Die geaktiveerde vorm van 'n tweede viervoudig geïnterpenetreerde hoogs poreuse MOF het 'n affiniteit vir koolstofdioksied, en toon ook 'n kleurverandering tydens bestraling aan. Die gebruik van 'n meer buigsame ligand het 'n tweevoud geïnterpenetreerde poreuse materiaal opgelewer wat by lae temperatuur geaktiveer word, maar nie ontruim kon word sonder verlies van kristalliniteit nie. Bestraling veroorsaak 'n kleur verandering, maar geen strukturele verandering nie. Die vierde raamwerk is 'n tweeledig geïnterpenetreerde struktuur wat ineenstort en 'n oënskynlik nie-poreuse struktuur vorm wanneer die oplosmiddel verwyder word. Bestraling van hierdie materiaal lei tot ring-sluiting van die diarieleteen ligand, wat met 'n kleurverandering gepaard gaan. Dit is opvallend dat al hierdie prosesse d.m.v. 'n SC-SC transformasie plaasvind. Dit is die eerste voorbeeld van die foto-geïnduseerde ring-sluiting van 'n diarieleteen ligand as deel van 'n MOF. Die vyfde raamwerk toon 'n hoë graad van interpenetrasie (viervoud), maar in teenstelling met al die vorige voorbeelde, veroorsaak bestraling met UV-lig geen sigbare kleurveranderinge en geen strukturele veranderinge nie.

ACKNOWLEDGEMENTS

Felix Frankfurter said it best when he wrote, “*gratitude is one of the least articulate of the emotions, especially when it is deep*”. Thus the notion of properly acknowledging all the people who helped shape this work, is almost more daunting than writing the actual thesis. To begin with I would like to thank my supervisor Len Barbour; who took me on without any experience and gave me room to flounder, grow in confidence and most importantly the opportunity to fall in love with an avenue of chemistry I now consider my own. After three years in your group I can honestly say I am a research chemist and will remain so for the rest of my life. The exceptional facilities, unwavering standard of expectation and ethos amongst your students make an extraordinary working environment and I count myself incredibly lucky to have been given such an opportunity. Another person who was instrumental in the direction of this work and, more importantly, the maintenance of my sanity is Delia Haynes. Words truly can not express how kind you have been and how much I owe you. Profound thanks must be given to Vincent Smith for his patience, insightful advice and willingness to help with seemingly endless CIF files. I would also like to thank Craig Grimmer, whose love of chemistry, endless stream of incredible ideas and support have guided me through my research career thus far.

Next I would like to thank all the technical staff in the de Beers Building; Debbie, Mary, Mubarak and Raymond, your willingness to help did not go unnoticed.

Thanks must of course be given to the Supramolecular group (current and past members) with particular emphasis on my fellow “horsemen of the apocalypse”; Leigh Loots, Laura Van Laeren and Helene Wahl. You girls are not only my best friends but strong women who constantly maintain an incredible standard of excellence in everything you undertake and who make the balance between geek and chic seem effortless. Your friendship continues to be one of my most prized possessions. To Dominic, for perspective, burritos and imgur.

Last but by no means least I would like to thank my family; to my parents, my sister Percy and Jeff, your love, kindness, patience and unwavering support means more than I could ever say.

PUBLICATIONS

1. M. P. Akerman, C. D. Grimmer, V. I. Nikolayenko and D. Reddy, *Acta Crystallogr. Section E*, 2011, E67(12), o3478-o3479.
2. M. P. Akerman, C. D. Grimmer, V. I. Nikolayenko and D. Reddy, *Acta Crystallogr. Section E*, 2012, E68(12), o2384-o2385.
3. M. P. Akerman, C. D. Grimmer, V. I. Nikolayenko and D. Reddy, *Acta Crystallogr. Section E*, 2012, E68(12), o2273-2273.
4. C. A. Slabber, C.D. Grimmer, R. S. Robinson, V. I. Nikolayenko, 1-[2 (benzyloxy)phenyl]ethanone, 2015, *Zeitschrift für Kristallographie - Crystalline Materials*
5. V. Nikolayenko, S. A. Herbert and L. Barbour, **2015**. In preparation
6. V. Nikolayenko and L. Barbour, **2015**. In preparation
7. V. Nikolayenko and L. Barbour, **2015**. In preparation
8. V. Nikolayenko and L. Barbour, **2015**. In preparation

CONFERENCES

Indaba7, **2012**, Kruger National Park

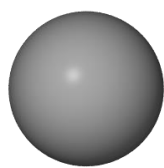
RSC YOUNG CHEMISTS SYMPOSIUM, UCT **2014** – First prize for oral presentation

POMOS **2014** – Oral and poster presented

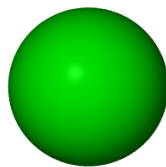
ABBREVIATIONS

1D	One dimensional
2D	Two dimensional
3D	Three dimensional
ASU	Asymmetric Unit
CIF	Crystallographic Information File
CSD	Cambridge Structural Database
EDX	Energy Dispersive X-ray spectroscopy
G	Guest
H	Host
H:G	Host:Guest ratio
IUPAC	International Union of Pure and Applied Chemistry
L	Ligand
FL1	Fluorinated ligand one
MOF	Metal-Organic Framework
PXRD	Powder X-ray Diffraction
SBU	Secondary Building Unit
SCD	Single-Crystal X-ray Diffraction
SEM	Scanning Electron Microscope
SC-SC	Single-Crystal to Single-Crystal Transformation
SPC	Soft Porous Crystal
TGA	Thermogravimetric Analysis
Z	Number of formula units per unit cell
DL	Diarylethene ligand

ATOMIC COLOUR KEY



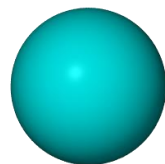
Hydrogen



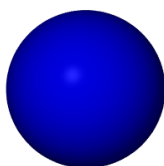
Fluorine



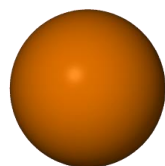
Carbon



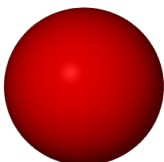
Zinc



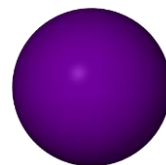
Nitrogen



Cadmium



Oxygen



Cobalt



Sulphur



Manganese

TABLE OF CONTENTS

DECLARATION	ii
ABSTRACT	iii
OPSOMMING	v
ACKNOWLEDGEMENTS	vii
PUBLICATIONS	viii
CONFERENCES	viii
ABBREVIATIONS	ix
ATOMIC COLOUR KEY	x
TABLE OF CONTENTS	xi

CHAPTER I: INTRODUCTION

1.1 SUPRAMOLECULAR CHEMISTRY.....	1
1.2 CRYSTAL ENGINEERING.....	2
1.3 SELF ASSEMBLY.....	3
1.4 INTERMOLECULAR INTERACTIONS.....	3
1.4.1 Directional Forces.....	4
1.4.1.1 Hydrogen bonding.....	4
1.4.1.2 Coordination bonding.....	5
1.4.2 Non-Directional Forces.....	6
1.4.2.1 Van der Waals Interactions.....	6
1.4.2.2 π - π stacking.....	6
1.5 METAL ORGANIC FRAMEWORKS.....	7
1.6 INCLUSION COMPOUNDS.....	8
1.7 POROSITY.....	12
1.8 GAS SORPTION.....	13
1.9 ISOSTRUCTURALITY.....	15
1.10 SOLID SOLUTIONS.....	15
1.11 EPITAXY.....	16
1.12 TOPOLOGY.....	16

1.13	SOLVATOMORPHISM	17
1.14	SINGLE-CRYSTAL TO SINGLE-CRYSTAL (SC-SC) TRANSFORMATIONS (LITHOTROPISM)	17
1.15	PLEOCHROISM	18
1.16	PHOTOCHROMISM	19
1.17	CYCLOADDITION	21
1.18	THESIS OUTLINE	23
1.19	REFERENCES	25

CHAPTER II: EXPERIMENTAL TECHNIQUES

2.1	SOLUTION NMR	30
2.2	SINGLE CRYSTAL X-RAY DIFFRACTION (SCD)	30
2.3	POWDER X-RAY DIFFRACTION (PXRD)	31
2.4	ENERGY DISPERSIVE XRAY SPECTROSCOPY (EDX)	31
2.5	THERMOGRAVIMETRIC ANALYSIS (TGA)	31
2.6	GRAVIMETRIC SORPTION(IGA)	32
2.7	GAS CHROMATOGRAPHY COUPLED TO A MASS SPECTROMETER (GCMS)	33
2.8	INFRA-RED ADSORPTION MEASUREMENTS (IR)	33
2.9	IRRADIATION EXPERIMENTS	33
2.10	SOLID-STATE UV-VISIBLE SPECTROSCOPY	34
2.11	COMPUTER PACKAGES	34
	2.11.1 The Cambridge structural database (CSD)	34
	2.11.2 Mercury	34
	2.11.3 Graphical illustrations and guest accessible surfaces	34
	2.11.4 PLATON/SQUEEZE	35
2.12	REFERENCES	36

CHAPTER III: STRUCTURAL ANALYSIS AND GAS SORPTION STUDIES

3.1	NATURE OF COMPONENTS	37
3.2	SOLVOTHERMAL CRYSTALLISATIONS	39
3.3	RESULTANT MOFS	39
	3.3.1 HC1 and HC2	42

3.3.2	CP1	43
3.3.3	CP2	46
3.3.4	CP3	51
3.3.5	CP4	53
3.3.6	CP5	55
3.3.7	CP5a	59
3.3.8	CP6	60
3.3.9	CP7	65
3.3.10	CP7a	67
3.3.11	CP7b	68
3.4	CONCLUSION	71
3.5	SYNTHESIS OF MOFs CP1-CP7b	71
3.6	CRYSTALLOGRAPHIC DATA TABLES	73
3.7	REFERENCES	80

CHAPTER IV: TUNING MOF SEQUESTRATION AND STORAGE

4.1	HC1	82
4.1.1	HC1'	84
4.2	SC-SC GUEST EXCHANGE EXPERIMENTS IN HC1	85
4.2.1	HC1·oxy	85
4.2.2	HC1·mxy	86
4.2.3	HC1·pxy	87
4.2.4	HC1·dioxane	88
4.3	GC-ANALYSED SELECTIVITY TESTING of HC1	89
4.4	GRAVIMETRIC GAS SORPTION FOR HC1	90
4.5	HC2	91
4.5.1	HC2'	92
4.6	GC-ANALYSED SELECTIVITY TESTING OF HC2	93
4.7	GRAVIMETRIC GAS SORPTION FOR HC2	94
4.8	PLEOCHROISM	95
4.9	SOLID SOLUTIONS	96
4.10	EPITAXIAL CRYSTAL GROWTH.....	101
4.11	CONCLUSION	102

4.12	SYNTHESIS OF MOFS HC1-HC6	103
4.13	CRYSTALLOGRAPHIC DATA TABLES	104
4.14	REFERENCES	107

CHAPTER V: GUEST INDUCED MOTION IN SOFT POROUS CRYSTALS

5.1	MOFS PREPARED USING FL1	110
5.1.1	SPC1a	111
5.1.2	SPC1a'	113
5.2	SC-SC GUEST EXCHANGE EXPERIMENTS IN SPC1a	114
5.2.1	SPC1a-CAN	116
5.2.2	SPC1a-Cl₃ACN	118
5.3	GRAVIMETRIC GAS SORPTION FOR SPC1a'	121
5.4	SPC1b	122
5.5	SPC2a	124
5.5.1	SPC2a'	128
5.5.2	SPC2a_Irrad	129
5.6	SC-SC GUEST EXCHANGE EXPERIMENTS IN SPC2a	130
5.7	GRAVIMETRIC GAS SORPTION FOR SPC2a'	132
5.8	SPC2b	133
5.9	CONCLUSION	138
5.10	SYNTHESIS OF MOFS SPC1-SPC2	139
5.11	CRYSTALLOGRAPHIC DATA TABLES	140
5.12	REFERENCES	145

CHAPTER VI: PHOTOCROMIC COMPOUNDS

6.1	INTRODUCTION	147
6.2	SOLVOTHERMAL CRYSTALLISATION CONDITIONS	154
6.3	RESULTANT MOFS	155
6.3.1	PCCP_1	155
6.3.1.1	Irradiation Experiments.....	157
6.3.1.2	Solid-State UV-visible Spectroscopy.....	158

6.3.2	PCCP_2	161
6.3.2.1	PCCP_2'	163
6.3.2.2	Super critical CO ₂ experiment.....	166
6.3.2.3	Irradiation Experiments.....	167
6.3.2.4	Solid-State UV-visible Spectroscopy.....	168
6.3.2.5	Variable Irradiation PXRD.....	170
6.3.2.6	Gravimetric gas sorption using CO ₂	173
6.3.3	PCCP_3	174
6.3.3.1	PCCP_3a	176
6.3.3.2	Irradiation Experiments.....	177
6.3.3.3	Solid State UV-visible Spectroscopy	177
6.3.4	PCCP_4	179
6.3.4.1	PCCP_4'	181
6.3.4.2	Irradiation Experiments.....	182
6.3.4.3	Solid State UV-visible Spectroscopy	183
6.3.5	PCCP_5	185
6.3.5.1	PCCP_5'	188
6.3.5.2	Irradiation Experiments.....	189
6.3.5.3	Solid State UV-visible Spectroscopy	189
6.4	CONCLUSION	190
6.5	SYNTHESIS OF MOFS PCCP_1-PCCP_5	192
6.6	CRYSTALLOGRAPHIC DATA TABLES	193
6.7	REFERENCES	199

CHAPTER VII: CONCLUSIONS AND FUTURE WORK

7.1	THESIS SUMMARY AND CONCLUDING REMARKS	201
7.2	PROPOSED FUTURE WORK	207

SUPPLEMENTARY INFORMATION

APPENDIX A (located on disc)

Ligand synthesis

Ligand NMR

Structure files (CIF and CIF check)

TGA thermograms

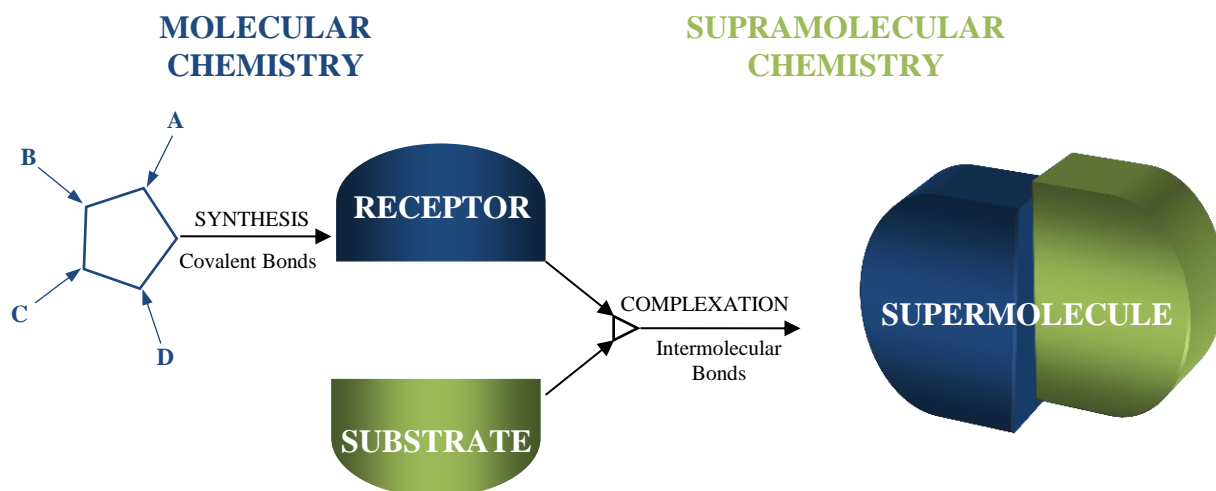
PXRD

Competition experiment data

IR data

1.1 Supramolecular chemistry

The work described in this dissertation falls under the ambit of supramolecular chemistry. However in order to define ‘supramolecular chemistry’, we must first consider a working definition of molecular chemistry. Molecular chemistry is concerned with the covalent bond, and its principal focus is to uncover and understand the rules that govern the structures, properties and transformations of molecular species.¹ Supramolecular chemistry can in turn be defined as “chemistry beyond the molecule”¹, in which two or more chemical species can associate with one another by means of noncovalent interactions to form entities of higher complexity. The term *supramolecular chemistry* was only used much later by the Nobel Laureate Jean-Marie Lehn in 1978 when he described it as “...the chemistry of molecular assemblies and of the intermolecular bond.”²⁻³ In other words, a supermolecule is an organised entity of higher complexity, consisting of molecules held together by intermolecular forces. **Scheme 1.1** illustrates the relationship between molecular and supramolecular chemistry. A typical supramolecular species consists of a molecular receptor bound to a substrate *via* intermolecular interactions to create a supermolecule (Übermolecule) a term first introduced by Wolf in the 1930s.^{4,5,6} This supermolecule is therefore of higher complexity and consists of two or more molecular entities. Guest molecules are often located within cavities present in the molecular host.



Scheme 1.1 The evolution of supramolecular chemistry from molecular chemistry.⁶

1.2 Crystal engineering

Crystal engineering is a vast and highly active discipline within the realm of supramolecular chemistry and in the simplest of terms may be regarded as an artefact of rational design. Desiraju famously described it as “*the understanding of intermolecular interactions in the context of crystal packing and in the utilisation of such understanding in the design of new solids with desired physical and chemical properties*”.⁷ A more modern definition is “*the bottom-up construction of functional materials, starting from molecular or ionic building blocks assembled by means of noncovalent interactions*”.⁸

Although Pepinsky⁹ was the first to utilise the term “crystal engineering” in a paper he presented in 1955 titled “Crystal Engineering: a new concept in crystallography,” it is generally accepted that the area was only truly established some sixteen years later by Schmidt as a result of his work regarding photodimerisation of olefins in the solid state.¹⁰ The systematic design of supramolecular architectures in the solid state may be achieved through a series of different strategies, one of which shall be discussed here. Desiraju *et al.* developed “supramolecular synthons” (combinations of intermolecular interactions) as a means to achieve supramolecular retrosynthesis. An organic crystal may be thought of as a simplified network in which the intermolecular interactions are linkages and the molecules are nodes. These features are required for one-, two- or three-dimensional architectures to be predicted. **Figure 1.1** provides examples of synthon involvement in retrosynthesis of a crystal.

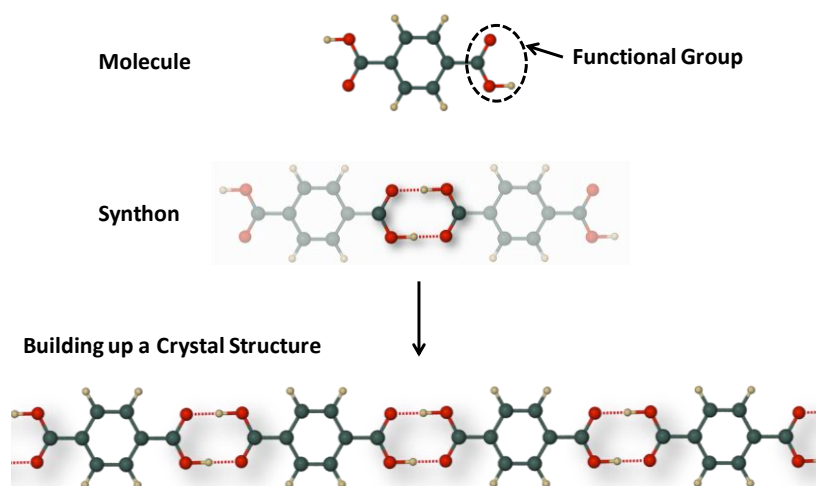


Figure 1.1 Example of a supramolecular synthon and the role it plays in the extended structure of a crystal.

1.3 Self assembly

Self assembly (**Figure 1.2**) is a core concept in supramolecular chemistry and concerns itself with the reproducible spontaneous association of a number of molecular building blocks through the use of reversible interactions to create higher order aggregates.¹¹ The reversible nature of self-assembling systems (often involving weak non-covalent interactions), enables the correction of any ‘errors’ incurred during the assembly process, thus allowing the most thermodynamically stable product to form. If several components are introduced into a system, the likelihood of those components only aligning in one configuration is slim. In all probability, several species will form, with one possessing the greatest thermodynamic stability, thus allowing its formation to occur more readily than the rest. Owing to their lability and high degree of directionality, metal to ligand interactions are the most commonly employed interactions in molecular self-assembly.¹¹ One way to realise predictable assemblies is to combine rigid ligands with metal ions that have well established coordination environments.

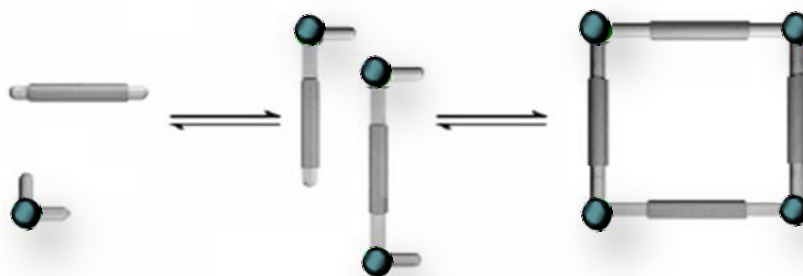


Figure 1.2 The thermodynamically stable assembly of a molecular square from molecular building blocks.¹²

1.4 Intermolecular interactions

Although considerably weaker than covalent interactions, non-covalent interactions can be used in a cooperative manner to form supramolecular complexes. These interactions represent the “glue” that holds supramolecular species together with dispersion interactions ranging from 2 kJ mol^{-1} to ion-ion interactions that can reach 300 kJ mol^{-1} .⁸

Crystallisation is an entropically unfavourable process, and the system needs to gain substantial enthalpy by balancing the attractive and repulsive forces between molecules in order to triumph over the dramatic decrease in entropy. Most intermolecular interactions (**Table 1.1**) may be further sub-divided into one of two categories. The forces responsible for structure formation are medium range (anisotropic) forces, also known as directional forces, while long range (isotropic) forces, or non-directional forces determine intermolecular orientations and functions.

Table 1.1 A selection of intermolecular interactions.¹²

	Intermolecular interaction	Energy (kJ mol⁻¹)	Examples
Anisotropic forces	Very strong hydrogen bonds	63- 167	OH...O ⁻
	Coordination bonds	84 - 188	M...N, M...O
	Strong hydrogen bonds	21 - 63	OH...O, NH...O
	Weak hydrogen bonds	4- 17	CH...O, OH... π
Isotropic forces	van der Waals interactions	2 - 8	CH ₃ ...CH ₃ , CH ₃ ...Ph
	Heteroatom interactions	4 - 8	N...Cl, C...Br
	π interactions	8 - 42	Ph...Ph, nucleobases

1.4.1 Directional Forces

1.4.1.1 Hydrogen bonding

Owing to its strength and highly directional nature, the hydrogen bond is considered the *master-key* anisotropic interaction and was first described by Linus Pauling in 1931.¹³ In 2011 the IUPAC defined the hydrogen bond as an attractive interaction between a hydrogen atom from a molecule or a molecular fragment D–H in which D is more electronegative than H, and an atom or a group of atoms in the same or a different molecule, in which there is evidence of bond formation.¹⁴ The D–H...A (D = donor and A = acceptor) bond is defined by the geometric parameters d , y , r , θ and ϕ ¹⁸ as shown in **Figure 1.3**.

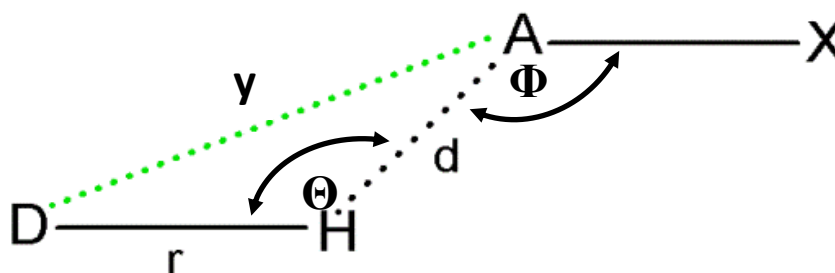


Figure 1.3 Important geometric parameters associated with the formation of a hydrogen bond. The D...A distance (shown as a green dashed line) is the principal parameter for identification of hydrogen bonds.

A typical hydrogen bond may be depicted as D-H...A-X. D-H represents the hydrogen bond donor. The acceptor may be an atom or an anion A, or a fragment of a molecule A-X, where A is bonded to X.⁸ In some cases, D and A are the same. In more specific cases, D and A are the same and D-H and A...H distances are similar as well, leading to symmetric hydrogen bonds. In any event, the acceptor is an electron rich region such as, but not limited to, a lone pair on A or π -bonded pair on A-X.⁸ Hydrogen bond strengths (4 to 167 kJ mol⁻¹) depend heavily on the nature of D and A as well as the geometry that the bond adopts. Such bonds can vary in length, strength and geometry and are consequently important electrostatic interactions for framework design.

1.4.1.2 Coordination bonding

When a labile metal containing a vacant coordination site comes into contact with a ligand capable of donating a lone pair of electrons, a coordination bond forms (ion-dipole interaction).¹⁵ Coordination bonds range between 84 - 188 kJ mol⁻¹ in strength and provide directionality. Owing to their strength, these bonds take precedence over other weaker bonds and are responsible for overall structure formation and network topology of coordination compounds.

1.4.2 Non-Directional Forces

1.4.2.1 Van der Waals Interactions

A species in close proximity to another induces oscillations in the overall electron distribution. These dispersion effects are known as van der Waals interactions and are composed of London interactions as well as exchange and repulsion interactions. Such weak electrostatic forces are the principal driving force for the encapsulation of guest molecules within a molecular host. An instantaneous dipole forms as the electron cloud moves about a molecule's momentary location. If two spontaneous dipoles attract one another, London interactions are produced. The Lennard-Jones model approximates the interaction between a pair of neutral atoms or molecules (Equation 1) and consists of a steep repulsive term, and a smoother attractive term:

$$V(r) = 4 \epsilon \left[\left(\frac{\sigma}{r} \right)^{12} - \left(\frac{\sigma}{r} \right)^6 \right] \quad \dots 1$$

ϵ is the depth of the potential well, σ is the finite distance at which the inter-particle potential is zero and r is the distance between the particles. The attraction decreases with the interatomic separation as r^{-6} , and depends approximately on the size of the molecules.¹⁶ Molecules are kept separate from one another by very important exchange forces that follow an r^{-12} rule, meaning that repulsion between atoms is strongest at short interatomic distances. As interatomic distances increase, the effects of these forces decrease rapidly.

1.4.2.2 π - π stacking

π - π interactions mostly occur between planar aromatic groups. Such forces are highly polarisable, providing enhanced stabilising dispersion interactions between adjacent aromatic molecules. These interactions are considered non-directional and occur in the energy range 8 - 42 kJ mol⁻¹.⁸ Computational studies have revealed that there are two types of orientation for π - π interactions; *edge-to-face* alignment (**Figure 1.4a**) in which a hydrogen atom (electron poor) of one aromatic ring is directed towards the central negative π -electron density of the other ring, and *offset face-to-face* (**Figure 1.4b and 1.4c**) in which parallel ring planes are offset from one another by a distance of about 3.5 Å. The interaction occurs between the edge of one ring and the centre of another.

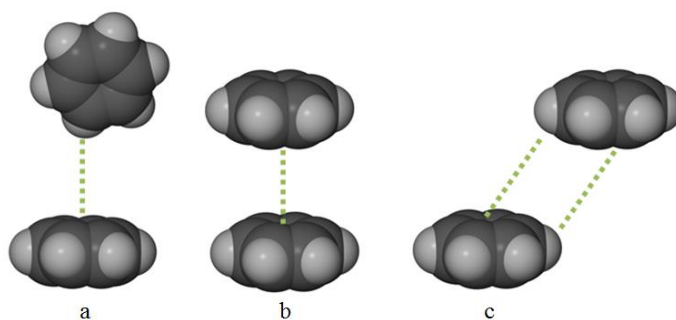


Figure 1.4 Types of π - π interactions **a)** *edge-to-face* **b)** *eclipsed-face-to-face* **c)** *offset face-to-face*.¹¹

1.5 Metal Organic Frameworks (MOFs)

Rigid metal organic frameworks (MOFs) are conceptually infinite scaffolds of interconnected structural units comprised of multivalent metals or metal clusters bridging organic ligands and contain guest-filled pores. First generation MOFs are materials that undergo complete and irreversible destruction upon guest removal.¹⁷ Second generation¹¹ MOFs differ in that they retain their form after guest removal, while third generation¹¹ MOFs undergo desolvation accompanied by a reversible host rearrangement.³ MOFs of this last type are flexible and dynamic and can respond reversibly to external stimuli such as guest uptake, temperature and light (**Figure 1.5**).

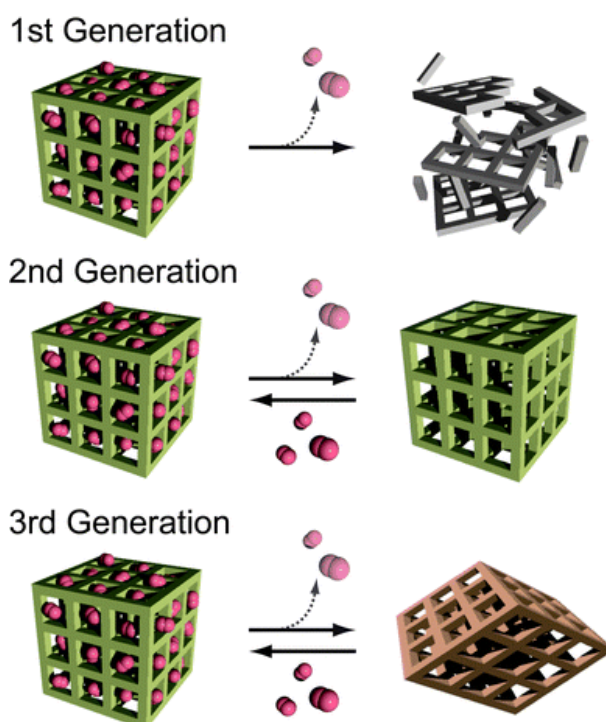


Figure 1.5 Diagrammatic representations of the three generations of MOFs.¹⁸

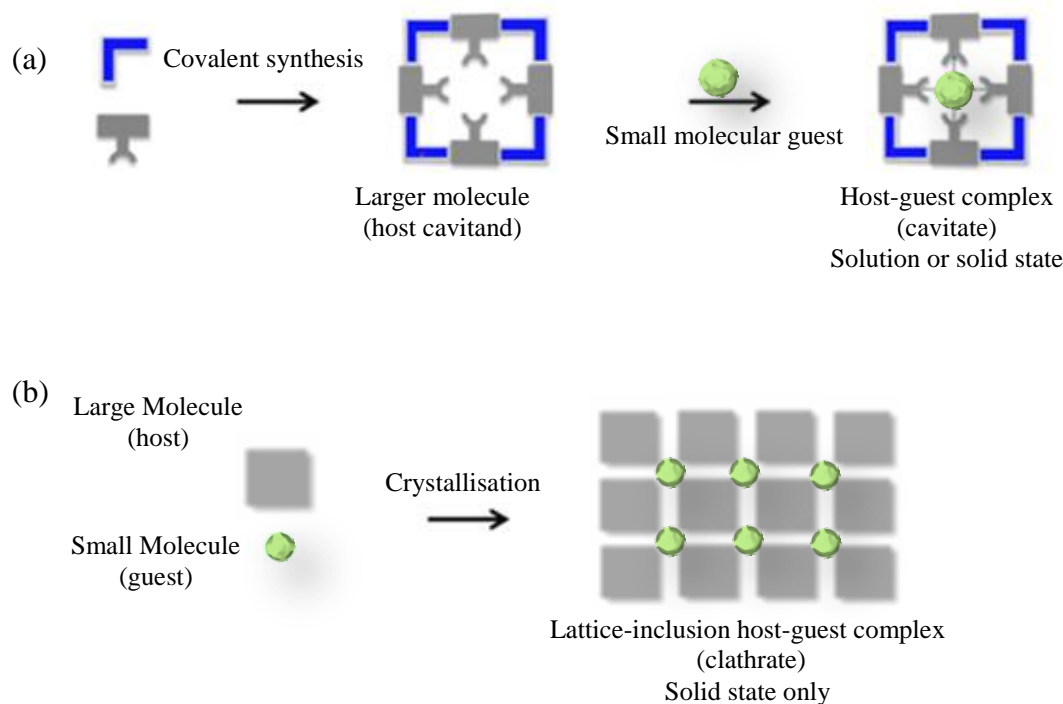
Such materials are considered hybrid coordination polymers that result when dative bonding occurs between organic bridging ligands and metal ions or clusters (secondary building units, SBU formation).¹⁹ The exact nature of the organic bridging unit may vary but, in most cases, neutral nitrogen containing ligands, carboxylate ligands or a combination thereof are the principal choice. MOF synthesis, also known as reticular synthesis (rational design) is a sub-class of crystal engineering and the term ‘reticular synthesis’ was coined by Yaghi *et al.*²⁰ Owing to the complete control over component selection and other variable parameters (nature of solvent, temperature, pH and crystallisation method) an infinite number of possible coordination arrangements exist. MOFs are therefore tuneable, highly versatile materials²¹ that can possess extraordinarily high surface areas and pore volumes. As a result, these materials are much sought after for industrial applications such as catalysis,²² gas separation and storage.¹⁷ The principal flaw associated with the industrial application of MOFs is their relatively poor thermal stability. Frameworks undergoing decomposition at low temperatures cannot be used in vapour phase reactions.^{14b} However, under milder conditions certain MOFs have been shown to outperform zeolites*.¹⁴

1.6 Inclusion Compounds

An inclusion compound may be thought of as the association (non-covalent connection) between a host molecule (enzyme, zeolite or MOF), and a smaller guest molecule trapped within its lattice.²³ The first system of this type to be identified was that of chlorine hydrate in 1811 by Sir Humphry Davy.²⁴ The discovery of other well-known inclusion compounds such as those of hydroquinone,²⁵ Dianin’s compound,²⁶ cyclodextrins,²⁷ Hofmann’s compound,²⁸ zeolites²⁹ and metal organic frameworks³⁰ followed throughout the 20th century. Powell³¹ reported the first structural elucidation of a host-guest (inclusion) complex in 1948 and coined the term *clathrate* (derived from the Latin word *clathratus*, meaning “enclosed by the bars of a grating”). The formation of inclusion compounds is governed by three underlying principles; fixation (Ehrlich introduced the idea that molecules do interact even if they do not bind),³² recognition (lock and key model developed by Fischer)³³ and coordination (Werner’s seminal work in the field of coordination chemistry, where he stated that selective binding must involve attraction or mutual affinity between host and guest).³⁴

* Zeolites are microporous aluminosilicate minerals commonly used as commercial absorbents.

In 1977 Cram³⁵ formalised the definition of a host-guest complex when he wrote: “*the host component is defined as an organic* molecule or ion whose binding sites converge in the complex... The guest component is defined as any molecule or ion whose binding sites diverge in the complex.*” Applications of inclusion compounds include entrapment of hazardous materials from the environment,³⁶ encapsulation of pharmaceutically active agents as a means to target specific tissue sites,³⁷ separation of closely related compounds within a mixture³⁸ and chemical sensors,³⁹ to name but a few. Host systems may be further subdivided into cavitands and clathrands (Scheme 1.2).⁴⁰ The former involve host molecules that completely surround the guest molecules possessing large cavities in both the solid state and in solution. Clathrands or intercalates are lattice inclusion compounds that typically only exist in the solid state. Host-guest complexes are held together by electrostatic forces such as hydrogen bonding and dipole-dipole interactions, while the terms ‘clathrates’ or ‘cavitates’ are used when the association is by non-directional forces such as van der Waals interactions.¹⁵



Scheme 1.2 a) Cavitates present in the solid or liquid state. b) Clathrate, only present in the solid state.

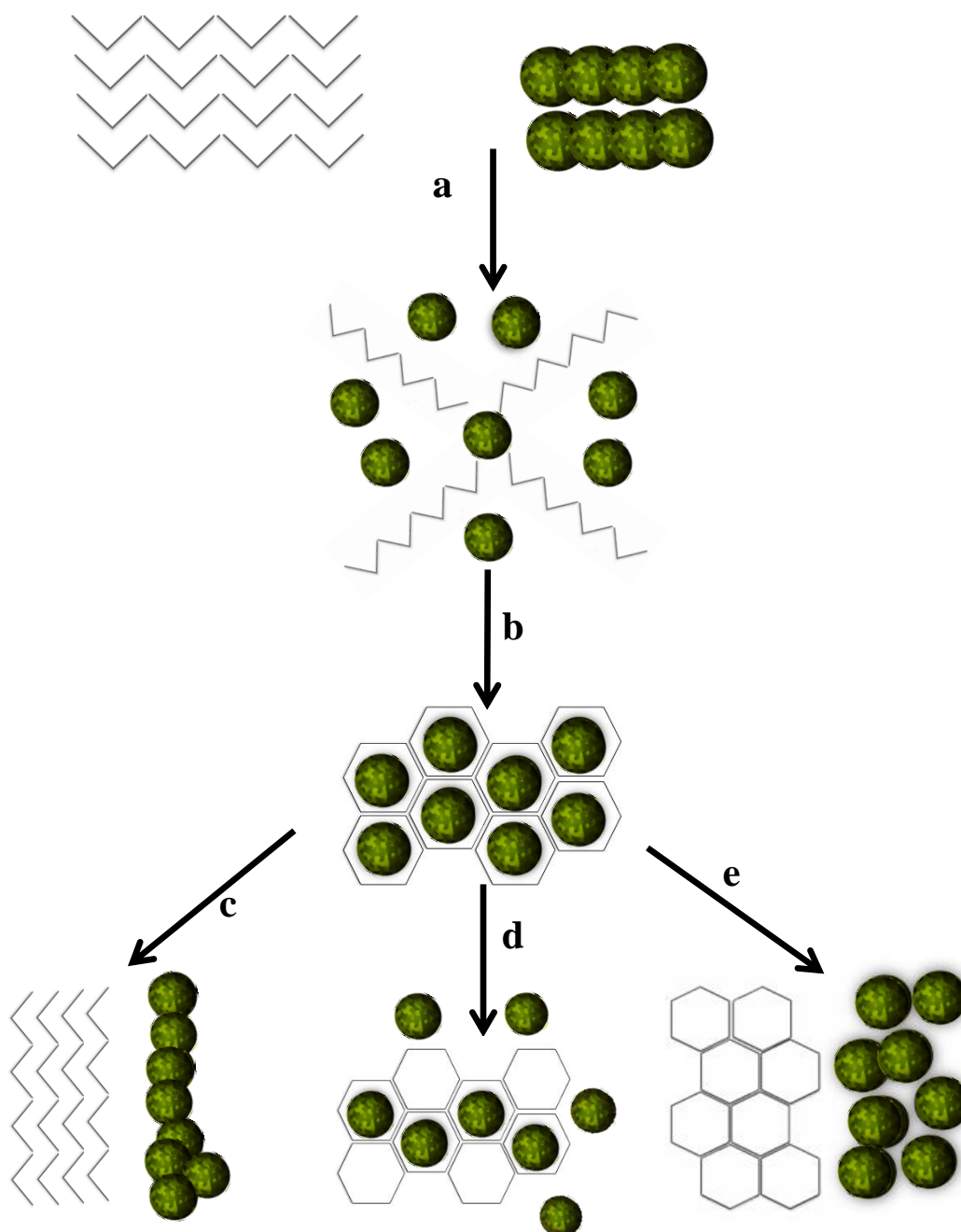
* Since the definition was proposed, the term “organic” has been removed from the description thus enabling the inclusion of various inorganic hosts.

Host-guest inclusion reactions can be described by the following equation:



where α represents the initial pure host phase H in the solid state, G the liquid or gaseous guest, β the phase of the new host-guest compound in the solid state and n the stoichiometric host-guest ratio. **Scheme 1.3** shows the processes of guest inclusion, phase transition and decomposition experienced by a host-guest compound.¹⁵

A complex typically forms when the host components are dissolved in a liquid guest. Weak hydrogen bonding and van der Waals interactions enable the liquid guest to interact with the host components and, as a result, influence the inclusion compound formed (**Scheme 1.3a**).⁴¹ Crystallisation of the complex results in the β -phase (**Scheme 1.3b**). Multiple factors such as temperature, types of guest utilised and pH determine the ultimate nature of this phase. Generally, if the β -phase is heated, one of three possible scenarios could ensue: (i) the host could expel the included solvent molecules and rearrange to form a new, more densely packed, non-porous α -host phase (**Scheme 1.3c**); (ii) the inclusion complex could undergo a phase transformation and alter its packing mode to produce a new γ -phase (**Scheme 1.3d**); (iii) the host expels the guest molecules without significant rearrangement of the host molecules to yield an empty β_o apohost structure capable of absorbing new guest molecules (**Scheme 1.3e**).³²



Scheme 1.3 Host-guest inclusion reactions involve: **a)** Dissolution of the apohost phase in the liquid guest. **b)** Crystallisation of the β phase. **c)** Desolvation and host rearrangement yielding the α phase. **d)** Partial desolvation to yield the γ phase or **e)** the apohost β_0 phase. Scheme adapted from reference 42.⁴²

1.7 Porosity

The word ‘pore’ is derived from the Greek word ‘poros’, meaning *passage* or *opening* and crystalline or amorphous materials possessing permanent apertures through which molecules are reversibly able to travel can be described as porous. Porosity at the molecular level is highly uncommon since materials are stabilised by attractive forces and molecules have an inherent tendency to close-pack in the solid state (one is reminded of Aristotle’s adage “*Nature abhors a vacuum*”). In this context, zeolites⁴³ and activated carbons⁴⁴ have been known for many centuries, having been utilised for a number of important technological applications. Since then, crystal engineering has implemented several strategies to induce the formation of porous materials in the hope of utilising such materials in industrial applications. One such example is the synthesis of infinite three-dimensional (3D) metal-organic framework materials (MOFs) or coordination polymers that include solvent molecules as guests in the framework apertures such that removal of the solvent yields porosity.

According to Barbour,⁴⁵ there are three distinct types of porosity and it is important to differentiate between them. *Virtual porosity* (false porosity) is generated by purposefully altering a data file by deleting or ignoring small molecules within the cavity, *transient porosity* (also described as porosity without pores) refers to a crystalline solid that possesses large voids without any permanent channels leading from the material’s surface to the voids and *conventional porosity* is generated by exchanging or completely removing the solvent molecules situated in the channels of the host, without framework collapse. Conventional porous MOFs can then be further subdivided into four categories based on pore size: ultramicroporous (pore size $< 5 \text{ \AA}$), microporous (pore size $5\text{-}20 \text{ \AA}$), mesoporous (pore size $20\text{-}500 \text{ \AA}$) and macroporous (pore size $> 500 \text{ \AA}$) in accordance with the guidelines provided by the IUPAC in 1985.⁴⁶ Not surprisingly, the study of porous materials has grown exponentially due to the many potential applications, including building technology, separation science, gas storage, soil science and catalysis, to name but a few.⁴⁷

1.8 Gas Sorption

When discussing porosity it is important to differentiate between absorption and adsorption. *Absorption* is the integration of one or more substances into a solid while *adsorption* is a purely two dimensional phenomenon occurring when one material accumulates on the surface of another. The distinction between absorption and adsorption is not always clear, and the generic term *sorption* is often used.⁴⁸ One can distinguish between the two types of sorption experimentally since absorption can be either endo- or exothermic, while adsorption is purely exothermic.⁴⁷ *Desorption* is the reverse of sorption and occurs when the guest taken up by a material is released. Gas sorption is measured by determining the amount gas taken up at a constant temperature as a function of the pressure of the gas at equilibrium; the amount sorbed (in moles, grams or cm³) is plotted against the relative equilibrium pressure (P/P^0), where P^0 is the saturation pressure of the adsorptive at the specified temperature. This relationship is known as the *sorption isotherm*. Generally, the sorption and desorption isotherms are plotted together. *Hysteresis* occurs when the two curves do not overlap.⁴⁹

Based on the strength and type of interaction, another important distinction must be made between the two types of sorption, namely *chemi-* and *physisorption*. *Chemisorption* is characterised by the formation of covalent bonds with an enthalpy of adsorption ranging between *ca* 105 and 397 kJ mol⁻¹. *Physisorption*, a notably weaker interaction, occurs when a gas is in contact with a solid surface, and is characterised by long range and weak van der Waals forces with an enthalpy often less than 42 kJ mol⁻¹. The amount of gas sorbed may be measured in one of two ways. The first is by gravimetric analysis, in which the increase in weight is recorded upon gas exposure. This is the type of analysis that was carried out during the course of this work. The second method is volumetric analysis whereby changes in pressure are measured at a fixed volume. The BDDT convention proposed by Brunauer *et al.*^{48b} was formalised by the IUPAC and states that experimentally obtained sorption isotherms may be classified into one of six types (**Figure 1.6**).⁵⁰ *Type I* isotherms, often referred to as Langmuir isotherms, possess a concave shape and are reversible.

Such isotherms are characteristic of microporous solids with small surface areas, examples of which include zeolites and activated carbon. *Type II* isotherms represent monolayer-multilayer adsorption and are reversible isotherms characteristic of nonporous or macroporous adsorbents. *Type III* isotherms are very uncommon having a convex shape and displaying reversibility over the entire pressure range, which can be attributed to weak host-guest interactions. *Type IV* isotherms display characteristic hysteresis; this is attributed to capillary condensation in mesoporous materials while the initial curvature (similar to type II) is attributed to monolayer-multilayer adsorption. *Type V* is another unusual isotherm and has a shape similar to that of the *Type III*, but is not reversible. This is due to weak adsorbent-adsorbate interactions. *Type VI* isotherms display a stepwise profile, which is attributed to layer-by-layer sorption on a uniform non-porous surface.⁴⁸

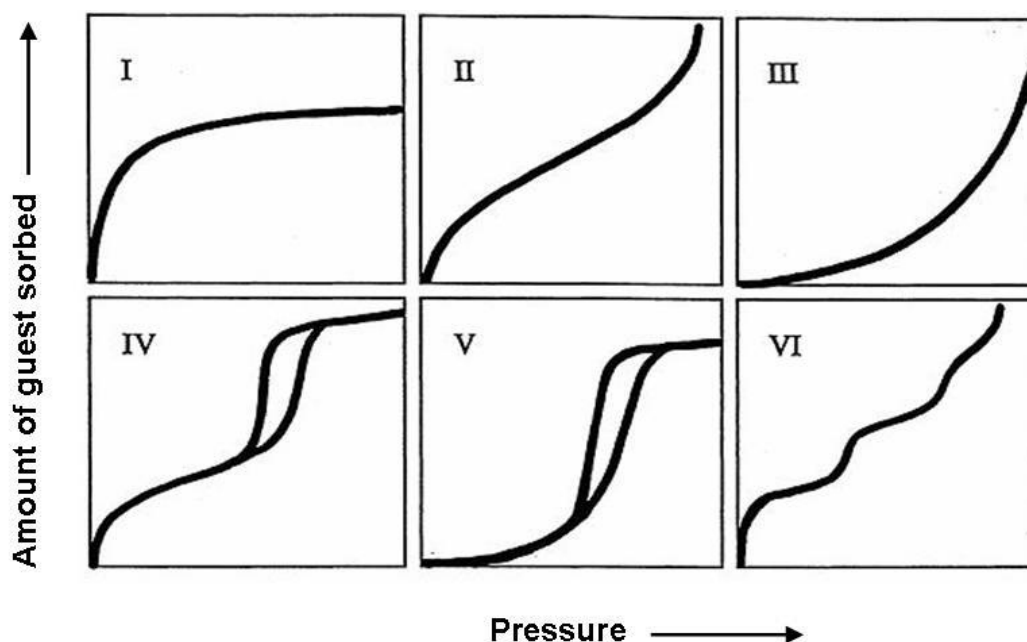


Figure 1.6 Idealised sorption isotherms as classified by the IUPAC.⁴⁸

Having presented an overview of supramolecular chemistry, the following sections will highlight some key concepts and definitions associated with the work undertaken in this thesis.

1.9 Isostructurality

Isomorphous is the term used to describe two crystals having the same external morphologies and was first introduced by Mitscherlich in 1819.⁵¹ Despite appearances, external morphologies provide no definitive information about the microscopic arrangements of atoms within a compound. Two materials are said to be *isostructural* (virtually superimposable)⁵² when they share the same three-dimensional packing arrangement of geometrically similar structural units in two different crystals, and as a result, crystallise in the same space group.¹² The study of isostructural compounds enables further elucidation of structure-property relationships as the arrangement of the host framework remains constant while the guest varies. Powder X-ray diffraction is an excellent technique when studying such compounds as the peak positions in the diffractograms of two isostructural compounds often overlap due to similar atomic lattice positions in the crystals, with any discrepancies being attributed to the different guest molecules located within the host assemblies.

1.10 Solid solutions

A solid solution (mixed crystal) is a monomorphic phase composed of two or more different atoms or molecules that are nonstoichiometrically interchanged within the crystal structure.⁵³ Formation of a solid solution is not always guaranteed and is dependent on the chemical and crystallographic properties of the substances in question. In accordance with the Hume-Rothery rule, such materials often form as the result of elements (generally metals) with similar atomic radii, electronegativities, valency or coordination modes undergoing reversible substitution reactions enabling the formation of a unique phase.⁵⁴ The solute may incorporate into the solvent crystal lattice substitutionally by replacing a solvent particle in the lattice, or interstitially by fitting into the space between solvent particles. Both of these types of solid solution affect the properties of the material by distorting the crystal lattice and disrupting the physical and electrical homogeneity of the solvent material.⁵⁵ Such solutions have significant commercial and industrial applications (metal alloys are solid solutions), as mixtures often have superior properties when compared to pure materials. Even small amounts of solute can affect the electrical and physical properties of the solvent *e.g.* doping of silicon.

1.11 Epitaxy

Epitaxy or *epitaxis* is the term used when one crystal is formed on the surface of another. Epitaxial growth involves the use of the surface of one crystal to seed the growth of a second form. If the two substances are isostructural, this is termed *homoepitaxy* while if the two forms are different the phenomenon is termed *heteroepitaxy*.

1.12 Topology

Chemical topology can be thought of as the connectivity between molecular entities. This concept was first introduced to the chemical community in the early 1960's by Wasserman.⁵⁶ The nature of the connection between two species is mechanical (interlocking) rather than chemical. In other words two or more species are considered entangled when they are irreversibly threaded around or through one another and uncoupling such an arrangement would require bond breaking.⁵⁷ Interpenetration (**Figure 1.7a**) is the term given to polymeric networks that pass through voids within each other to become topologically entangled such that they are inseparable.⁵⁸ This occurs during the crystallisation process as a means of minimising pore size and to thus stabilise the overall structure. Self-penetrating nets have two types of topology: parallel interpenetration of corrugated layers leading to a two dimensional network (generally) and inclined interpenetration of laminated nets resulting in a three-dimensional structure. Interdigitation (**Figure 1.7b**) is the interlocking of two moieties like the teeth of two combs. Such an entanglement can be separated without bond breaking and must not be confused with interpenetration.

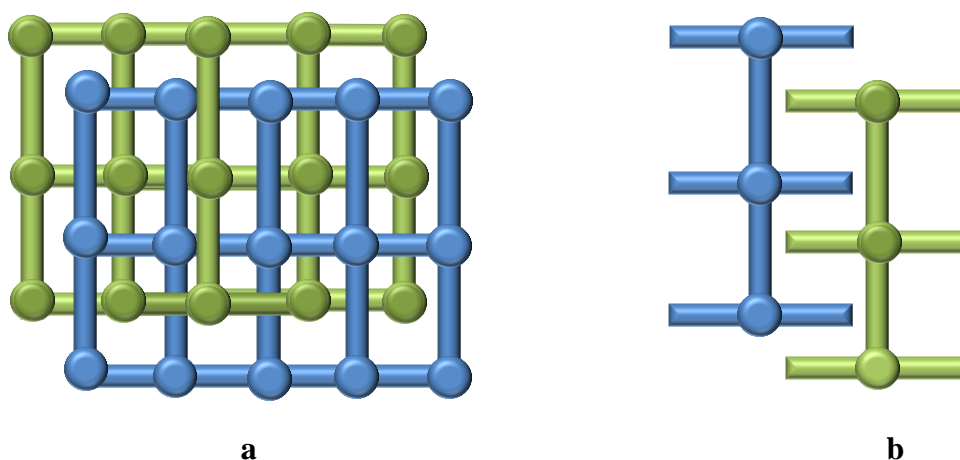


Figure 1.7 Diagram differentiating between **a**) interpenetration and **b**) interdigitation.⁴⁴

1.13 Solvatomorphism

Solvate refers to a material that has solvent molecules from the crystallisation process incorporated into the crystal lattice.⁵⁹ Favourable intermolecular interactions or improved packing, induced by the inclusion of solvent molecules, provides solvate stability. Solvates in which the guest changes but the host stays the same are *solvatomorphs*.

1.14 Single-crystal to single-crystal (SC-SC) transformations (lithotropism)

When a material in the solid state is exposed to physical or chemical stimuli, atomic or molecular rearrangement may occur.⁶⁰ If this response occurs in a concerted manner with minimal mechanical stress, the crystal may retain its mosaicity (or singularity) and may be said to have undergone a *single-crystal to single-crystal* transformation. Owing to the rigidity of a host lattice or framework, even minor changes in packing often induce crystal disintegration and, as a result, materials capable of surviving such transformations are still comparatively rare. Most SC-SC transformations are to be found in host-guest complexes, where the removal of the guest enables the host to undergo a rearrangement into its more stable close-packed conformation. If the host is invariant (except for small atomic displacements or adjustments), empty space or voids in the form of discrete pockets or channels may result upon guest departure. A guest exchange may be achieved by exposing the crystal to a different solvent or gas environment. The direct study of these single-crystal to single-crystal transformations by SCD analysis provides an opportunity for understanding solid-state dynamics and is evidence of the phenomenon of molecular cooperativity in the solid state.⁶¹

1.15 Pleochroism

Pleochroism arises from the Greek words *pleion* meaning more and *chroma* meaning colour. This is an optical phenomenon in which double refraction of light by a substance causes crystals to appear to have different colours at different angles of rotation, especially when studied under plane polarised light (**Figure 1.8**). Such crystals are able to bend light of different polarisations by different amounts, thus creating different paths through the crystal. The components of a divided light beam follow these paths and travel at different speeds enabling each path to absorb different colours of light. An important distinction must be made between pleochroism and birefringence. Bassett said it best; “a crystal must be anisotropic in order to show pleochroism and a crystal must be anisotropic to show birefringence, but a crystal needn't be birefringent in order to show pleochroism. It could have a birefringence of zero and still show strong pleochroism.”⁶²

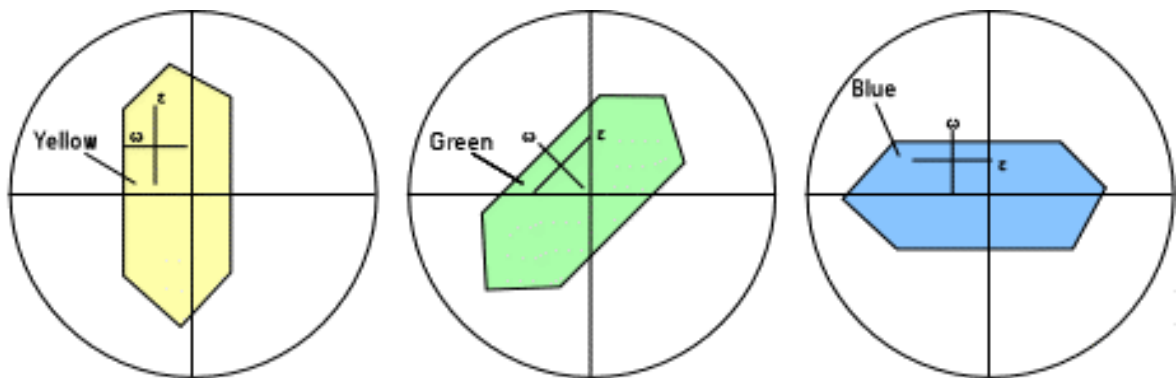
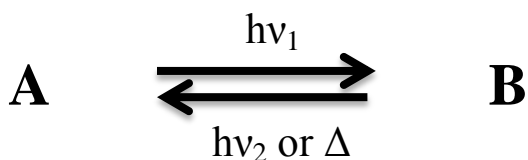


Figure 1.8 Schematic representation of a pleochromic crystal at 0° , 45° and 90° to the plane-polarised incident light.

1.16 Photochromism

Photochromism is derived from the Greek words *phos* meaning light and *chroma* meaning colour. It is described as the reversible transformation of two chemical species that have different absorption spectra in the visible region and is induced by absorption of electromagnetic radiation (**Scheme 1.4**).⁶³ With regard to this study, this implies the reversible photoinduced colouration of an ensemble of molecules in the crystalline state. Photochromic systems may be subdivided into two categories. The T-type (thermally reversible type) represents the most common group of chromophores and occurs when the post-irradiation isomer (B) is unstable and reverts to its original form (A), often upon heating. The second group is the P-type (photochemically reversible type) wherein isomers are far more stable and may be converted to their original form photochemically but not thermally.



Scheme 1.4 Photochromism as a reversible transformation between two forms.

Fritzsche is credited with reporting the first photochromic compound in 1867 when he observed the bleaching of an orange-coloured solution of tetracene in daylight and regeneration of the colour after leaving the solution in the dark.⁶⁴ Unfortunately, due to the poorly developed spectroscopic techniques of the time, this field remained largely unexplored until some forty years ago.^{65,66,67,68} With the advancement of analytical instrumentation and techniques, numerous families of organic molecules with photochromic properties have been identified and studied in great detail. Examples of such materials include spiropyrans, quinones, azobenzenes and diarylethenes (**Figure 1.9**).⁵⁸ In all these compounds, the colouration-decolouration process occurs as a result of unimolecular reactions, involving either ring closing and opening steps or a *cis-trans* isomerisation. Due to the wide range of potential applications, including ophthalmic lenses (corrective lenses), molecular switches, biomedical research and information technology (data storage), the use of molecular engineering to fine-tune photochromic compounds is a rapidly growing field.⁶⁹⁻⁷⁰

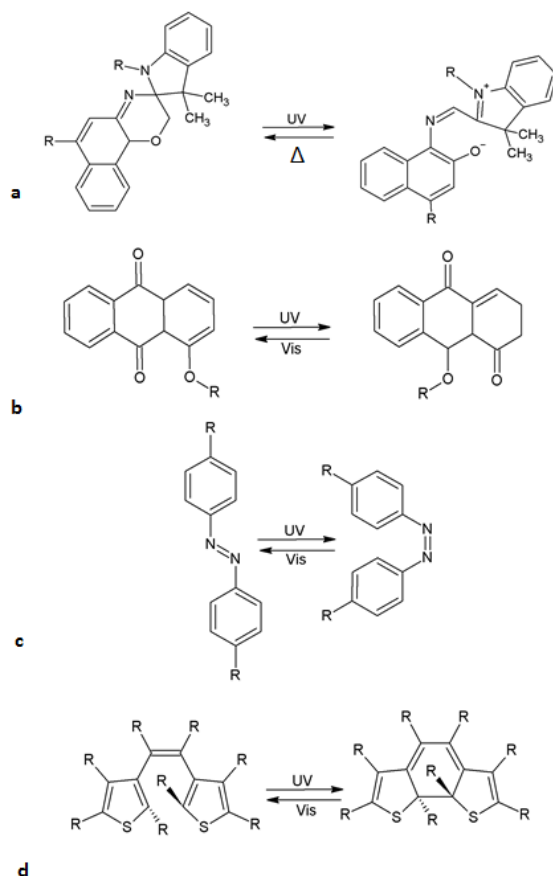


Figure 1.9 Examples of well-known photochromic compounds: **a)** spiropyrans **b)** quinones **c)** azobenzene **d)** diarylethenes.⁵⁸

1,2-Diphenylethene, or stilbene, is the best known diarylethene compound and has been shown to undergo *cis-trans* isomerisation as well as photocyclisation. It is important to note that, upon exposure to air or oxidants, the dihydrophenanthrene converts irreversibly to the phenanthrene while, in the absence of such agents, the dihydrophenanthrene thermally or photochemically reverts back to the initial stilbene form (**Figure 1.10**).⁷¹ The introduction of substituents (such as methyl groups) at the 2- and 6-positions of the phenyl ring stabilises the system and prevents unwanted oxidation.⁷²

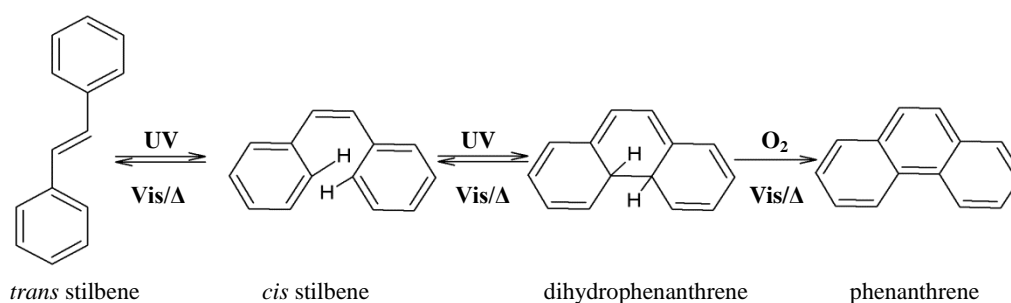


Figure 1.10 Isomerisation, photocyclisation and oxidation of stilbene.⁶⁹

Since thermal reversion is generally undesirable (the target function of such materials is formation of light-triggered molecular switches), numerous aryl groups have been studied in an attempt to prepare a P-type chromophore. Of all the groups investigated, stilbenes with five membered heterocyclic rings were found to be the best switches as both isomers are thermally stable and ring closing/opening may occur continuously without loss of performance.⁷³ In order to eliminate any competition, the dual nature of the stilbenes was eliminated by constraining the central ethene bond so that *cis-trans* isomerisation could not occur. **Figure 1.11** shows the carefully designed diarylethenes with various substituents and the effect that these substituents have on the colour observed upon irradiation with ultra-violet light.

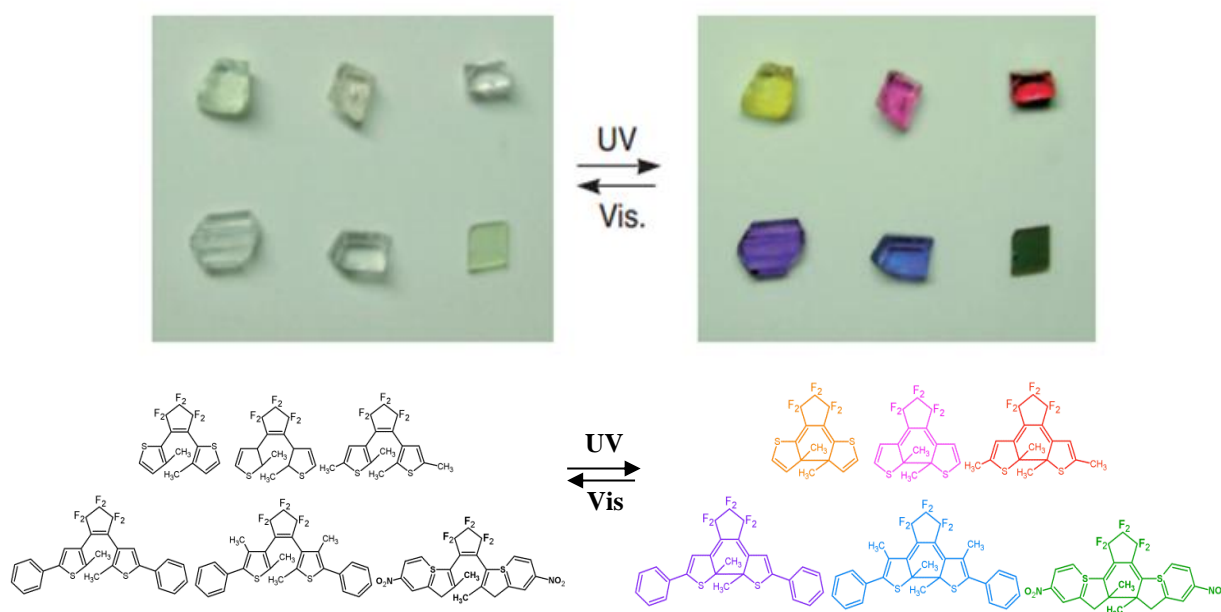


Figure 1.11 Variable colour changes associated with several diarylethene single crystals upon photoirradiation.⁷⁴

1.17 Cycloaddition

Cycloaddition reactions are pericyclic chemical reactions wherein two or more unsaturated molecules (or parts of the same molecule) combine with the formation of a cyclic adduct wherein there is a net reduction of the bond multiplicity.⁷⁵ These types of addition reactions enable carbon-carbon bond formation without the need of a nucleophile or electrophile. There are two types of cycloaddition reactions; thermal cycloaddition reactions involve the reactants being in the ground state and occur due to orbital overlap in a suprafacial-suprafacial or antarafacial-antarafacial manner.⁷⁴

Less common examples of thermal cycloadditions involve suprafacial-antarafacial pairing, an example of which is the [2 + 2] cycloaddition reaction. Photochemical cycloadditions (introduced by Schmidt⁷⁶ in the 1960's) involve the promotion of an electron from the HOMO (π bonding) to the LUMO (π^* anti-bonding) allowing the reaction to proceed via a suprafacial-suprafacial manner. Schmidt postulated that “*the reaction in the solid state occurs with a minimum atomic or molecular movement*”. This inevitably led to the introduction of specific geometric criteria required for such cycloaddition reactions whereby the olefinic bonds of the reacting molecules need to be aligned parallel to each other and separated by a distance of ≤ 4.2 Å.⁷⁵ The photochemical dimerization of cinnamic acid (Figure 1.12) is a well-known example of such a reaction and involves two *trans* alkenes reacting in a head-to-tail manner.⁷⁷

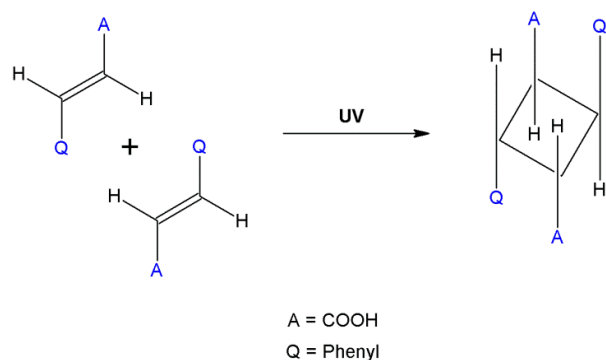


Figure 1.12 Photochemical dimerization of cinnamic acid.⁷⁵

MacGillivray *et al.*⁷⁸ have shown that supramolecular effects also play a profound role in directing cycloaddition by fine tuning hydrogen bond strength and directionality using “clip-like” templates such as resorcinol to help orient the double bonds in molecules such as bipyridyl ethene (bpe). This enables the C=C bonds to align parallel to one another with a distance of 3.65 Å between them. Such an arrangement conforms to the criteria set out by Schmidt for a [2 + 2] photoreaction in a solid.

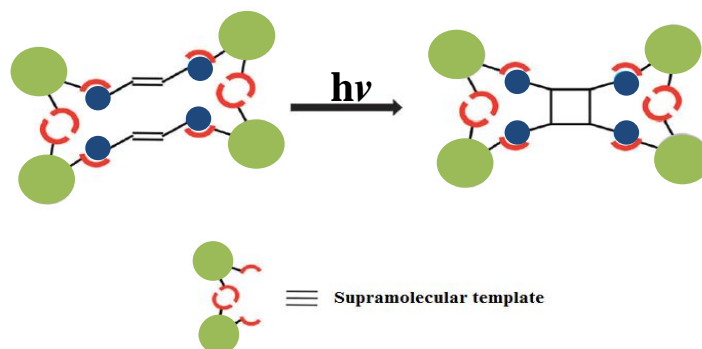


Figure 1.13 Template directed supramolecular [2 + 2] photocycloaddition.⁷⁷

Charge driven hydrogen bonds involving cations and anions, as well as cation- π interactions have also been used to align olefins for photoreaction.⁷⁹ In addition to hydrogen bonding, the presence of chloro-,⁸⁰ fluoro-,⁸¹ alkoxyaryl,⁸² as well as electron donor/acceptor⁸³ groups has promoted olefinic molecule alignment in crystals for [2 + 2] photodimerization. Metal ions can also direct photochemical [2 + 2] cycloadditions of olefins in the solid state by making use of their predictable and well-defined coordination numbers and geometries.⁸⁴ Discrete dinuclear complexes as well as MOFs formed from metallophilic interactions with bridging ligands provide intriguing platforms to control the photodimerization owing to bulk physical property changes that can occur in porous frameworks.⁸⁵

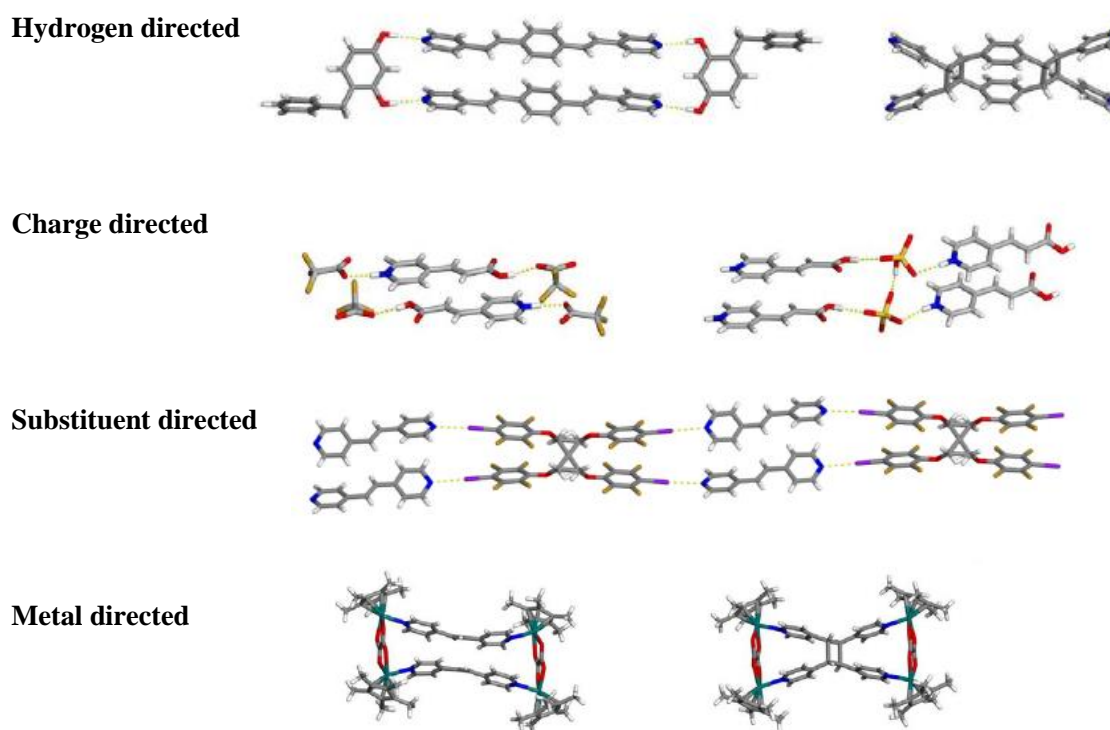


Figure 1.14 Types of supramolecular effects used to drive [2 + 2] addition reactions.⁷⁷⁻⁸³

1.18 Thesis outline

The objective of this work was to synthesise dynamic second and third generation MOFs and to study their liquid and vapour sequestration and storage capabilities using a variety of analytical techniques, including single crystal X-ray diffraction (SCD), thermogravimetric analysis (TGA), powder X-ray diffraction (PXRD) and sorption.

CHAPTER II describes the instrumentation and software used in this work.

CHAPTER III introduces the reader to a collection of four ditopic pillaring ligands (**L1-L4**) as well as the acids selected to act as secondary ligands. The novel frameworks assembled from these building blocks together with four divalent metal ion salts (zinc nitrate, cadmium nitrate, cobalt nitrate and magnesium nitrate) under solvothermal conditions are described in full. Sorption studies were carried out on frameworks that could be obtained with bulk phase purity.

CHAPTER IV describes the formation of a novel threefold interpenetrated zinc framework containing honeycomb channels. This material was formed from the solvothermal reaction of **L1** with **OBA** and zinc nitrate. It may be activated without loss of crystal singularity; thus a series of single-crystal to single-crystal guest exchange experiments were performed. The results of this work prompted subsequent gas chromatographic competition experiments and gas sorption experiments. An isostructural cobalt framework was then formed and treated in a similar manner in the hope of elucidating what, if any, effect a change in metal would elicit. An epitaxial crystal was also obtained.

CHAPTER V describes the effect that fluorination of ligand **L1** (**FL1**) has on framework formation, as well as the role that certain solvents play in initiating crank-handle-motion and cycloaddition in soft porous crystals.

CHAPTER VI acquaints the reader with two pyridyl-substituted diarylethene ligands (**DL1** and **DL2**). These known photochromic compounds were incorporated into a selection of frameworks and their response to light stimuli (visible and ultraviolet) is discussed.

CHAPTER VII provides a brief overview of the outcomes of this work, as well as suggestions for future work.

SUPPLEMENTARY INFORMATION

1.19 References

- 1 J. -M. Lehn, *Angew. Chem. Int. Ed.*, **1988**, 27, 89.
- 2 J. -M. Lehn, *Acc. Chem. Res.*, **1978**, 11, 49.
- 3 J. -M. Lehn, *Pure Appl. Chem.*, **1978**, 50, 871.
- 4 K. L. Wolf, H. Frahm, H. Harms, *Z. Physik. Chem.*, **1937**, B36, 237.
- 5 K. L. Wolf, H. Dunken, K. Merkel, *Z. Physik. Chem.*, **1940**, B46, 287.
- 6 K. L. Wolf, R. Wolff, *Angew. Chem.*, **1949**, 61, 191.
- 7 G. R. Desiraju, *Crystal Engineering, the Design of Organic Solids*, Elsevier: Amsterdam, **1989**.
- 8 J. L. Atwood, J. W. Steed, *Encyclopaedia of Supramolecular Chemistry*, **2004**; Vol. 2.
- 9 R. Pepinsky, *Phys. Rev.*, **1955**, 100, 971.
- 10 G. M. J. Schmidt, *Pure Appl. Chem.*, **1971**, 27, 647.
- 11 J. W. Steed, D. R. Turner, K. J. Wallace, *Core Concepts in Supramolecular Chemistry and Nanochemistry*, Wiley, **2007**.
- 12 A. Nangia, *J. Chem. Sci.*, **2010**, 122, 295.
- 13 L. Pauling, *J. Am. Chem. Soc.*, **1931**, 53, 1367.
- 14 E. Arunan¹, G. R. Desiraju, R. A. Klein, J. Sadlej, S. Scheiner, I. Alkorta, D. C. Clary, R. H. Crabtree, J. J. Dannenberg, P. Hobza, H. G. Kjaergaard, A. C. Legon, B. Mennucci, D. J. Nesbitt, *Pure Appl. Chem.*, **2011**, 83, 1637.
- 15 F. A. Cotton, G. Wilkinson, P. L. Gaus, *Basic Inorganic Chemistry*, John Wiley and Sons, **1995**.
- 16 G. R. Desiraju in *Comprehensive Supramolecular Chemistry*; J. L. Atwood, D. Davies, D. D. MacNicol, F. Vögtle, Eds.; Pergamon: Oxford, **1996**.
- 17 S. Kitagawa, R. Kitaura, S.-I. Noro, *Angew. Chem. Int. Ed.*, **2004**, 43, 2334.
- 18 S. Horike, S. Shimomura, S. Kitagawa, *Nat. Chem.*, **2009**, 1, 695
- 19 L. J. Murray, M. Dincă, J. R. Long, *Chem. Soc. Rev.*, **2009**, 38, 1294.
- 20 a) M. Eddaoudi, J. Kim, N. Rosi, D. Vodak, J. Wachter, M. O'Keefe, O. M. Yaghi, *Science*, **2002**, 295, 469.; b) O. M. Yaghi, M. O'Keefe, N. W. Ockwig, H. K. Chae, M. Eddaoudi, J. Kim, *Nature*, **2003**, 423, 705.; c) N. W. Ockwig, O. Delgado-Friedrichs, M. O'Keefe, O. M. Yaghi, *Acc. Chem. Res.*, **2005**, 38, 176.
- 21 A. U. Czaja, N. Trukhan, U. Muller, *Chem. Soc. Rev.*, **2009**, 38, 1284.

- 22 a) A. Dhakshinamoorthy, M. Alvaro, H. Garcia, *Chem. Eur. J.*, **2010**, *16*, 8530.; b) A. Dhakshinamoorthy, M. Alvaro, A. Corma, H. Garcia, *Dalton Trans.*, **2011**, *40*, 6344.
- 23 D. J. Cram, *Angew. Chem. Int. Ed.*, **1986**, *25*, 1039.
- 24 H. Davy, *Phil. Trans. R. Soc. Lond.*, **1811**, *101*, 155.
- 25 T. C. W. Mak, C. -K. Lam, *Encyclopaedia of Supramolecular Chemistry*, Eds. J. L. Atwood, J. W. Steed, Marcel Dekker, Inc., New York; Basel, **2004**, 679.
- 26 a) K. J. Harrington, *Sep. Sci. Technol.*, **1982**, *17*, 1443.; b) S. G. Frank, *J. Pharm. Sci.*, **1975**, *64*, 1585.
- 27 J. Szejtli, *Comprehensive Supramolecular Chemistry* Eds. J. L. Atwood, J. E. D. Davies, D. D. MacNichol, F. Vögtle, Pergamon, **1996**, 189.
- 28 B. H. Davis, K. S. W. Sing, *Handbook of Porous Solids, Vol. 2*, Wiley, Weinheim, **2002**.
- 29 a) R. M. Barrer, *J. Inclusion Phenom. Macrocyclic Chem.*, **1983**, *1*, 105.; b) T. Bein, *Inclusion Chemistry of Organometallics on Zeolites*, Pergamon, **1996**.
- 30 a) W. Morris, C. J. Doonan, H. Furukawa, R. Banerjee, O. M. Yaghi, *J. Am. Chem. Soc.*, **2008**, *130*, 12626.; b) R. Banerjee, A. Phan, B. Wang, C. Knobler, H. Furukawa, M. O'Keeffe, O. M. Yaghi, *Science*, **2008**, *319*, 939.; c) M. H. Alkordi, Y. Liu, R. W. Larsen, J. F. Eubank, M. Eddaoudi, *J. Am. Chem. Soc.*, **2008**, *130*, 12639.; d) J. E. D. Davies, *J. Incl. Phenom.*, **1998**, *32*, 499.
- 31 J. W. Steed, J. L. Atwood, *Supramolecular Chemistry*, John Wiley and Sons, Ltd, **2000**.
- 32 P. Ehrlich, *Studies on Immunity* Wiley; New York, **1906**.
- 33 E. Fischer, *Ber. Deutsch. Chem. Ges.*, **1894**, *27*, 2985.
- 34 A. Werner, *Zeitschr. Anorg. Chem.*, **1893**, *3*, 267.
- 35 E. P. Kyba, R. C. Helgeson, K. Madan, G. W. Gokel, T. L. Tarnowski, S. S. Moore, D. J. Cram, *J. Am. Chem. Soc.*, **1977**, *99*, 2564.
- 36 a) E. Hughes; J. Jordan; T. Gullion, *J. Phys. Chem. B.*, **2001**, *105*, 5887.; b) S. Erdemir, M. Bahadir; M. Yilmaz, *J. Hazard Mater.*, **2009**, *168*, 1170.
- 37 Y. Y. Cheng; J. R. Wang; T. L. Rao, X. X. He, T. W. Xu, *Front. Biosci-Landmrk.*, **2008**, *13*, 1447.
- 38 Q. K. Liu, J. P. Ma, Y. B. Dong, *J. Am. Chem. Soc.*, **2010**, *132*, 7005.
- 39 E. V. Anslyn, *J. Org. Chem.*, **2007**, *72*, 687.

- 40 S. Potts, *Inclusion Studies of Metal Organic Hosts*, PhD dissertation, Stellenbosch University, Stellenbosch, **2011**.
- 41 H. Reuter, *Angew. Chem. Int. Ed., Engl.*, **1992**, *31*, 1185.
- 42 A. Werner, *Zeitschr. Anorg. Chem.*, **1893**, *3*, 267.
- 43 H. van Bekkum, E. M. Flanigen, J. C. Jansen, *Introduction to zeolite science and practise*, Amsterdam, **1991**, 13.
- 44 J. W. McBain, *The Sorption of Gases by Solids*, Routledge, London, **1932**.
- 45 L. J. Barbour, *Chem. Commun.*, **2006**, 1163.
- 46 a) K. S. W. Sing, D. H. Everett, R. A. W. Haul, L. Moscou, R. A. Pierotti, J. Rouquerol, T. Siemieniewska, *Pure Appl. Chem.*, **1985**, *57*, 603.; b) J. Rouquerol, D. Avnir, C. W. Fairbridge, D. H. Everett, J. H. Haynes, N. Pernicone, J. D. F. Ramsay, K. S. W. Sing, K. K. Unger, *Pure Appl. Chem.*, **1994**, *66*, 1739.; c) A. Nangia, in *Encyclopedia of Supramolecular Chemistry*, ed. J. W. Steed and J. L. Atwood, **2004**, Marcel Dekker, Inc., Amsterdam, 967.
- 47 B. H. Davis, K. S. W. Sing, in *Handbook of Porous Solids, Vol. 1* (Eds; F. Schüth, K. S. W. Sing, J. Weitkamp), Wiley, Weinheim, **2002**, 3.
- 48 K. S. W. Sing, D. H. Everett, R. A. W. Haul, L. Moscou, R. A. Pierotti, J. Rouquerol, T. Siemieniewska, *Pure Appl. Chem.*, **1985**, *57*, 603.
- 49 a) K. S. W. Sing, S. J. Gregg, *Adsorption, Surface Area and Porosity*, **1984**, Academic Press, London.; b) S. Brunauer, L. S. Deming, W. S. Deming, E. Teller, *J. Am. Chem. Soc.*, **1940**, *62*, 1723.
- 50 K. S. W. Sing, D. H. Everett, R. A. W. Haul, L. Moscou, R. A. Pierotti, J. Rouquerol, T. Siemieniewska, *Pure Appl. Chem.*, **1985**, *57*, 603.
- 51 E. Mitscherlich, *Ann. Chim. Phys.*, **1822**, *19*, 350.
- 52 M. R. Caira, *Encyclopaedia of Supramolecular Chemistry*, Eds. J. L. Atwood, J. W. Steed, Marcel Dekker, Inc., New York; Basel, **2004**, 767.
- 53 L. J. Barbour, D. Das, T. Jacobs, G. O. Lloyd, V. J. Smith, in *Supramolecular Chemistry: From Molecules to Nanomaterials*. Eds. P. A. Gale, J. W. Steed, John Wiley and Sons, Ltd, United Kingdom, 1st Eds., **2012**, *6*, 2887.
- 54 A. H. Cottrell, *An Introduction to Metallurgy*. Institute of Materials, **1967**.
- 55 W. D. Callister Jr., *Materials Science and Engineering: An Introduction* (7th ed.). John Wiley and Sons. **2006**.
- 56 E. Wasserman, *J. Am. Chem. Soc.*, **1960**, *82*, 4433.

- 57 J. W. Steed, D. R. Turner, K. J. Wallace, *Core Concepts in Supramolecular Chemistry and Nanochemistry*, Wiley, **2007**.
- 58 E. R. T. Tiekink, J. J. Vittal, *Frontiers in Crystal Engineering*, Wiley, **2006**.
Department of Chemistry, University of Texas at San Antonio.
- 59 T. Hosokawa, S. Datta, A. R. Sheth, N. R. Brooks, V. G. Young, D. J. W. Grant, *Cryst. Growth Des.*, **2004**, *4*, 1195.
- 60 L. J. Barbour, *Aust. J. Chem.*, **2006**, *59*, 595.
- 61 T. Jacobs, *Self-assembly of new porous materials*, PhD dissertation, Stellenbosch University, Stellenbosch, **2009**.
- 62 <http://www.nordskip.com/iolite.html> accessed 14.08.2014
- 63 N. K. Nath, M. K. Panda, S. C. Sahoo, P. Naumov, *CrystEngComm.*, **2014**, *16*, 1850.
- 64 J. Fritzsche. *Comptes Rendus Acad. Sci.*, Paris, **1867**, *69*, 1035 .
- 65 G. H. Dorion, A. F. Wiebe, *Photochromism*, Focal Press, New York, **1970**.
- 66 G. H. Brown, *Photochromism*, Wiley, New York, **1971**.
- 67 H. Dürr, H. Bouas-Laurent, *Photochromism: Molecules and Systems*, Eds Elsevier, Amsterdam, **1990**.
68. J. C. Crano, R. Guglielmetti, *Organic Photochromic and Thermochromic Compounds*, Plenum Press, New York, **1999**.
- 69 a) C. B. McArdle, Blackie, *Applied Photochromic Polymer Systems*, ed. Glasgow, **1992**; b) M. Irie, *Photo-Reactive Materials for Ultrahigh Density Optical Memory*, Elsevier, Amsterdam, **1994**.
- 70 M. Irie, *Chem. Rev.*, **2000**, *100*, *5*, 1683.
- 71 a) J. Saltiel, J. D'Agostino, E. D. Megarity, J. Metts, K. R. Neuberger, M. Wrighton, O. Zafirov, *Org. Photochem.*, **1973**, *3*, *1*.; b) K. A. Muszkat, E. J. Fischer, *J. Chem. Soc.*, **1967**, 662.; c) K. A. Muszkat, *Top. Curr. Chem.*, **1980**, *88*, 89.
- 72 K. Uchida, S. Nakamura, M. Irie, *M. Res. Chem. Intermed.*, **1995**, *21*, 861.
- 73 R. M. Kellogg, M. B. Groen, H. J. Wynberg, *Org. Chem.*, **1967**, *32*, 3093.
- 74 S. Takami, L. Kuroki, M. Irie, *J. Am. Chem. Soc.*, **2007**, *129*, 7319.
- 75 International Union of Pure and Applied Chemistry (IUPAC). "Cycloaddition". Retrieved 15 July 2015.
- 76 (a) M. D. Cohen, G. M. J. Schmidt, *J. Chem. Soc.*, **1964**, 2000.; b) G. M. J. Schmidt, *Pure Appl. Chem.*, **1971**, *27*, 647.
- 77 S. M. Hein, Sara M. *Journal of Chemical*, **2006**, *83*, 940

- 78 a) L. R. MacGillivray, J. L. Atwood, *J. Am. Chem. Soc.*, **1997**, *119*, 6931.; b) L. R. MacGillivray, J. L. Reid, J. A. Ripmeester, *J. Am. Chem. Soc.*, **2000**, *122*, 7817.
- 79 a) J. Hu, L. J. Barbour, G. W. Gokel, *New J. Chem.* **2004**, *28*, 907.; b) G. W. Gokel, *Chem. Commun.* **2003**, *23*, 3251.
- 80 J. A. R. P. Sarma, G. R. Desiraju, G. R. *J. Chem. Soc., Chem. Commun.* **1984**, 145.
- 81 K. Vishnumurthy, T. N. G. Row, K. Venkatesan, *J. Chem. Soc., Perkin Trans. 2*, **1997**, 615.
- 82 G. R. Desiraju, R. Kamala, B. H. Kumari, J. A. R. P. Sarma, *J. Chem. Soc., Perkin Trans. 2*, **1984**, 181.
- 83 C. V. K. Sharma, K. Panneerselvam, L. Shimoni, H. Katz, H. L. Carrell, G. R. Desiraju, *Chem. Mater.* **1994**, *6*, 1282.
- 84 I. G. Georgiev, L. R. MacGillivray, *Chem. Soc. Rev.*, **2007**, *36*, 1239.
- 85 D.-K. Bučar, G. S. Papaefstathiou, T. D. Hamilton, Q. Chu, I. G. Georgiev, L. R. MacGillivray, *Eur. J. Inorg. Chem.*, **2007**, *29*, 4559.

Experimental Techniques

This chapter describes the analytical instrumentation as well as the software packages used during the course of this study. Common instrumental techniques and routine methodology are discussed briefly, while those adapted specifically for this work are elaborated upon further.

2.1 Solution NMR

Proton NMR spectra of all seven ligands used throughout this work were recorded on a Bruker Avance III 400 spectrometer operating at a frequency of 400 MHz. A 5 mm BBFO-Z probe was used. All experiments were carried out at 30 °C with all chemical shifts reported in units of ppm.

2.2 Single Crystal X-ray Diffraction (SCD)

Crystals of suitable size and with the appropriate morphology, transparency and ability to extinguish plane-polarised light were glued onto a fibre, where necessary, using epoxy or attached to the tip of a MiTeGen mount¹ using Paratone®N oil. X-ray intensity data were recorded on a Bruker SMART-APEX II or Bruker APEX II DUO diffractometer. The SMART instrument is equipped with a molybdenum fine-focus sealed tube, a 0.5 mm Monocap collimator and an APEX II detector. The DUO instrument is equipped with Incoatec I μ S molybdenum and copper microfocus X-ray sources and an APEX II detector. Both diffractometers are fitted with an Oxford Cryosystems cryostat (700 Series Cryostream Plus), which is used to control the sample temperature. Data reduction and absorption corrections were carried out using the SAINT² and SADABS³ programs, respectively. The unit cell dimensions were refined on all data and space groups were assigned based on systematic absences and intensity statistics. The structures were solved by direct methods or a combination of Patterson and partial structure expansion using SHELXS-97⁴ and refined with SHELXL-97³ using the X-Seed⁵ graphical user interface. Non-hydrogen atoms were refined anisotropically. Hydrogen atoms were placed in calculated positions. Illustrations of all crystal structures were generated using the program POV-Ray.⁶

2.3 Powder X-ray Diffraction (PXRD)

A PANalytical XPERT-PRO diffractometer was used to record experimental patterns. The diffractometer utilises Bragg-Brentano geometry and Cu K α radiation ($\lambda = 1.5418 \text{ \AA}$) as the incident beam. Intensity data were recorded using a flat stage or capillary spinner. In the case of the flat stage, samples were finely ground using a mortar and pestle, loaded onto a zero-background sample holder and levelled with a glass slide. The samples were scanned between 5° and 40° with a scan step size of 0.017° and a varying scan speed, which was dependent on the nature of the sample.

2.4 Energy-dispersive X-ray Spectroscopy (EDX)

Backscattering electron energy disperse spectroscopy (BSE-EDS) analysis was accomplished using a Zeiss EVO® MA15 Scanning Electron Microscope. Prior to analysis the samples were coated with a thin layer of gold in order to provide electrical conductivity. The analyses in area mode were carried out using a backscattered electron detector. The phase compositions of the samples were quantified by energy-dispersive spectrometry using an Oxford Instruments® X-Max 20 mm² detector and Oxford INCA software. Beam conditions during the qualitative analysis were 20 kV, with a working distance of 8.5 mm and a beam current of approximately -20 nA. The counting time was 10 seconds live-time. The elemental data (in weight %) were normalised to 100%.

2.5 Thermogravimetric Analysis (TGA)

A TGA trace was generated by measuring the percentage mass as the sample was heated at a constant rate. A TA Instruments Q500 thermogravimetric analyser was used and sample weights typically ranged from 2-10 mg. N₂ gas flowing at a rate of 50 ml min⁻¹ was used to purge the furnace. The temperature was ramped from room temperature to $\sim 600^\circ\text{C}$ at a constant heating rate of $10^\circ\text{C min}^{-1}$. The resulting thermograms were analysed using the TA Instruments Universal Analysis program.

2.6 Gravimetric Sorption

Gravimetric gas sorption experiments were carried out on an Intelligent Gravimetric Analyser (IGA) supplied by Hiden Isochema, Warrington, UK.⁷ The instrument (**Figure 2.1**) facilitates precise measurement of mass change and control of pressure and temperature, and is equipped with an enhanced pressure rating that allows measurements up to 20 bar, with buoyancy effects being corrected automatically. The temperature of the experiment was controlled by a refrigerated recirculation bath maintained at 25 °C. Every experiment utilises ultra-high purity gases and outgassing occurs upon loading a new sample and between changing gas cylinders. The data were monitored by real time software that continually analyses the pressure and weight equilibrium using least-squares regression to extrapolate the value of the asymptote.^{8,9,10,11,12,13} A Linear Driving Force (LDF) relaxation model was used, with each point recorded once 95% fit with the model was achieved, or the time-out was reached (set to 120 minutes). The data were exported as values of mmol per gram of host, which can easily be converted to number of guest molecules per asymmetric unit of host.



Figure 2.1 Photograph of the Intelligent Gravimetric Analyser (IGA-002) and gas cylinders.

2.7 Gas Chromatography coupled to a Mass Spectrometer (GCMS)

Gas chromatographic analysis of *ortho*, *meta* and *para*-xylene was carried out using a Hewlett Packard 5890 Series II GC (Agilent, Little Falls, Wilmington, USA) equipped with a HP INNOWAX capillary GC column with dimensions 30 m length \times 0.25 mm i.d. \times 0.5 μ m film thickness (f.t.) (Agilent). Injection (1 μ L) was performed in split mode (1:20 ratio) at 240 °C and a Flame Ionisation Detector (FID) was used at 240 °C with hydrogen flow of 35 ml min⁻¹ and air of 350 ml min⁻¹. The carrier gas was helium with a flow rate of 1 ml min⁻¹. The initial oven temperature was 30 °C for one minute, after which the temperature was increased by 5 °C min⁻¹ to 80 °C and thereafter 10 °C min⁻¹ to 240 °C at which it was held constant for five minutes. Under these conditions *ortho*, *meta* and *para*-xylene eluted at 11.36, 11.55 and 12.77 minutes, respectively.

2.8 Infra-Red Absorption Measurements

IR absorption spectra were measured using a Nexus Thermo-Nicolet FT-IR instrument with an ATR attachment.

2.9 Irradiation Experiments

Photochromic samples were converted between the open and closed forms using high intensity lasers or photodiodes. The ultraviolet photodiode has a wavelength 365 nm and that of the green laser (used in place of white light, as the laser provided a high intensity) is 532 nm. In order to perform continuous irradiation experiments while recording diffraction data, it was necessary to design a suitable location to house the photodiode that would provide sufficient intensity without impeding detector motion. After numerous attempts of various design scenarios, it was determined that the best location for the source would be directly under the crystostream. The problem with such a configuration is that irradiation and cooling cannot occur simultaneously as one runs the risk of cracking the glass window located in the photodiode. As a result, continuous irradiation experiments were performed at room temperature. A photograph of this setup is located in Chapter VI on page 151.

2.10 Solid-State UV-visible Spectroscopy

Solid-state UV/visible absorption spectra were recorded for all photochromic materials using an Analytik Jena SPECORD 210 PLUS spectrophotometer. All measurements were performed in an environment thermostated within ± 0.1 °C. All data were graphically analysed using the software package WinAspect PLUS 3.9.14.

2.11 Computer Packages

A number of computer software packages were used during the course of this study. These are briefly discussed below.

2.11.1 The Cambridge Structural Database (CSD)

The CSD¹⁴ is a virtual repository containing single crystal and powder structural data for compounds that have been determined by X-ray and neutron diffraction studies and deposited as published or unpublished results. The CSD is an invaluable tool for structural analysis.

2.11.2 Mercury

Mercury¹⁵⁻¹⁶ can be used for structure exploration and visualisation. Among its many useful features the program offers powder pattern simulation, overlaying of multiple structures, solvent-accessible void space calculation and visualisation as well as morphology calculations.

2.11.3 Graphical illustrations and guest accessible surfaces

High quality molecular graphics were obtained using the ray-tracing program POV-Ray, which can be accessed from within the X-Seed⁵ interface. Solvent-accessible voids can be visualised by calculating Connolly surfaces using MS-ROLL,¹⁷ another program incorporated into X-Seed. Based on the seminal work of Lee and Richards,¹⁸ the *accessible surface* is defined as the trace left by the probe sphere centre as it rolls through the structure of interest. The surface mapped by the exterior of the probe is designated the *contact surface*.

A typical mapping procedure involves deletion of the guest molecules from the atom list and selection of an appropriate probe radius. The output file name .cav is imported into X-Seed and the mapped surface can be incorporated into the final structure visualisation using POV-Ray. Images can be rendered with the guest molecules reinstated to show their location in these voids.

2.11.4 PLATON/SQUEEZE

PLATON¹⁹/SQUEEZE²⁰ is a program that calculates the number of electrons located within the solvent-accessible voids of a crystal structure. The program is also able to determine the volume of the solvent-accessible space. In order to obtain accurate results, high quality complete data with high and low-angle reflections are required.

2.12 References

- 1 <http://www.mitegen.com/> accessed 21.08.14
- 2 SMART Data Collection Software, Version 5.629; **2003**, WI, Bruker AXS Inc., Madison.
- 3 SADABS, Version 2.05; **2002**, WI, Bruker AXS Inc., Madison.
- 4 G. M. Sheldrick, *Acta Crystallogr. Sect. A: Found. Crystallogr.*, **2008**, *64*, 112.
- 5 L. J. Barbour, *J. Supramol. Chem.*, **2001**, *1*, 189.
- 6 POV-Ray™, Version 3.6. **2004** Williamstone, Persistence of Vision Raytracer Pty. Ltd.
- 7 D. K. Ross, M.J. Benham, *Z., Phys. Chem.*, **1989**, *163*, 25.
- 8 C.R. Reid, I. P. O'koye, K.M. Thomas, *Langmuir*, **1998**, *14*, 2415.
- 9 A.W. Harding, N. J. Foley, P.R. Norman, D.C. Francis, K.M. Thomas, *Langmuir*, **1998**, *14*, 3858.
- 10 I. P. O'Koye, M. Benham, K.M. Thomas, *Langmuir*, **1997**, *13*, 4054.
- 11 N.J. Foley, K. M. Thomas, P.L. Forshaw, D. Stanton, P.R. Norman, *Langmuir*, **1997**, *13*, 2083.
- 12 A. J. Fletcher, K. M. Thomas, *Langmuir*, **1999**, *15*, 6908.
- 13 A. J. Fletcher, K. M. Thomas, *Langmuir*, **2000**, *16*, 6253.
- 14 *Cambridge Structural Database and Cambridge Structural Database System, Version 3.55* (February **2015**), Cambridge Crystallographic Data Centre, University Chemical Laboratory, Cambridge, England.
- 15 C. F. Macrae, I. J. Bruno, J. A. Chisholm, P. R. Edgington, P. McCabe, E. Pidcock, L. Rodriguez-Monge, R. Taylor, J. van de Streek, P. A. Wood, *J. Appl. Cryst.*, **2008**, *41*, 466.
- 16 C. F. Macrae, P. R. Edgington, P. McCabe, E. Pidcock, G. P. Shields, R. Taylor, M. Towler, J. van de Streek, *J. Appl. Cryst.*, **2006**, *39*, 453.
- 17 (a) M. L. Connolly, *Science*, **1983**, *221*, 709.; (b) M. L. Connolly, *J. Mol. Graphics* **1993**, *11*, 139.
- 18 B. Lee and F. M. Richards, *J. Mol. Biol.*, **1971**, *55*, 379.
- 19 A. L. Spek, *Acta Crystallogr., Sect. D*, **2009**, *65*, 148.
- 20 P. Van Der Sluis, A. L. Spek, *Acta Crystallogr., Sect. A*, **1990**, *46*, 194.

STRUCTURAL ANALYSIS AND GAS SORPTION STUDIES

The work presented in this chapter focuses on the systematic synthesis of novel MOFs designed from a selection of carefully chosen components with the hope of engineering second- and third-generation materials possessing interesting properties. This chapter also serves as a general introduction to the direction of the experimental work undertaken for this dissertation, with the next three chapters describing more detailed analyses of specific materials. The enormity of the field of MOF crystal engineering is illustrated by the practically infinite number of combinations of organic bridging ligands and metals possessing different coordination geometries for the construction of framework materials. Since these choices affect the topology, pore size and physical properties of the MOFs formed, component selection is important. Although crystal engineering has not yet reached the point where one can reliably predict the outcome of a set of crystallisation components, work such as this is intended to widen the general knowledge such that guidelines may eventually be established that will enable target-directed MOF design. An assortment of MOFs were obtained in this study. However, not all were characterised in detail owing to lack of crystallinity or insufficient bulk phase purity.

3.1 Nature of Components

Four known symmetrical nitrogen donor ligands (**Figure 3.1**) were synthesised according to literature methods.^{1,2,3,4} These ligands were selected because of their high yielding synthetic procedures, variable length and variable degree of flexibility (two rigid* and two with rotatable carbon-carbon bonds*). It was believed that by selecting a ligand from each of the four categories (short-rigid, long-rigid, short-flexible and long-flexible), a variety of MOFs could be formed.

* One short and one long ligand.

CHAPTER III: STRUCTURAL ANALYSIS AND GAS SORPTION STUDIES

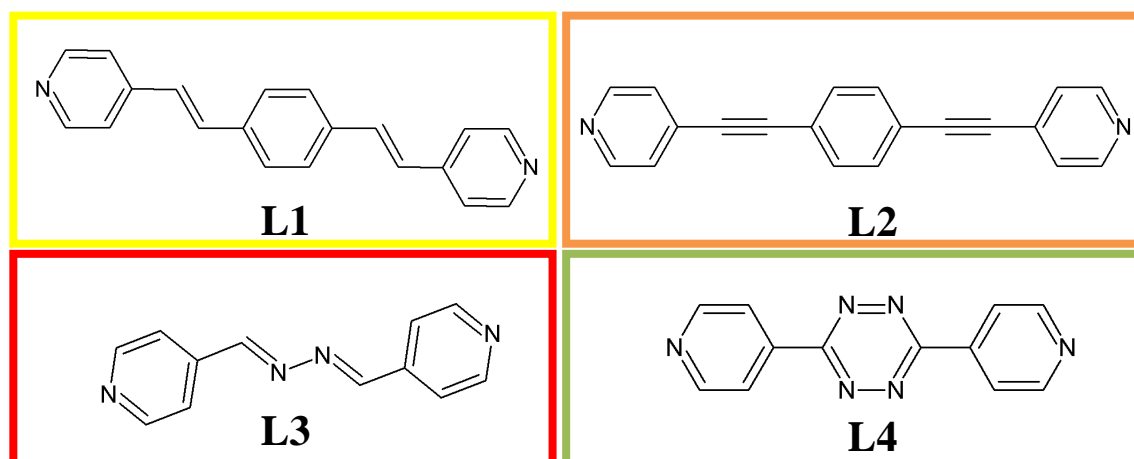


Figure 3.1 Pyridyl ligands used in this study: 1,4'-bis-(pyridyl-ethenyl) benzene (**L1**), 1,4'-bis-(pyridyl-ethyne)-benzene (**L2**), 1,4'-bis-(pyridyl-ethenyl)-hydrazine (**L3**) and 1,4'-bis-(pyridyl)-tetrazine (**L4**). *

Although the literature already contains some examples of coordination compounds with the selected ligands, this area was developed further by the incorporation of a second, ligand to provide structural support and enable the formation of interesting 3D structures. Several commercially available carboxylic acids, namely 4,4'-oxybisbenzoic acid (**OBA**), 4,4'-azodibenzoic acid (**ADB**), 2,5-pyridine dicarboxylic acid (**PDC**) and the asymmetric hybrid 4-[2-(4-pyridyl)ethenyl]benzoic acid (**PYEB**) (**Figure 3.2**) were selected for this study. The incorporation of carboxylic acids ensures formation of neutral frameworks devoid of cumbersome counter ions that could potentially block pores. The two types of ligands were crystallised with a variety of nitrate salts ($M = \text{Zn, Cd, Co}$ and Mn) with a view to obtaining third generation porous coordination polymers.

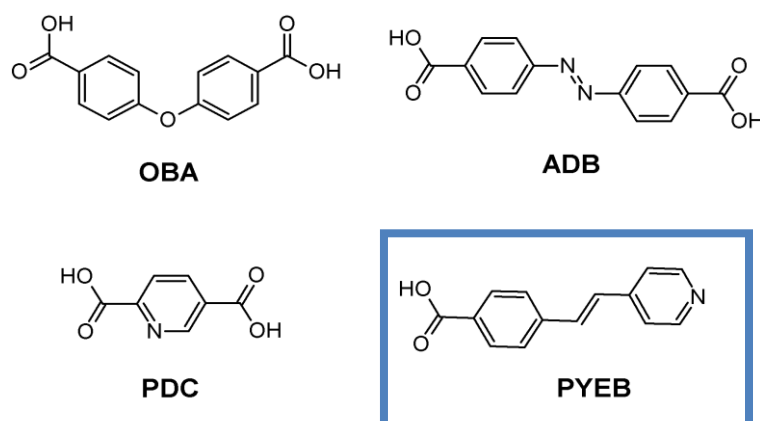


Figure 3.2 Commercially available carboxylic acids employed in this study.

* Experimental procedures and NMR data for synthesised ligands are provided in the supplementary information. Coloured boxes correspond to the information presented in **Table 3.1**.

CHAPTER III: STRUCTURAL ANALYSIS AND GAS SORPTION STUDIES

3.2 Solvothermal Crystallisations

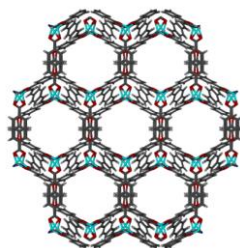
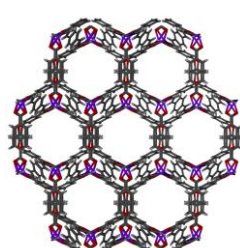
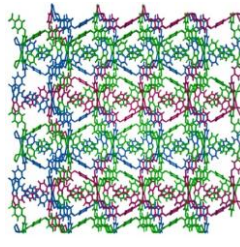
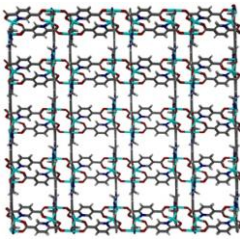
Solvothermal crystallisation is a common technique used in MOF formation and involves the total or partial dissolution of a ligand and a metal salt in a single or a binary solvent mixture. The solution is then sealed inside a Teflon-lined steel autoclave and heated in an oven. MOFs may be constructed by varying ligand components, or by using one set of components but varying factors such as concentration, molar ratios of the components, solvent nature, pH, crystallisation temperature, cooling rate and reaction duration, all of which can produce very different assemblies and thus different products. Optimal conditions (various combinations of the aforementioned parameters were attempted) related to framework formation in this study involved dissolution of the pyridyl ligand (0.03 mmol), the carboxylate ligand (0.05 mmol) and the metal salt (0.05 mmol) in a 5 mL solution of DMF, DMA, EtOH, DMSO or a combination thereof. Three different temperature programs were utilised. In the first two, sintered glass vials were placed in an oven preheated to either 80 or 100 °C and left for 24 hours, after which they were allowed to cool to ambient temperature before opening. In the third instance, the autoclave temperature was ramped from ambient to 120 °C over a 15 minute period, kept isothermal for 24 hours and then slowly cooled to ambient temperature over 12 hours. Owing to the teflon insert and steel autoclave, the crystallisation process cannot be observed and it is thus difficult to conclusively determine whether MOF crystallisation occurs as a result of slow cooling or because of the high-pressure-high-temperature environment established.

3.3 Resultant MOFs

During this work, several hundred crystallisation experiments were carried out. Those performed using slow evaporation, diffusion crystallisation or solvothermal crystallisation with methanol or water resulted in no crystalline products while solvothermal crystallisations involving DMF, DMA, EtOH, DMSO or a combination thereof yielded 61 novel materials. This chapter will focus on 21 of these frameworks. The crystallographic information supplied in **Table 3.1** provides a brief description and summary of the frameworks with ligands **L1-L4** and **PYEB** that are described in this chapter (the left-hand column of **Table 3.1** is coloured according to the ligand used). Selected frameworks exhibiting interesting phenomena are discussed in detail further along in the chapter.

CHAPTER III: STRUCTURAL ANALYSIS AND GAS SORPTION STUDIES

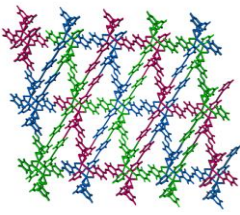
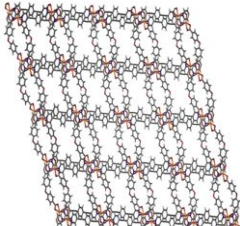
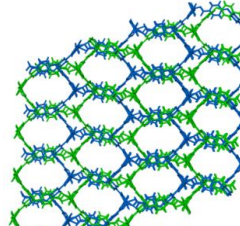
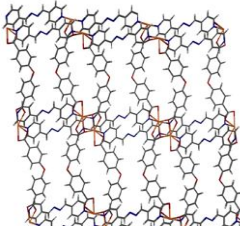
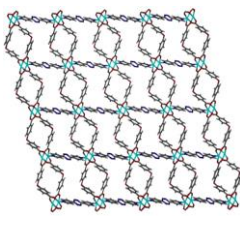
Table 3.1 Overview of the MOFs obtained with ligands **L1-L4** (guest deleted from the figures to illustrate pores).*

Name	Crystallisation conditions	Crystallographic data	Systematic name and description	Packing diagram	Additional studies [†]
HC1	L1 OBA Zn(NO ₃) ₂ ·6H ₂ O in DMF, 100 °C	<i>C2/c</i> $a = 15.078(6) \text{ \AA}$ $b = 24.074(3) \text{ \AA}$ $c = 15.823(3) \text{ \AA}$ $\beta = 110.83(1)^\circ$ $V = 5368.3(2) \text{ \AA}^3$	$\{[\text{Zn}(\text{L1})_{0.5}\text{OBA}]\cdot\text{DMF}\}_n$ 3D threefold interpenetrated framework with honeycomb channels viewed along [0 1 0] containing DMF guest molecules.	 [1 0 1]	Detailed discussion presented in Chapter IV
HC2	L1 OBA Co(NO ₃) ₂ ·6H ₂ O in DMA_DMSO, 120 °C	<i>C2/c</i> $a = 15.010(9) \text{ \AA}$ $b = 24.101(4) \text{ \AA}$ $c = 44.318(7) \text{ \AA}$ $\beta = 94.46(7)^\circ$ $V = 15985.0(8) \text{ \AA}^3$	$\{[\text{Co}_3(\text{L1})_{1.5}\text{OBA}_3]\cdot\text{DMA}\}_n$ 3D threefold interpenetrated framework with honeycomb channels viewed along [0 1 0] containing DMA guest molecules.	 [1 0 1]	Detailed discussion presented in Chapter IV
CP1	L1 OBA Co(NO ₃) ₂ ·6H ₂ O in DMF-DMSO 120 °C	<i>P2₁/n</i> $a = 13.737(2) \text{ \AA}$ $b = 24.621(3) \text{ \AA}$ $c = 16.218(5) \text{ \AA}$ $\beta = 113.48(3)^\circ$ $V = 5031.2(2) \text{ \AA}^3$	$\{[\text{Co}_2(\text{L1})(\text{OBA})_2]\cdot 2\text{DMF}\cdot\text{H}_2\text{O}\}$ 3D threefold interpenetrated framework with discrete voids viewed along [0 0 1] containing DMF-DMSO and water molecules. The L1 ligand is disordered.	 [0 0 1]	TGA revealed guest loss at 175 °C with framework decomposition setting in at 400 °C. Crystal quality is not maintained post guest removal.
CP2	L1 PDC Zn(NO ₃) ₂ ·6H ₂ O in DMF 100 °C	<i>P2₁/n</i> $a = 13.985(0) \text{ \AA}$ $b = 12.144(1) \text{ \AA}$ $c = 14.660(5) \text{ \AA}$ $\beta = 105.89(5)^\circ$ $V = 2394.6(7) \text{ \AA}^3$	$\{[\text{Zn}_2(\text{PDC})_2(\text{DMF})_2]\cdot 2\text{DMF}\}$ 3D non-interpenetrated net composed solely of PDC ligands with two types of rectangular DMF solvent filled channels along [0 1 0].	 [0 1 0]	TGA revealed guest loss at 175 °C with framework decomposition setting in at 400 °C. SC-SC guest exchange study performed

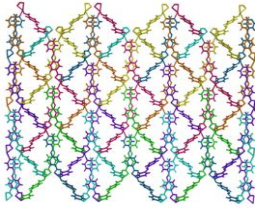
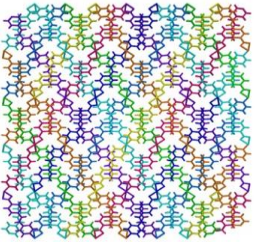
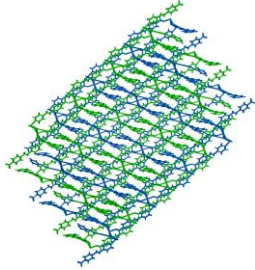
* Colour denotes degree of interpenetration, with non-interpenetrated structures remaining CPK coloured.

[†] Additional data such as TGA and phase-purity PXRD may be found in the supplementary information.

CHAPTER III: STRUCTURAL ANALYSIS AND GAS SORPTION STUDIES

CP3	L2 ADB Cd(NO ₃) ₂ ·4H ₂ O in DMF 100 °C	$P\bar{1}$ $a = 12.281(6) \text{ \AA}$ $b = 13.356(4) \text{ \AA}$ $c = 13.852(5) \text{ \AA}$ $\alpha = 78.08(3)^\circ$ $\beta = 77.17(5)^\circ$ $\gamma = 76.53(5)^\circ$ $V = 2125.8(4) \text{ \AA}^3$	$\{[\text{Cd}(\text{L}2)(\text{ADB})] \cdot 3\text{DMF}\}$ 3D threefold interpenetrated framework with corrugated channels along [1 0 0].	 [1 0 0]	TGA shows that desolvation of the DMF guest is complete at 180 °C, and decomposition begins at 275 °C. Crystal quality is not maintained post guest removal. Sorption study was performed
CP4	L2 OBA Cd(NO ₃) ₂ ·4H ₂ O in DMF-DMSO 100 °C	$C2/c$ $a = 32.436(6) \text{ \AA}$ $b = 8.982(3) \text{ \AA}$ $c = 30.100(3) \text{ \AA}$ $\beta = 109.70(5)^\circ$ $V = 8256.3(3) \text{ \AA}^3$	$\{[\text{Cd}(\text{L}2)(\text{OBA})] \cdot 2\text{DMF}\}$ 3D non-interpenetrated framework with nets superimposed upon one another. Channels viewed along [0 1 0].	 [0 1 0]	TGA revealed guest loss at 175 °C with framework decomposition setting in at 330 °C. Crystal quality is not maintained post guest removal
CP5	L3 OBA Zn(NO ₃) ₂ ·6H ₂ O in DMF 120 °C	$P2_1/n$ $a = 12.257(3) \text{ \AA}$ $b = 26.651(7) \text{ \AA}$ $c = 15.530(1) \text{ \AA}$ $\beta = 96.37(5)^\circ$ $V = 5041.97 \text{ \AA}^3$	$\{[\text{Zn}_2(\text{L}3)(\text{OBA})_2] \cdot 3\text{DMF}\}$ 3D twofold interpenetrated nets that form elongated “honeycomb” channels along [1 0 1] that house DMF guest molecules.	 [1 0 1]	TGA shows that desolvation of the DMF guest is complete at 150 °C, and decomposition begins at 320 °C. SC-SC guest exchange study performed Sorption study was performed
CP5a	L3 OBA Cd(NO ₃) ₂ ·4H ₂ O in DMA-DMSO 100 °C	$P2_1/c$ $a = 12.236(1) \text{ \AA}$ $b = 10.034(8) \text{ \AA}$ $c = 29.669(5) \text{ \AA}$ $\beta = 100.64(5)^\circ$ $V = 3580.33 \text{ \AA}^3$	$\{[\text{Cd}(\text{L}3)\text{OBA}] \cdot 2\text{DMA} \cdot \text{H}_2\text{O}\}_n$ 3D non-interpenetrated net with DMA and water guest molecules present in the channels.	 [0 1 0]	TGA shows that desolvation of the guests is complete at 120 °C, and decomposition begins at 280 °C. Crystal quality is not maintained post guest removal
CP6	L4 OBA Zn(NO ₃) ₂ ·6H ₂ O in DMF-EtOH 80 °C	$C2/c$ $a = 27.760(7) \text{ \AA}$ $b = 7.530(1) \text{ \AA}$ $c = 23.781(8) \text{ \AA}$ $\beta = 105.51(4)^\circ$ $V = 4790.2(4) \text{ \AA}^3$	$\{[\text{Zn}(\text{L}4)_{0.5}(\text{OBA})] \cdot \text{DMF} \cdot \text{EtOH}\}$ 2D non-interpenetrated net with hourglass-shaped solvent-containing channels running along [0 1 0].	 [0 1 0]	TGA shows that desolvation of the DMF guest is complete at 150 °C, and decomposition sets in at 275 °C. Xylene-induced transformation

CHAPTER III: STRUCTURAL ANALYSIS AND GAS SORPTION STUDIES

CP7	PYEB Zn(NO ₃) ₂ ·6H ₂ O in DMF-EtOH 80 °C	<i>Cc</i> $a = 13.344(1) \text{ \AA}$ $b = 25.702(1) \text{ \AA}$ $c = 8.411(0) \text{ \AA}$ $\beta = 97.73(5)^\circ$ $V = 2843.21 \text{ \AA}^3$	{[Zn(PYEB)₂]-DMF} 3D sevenfold interpenetrated nets that form triangular channels along [0 0 1] with DMF molecules located in the channel.	 [0 0 1]	TGA revealed guest loss at 200 °C with framework decomposition setting in at 420 °C. Crystal quality is not maintained post guest removal
CP7a	PYEB Co(NO ₃) ₂ ·6H ₂ O in DMF-EtOH 80 °C	<i>Aba2</i> $a = 13.008(1) \text{ \AA}$ $b = 21.879(4) \text{ \AA}$ $c = 8.674(9) \text{ \AA}$ $V = 2468.9(6) \text{ \AA}^3$	{[Co(PYEB)]} Non-porous 3D eightfold interpenetrated MOF.	 [0 0 1]	TGA revealed no guest loss with framework decomposition setting in at 420 °C.
CP7b	PYEB Mn(NO ₃) ₂ ·4H ₂ O in DMF-EtOH 80 °C	<i>P2₁/c</i> $a = 13.453(9) \text{ \AA}$ $b = 18.746(9) \text{ \AA}$ $c = 15.938(5) \text{ \AA}$ $\beta = 101.76(8)^\circ$ $V = 3930.23 \text{ \AA}^3$	{[Mn₃(PYEB)₆]-DMF-EtOH}_n 3D twofold interpenetrated nets with small corrugated channels viewed along [0 1 0].	 [0 0 1]	TGA revealed guest loss at 200 °C with framework decomposition setting in at 410 °C. SC-SC activation

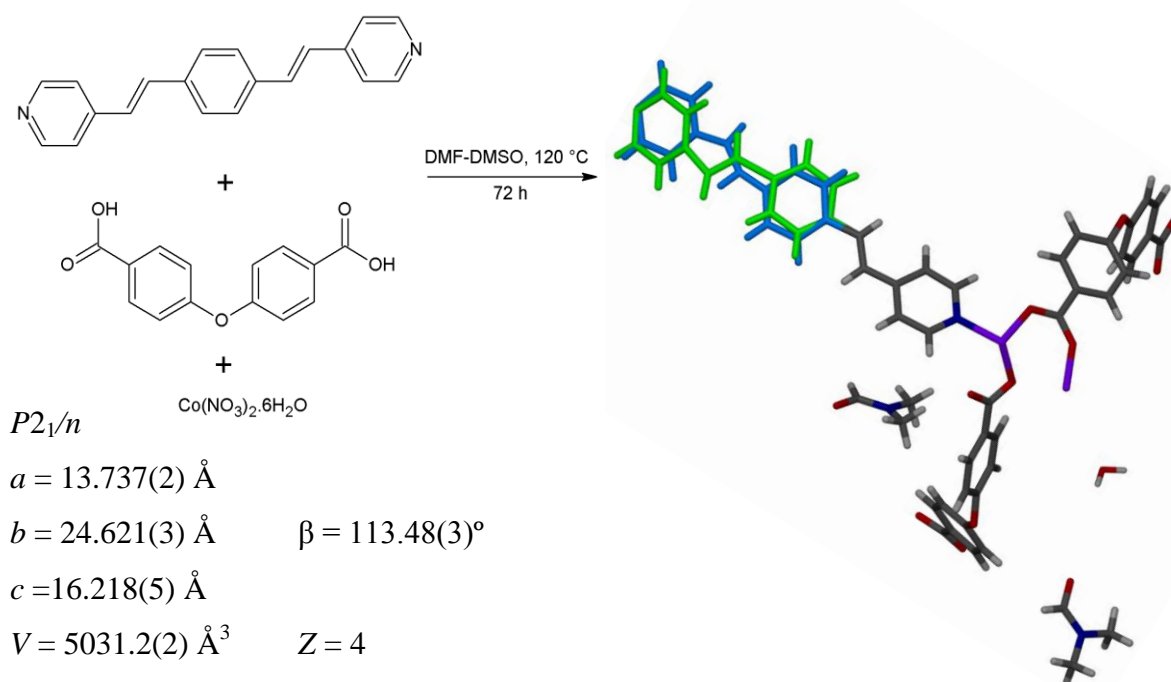
3.3.1 **{[Zn(L1)_{0.5}OBA]-DMF}_n and {[Co₃(L1)_{1.5}OBA₃]-DMA}_n**

The zinc MOF, **HC1** (Honeycomb 1) was the first material to be synthesised during the course of this study. However, due to the versatility of this material and the various interesting properties it was found to possess, **HC1** and its cobalt analogue **HC2** have been assigned a separate chapter (Chapter 4) wherein they are discussed in full. Inclusion of these materials in this chapter serves merely to aid the reader in understanding the approach taken in this work.

CHAPTER III: STRUCTURAL ANALYSIS AND GAS SORPTION STUDIES

3.3.2 $\{[Co_2(L1)OBA_2] \cdot 2DMF \cdot H_2O\}_n$ or CP1

CP1 crystallises in the monoclinic space group $P2_1/n$. Despite the presence of DMSO during crystallisation, no DMSO was found in the structure. The asymmetric unit of **CP1** contains two cobalt cations, one **L1** ligand (a portion of which is disordered over two positions), two **OBA** ligands, two DMF molecules and one water molecule (**Scheme 3.1**). Both cobalt ions have a highly distorted square pyramidal environment comprised of four oxygen atoms from two **OBA** ligands and one nitrogen atom from the **L1** ligand situated in the axial position (**Figure 3.3**). Although the two metal ions have the same coordination mode, the di-coordinated acid chelating Co1 is twisted inward by 18° when compared with the di-coordinated acid chelating Co2. The conformation of the ligand **L1** in **CP1** is interesting because it appears that a portion of the ligand is disordered between the *anti*- (blue) and the *syn*-conformations (green).*



Scheme 3.1 Synthesis of **CP1** from the solvothermal reaction of **L1**, **OBA** and cobalt(II) nitrate in a DMF-DMSO mixture at 120°C , with selected crystallographic information.

* Ligands such as **L1** have been shown to undergo ‘crank-handle’ motion wherein the two-pyridyl rings of the molecule move simultaneously in opposite directions like independent crank-handles; enabling conformational change from the *anti* to the *syn* conformer, (**Chapter V** discusses this phenomenon in greater detail). It must however be noted that in order to determine whether the disorder in **CP1** is in fact dynamic or merely an average of two molecular orientations, one would have to do variable temperature SC-SC collections. If the ratio of the two forms was seen to alter with temperature then the structure would be deemed dynamic. Future work would involve such analysis.

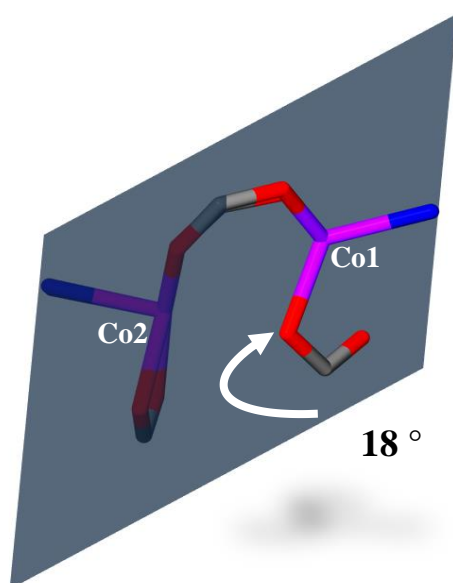


Figure 3.3 CP1 distorted half paddlewheel (each metal has the same coordination mode).

A consequence of molecular and packing symmetry is the formation of this highly unusual distorted “half paddlewheel” SBU. Of the four-carboxylate oxygen atoms, two are chelating a single metal centre while the other two are bridging two metal centres (**Figure 3.4**). This unusual SBU formation is attributed to the reduction of the steric hindrance by the angular **OBA** ligand. In **CP1** the angles between the *para*-position carbon atoms connecting the two phenyl rings is $116.2(6)^\circ$ and $118.0(6)^\circ$. This bending of the **OBA** ligand causes steric crowding, which is responsible for the type of SBU formed.

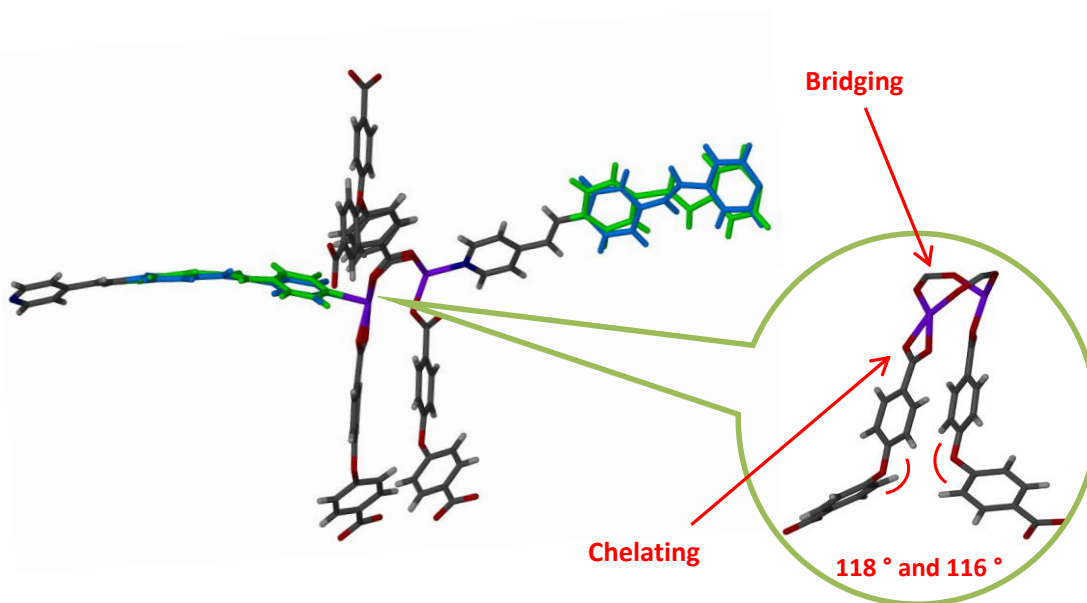


Figure 3.4 Half paddlewheel of **CP1** showing bent **OBA** ligands.

CHAPTER III: STRUCTURAL ANALYSIS AND GAS SORPTION STUDIES

The framework in **CP1** is threefold interpenetrated. An investigation of a single net reveals large ‘honeycomb’ channels that are already partially filled by the bent **OBA** ligands (**Figure 3.5a**). Two further nets are present, filling this space and stabilising the overall structure. In spite of significant interpenetration, the structure contains a herringbone arrangement of discrete pockets, which are occupied by ordered dimethylformamide molecules (**Figure 3.5b**) (four DMF molecules per void)

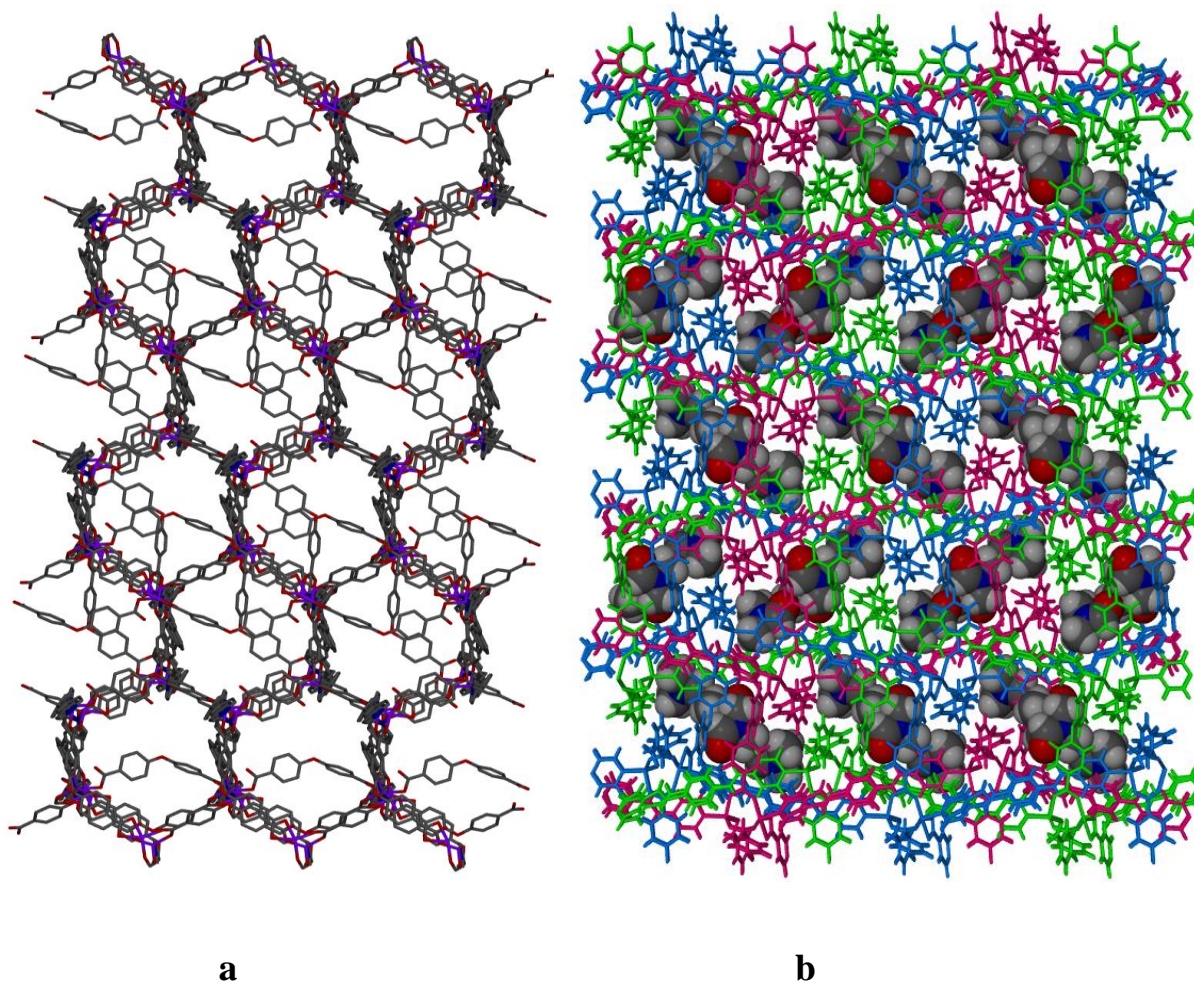


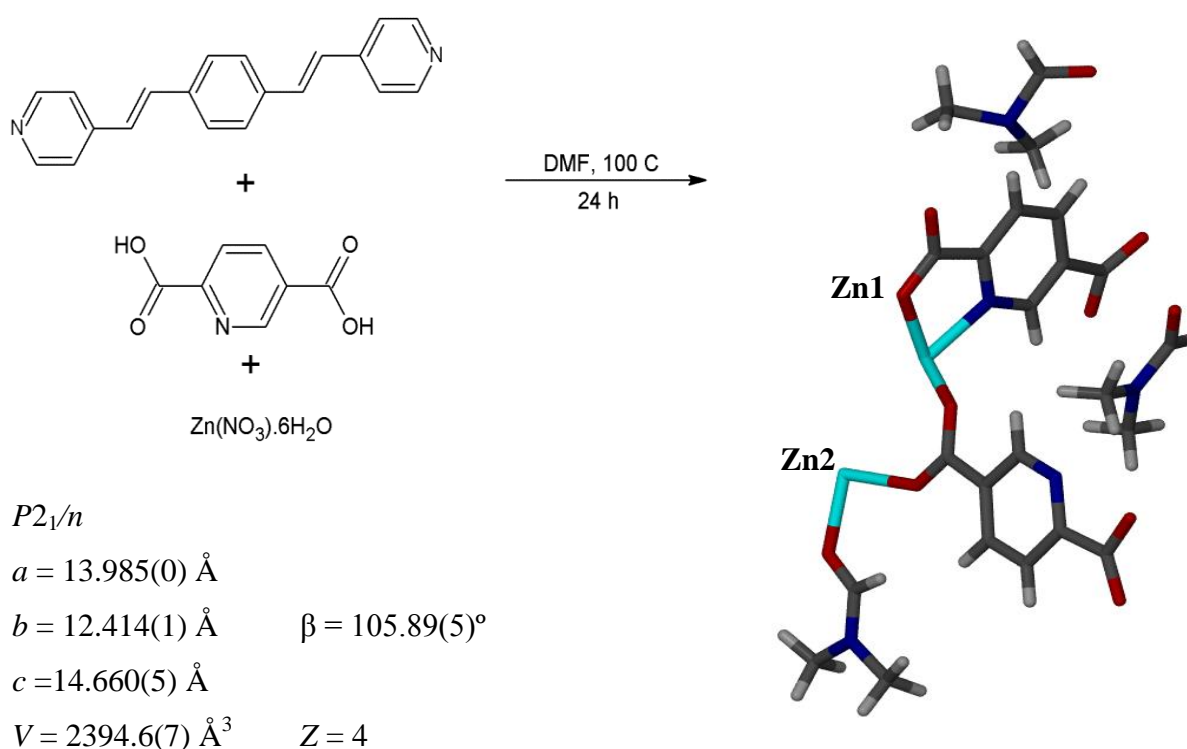
Figure 3.5 a) Single net showing partially filled “honeycomb” channels. b) Packing diagram showing DMF-filled discrete pockets.

The thermogram of **CP1** shows a mass loss of 11.53 wt% (two DMF and one water molecule per ASU) in the temperature range 60 - 200 °C. The material is then stable until decomposition at 400 °C. Desolvation induced deterioration of the crystals and therefore no further analysis was carried out.

CHAPTER III: STRUCTURAL ANALYSIS AND GAS SORPTION STUDIES

3.3.3 $\{[\text{Zn}_2(\text{PDC})_2(\text{DMF})\cdot 2\text{DMF}]_n\}$ or CP2

CP2 was formed by the solvothermal reaction of L1 with PDC and Zn(II) nitrate hexahydrate in DMF. The framework crystallises in the monoclinic space group $P2_1/n$. Although L1 was present during the crystallisation process, it is not incorporated into the framework. When the crystallisation experiment was repeated without ligand L1, no crystals were obtained. Thus it is believed that the presence of L1 is essential for framework formation and that it acts as a templating agent. The asymmetric unit of CP2 consists of two zinc cations, two PDC ligands, one coordinated DMF molecule and two guest DMF molecules, one of which is located about a centre of inversion (Scheme 3.2). Extension of the ASU shows that the framework contains an unusual paddlewheel SBU in which each metal has a unique coordination environment. Zn1 has trigonal bipyramidal geometry comprising four PDC ligands while Zn2 has an octahedral coordination environment comprised of four PDC ligands (one coordinated via the nitrogen and four via an oxygen) and a DMF molecule bound via its oxygen atom (Figure 3.6a). These unusual paddlewheels assemble into a non-interpenetrated 3D net with DMF guest molecules located in the channels (Figure 3.6b).



Scheme 3.2 Synthesis of CP2 from the solvothermal reaction of L1, PDC and zinc(II) nitrate in DMF at 100 °C, with selected crystallographic information.

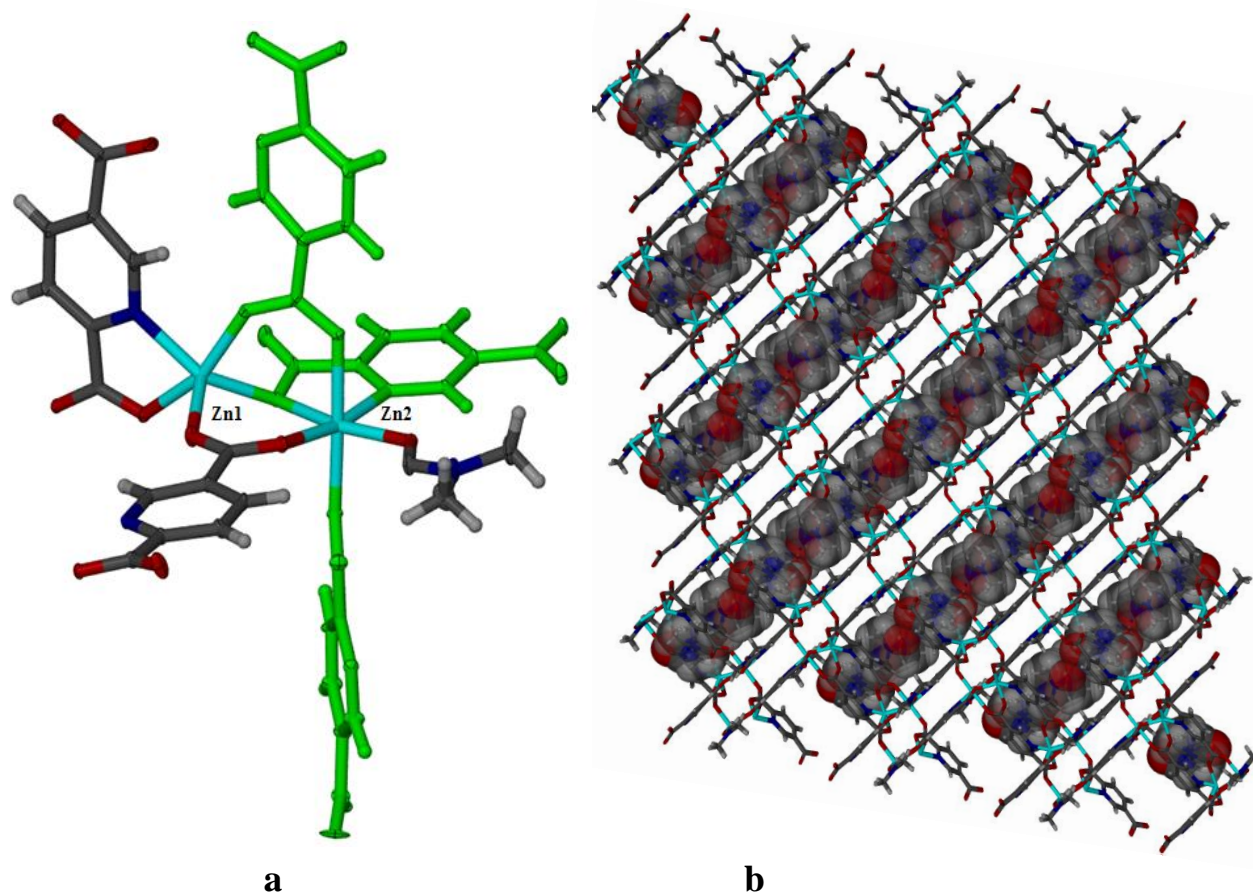
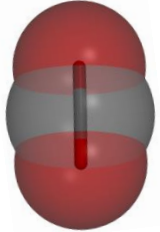
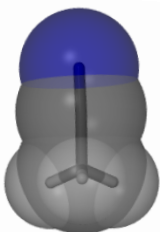
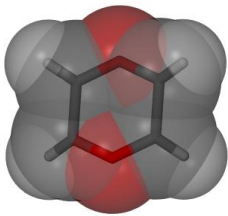
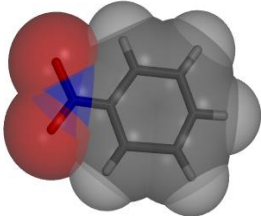


Figure 3.6 a) The unusual zinc paddlewheel in **CP2** with the ASU represented in CPK colours. b) Packing diagram of **CP2** viewed down *b*, showing DMF guest molecules.

Thermogravimetric analysis indicates that the framework undergoes complete desolvation by 175 °C with a 19.01 wt% loss (two DMF molecules per ASU). The coordinated DMF detaches between 275 - 375 °C with a further 8.32 wt% mass loss. The onset of decomposition is observed at 400 °C. Although no activated SC structure could be obtained due to crystal decomposition, several SC-SC guest exchange experiments were carried out. Crystals of **CP2** were exposed to guests such as acetonitrile, supercritical CO₂, dioxane and nitrobenzene. In all instances, the relevant guest replaced the DMF molecules. **Table 3.2** presents the crystallographic data obtained from these exchanges.

CHAPTER III: STRUCTURAL ANALYSIS AND GAS SORPTION STUDIES

Table 3.2 CP2 crystallographic data for SC-SC solvent exchange experiments.*

<i>P2₁/n</i>			
			
CP2·SCO₂	CP2·ACN	CP2·Dioxane	CP2·NB
$a = 14.187(3) \text{ \AA}$	$a = 14.050(8) \text{ \AA}$	$a = 14.006(2) \text{ \AA}$	$a = 13.795(9) \text{ \AA}$
$b = 12.112(6) \text{ \AA}$	$b = 11.921(6) \text{ \AA}$	$b = 12.191(3) \text{ \AA}$	$b = 12.211(2) \text{ \AA}$
$c = 14.322(1) \text{ \AA}$	$c = 14.327(4) \text{ \AA}$	$c = 14.621(4) \text{ \AA}$	$c = 14.855(9) \text{ \AA}$
$\beta = 105.15(3)^\circ$	$\beta = 105.18(7)^\circ$	$\beta = 105.29(4)^\circ$	$\beta = 105.89(1)^\circ$
$V = 2375.6(1) \text{ \AA}^3$	$V = 2316.1(4) \text{ \AA}^3$	$V = 2408.2(4) \text{ \AA}^3$	$V = 2407.0(5) \text{ \AA}^3$
Although the guest could not be modelled, SQUEEZE indicated the presence of two CO ₂ molecules. IR confirmed the asymmetric CO ₂ stretch at 2334 cm ⁻¹	Two half-occupancy molecules	Two molecules with one disordered over two positions (32% and 68% occupancy) while the second is located on a centre of inversion	One full-occupancy molecule

In the case of **CP2·CO₂**, although the guest could not be modelled, IR[†] confirmed the presence of CO₂ with SQUEEZE indicating approximately two molecules of guest per ASU. The guest molecules were modelled in all other exchange experiments. **CP2·ACN** has two half-occupancy acetonitrile molecules per ASU with one acetonitrile molecule located on a centre of inversion. **CP2·Dioxane** has two dioxane molecules with one disordered over two positions (68% and 32% occupancy), while the second is located on a centre of inversion with 60% site occupancy. **CP2·NB** has one full-occupancy nitrobenzene guest molecule.

* Relevant TGA data may be located in the supplementary information.

† IR spectrum is located in the supplementary information.

CHAPTER III: STRUCTURAL ANALYSIS AND GAS SORPTION STUDIES

Figure 3.7 shows the solvent-accessible space available in **CP2** and the manner in which each solvent occupies said accessible surface.⁵ **Figure 3.7a** shows the channels running down the *b* axis. When the structure is viewed down the *a* axis (**Figure 4b**), small diagonal interconnecting channels are observed, allowing for the formation of a network of interconnected solvent accessible space.

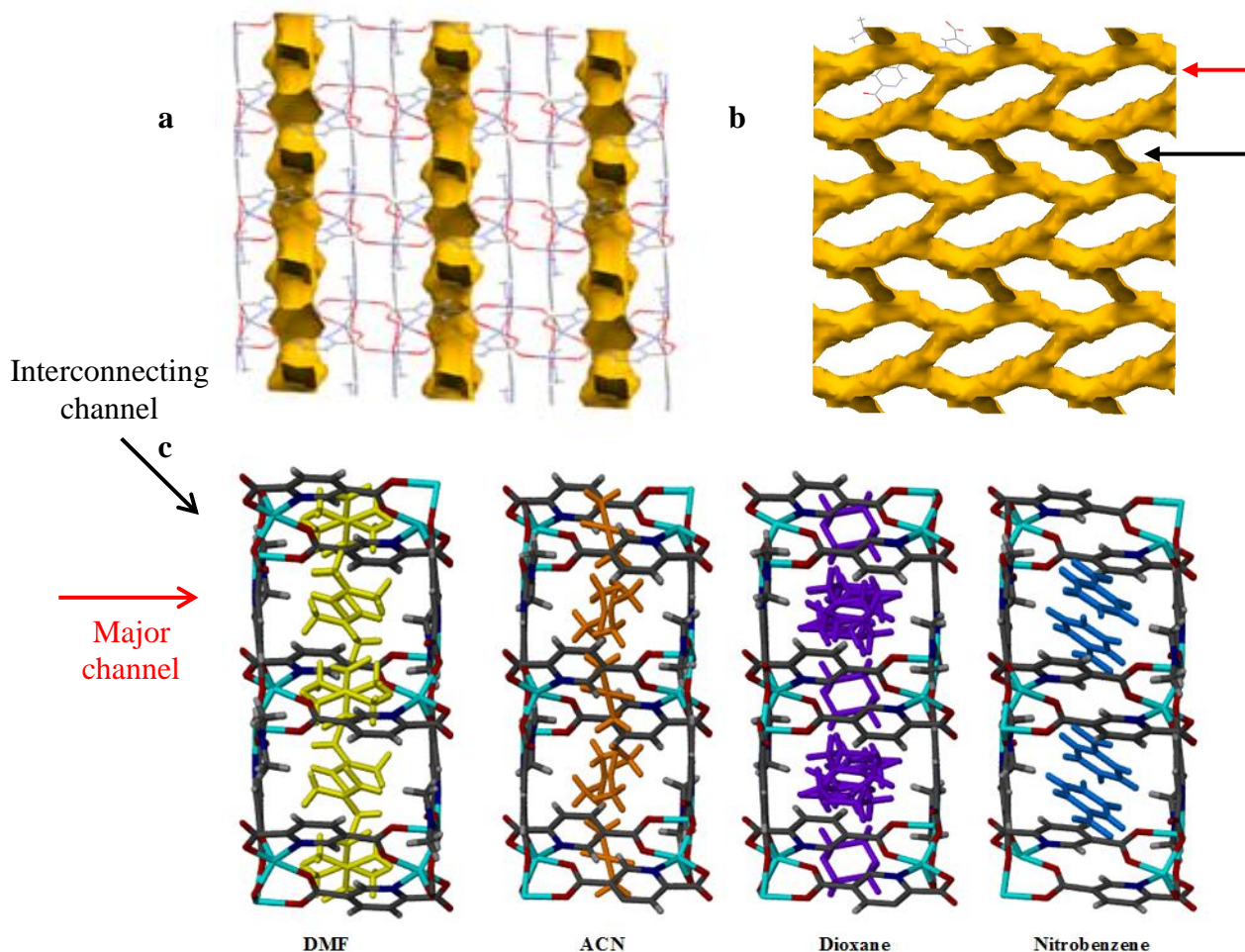


Figure 3.7 a) Solvent accessible channels present in **CP2** viewed down the *b* axis. b) Smaller interconnecting channels viewed down the *a* axis. c) Comparison of solvent orientation in each of the **CP2** solvates (**CP2**·**CO₂** is excluded as the guest could not be modelled).

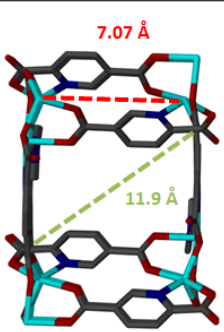
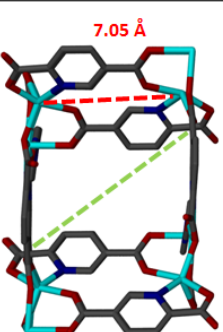
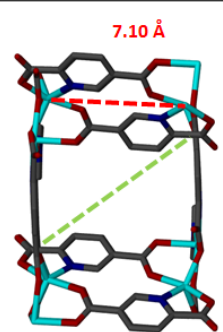
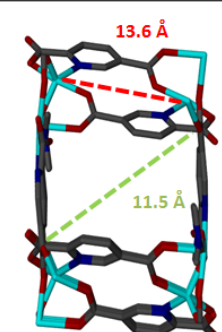
In the cases of solvates **CP2**·**DMF**, **CP2**·**ACN** and **CP2**·**Dioxane** the guest molecules are relatively small and are thus located in both the main channel as well as in the smaller interconnecting spaces (**Figure 3.7c**). It is believed that, due to its close size and shape resemblance to acetonitrile, **CO₂** probably behaves in a similar manner. **CP2**·**NB** differs in that nitrobenzene is not only larger in molecular volume compared to all the previous guests (**CO₂**, acetonitrile, **DMF** and **dioxane**), but also has a bulky nitro tail, thus ensuring that nitrobenzene molecules are only located in the major channel.

CHAPTER III: STRUCTURAL ANALYSIS AND GAS SORPTION STUDIES

Examination of the unit cell parameters indicates several trends, which include the *a* axis decreasing with an increase in guest size while the *c* axis increases with an increase in guest size. Comparison of a single pore of each of the solvates provides a clearer understanding of the effect each solvent has on the host structure. **Table 3.3** shows that as larger guests are incorporated, the metal-to-metal distance increases from 7.07 Å for CO₂ to 13.6 Å for nitrobenzene. This in turn causes an alteration of the cavity shape (diagonal decrease from 11.9 to 11.5 Å). It is believed that the host undergoes structural changes to accommodate the guest in a “best fit” scenario.

Overall density (host + guest) appears to increase with an increase in molecular volume of the guest. However, despite the fact that dioxane has a smaller volume than nitrobenzene does, **CP2·Dioxane** has a higher density, implying that this is the most stable of all the solvates. The reason for this relates back to the packing diagram presented in **Figure 3.7c**. **CP2·Dioxane** is able to accommodate more dioxane molecules (the shape and size of the guest are optimum for inclusion in both the channel and the interstitial space) making it the most thermodynamically favourable solvate. A comparison of the expected and experimental occupancy numbers shows good correlation. **Table 3.3** also illustrates that **CP2** takes up the maximum number of acetonitrile, dioxane and nitrobenzene molecules possible (2, 2 and 1, respectively).

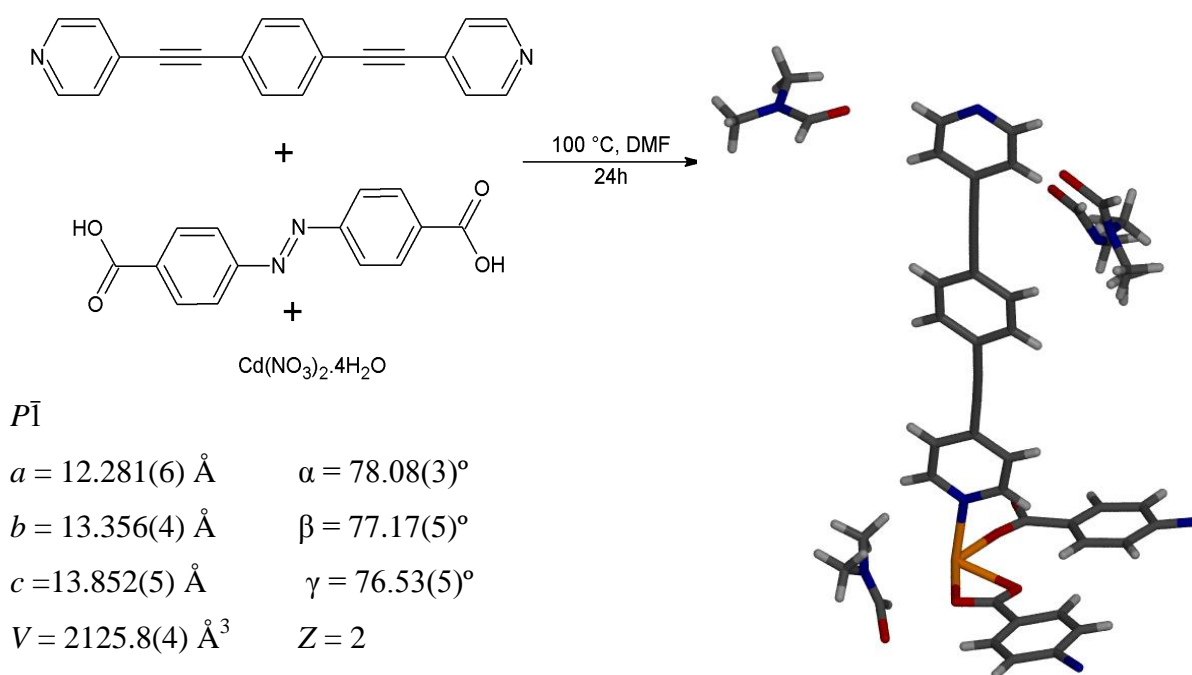
Table 3.3. Tabulated data for the **CP2** pore system in response to occlusion of a selection of guests.

GUEST SIZE →				
				
	SCO ₂	ACN	Dioxane	Nitrobenzene
Crystal density	1.49 g cm ⁻³	1.71 g cm ⁻³	1.83 g cm ⁻³	1.74 g cm ⁻³
Guest Molecular volume	33 Å ³	46 Å ³	80 Å ³	102 Å ³
Solvent accessible void	117 Å ³	107 Å ³	138 Å ³	117 Å ³
Expected occupancy	3.5	2	2	1
Experimental occupancy	2	2	2	1

CHAPTER III: STRUCTURAL ANALYSIS AND GAS SORPTION STUDIES

3.3.4 $\{[\text{Cd}(\text{L}2)\text{ADB}] \cdot 3\text{DMF}\}_n$ or CP3

CP3* was formed by the reaction of **L2**, **ADB** and Cd(II) nitrate tetrahydrate under solvothermal conditions (100 °C, DMF-DMSO). **CP3** crystallises in the triclinic space group $P\bar{1}$. The ASU consists of one cadmium cation, one **ADB** ligand, one **L2** ligand and three DMF molecules, one of which is disordered over two positions with 50:50 site occupancy (**Scheme 3.3**).



Scheme 3.3 Synthesis of **CP3** from the solvothermal reaction of **L2**, **ADB** and zinc(II) nitrate in DMF at 100 °C, with selected crystallographic information.

The framework contains an SBU comprised of four acid groups bridging two Cd ions, with four pyridyl moieties situated in the axial positions (**Figure 3.8a**). The threefold-interpenetrated structure contains triangular channels housing dimethylformamide molecules (**Figure 3.8**).

* It should be noted that the crystals of **CP3** are very poor. Diffraction data for multiple crystals was recorded and attempts at growing better quality crystals were made but proved unsuccessful.

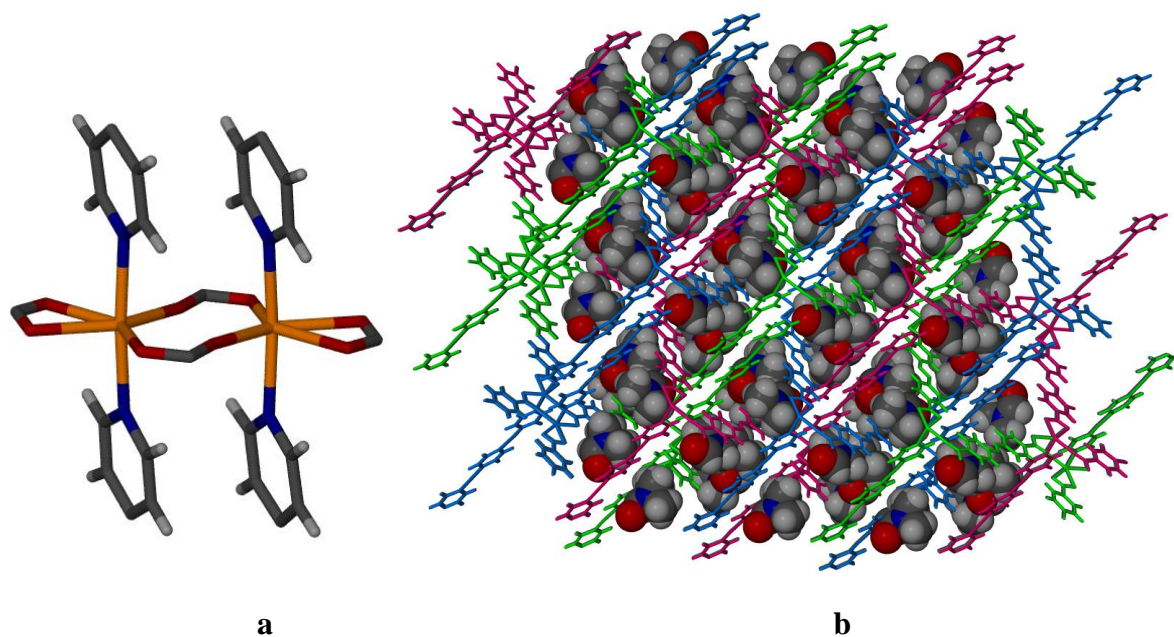


Figure 3.8 a) Cadmium SBU in CP3. b) Packing diagram of CP3 viewed down the *c* axis showing interpenetration and DMF guest molecules.

TGA is in agreement with SQUEEZE and indicates that the framework undergoes complete desolvation by 180 °C with a 25.41 wt% loss (three DMF molecules). The onset of decomposition occurs at 275 °C. Although desolvation induced crystal deterioration, a comparison of the experimental and generated PXRD traces (see supplementary information) of the activated forms indicates that the framework did not undergo decomposition upon guest loss. The gas sorption properties of the desolvated phase of CP3 were measured at 25 °C using CO₂, methane, ethane, propane and butane (**Figure 3.9**). CP3 shows Type I sorption behaviour for all selected guests, absorbing approximately one and a half molecules of CO₂ (4.8 wt%) or one molecule each of methane (3.3 wt%), ethane (5.6 wt %), propane (7.0 wt%) or butane (6.7 wt%) per ASU. CP3 could potentially accommodate more of all the guest molecules.* All but one of the isotherms (butane) show stepless hysteresis[†], with the trend for potential selectivity as follows: CO₂ > methane > ethane > propane > butane. The butane sorption isotherm shows a small step, which is not evident in the desorption isotherm.

* Maximum gas uptake is indicated by a plateau in the sorption isotherm.

[†] *Hysteresis* occurs when the two curves do not overlap and is indicative of a host-guest interaction. The ethane isotherm exhibits the highest amount of hysteresis and future experiments would involve studying these host-guest interactions using our in-house developed gas cell.

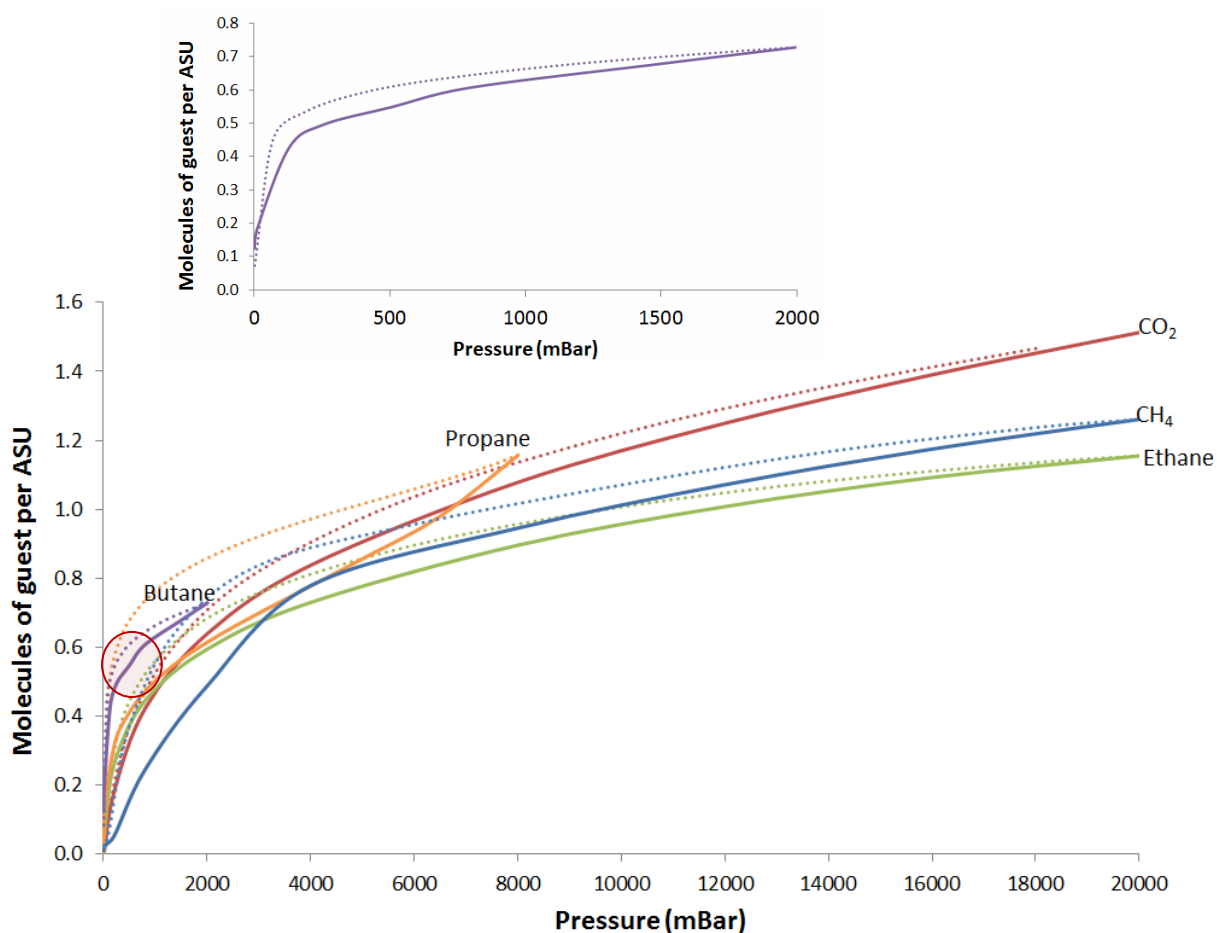
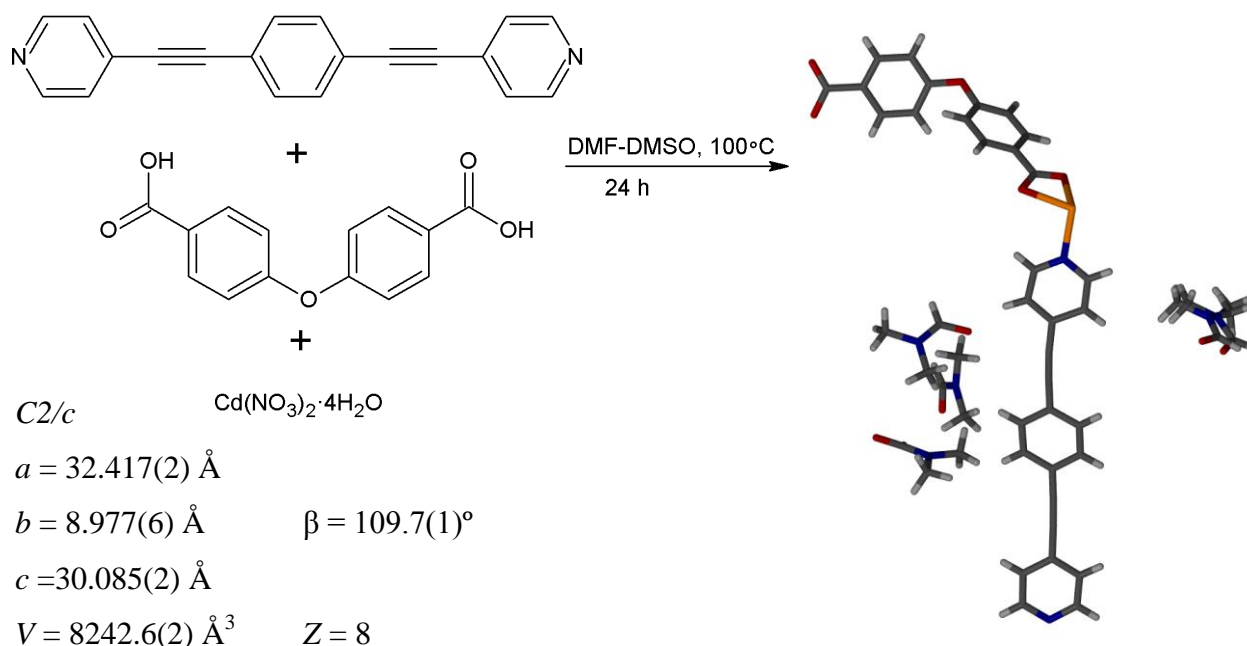


Figure 3.9 CO₂ and selected alkane sorption and desorption isotherms for **CP3** at 25 °C. Solid lines represent absorption and dashed lines represent desorption. Inset graph shows magnified butane isotherm.

3.3.5 {[Cd(L2)(OBA)]·2DMF}_n or CP4

CP4 was formed by the reaction of **L2**, **OBA** and Cd(II) nitrate tetrahydrate under solvothermal conditions (100 °C, DMF-DMSO). **CP4** crystallises in the monoclinic space group *C2/c*. **Scheme 3.4** shows the ASU consisting of one cadmium cation, one **OBA** ligand, one **L2** ligand and two DMF molecules (one of which is disordered over two positions of 67:33 site occupancy while the second is disordered over three positions with 41:34:25 site occupancy). Once again, although **CP4** was grown from DMSO, no DMSO is present in the structure. This structure consists of non-interpenetrated 2D nets with two interconnected corrugated types of channels, both containing DMF guest molecules (**Figure 3.10**).

CHAPTER III: STRUCTURAL ANALYSIS AND GAS SORPTION STUDIES



Scheme 3.4 Synthesis of **CP4** from the solvothermal reaction of **L2**, **OBA** and cadmium(II) nitrate in DMF-DMSO at 100 °C, with selected crystallographic information.

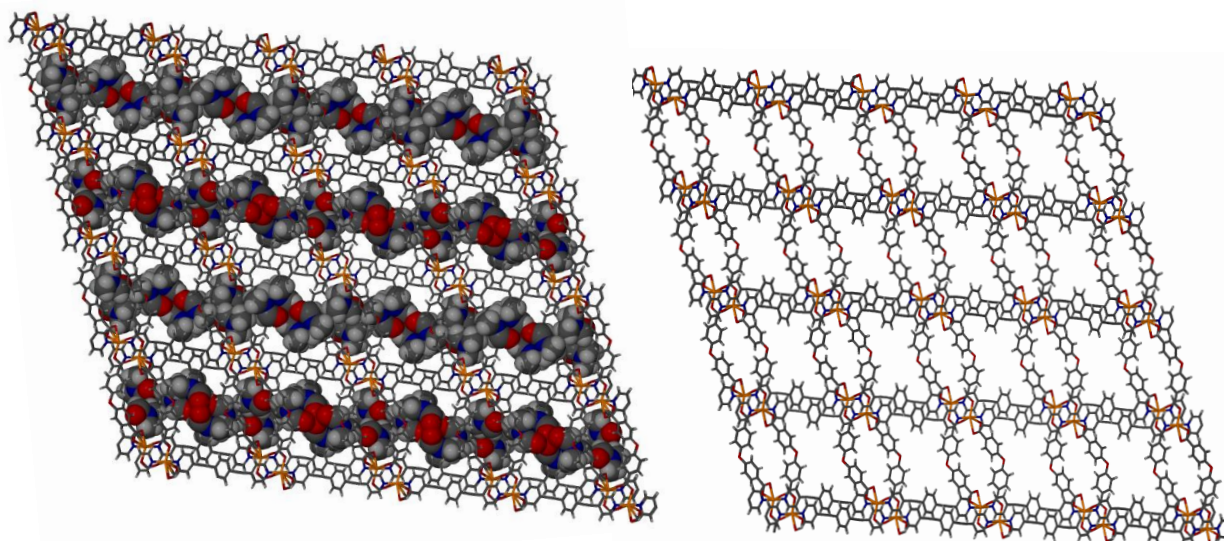


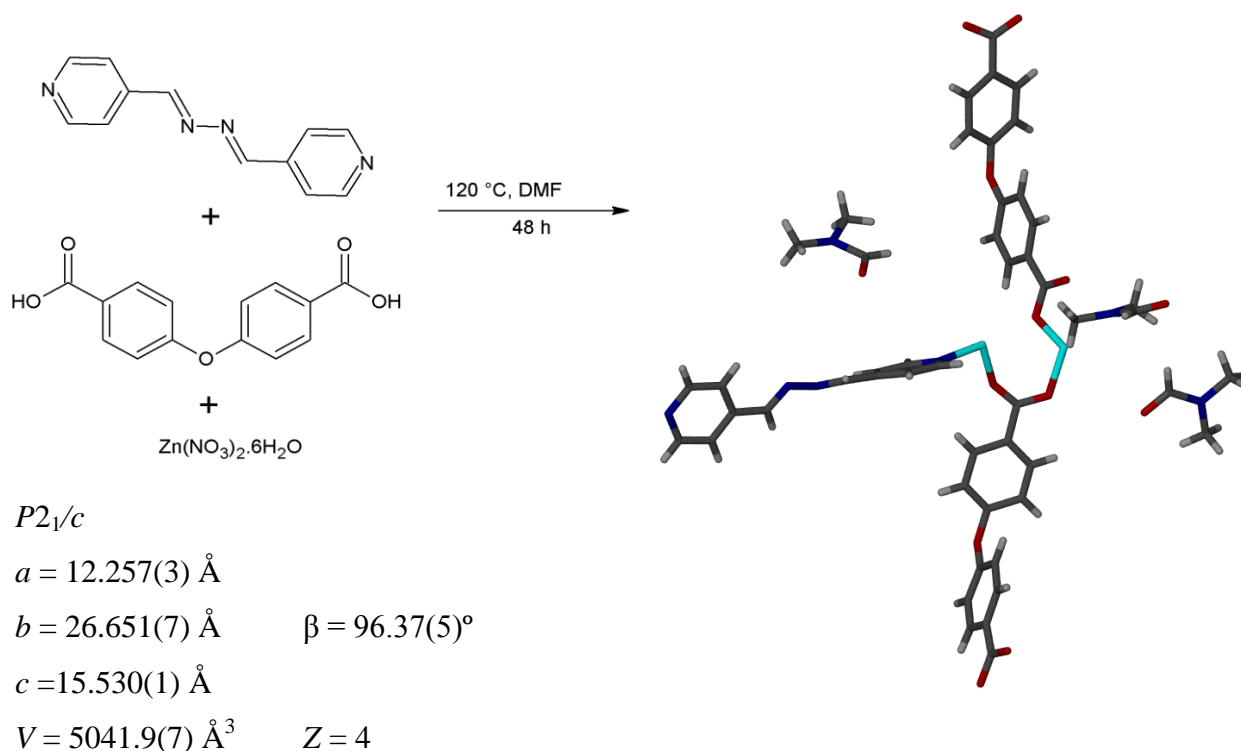
Figure 3.10 Packing diagram of **CP4** viewed along the b axis showing solvent-occupied (left) and solvent-free (right) channels.

TGA is in agreement with SQUEEZE, showing some initial surface solvent loss and then 18.56 wt% loss (two DMF molecules) between 60 - 175 °C. The onset of decomposition occurs at 330 °C. Desolvation induced crystal deterioration and thus no further analysis was performed.

CHAPTER III: STRUCTURAL ANALYSIS AND GAS SORPTION STUDIES

3.3.6 $\{[\text{Zn}_2(\text{L3})(\text{OBA})_2]\cdot 3\text{DMF}\}_n$ or CP5

By combining **L3** with **OBA** and zinc(II) nitrate hexahydrate in DMF at 120 °C, crystals of **CP5** were obtained. This framework crystallises in the space group $P2_1/c$ with one **L3** ligand, two **OBA** ligands, two zinc ions and three DMF guest molecules in the ASU (**Scheme 3.5**). The framework contains the unusual paddlewheel also observed in **CP1** (**Figure 3.11a**). The 2D sheets created by the **OBA** ligands are connected by the linear **L3** ligands and the framework thus propagates in all three directions. In 2014 Maspoch *et al.*⁶ published this framework in the context of an azine MOF's ability to selectively capture CO₂.



Scheme 3.5 Synthesis of **CP5** from the solvothermal reaction of **L3**, **OBA** and zinc nitrate in DMF at 120 °C, with selected crystallographic information.

The framework is twofold interpenetrated with 1D elongated honeycomb channels running along $[1\ 0\ 1]$ (**Figure 3.11b**). An examination of a single corrugated channel shows that the DMF molecules are grouped into sets of four, with each of the molecules orientated in a different direction (**Figure 3.11c**). Thermogravimetric analysis indicates that the framework experiences an 18.23 wt% loss in the range of 30 - 150 °C (three DMF molecules), with the material remaining stable until framework decomposition at 320 °C.

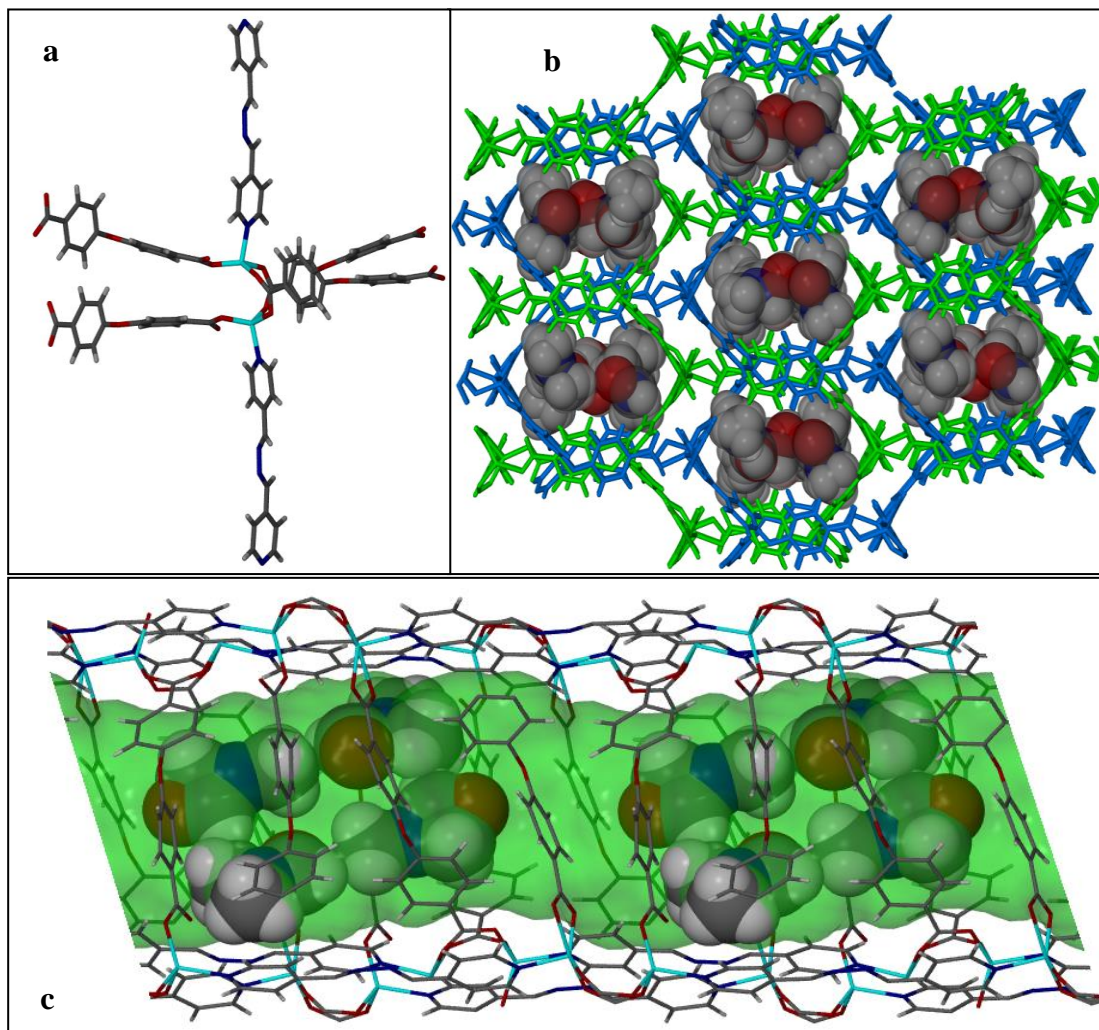


Figure 3.11 a) The unusual paddlewheel of CP5. b) DMF molecules located within the elongated honeycomb channels of CP5 as viewed down [1 0 1]. c) Connolly-mapped channel viewed perpendicular to the *ac* plane, showing the DMF grouping.

Having ascertained that the material can be activated without loss of porosity, a SC-SC transformation was carried out by heating the solvate at 150 °C under reduced pressure for 24 h. The cell parameters undergo a slight change (**Figure 3.12**). However, the framework of the empty phase (CP5') remains the same as that of the as-synthesised phase. Examination of the porous structure shows that it possesses 690 Å³ of solvent-accessible space per unit cell. **Figure 3.13** shows the solvent accessible space as crenelated channels.

CHAPTER III: STRUCTURAL ANALYSIS AND GAS SORPTION STUDIES



$C2/c$

$a = 12.545(2) \text{ \AA}$

$b = 24.412(1) \text{ \AA}$ $\beta = 97.88(6)^\circ$

$c = 15.711(9) \text{ \AA}$ $Z = 4$

$V = 5156.8(1) \text{ \AA}^3$

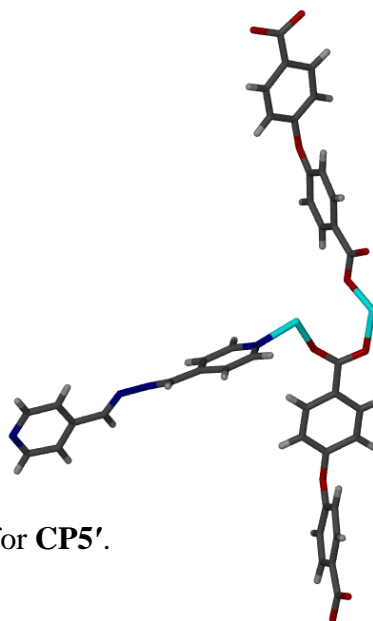


Figure 3.12 ASU and crystallographic information for CP5'.

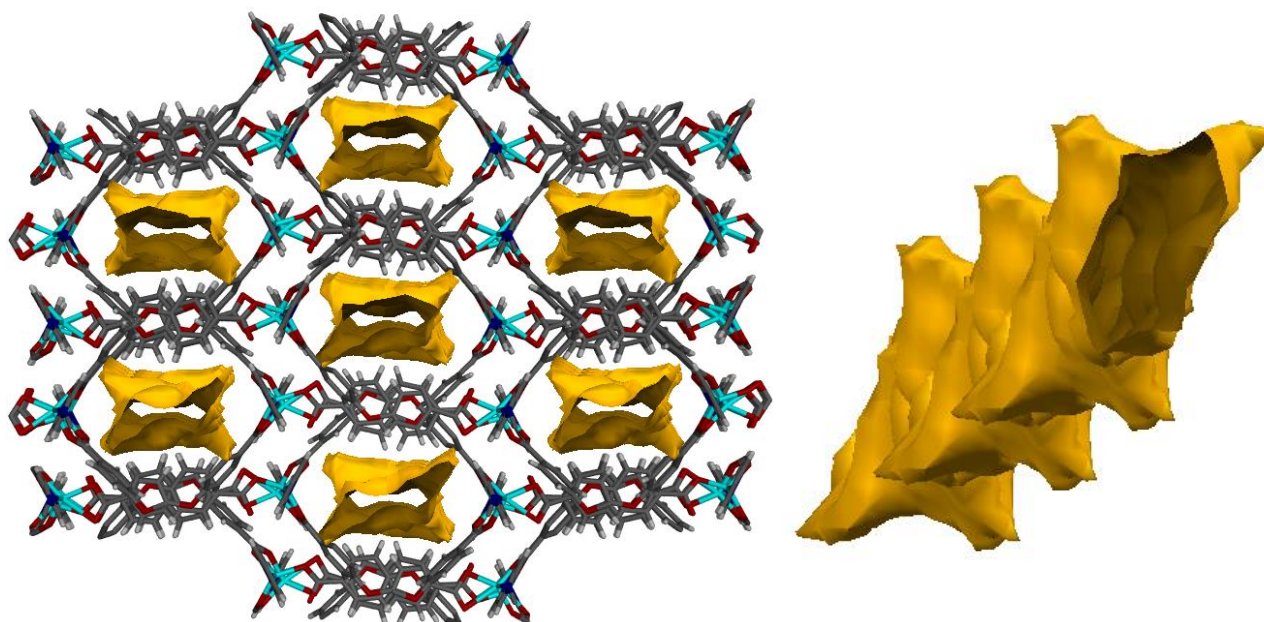


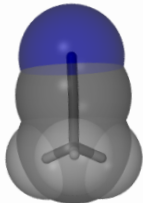
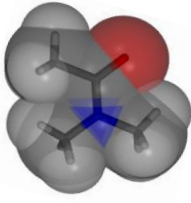
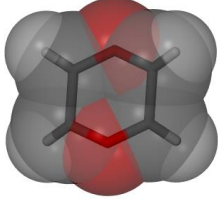
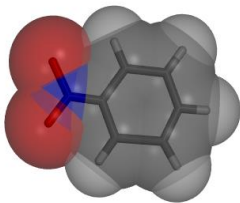
Figure 3.13 Extended view of CP5' along [1 0 1] showing solvent-accessible space.

Several SC-SC guest-exchange experiments were carried out. Crystals of the apohost CP5' were exposed to guests such as acetonitrile, DMA, dioxane and nitrobenzene. In all instances the relevant guest molecules were located within the channels of CP5' using SCD. Table 3.4 presents the relevant crystallographic data obtained for these exchanges.

* Prime denotes activation.

CHAPTER III: STRUCTURAL ANALYSIS AND GAS SORPTION STUDIES

Table 3.4 CP5' crystallographic data for SC-SC solvent exchange experiments.

<i>C2/c</i>			
			
CP5'·ACN	CP5'·DMA	CP5'·Dioxane	CP5'·NB
$a = 12.145(7) \text{ \AA}$	$a = 12.619(6) \text{ \AA}$	$a = 12.371(7) \text{ \AA}$	$a = 13.158(3) \text{ \AA}$
$b = 25.666(4) \text{ \AA}$	$b = 26.404(8) \text{ \AA}$	$b = 26.508(8) \text{ \AA}$	$b = 25.905(5) \text{ \AA}$
$c = 16.392(1) \text{ \AA}$	$c = 15.617(8) \text{ \AA}$	$c = 15.622(9) \text{ \AA}$	$c = 15.347(5) \text{ \AA}$
$\beta = 100.82(2)^\circ$	$\beta = 98.04(3)^\circ$	$\beta = 97.29(4)^\circ$	$\beta = 98.81(9)^\circ$
$V = 5019.0(6) \text{ \AA}^3$	$V = 5152.9(8) \text{ \AA}^3$	$V = 5082.21 \text{ \AA}^3$	$V = 5169.6(9) \text{ \AA}^3$
Two and a half acetonitrile molecules, one of which is disordered over four positions (46:22:14:18)	Two DMA molecules, each disordered over two positions (54:46 and 52:48 occupancy)	Two molecules located over three positions with 70, 70 and 60 % occupancy	Two nitrobenzene molecules, one of which is disordered over two positions (62:38 site occupancy). NB induces crystal deterioration.

The SC-SC exchange experiments did not induce any significant changes in the host structure. They did however reveal the susceptibility of the framework toward guest size and shape. The *a* axis increases with an increase in guest size while the *c* axis decreases. The gas sorption properties of CP5' were measured using CO₂, methane, ethane, propane and butane (**Figure 3.14**). CP5' shows Type I sorption behaviour for all selected guests, absorbing approximately three molecules of CO₂ (7.8 wt%), two molecules of methane (4.7 wt%), ethane (8.8 wt%), propane (10 wt%) or one molecule of butane (9.0 wt%) per ASU. Ethane was the only gas to attain full occupancy in the pressure range tested. It therefore appears that the framework could potentially accommodate more of the other guest molecules. All isotherms show stepless sorption with the order for potential selectivity as follows: CO₂ > ethane = methane > propane > butane. The framework absorbed CO₂ and ethane with no hysteresis while methane, propane and butane isotherms showed hysteresis with 0.5 molecules of methane remaining encapsulated post desorption. These gases are experiencing host-guest interactions and warrant future studies.

CHAPTER III: STRUCTURAL ANALYSIS AND GAS SORPTION STUDIES

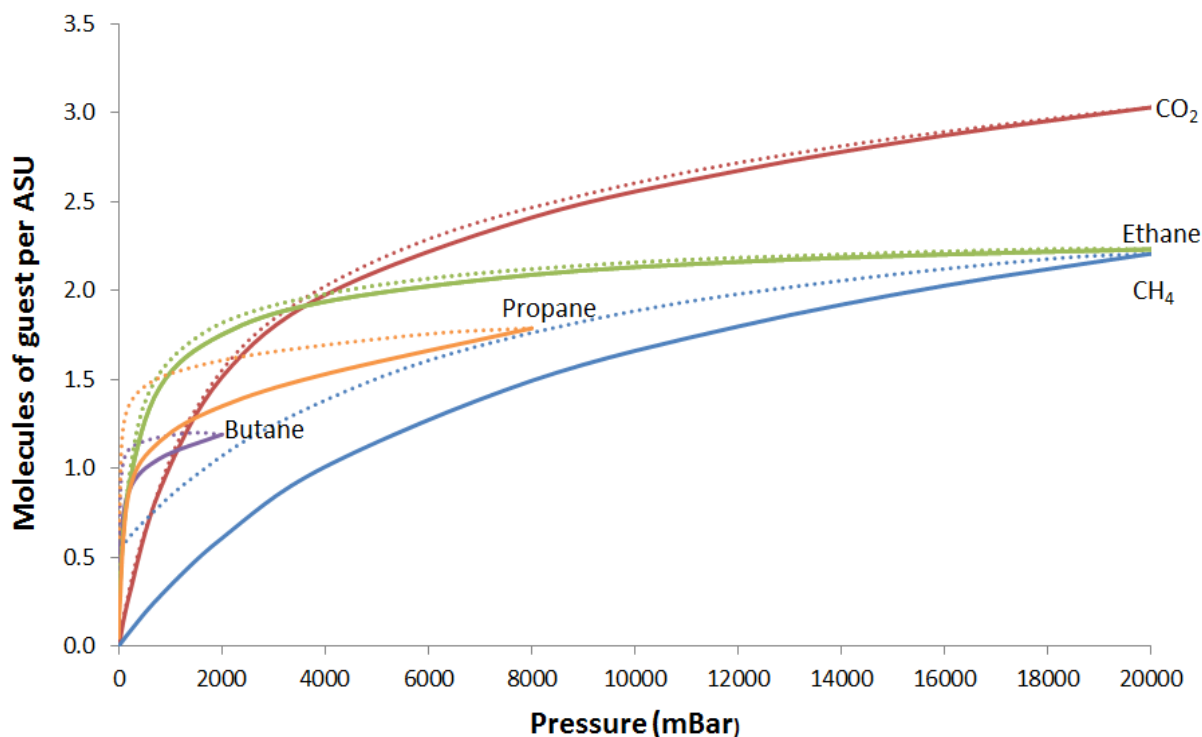


Figure 3.14 CO₂ and selected alkane sorption and desorption isotherms for **CP5'** at 25 °C. Solid lines represent absorption and dashed lines represent desorption.

Repetition of the crystallisation process, but substituting cadmium for zinc, yielded **CP5a**.

3.3.7 {[Cd(L3)OBA]·2DMA·H₂O}_n or CP5a

CP5a crystallises in the monoclinic space group $P2_1/c$ with one cadmium metal ion, one **OBA** ligand and one **L3** ligand in the ASU. In addition, there are two DMA guest molecules, each disordered over two positions (64:34 and 82:18 site occupancy) and one water molecule in the ASU (**Figure 3.15**).

$P2_1/c$

$a = 12.256(4) \text{ \AA}$

$b = 10.093(9) \text{ \AA}$

$c = 29.729(5) \text{ \AA}$

$V = 3617.3(5) \text{ \AA}^3$

$\beta = 100.41(8)^\circ$

$Z = 4$

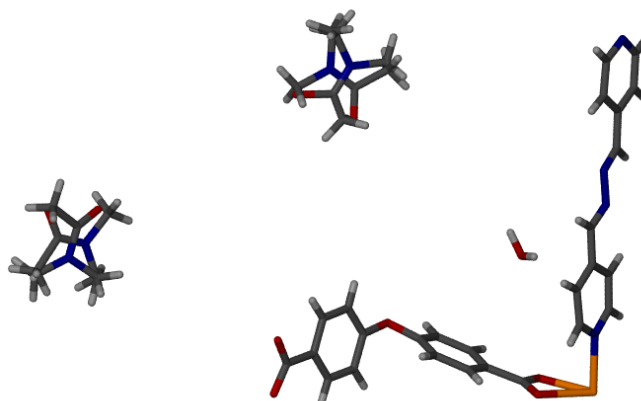


Figure 3.15 ASU and crystallographic information for **CP5a**.

CHAPTER III: STRUCTURAL ANALYSIS AND GAS SORPTION STUDIES

Figure 3.16a shows that the disordered DMA molecules are hydrogen bonded to one another via a water molecule. **CP5a**, is a non-interpenetrated 3D MOF with guest molecules located in the large and small channels (**Figure 3.16b**).

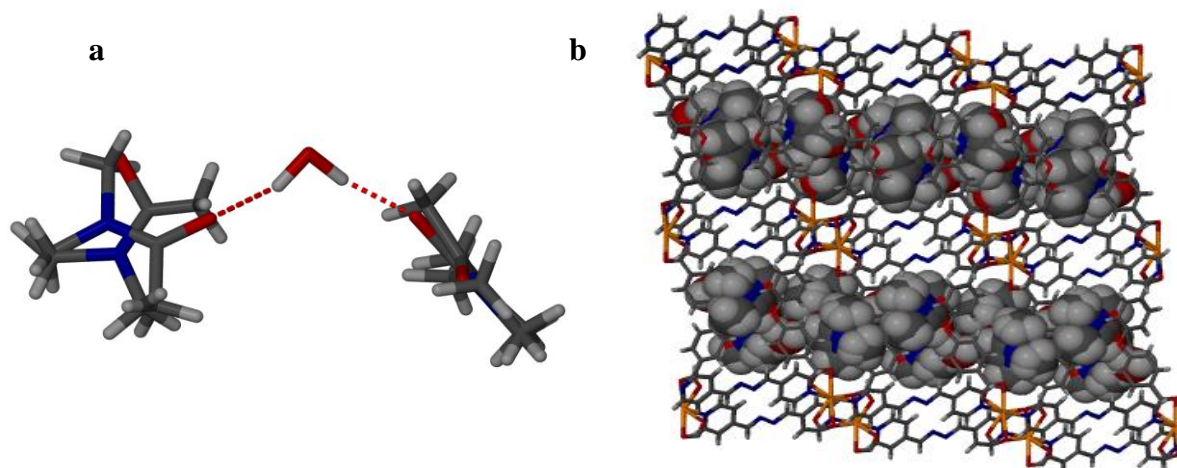


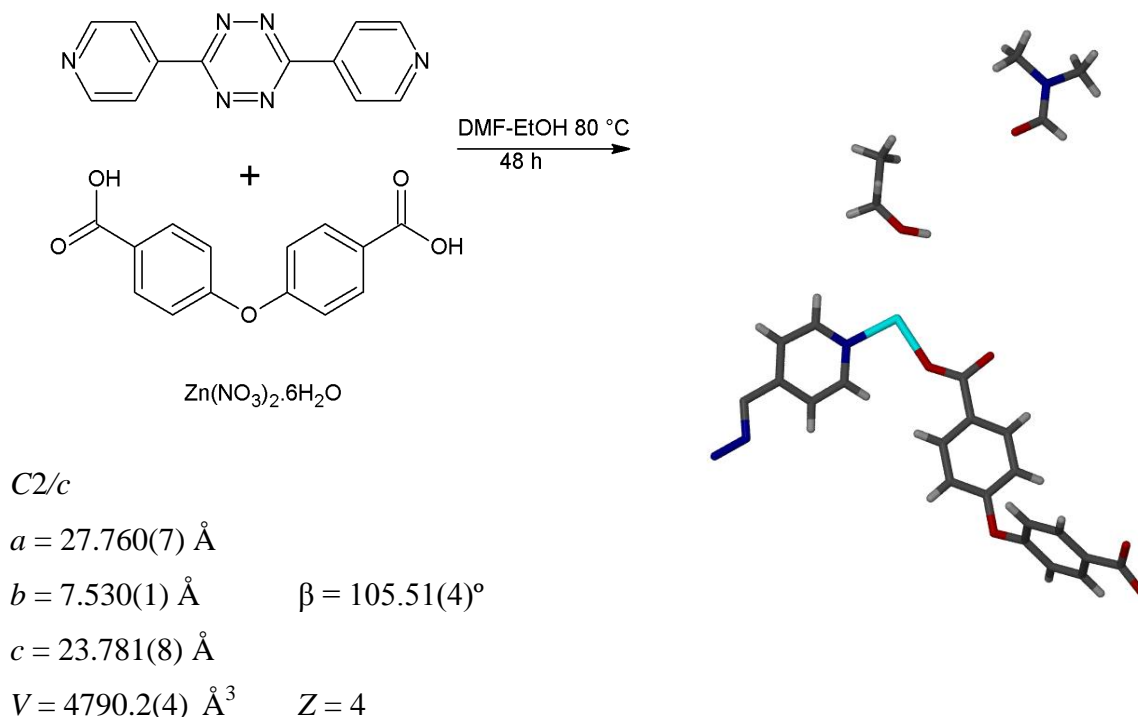
Figure 3.16 a) Hydrogen bonding between water and DMA molecules. b) Packing diagram of **CP5a**, viewed down *b*, showing DMA and water in both channels.

TGA is in agreement with SQUEEZE, showing some initial surface solvent loss and then a 19.64 wt% loss (two DMA molecules) between 30 – 120 °C. The onset of decomposition occurs at 280 °C. Desolvation induced single crystal deterioration and no further analysis was thus performed.

3.3.8 $\{[\text{Zn}(\text{L4})_{0.5}\text{OBA}]\cdot\text{DMF}\cdot\text{EtOH}\}_n$ or **CP6**

CP6 was obtained by combining **L4**, **OBA** and zinc(II) nitrate hexahydrate under solvothermal conditions (80 °C, DMF-EtOH). This framework crystallises in the monoclinic space group *C2/c*. The ASU comprises one zinc cation, one **OBA** ligand, half an **L4** ligand, one DMF molecule and an ethanol molecule located around a centre of inversion with 51% occupancy (**Scheme 3.6**). The framework contains the well-documented zinc paddlewheel moiety. Four **OBA** ligands linked to two **L4** ligands by two metal salts form a distorted 2D rhombic grid. The structure is a non-interpenetrated 2D coordination polymer with two types of corrugated channels containing dimethylformamide and ethanol guest molecules which may be viewed along $[0\ 1\ 0]$ (**Figure 3.17**).

CHAPTER III: STRUCTURAL ANALYSIS AND GAS SORPTION STUDIES



Scheme 3.6 Synthesis of **CP6** from the solvothermal reaction of **L4**, **OBA** and zinc nitrate in a DMF-EtOH mixture at 80 °C, with selected crystallographic information.

The larger hour-glass channel (guest is surrounded by pyridyl ligand and acid) is occupied by DMF molecules with the orientation of DMF molecules alternating in every second channel (**Figure 3.17**, yellow and orange). The ethanol molecules are located in the much smaller channel (**Figure 3.17**, light and dark blue) comprised of two **OBA** molecules arranged in a bent conformation. After characterisation, it was discovered that Feng *et al.*⁷ had published a similar framework in 2011 with only DMF guest molecules located in the channels.

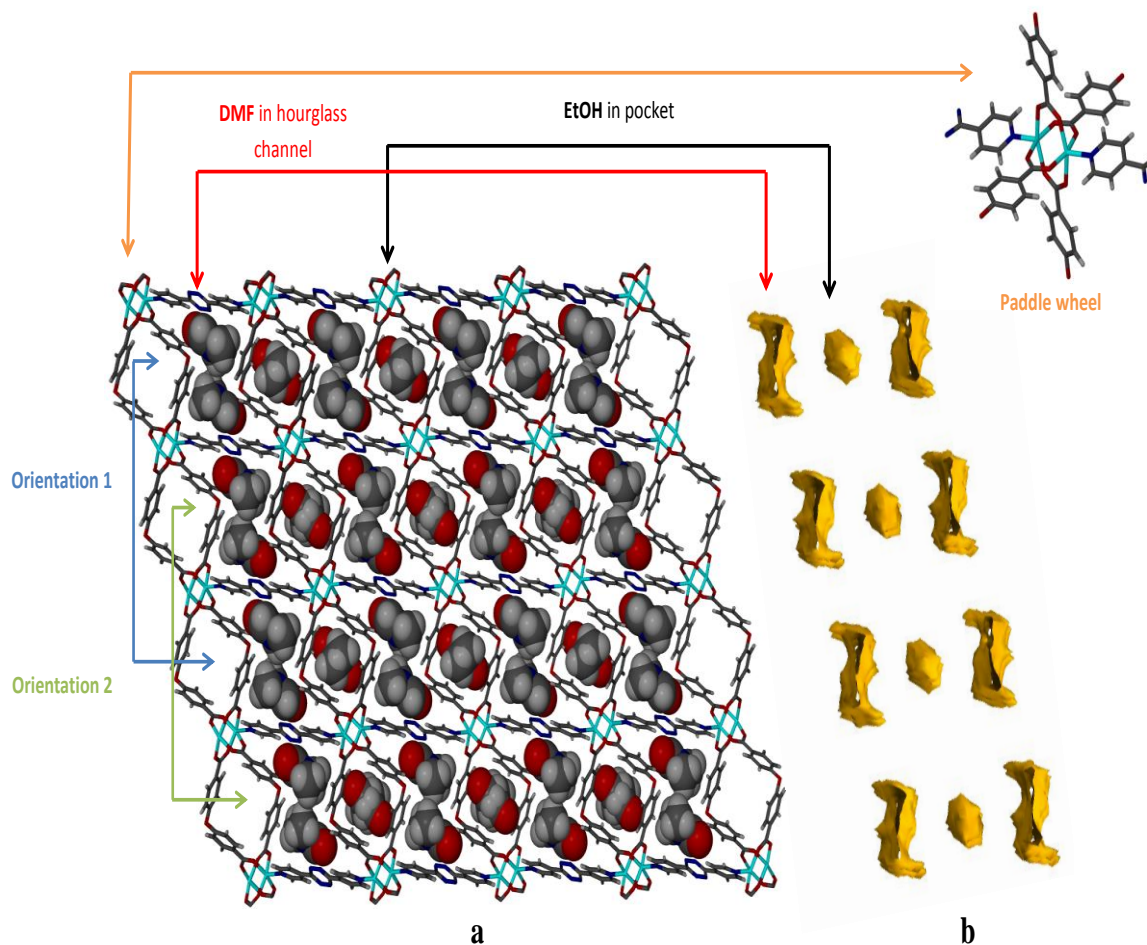


Figure 3.17 Packing diagram of **CP6** viewed along $[0\ 1\ 0]$ showing DMF and ethanol molecules in CPK representation. **b)** Two distinct solvent-accessible voids present in **CP6**.

Thermogravimetric analysis indicates that the framework undergoes complete desolvation by 150 °C with a 17.03 wt% loss (one DMF and one ethanol molecule per ASU). The onset of decomposition is observed at 275 °C. Crystals of **CP6** are unusual in that they may be left exposed to air for extended periods with no visible deterioration; however, desolvation, activation with supercritical CO₂ or any attempt at solvent exchange (acetone, acetonitrile, chloroform, dimethylacetamide, dioxane, ethanol, methanol, toluene and water) induces rapid and extensive crystal disintegration. It was by a process of elimination that crystals of **CP6** were placed in a mixture of the three xylene isomers (*ortho*, *meta* and *para*) overnight. Although the crystals underwent some cracking and degradation (**Figure 3.18**), they did not disintegrate completely, and thus X-ray diffraction data were recorded.

CHAPTER III: STRUCTURAL ANALYSIS AND GAS SORPTION STUDIES

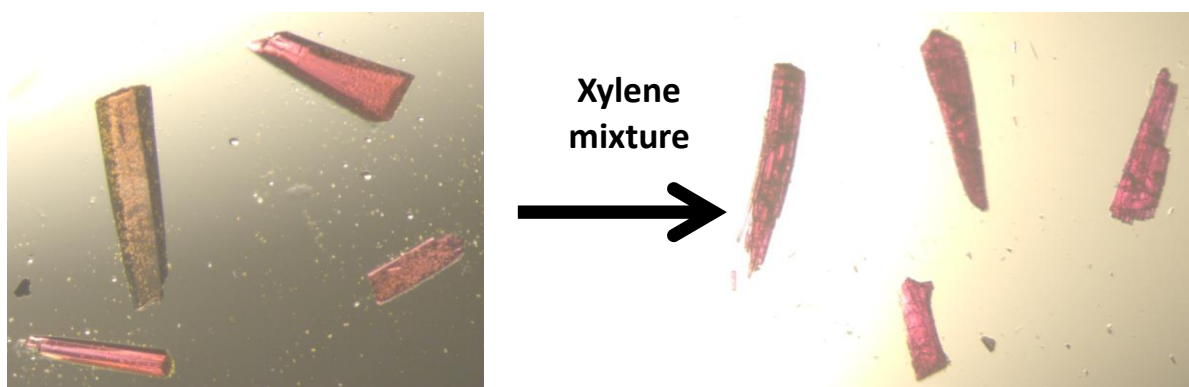


Figure 3.18 Photographs showing original **CP6** crystals (left) and **CP6** crystals after exposure to xylene (right).

$$\{[\text{Zn}(\text{L}5)_{0.5}\text{OBA}] \cdot \text{xylene}\}_n \text{ or } \text{CP6} \cdot \text{xymix}$$

Despite poor crystal quality, a structure of the transformed species (**CP6·xymix**) was obtained. Due to the sensitivity of the framework (tetrazine ligands are highly reactive) toward stimuli (temperature or solvent), the data obtained were not of publishable quality. However, the structure does provide some idea regarding the effect xylene has on **CP6**. **CP6·xymix** crystallises in the space group $P2/c$ and the ASU comprises two zinc cations, two **OBA** ligands and two independent halves of ligand **L4** (**Figure 3.19**).

$P2/c$

$a = 14.065(0) \text{ \AA}$

$b = 23.366(7) \text{ \AA}$ $\beta = 106.22(6)^\circ$

$c = 15.686(6) \text{ \AA}$ $Z = 4$

$V = 4950.2(4) \text{ \AA}^3$

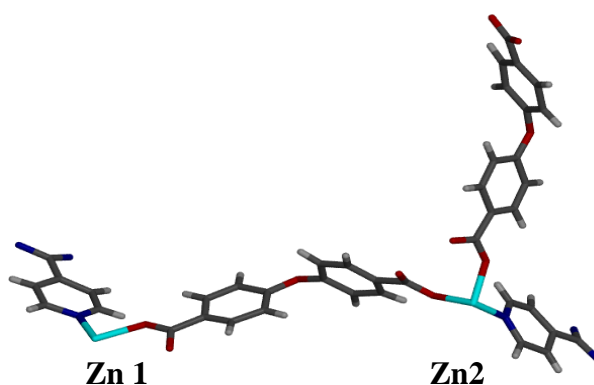


Figure 3.19 ASU and selected crystallographic parameters for **CP6·xymix**.

Unfortunately, due to the quality of the data, no xylene molecules could be modelled. However, SQUEEZE and TGA (17.46 wt% loss between 75 – 200 °C) data indicate the presence of one xylene molecule per ASU. Symmetry-lowering (*i.e.* the space group change from $C2/c$ for **CP6** to $P2/c$ for **CP6·xymix**) is due to distortion of half of the SBUs relative to the other half as a result of xylene uptake.

CHAPTER III: STRUCTURAL ANALYSIS AND GAS SORPTION STUDIES

A comparison of the paddlewheels as well as the extended structures of the **CP6** and **CP6·xymix** frameworks (**Figure 3.20**) shows this effect. It appears that the incorporation of xylene induces straightening of the previously slanted **OBA** paddlewheel moiety, with the **L4** ligand also experiencing a conformational change. The previously planar ligand now has its tetrazine portion twisted in relation to the two pyridyl ligands. As a result, the structure is transformed from a slanted pillared structure to a vertically pillared structure. Furthermore, doubling of ligands in **CP6·xymix** results in the channel previously containing ethanol to reduce in volume.

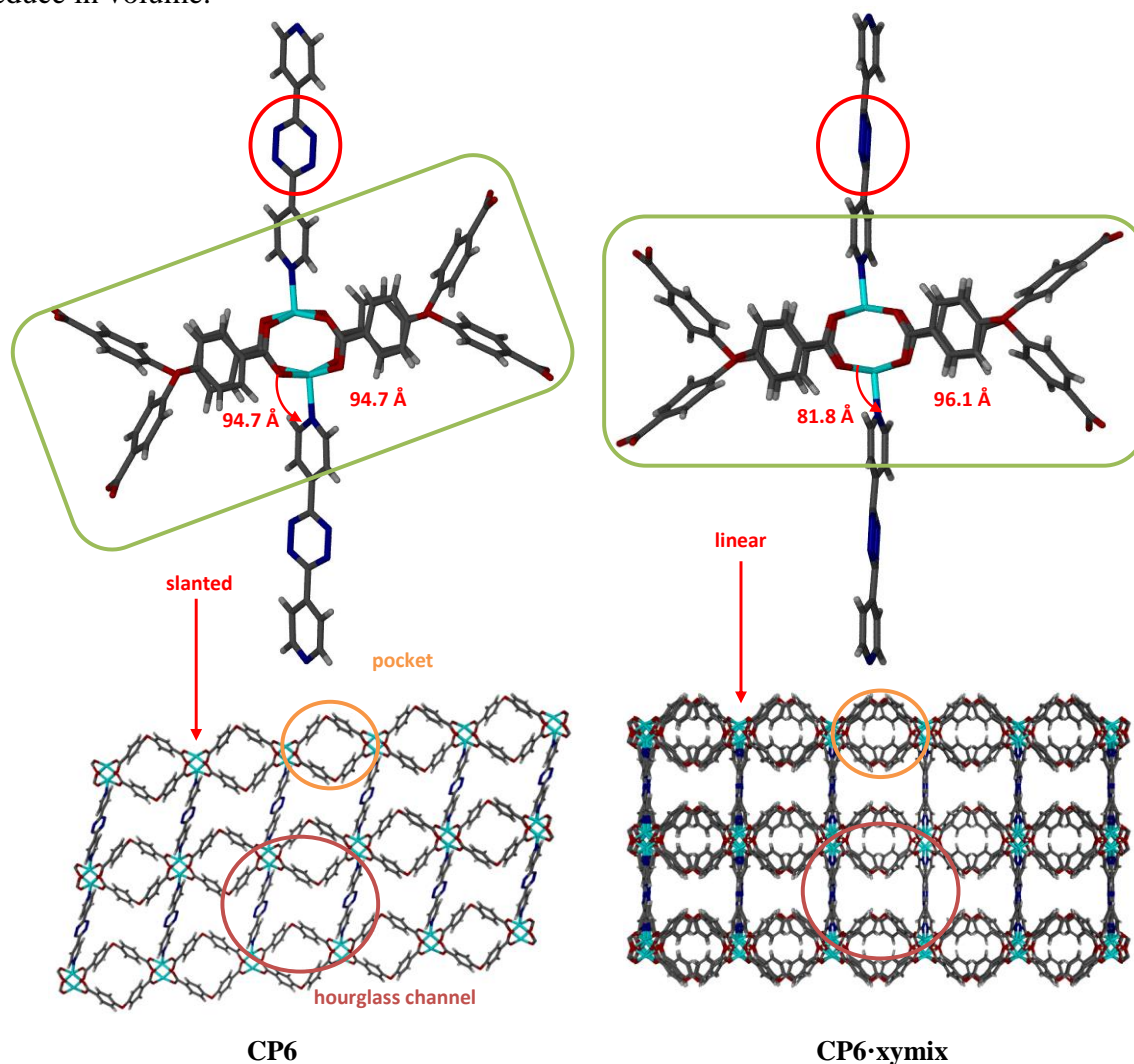


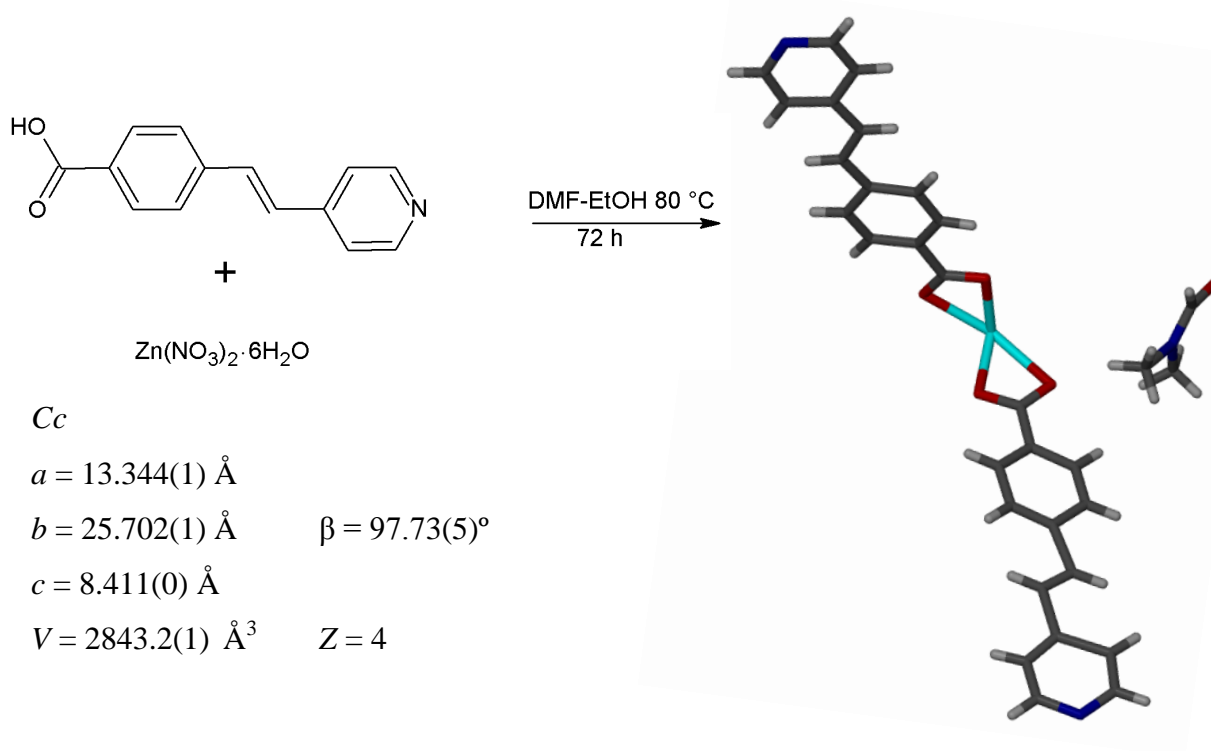
Figure 3.20 Comparison of individual paddlewheels and extended structures of **CP6** and **CP6·xymix**, both viewed along [0 1 0].

CHAPTER III: STRUCTURAL ANALYSIS AND GAS SORPTION STUDIES

3.3.9 $\{[\text{Zn}(\text{PYEB})_2]\cdot\text{DMF}\}_n$ or CP7

In 2011 Bharadwaj *et al.*⁸ reported a sevenfold interpenetrated porous framework containing the asymmetric ligand **PYEB** and zinc. The paper provided a detailed analysis of the framework as well as several SC-SC guest-exchange experiments. Although no activated form was described, a porous framework with such an unusually high degree of interpenetration and existing SC-SC guest exchange experiments seemed like an ideal candidate for gas-cell structural studies. The challenge of remaking this material was undertaken with the hope of activating the crystals and performing gas cell experiments with a view to modelling various gas molecules.

Using the solvothermal reaction described by Bharadwaj *et al.* **CP7** crystallises in the monoclinic space group *Cc* with the asymmetric unit comprising two **PYEB** ligands, one zinc cation and one DMF guest molecule (**Scheme 3.7**).



Scheme 3.7 Synthesis of **CP7** from the solvothermal reaction of **PYEB** and zinc nitrate in a DMF-EtOH mixture at 80 °C, with selected crystallographic information.

CHAPTER III: STRUCTURAL ANALYSIS AND GAS SORPTION STUDIES

The structure obtained is the same as that described in the literature. Each metal centre is coordinated to four **PYEB** ligands (two pyridine nitrogen atoms and three oxygen atoms) forming a distorted trigonal bipyramidal geometry (**Figure 3.21**). The **PYEB** ligand is co-planar with the pyridyl moiety twisted relative to the phenyl ring (dihedral angle 13.01°). The DMF molecule was modelled with full occupancy and the amount of guest present was further verified by thermogravimetric analysis, which shows a 12.4 wt% loss (1 DMF molecule per ASU) in the range 100 - 200 °C. The framework was then stable until decomposition at 420 °C.

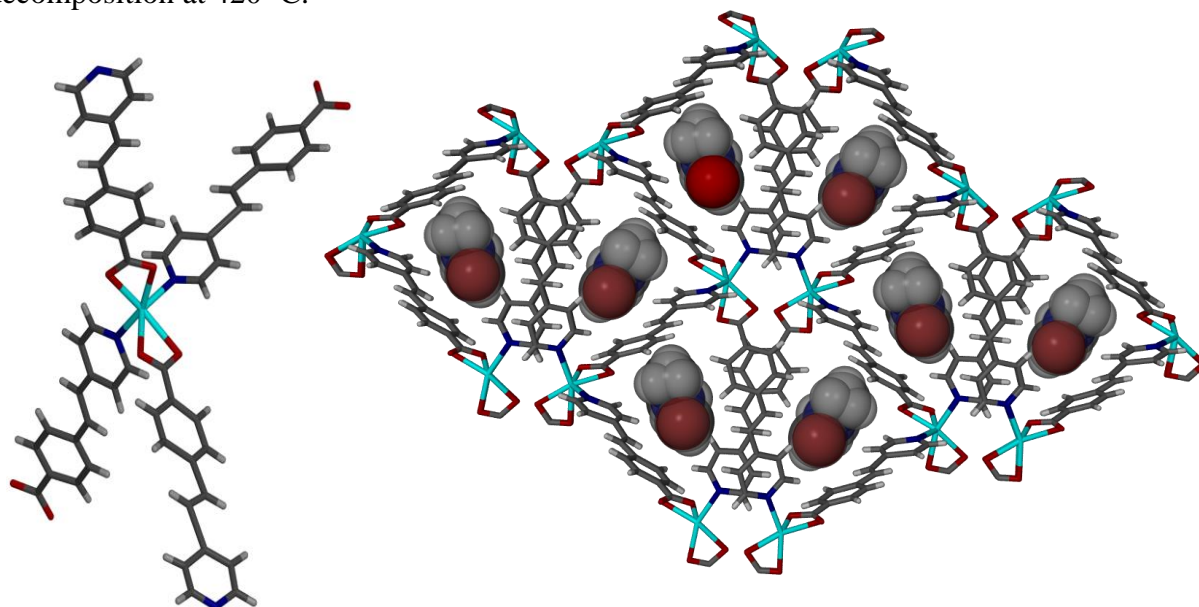


Figure 3.21 Distorted trigonal bipyramidal moiety (left) and extended view of **CP7** along [0 0 1] showing channels occupied by DMF molecules (right).

Gradual heating or exposure to supercritical CO₂ (a standard method for material activation) proved ineffective as the crystals of **CP7** immediately disintegrated. Solvent exchange experiments were then attempted in the hope that a smaller, more volatile guest would be able to vacate the channel more readily than DMF. Unfortunately, this was also unsuccessful and once again yielded polycrystalline powder. Attempts to replicate the solvent exchange experiments performed previously proved unsuccessful. Activation of **CP7**, without crystal deterioration also proved unsuccessful (in spite the fact that one of the co-authors recently joined the Barbour group and could also not explain why the study could not be repeated). The zinc salt was first replaced by cobalt(II) nitrate and then by manganese(II) nitrate in the hope of generating a similar porous highly interpenetrated MOF that would allow activation in a SC-SC manner.

CHAPTER III: STRUCTURAL ANALYSIS AND GAS SORPTION STUDIES

Substitution of Co(II) nitrate hexahydrate for the zinc salt, yielded **CP7a**.

3.3.10 $\{[\text{Co}(\text{PYEB})]\}_n$ or **CP7a**

This MOF crystallises in the orthorhombic space group *Aba2* with one **PYEB** and one cobalt metal in the ASU (**Figure 3.22**). Each metal centre is coordinated to four **PYEB** ligands (two pyridine nitrogen atoms and four oxygen atoms) possessing the same distorted trigonal bipyramidal geometry as **CP7**. Examination of the extended structure shows **CP7a** to be eightfold interpenetrated with the incorporation of an additional net weaving through the previously accessible pores, making this material non-porous (**Figure 3.23**).

Aba2

$$a = 13.008(1) \text{ \AA}$$

$$b = 21.879(4) \text{ \AA}$$

$$c = 8.674(9) \text{ \AA}$$

$$V = 2468.9(6) \text{ \AA}^3$$

$Z = 4$

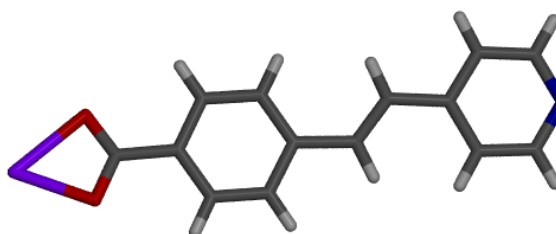


Figure 3.22 The ASU and selected crystallographic parameters for **CP7a**.

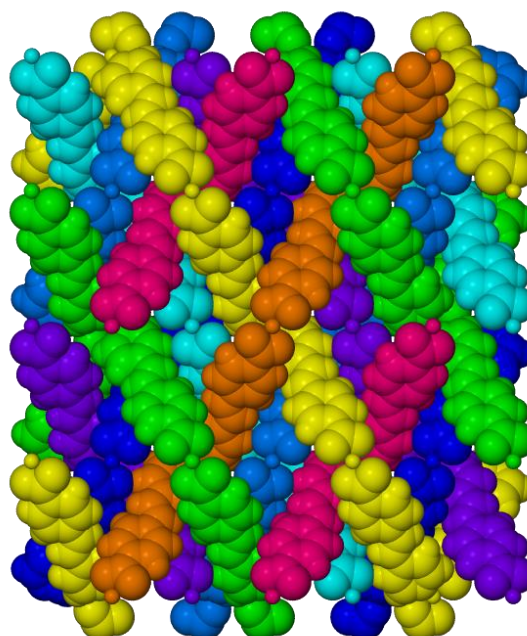


Figure 3.23 Space-fill packing diagram of **CP7a** viewed along $[0\ 0\ 1]$ showing the non-porous nature.

CHAPTER III: STRUCTURAL ANALYSIS AND GAS SORPTION STUDIES

Thermogravimetric analysis and SQUEEZE are in agreement, indicating no guest loss. Framework decomposition begins at 420 °C.

3.3.11 $\{[\text{Mn}_3(\text{PYEB})_6]\cdot\text{DMF}\cdot\text{EtOH}\}_n$ or **CP7b**

In a final attempt to obtain a highly interpenetrated activated MOF, the cobalt salt was replaced by a manganese salt and the crystallisation repeated. MOF **CP7b** crystallises in the monoclinic space group $P2_1$ and comprises three manganese metal centres, six **PYEB** ligands (one of which is disordered over two positions, 64:36 site occupancy), one DMF solvent molecule and one ethanol molecule (**Figure 3.24**). Unlike all the previous examples of MOFs with the **PYEB** ligands, **CP7b** involves a unique three-metal paddlewheel moiety wherein two manganese metal ions have octahedral coordination geometry while the third central ion is tetrahedral (**Figure 3.25**). Both the central metal and one of the peripheral metals are located on special positions. Another point of interest is that, of the ten ligands present in the paddlewheel moiety, two remain mono-coordinated (**Figure 3.25**). As a result this framework is only twofold interpenetrated with DMF and ethanol guest molecules present in the channels (**Figure 3.26**).

$P2_1$

$a = 13.467(8) \text{ \AA}$

$b = 18.637(1) \text{ \AA}$

$c = 15.833(7) \text{ \AA}$

$V = 3879.5(1) \text{ \AA}^3$

$\beta = 102.53(7)^\circ$

$Z = 2$

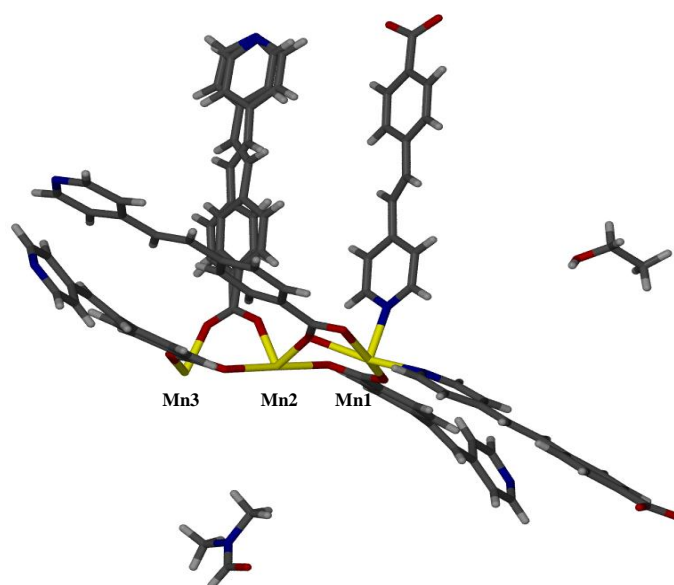


Figure 3.24 Synthesis of **CP7b** from the solvothermal reaction of **PYEB** and manganese nitrate in a DMF-EtOH mixture at 80 °C, with selected crystallographic information.

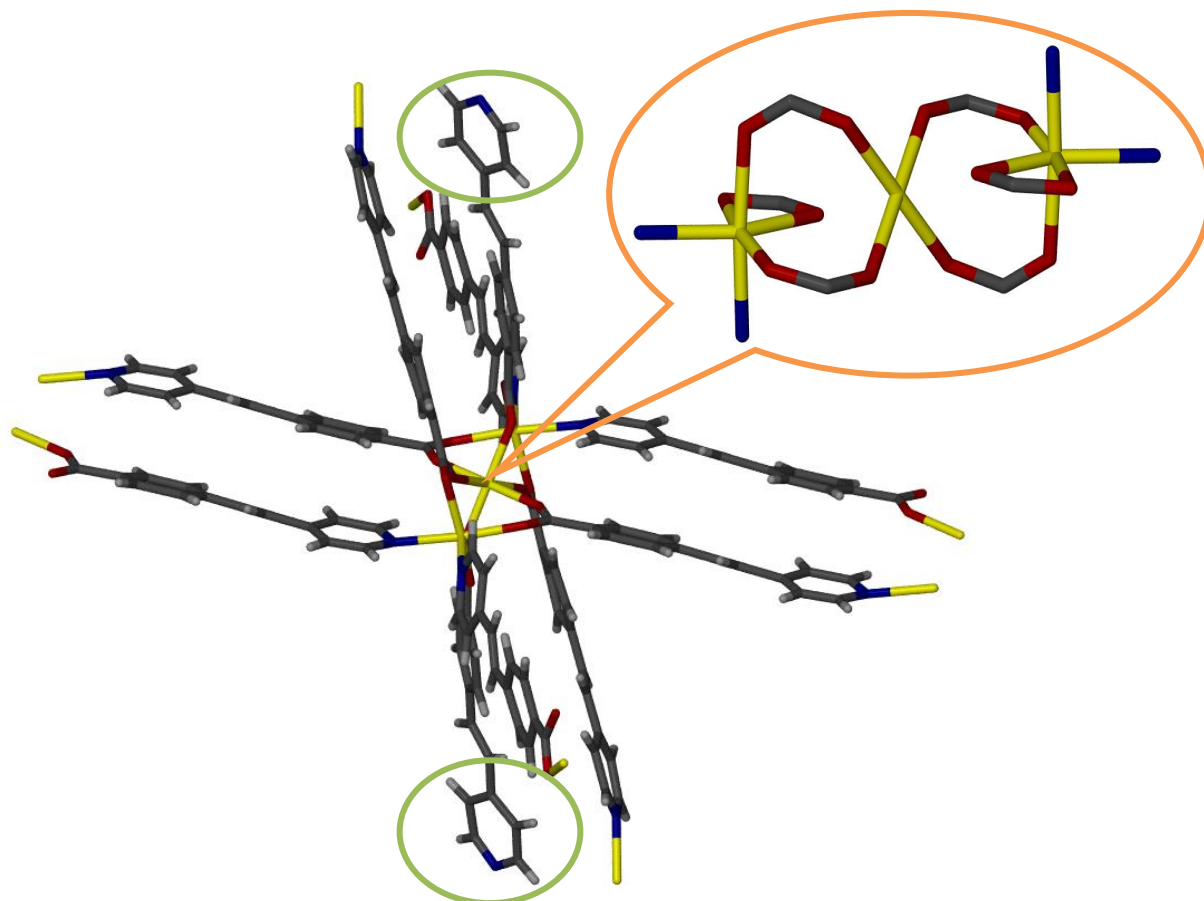


Figure 3.25 CP7b paddlewheel geometry and mono-coordinated ligands ringed in green.

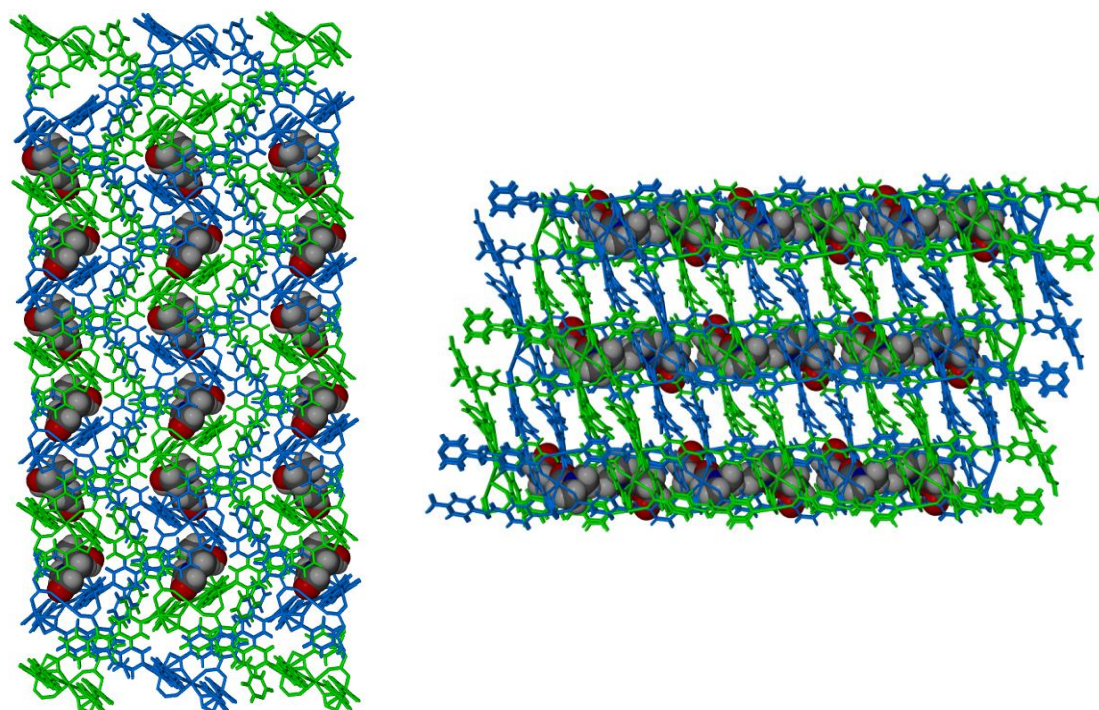


Figure 3.26 Extended view of CP7b along [0 0 1] (left) and [0 1 0] (right) showing channels occupied by DMF.

CHAPTER III: STRUCTURAL ANALYSIS AND GAS SORPTION STUDIES

TGA analysis agrees with SQUEEZE, showing a 6.79 wt% loss in the region 125 - 225 °C (one DMF and one ethanol molecule per ASU), with decomposition setting in at 410 °C. The apohost form (**CP7b'**) was generated by heating the solvate at 200 °C under reduced pressure for 24 h. Due to the robust nature of the framework, this occurred as a SC-SC transformation. The space group changed from $P2_1$ to $P2_1/c$ with the cell parameters experiencing some reduction in length (**Figure 3.27**). The framework is found to be non-porous. Although a framework composed of solely **PYEB** ligands coordinated to metal ions was obtained and activated as a SC-SC transformation, no highly interpenetrated form was acquired (**Figure 3.28**).

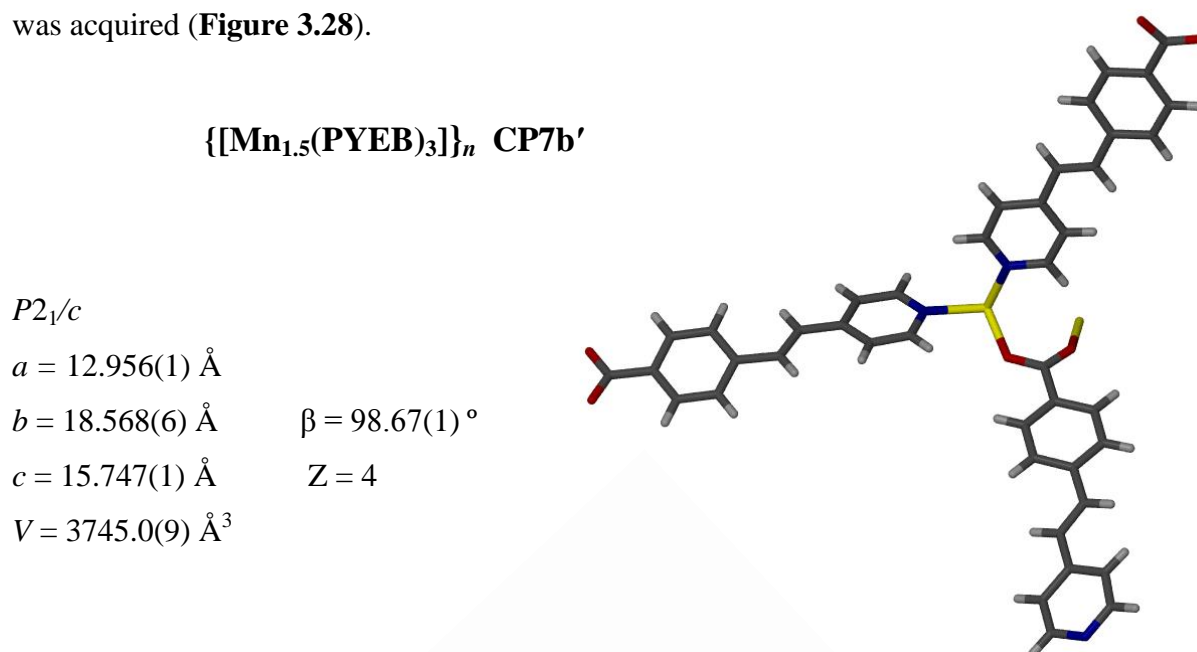


Figure 3.27 The ASU of **CP7b'**, with selected crystallographic parameters.

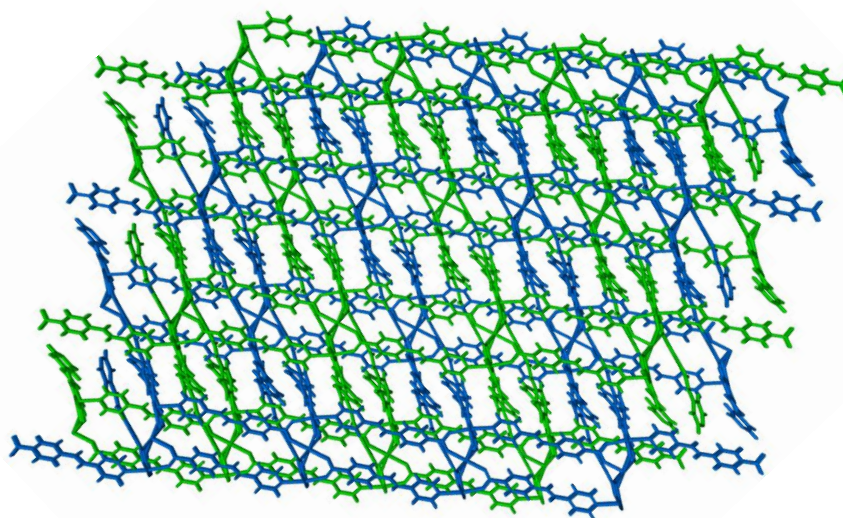


Figure 3.28 Extended view of **CP7b'** along $[0\ 1\ 0]$ showing unoccupied channels.

3.4 Conclusion

By combining the four symmetrical N-donor ligands (**L1-L4**) selected from the literature with a selection of aryl dicarboxylic acid ligands varying in length and flexibility, with a series of divalent metal salts, a succession of structurally diverse MOFs were obtained. The 2D and 3D frameworks show varying degrees of interpenetration and porosity. Although not all materials retained crystallinity or bulk phase purity, gas sorption experiments were performed on **CP3** and **CP5'**. In addition to this, **CP3**, **CP5**, **CP6** and **CP7b** all underwent SC-SC exchange experiments. This study shows that variation of MOF properties may be achieved through modification of the components as well as use of the same crystallisation components treated under different crystallisation conditions. This study has generated twenty-one new MOFs and further examination of such materials may prove useful in establishing a set of protocols in order to rationally design targeted functional materials for a broad range of applications.

3.5 Synthesis of metal organic frameworks CP1-CP7b

CP1: A mixture of $\text{Co}(\text{NO}_3)_2 \cdot 6\text{H}_2\text{O}$ (15 mg 0.05 mmol), **OBA** (13 mg 0.05 mmol) and **L1** (8.5 mg 0.03 mmol) in a DMF:DMSO solution (4.5:0.5 mL) was heated to 120 °C in a sintered glass vial for 24 h. Purple-red diamond-shaped crystals were obtained.

CP2: A mixture of $\text{Zn}(\text{NO}_3)_2 \cdot 6\text{H}_2\text{O}$ (15 mg, 0.05 mmol), **PDC** (8 mg 0.05 mmol) and **L1** (8.5 mg 0.03 mmol) in DMF (5 mL) was heated to 100 °C in a sintered glass vial for 24 h. Colourless block-shaped crystals were obtained.

CP3: A mixture of $\text{Cd}(\text{NO}_3)_2 \cdot 4\text{H}_2\text{O}$ (9 mg, 0.04 mmol), **ADB** (14 mg 0.05 mmol) and **L2** (8 mg 0.03 mmol) in DMF (5 mL) was heated to 100 °C in a sintered glass vial for 24 h. Yellow rectangular crystals were obtained.

CP4: A mixture of $\text{Cd}(\text{NO}_3)_2 \cdot 4\text{H}_2\text{O}$ (9 mg, 0.04 mmol), **OBA** (13 mg 0.05 mmol) and **L2** (8.5 mg 0.03 mmol) in a DMF:DMSO solution (4.5:0.5 mL) was heated to 100 °C in a sintered glass vial for 24 h. Colourless block-shaped crystals were obtained.

CHAPTER III: STRUCTURAL ANALYSIS AND GAS SORPTION STUDIES

CP5: A mixture of $\text{Zn}(\text{NO}_3)_2 \cdot 6\text{H}_2\text{O}$ (15 mg 0.05 mmol), **OBA** (13 mg 0.05 mmol) and **L3** (6.3 g 0.03 mmol) in DMF (5 mL) was heated to 120 °C in a sintered glass vial for 48h. Yellow block-shaped crystals were obtained.

CP5a: A mixture of $\text{Cd}(\text{NO}_3)_2 \cdot 4\text{H}_2\text{O}$ (9 mg, 0.04 mmol), **OBA** (13 mg 0.05 mmol) and **L3** (6.3 mg 0.03 mmol) in a DMA:DMSO solution (4.5:0.5 mL) was heated to 120 °C in an autoclave for 24 h. Colourless rectangular crystals were obtained.

CP6: A mixture $\text{Zn}(\text{NO}_3)_2 \cdot 6\text{H}_2\text{O}$ (29 mg 0.10 mmol), **OBA** (26 mg 0.10 mmol) and **L4** (24 mg 0.10 mmol) in 50:50 v/v solution of DMF-EtOH (5 mL) was heated to 80 °C in an autoclave for 24 h. Pink rectangular needle-shaped crystals were obtained.

CP7: A mixture of $\text{Zn}(\text{NO}_3)_2 \cdot 6\text{H}_2\text{O}$ (149 mg 0.50 mmol) and **PYEB** (113 mg 0.50 mmol) in 50:50 v/v solution of DMF-EtOH (4 mL) was heated to 80 °C in an autoclave for 72 h. Pale orange needle-shaped crystals were obtained.

CP7a: A mixture of $\text{Co}(\text{NO}_3)_2 \cdot 6\text{H}_2\text{O}$ (146 mg 0.50 mmol) and **PYEB** (113 mg 0.50 mmol) in an 50:50 v/v solution of DMF-EtOH (4 mL) was heated to 80 °C in an autoclave for 72 h. Red needle-shaped crystals were obtained.

CP7b: A mixture of $\text{Mn}(\text{NO}_3)_2 \cdot 6\text{H}_2\text{O}$ (126 mg 0.50 mmol) and **PYEB** (113 mg 0.50 mmol) in an 50:50 v/v solution of DMF-EtOH (4 mL) was heated to 80 °C in an autoclave for 72 h. Yellow block-shaped crystals were obtained.

CHAPTER III: STRUCTURAL ANALYSIS AND GAS SORPTION STUDIES

	CP1	CP2	CP2_SCO ₂
Empirical formula	C ₅₃ H ₄₃ Co ₂ N ₄ O ₁₃	C ₂₀ H ₂₀ N ₄ O ₉ Zn ₂	C ₁₇ H ₁₃ N ₃ O ₉ Zn ₂
Formula weight	1049.76	637.15	534.08
Temperature (K)	100 K	100 K	100 K
Wavelength (Å)	0.71073	0.71073	0.71073
Crystal system	Monoclinic	Monoclinic	Monoclinic
<i>a</i> /Å	13.737(3)	13.985(2)	14.187(4)
<i>b</i> /Å	24.621(5)	12.144(2)	12.113(2)
<i>c</i> /Å	16.219(3)	14.661(2)	14.322(4)
α /°	90.0	90.0	90.0
β /°	113.483(2)	105.895(2)	105.153(3)
γ /°	90.0	90.0	90.0
Space group	<i>P</i> 21/ <i>n</i>	<i>P</i> 21/ <i>n</i>	<i>P</i> 21/ <i>n</i>
Volume (Å ³)	5031.3(2)	2394.7(6)	2375.6(1)
<i>Z</i>	4	4	4
Calculated density (g cm ⁻³)	1.386	1.767	1.493
Absorption coefficient (mm ⁻¹)	0.726	2.072	2.067
<i>F</i> ₀₀₀	2164.8	1297.6	1072.0
θ range for data collection (°)	1.60 to 28.21	1.78 to 28.32	2.24 to 28.20
Miller index ranges	-17 ≤ <i>h</i> ≤ 16, -28 ≤ <i>k</i> ≤ 32, -19 ≤ <i>l</i> ≤ 21	-18 ≤ <i>h</i> ≤ 14, -15 ≤ <i>k</i> ≤ 16, -14 ≤ <i>l</i> ≤ 18	-17 ≤ <i>h</i> ≤ 8, -15 ≤ <i>k</i> ≤ 15, -17 ≤ <i>l</i> ≤ 18
Reflections collected	30340	14696	12977
Independent reflections	11611	5565	5437
Completeness to θ_{\max} (%)	93.6	93.0	93.1
Max. and min. transmission	0.9784, 0.9047	0.7716, 0.5300	0.7099, 0.3854
Refinement method	Full-matrix least-squares on <i>F</i> ²	Full-matrix least-squares on <i>F</i> ²	Full-matrix least-squares on <i>F</i> ²
Data / restraints / parameters	8499/ 2/604	4572/16/417	3604/0/283
Goodness-of-fit on <i>F</i> ²	1.042	1.028	1.041
Final <i>R</i> indices [<i>I</i> > 2 σ (<i>I</i>)]	<i>R</i> 1 = 0.0460, <i>wR</i> 2 = 0.0608	<i>R</i> 1 = 0.0363, <i>wR</i> 2 = 0.0863	<i>R</i> 1 = 0.0660, <i>wR</i> 2 = 0.01740

CHAPTER III: STRUCTURAL ANALYSIS AND GAS SORPTION STUDIES

	CP2_ACN	CP2_Dioxane	CP2_NB
Empirical formula	C ₁₉ H ₁₆ N ₄ O ₉ Zn ₂	C ₂₂ H ₂₃ N ₃ O ₁₂ Zn ₂	C ₄₂ H ₃₃ N ₇ O ₂₁ Zn ₄
Formula weight	575.14	650.0	620.26
Temperature (K)	100 K	100 K	100 K
Wavelength (Å)	0.71073	0.71073	0.71073
Crystal system	Monoclinic	Monoclinic	Monoclinic
<i>a</i> /Å	14.063(2)	14.006(5)	13.796(6)
<i>b</i> /Å	12.0287(2)	12.191(5)	12.211(6)
<i>c</i> /Å	14.381(2)	14.621(6)	14.856(7)
α /°	90.0	90.0	90.0
β /°	105.108(2)	105.294(5)	105.891(5)
γ /°	90.0	90.0	90.0
Space group	<i>P</i> 21/ <i>n</i>	<i>P</i> 21/ <i>n</i>	<i>P</i> 21/ <i>n</i>
Volume (Å ³)	2348.6(6)	2408.1(2)	2407.0(2)
<i>Z</i>	4	4	4
Calculated density (g cm ⁻³)	1.627	1.793	1.712
Absorption coefficient (mm ⁻¹)	2.098	2.064	2.058
<i>F</i> ₀₀₀	1160.0	1324.4	1251.2
θ range for data collection (°)	1.80 to 28.23	1.79 to 28.24	2.19 to 28.26
Miller index ranges	-18 ≤ <i>h</i> ≤ 11, -14 ≤ <i>k</i> ≤ 15, -10 ≤ <i>l</i> ≤ 19	-18 ≤ <i>h</i> ≤ 18, -15 ≤ <i>k</i> ≤ 13, -15 ≤ <i>l</i> ≤ 18	-17 ≤ <i>h</i> ≤ 17, -12 ≤ <i>k</i> ≤ 16, -19 ≤ <i>l</i> ≤ 15
Reflections collected	14530	13900	11311
Independent reflections	5372	5559	5163
Completeness to θ_{\max} (%)	92.9	93.2	81.3
Max. and min. transmission	0.7563, 0.5642	0.7957, 0.6595	0.8206, 0.6198
Refinement method	Full-matrix least-squares on <i>F</i> ²	Full-matrix least-squares on <i>F</i> ²	Full-matrix least-squares on <i>F</i> ²
Data / restraints / parameters	3546/6/302	3990/22/339	3019/6/319
Goodness-of-fit on <i>F</i> ²	0.951	1.088	0.998
Final <i>R</i> indices [<i>I</i> > 2σ(<i>I</i>)]	<i>R</i> 1 = 0.0502, <i>wR</i> 2 = 0.1299	<i>R</i> 1 = 0.0666, <i>wR</i> 2 = 0.1747	<i>R</i> 1 = 0.0813 <i>wR</i> 2 = 0.1910

CHAPTER III: STRUCTURAL ANALYSIS AND GAS SORPTION STUDIES

	CP3	CP4	CP5
Empirical formula	C ₄₃ H ₄₁ CdN ₇ O ₇	C ₄₀ H ₃₄ CdN ₄ O ₇	C ₄₆ H ₄₁ N ₆ O ₁₂ Zn ₂
Formula weight	880.24	795.20	1009.71
Temperature (K)	100 K	100 K	100 K
Wavelength (Å)	0.71073	0.71073	0.71073
Crystal system	Triclinic	Monoclinic	Monoclinic
<i>a</i> /Å	12.282(2)	32.417(2)	12.257(6)
<i>b</i> /Å	13.356(3)	8.978(5)	26.652(1)
<i>c</i> /Å	13.852(3)	30.085(2)	15.530(7)
α /°	78.083(1)	90.0	90.0
β /°	77.175(9)	109.711(5)	96.375(5)
γ /°	76.535(9)	90.0	90.0
Space group	<i>P</i> $\bar{1}$	<i>C</i> 2/ <i>c</i>	<i>P</i> 2 ₁ / <i>c</i>
Volume (Å ³)	2125.8(8)	8243(8)	1009.71
<i>Z</i>	2	8	4
Calculated density (g cm ⁻³)	1.375	1.281	1.330
Absorption coefficient (mm ⁻¹)	0.571	0.579	1.015
<i>F</i> ₀₀₀	904.0	3248.3	2078.1
θ range for data collection (°)	1.53 to 28.93	2.27 to 28.33	1.67 to 28.33
Miller index ranges	-16 ≤ <i>h</i> ≤ 16, -18 ≤ <i>k</i> ≤ 18, -18 ≤ <i>l</i> ≤ 18	-35 ≤ <i>h</i> ≤ 41, -11 ≤ <i>k</i> ≤ 11, -37 ≤ <i>l</i> ≤ 38	-15 ≤ <i>h</i> ≤ 13, -25 ≤ <i>k</i> ≤ 35, -15 ≤ <i>l</i> ≤ 19
Reflections collected	82668	21780	26682
Independent reflections	10737	9455	11332
Completeness to θ_{\max} (%)	95.5	92.1	90.0
Max. and min. transmission	0.924, 0.761	0.955, 0.899	0.938, 0.595
Refinement method	Full-matrix least-squares on <i>F</i> ²	Full-matrix least-squares on <i>F</i> ²	Full-matrix least-squares on <i>F</i> ²
Data / restraints / parameters	5988/4/455	3990/39/484	4863/600/650
Goodness-of-fit on <i>F</i> ²	2.175	0.969	1.023
Final <i>R</i> indices [<i>I</i> > 2 σ (<i>I</i>)]	<i>R</i> 1 = 0.2154, <i>wR</i> 2 = 0.5436	<i>R</i> 1 = 0.0968, <i>wR</i> 2 = 0.2286	<i>R</i> 1 = 0.1066, <i>wR</i> 2 = 0.2570

CHAPTER III: STRUCTURAL ANALYSIS AND GAS SORPTION STUDIES

	CP5'	CP5'_ACN	CP5'_DMA
Empirical formula	C ₄₀ H ₂₆ N ₄ O ₁₀ Zn ₂	C ₄₅ H ₃₄ N ₇ O ₁₀ Zn ₂	C ₄₈ H ₄₃ N ₆ O ₁₂ Zn ₂
Formula weight	853.43	962.43	1026.66
Temperature (K)	100 K	100 K	100 K
Wavelength (Å)	0.71073	0.71073	0.71073
Crystal system	Monoclinic	Monoclinic	Monoclinic
<i>a</i> /Å	12.5541(2)	12.1457(7)	12.620(3)
<i>b</i> /Å	26.415(4)	25.6660(1)	26.405(6)
<i>c</i> /Å	15.696(3)	16.3921(9)	15.618(4)
α /°	90.0	90.0	90.0
β /°	97.845(2)	100.822(1)	98.040(3)
γ /°	90.0	90.0	90.0
Space group	<i>P</i> 2 ₁ / <i>c</i>	<i>P</i> 2 ₁ / <i>c</i>	<i>P</i> 2 ₁ / <i>c</i>
Volume (Å ³)	5156.3	5019.1(5)	5153(2)
<i>Z</i>	4	4	4
Calculated density (g cm ⁻³)	1.099	1.274	1.323
Absorption coefficient (mm ⁻¹)	0.977	1.014	0.994
<i>F</i> ₀₀₀	1736	1968	2116
θ range for data collection (°)	1.52 to 28.24	1.59 to 28.30	1.53 to 28.34
Miller index ranges	-15 ≤ <i>h</i> ≤ 16, -32 ≤ <i>k</i> ≤ 35, -20 ≤ <i>l</i> ≤ 10	-15 ≤ <i>h</i> ≤ 16, -33 ≤ <i>k</i> ≤ 23, -18 ≤ <i>l</i> ≤ 20	-16 ≤ <i>h</i> ≤ 15, -34 ≤ <i>k</i> ≤ 29, -20 ≤ <i>l</i> ≤ 19
Reflections collected	30655	31481	30169
Independent reflections	11852	11435	11820
Completeness to θ_{\max} (%)	93.0	91.6	92.0
Max. and min. transmission	0.808, 0.498	0.869, 0.663	0.774, 0.494
Refinement method	Full-matrix least-squares on <i>F</i> ²	Full-matrix least-squares on <i>F</i> ²	Full-matrix least-squares on <i>F</i> ²
Data / restraints / parameters	5113/488/505	8902/438/609	8934/552/687
Goodness-of-fit on <i>F</i> ²	1.059	1.049	1.107
Final <i>R</i> indices [<i>I</i> > 2 σ (<i>I</i>)]	<i>R</i> 1 = 0.1152, <i>wR</i> 2 = 0.3529	<i>R</i> 1 = 0.0565, <i>wR</i> 2 = 0.1625	<i>R</i> 1 = 0.1186, <i>wR</i> 2 = 0.3155

CHAPTER III: STRUCTURAL ANALYSIS AND GAS SORPTION STUDIES

	CP5'_Dioxane	CP5'_NB	CP5a
Empirical formula	C ₄₉ H ₄₃ N ₄ O ₁₄ Zn ₂	C ₅₂ H ₃₇ N ₆ O ₁₄ Zn ₂	C ₃₄ H ₃₈ CdN ₆ O ₈
Formula weight	1041.00	1100.66	771.11
Temperature (K)	100 K	100 K	100 K
Wavelength (Å)	0.71073	0.71073	0.71073
Crystal system	Monoclinic	Monoclinic	Monoclinic
<i>a</i> /Å	12.372(4)	13.158(6)	12.256(6)
<i>b</i> /Å	26.509(8)	25.905(1)	10.094(5)
<i>c</i> /Å	15.623(5)	15.347(8)	29.730(2)
α /°	90.0	90.0	90.0
β /°	97.294(4)	98.819(6)	100.418(7)
γ /°	90.0	90.0	90.0
Space group	<i>P</i> 2 ₁ / <i>c</i>	<i>P</i> 2 ₁ / <i>c</i>	<i>P</i> 2 ₁ / <i>c</i>
Volume (Å ³)	5082(3)	5169(4)	3617(3)
<i>Z</i>	4	4	4
Calculated density (g cm ⁻³)	1.361	1.414	1.416
Absorption coefficient (mm ⁻¹)	1.011	0.999	0.660
<i>F</i> ₀₀₀	2411.8	2252.0	1584
θ range for data collection (°)	1.52 to 28.31	1.5 to 28.35	1.69 to 28.30
Miller index ranges	-16 ≤ <i>h</i> ≤ 10, -33 ≤ <i>k</i> ≤ 31, -20 ≤ <i>l</i> ≤ 20	-17 ≤ <i>h</i> ≤ 15, -32 ≤ <i>k</i> ≤ 31, -17 ≤ <i>l</i> ≤ 19	-16 ≤ <i>h</i> ≤ 16, -13 ≤ <i>k</i> ≤ 13, -39 ≤ <i>l</i> ≤ 39
Reflections collected	27315	8312	94192
Independent reflections	11480	6350	8979
Completeness to θ_{\max} (%)	90.8	98.0	99.7
Max. and min. transmission	0.882, 0.644	0.828, 0.600	0.930, 0.738
Refinement method	Full-matrix least-squares on <i>F</i> ²	Full-matrix least-squares on <i>F</i> ²	Full-matrix least-squares on <i>F</i> ²
Data / restraints / parameters	8416/629/671	4241/1284/605	8146/384/494
Goodness-of-fit on <i>F</i> ²	1.156	1.056	1.193
Final <i>R</i> indices [<i>I</i> > 2 σ (<i>I</i>)]	<i>R</i> 1 = 0.1345, <i>wR</i> 2 = 0.3110	<i>R</i> 1 = 0.0995, <i>wR</i> 2 = 0.2646	<i>R</i> 1 = 0.0727, <i>wR</i> 2 = 0.1811

CHAPTER III: STRUCTURAL ANALYSIS AND GAS SORPTION STUDIES

	CP6	CP6_xymix	CP7
Empirical formula	C ₂₄ H ₂₂ N ₄ O ₇ Zn	C ₄₀ H ₂₄ N ₆ O ₁₀ Zn ₂	C ₃₁ H ₂₇ N ₃ O ₅ Zn
Formula weight	535.46	879.43	586.95
Temperature (K)	100 K	100 K	289 K
Wavelength (Å)	0.71073	0.71073	0.71073
Crystal system	Monoclinic	Monoclinic	Monoclinic
<i>a</i> /Å	27.739(5)	14.065 (2)	13.344(4)
<i>b</i> /Å	7.536(1)	23.367(3)	25.700(7)
<i>c</i> /Å	23.793(5)	15.686(6)	8.410(2)
α /°	90.0	90.0	90.0
β /°	105.579(2)	106.220(6)	99.735(5)
γ /°	90.0	90.0	90.0
Space group	<i>C2/c</i>	<i>P2/c</i>	<i>Cc</i>
Volume (Å ³)	4791.0(2)	4950.3(1)	2842.6(1)
<i>Z</i>	8	4	4
Calculated density (g cm ⁻³)	1.485	1.180	1.372
Absorption coefficient (mm ⁻¹)	1.075	1.021	0.908
<i>F</i> ₀₀₀	2204.5	1784.0	1216
θ range for data collection (°)	1.78 to 28.25	1.51 to 28.43	1.74 to 28.22
Miller index ranges	-31 ≤ <i>h</i> ≤ 35, -9 ≤ <i>k</i> ≤ 9, -30 ≤ <i>l</i> ≤ 31	-18 ≤ <i>h</i> ≤ 18, -30 ≤ <i>k</i> ≤ 31, -20 ≤ <i>l</i> ≤ 20	-17 ≤ <i>h</i> ≤ 17, -32 ≤ <i>k</i> ≤ 23, -11 ≤ <i>l</i> ≤ 10
Reflections collected	13122	197368	8941
Independent reflections	5438	12271	5635
Completeness to θ_{\max} (%)	92.0	98.4	98.0
Max. and min. transmission	0.897, 0.584	0.903, 0.565	0.913, 0.835
Refinement method	Full-matrix least-squares on <i>F</i> ²	Full-matrix least-squares on <i>F</i> ²	Full-matrix least-squares on <i>F</i> ²
Data / restraints / parameters	3951/3/334	4185/498/506	3159/6/365
Goodness-of-fit on <i>F</i> ²	1.070	2.179	0.976
Final <i>R</i> indices [<i>I</i> > 2 σ (<i>I</i>)]	<i>R</i> 1 = 0.0500, <i>wR</i> 2 = 0.1149	<i>R</i> 1 = 0.2839, <i>wR</i> 2 = 0.6185	<i>R</i> 1 = 0.0682, <i>wR</i> 2 = 0.1105

CHAPTER III: STRUCTURAL ANALYSIS AND GAS SORPTION STUDIES

	CP7a	CP7b	CP7b'
Empirical formula	C ₂₈ H ₂₀ Co N ₂ O ₄	C ₈₉ H ₇₄ Mn ₃ N ₇ O ₁₄	C ₈₄ H ₆₀ Mn ₃ N ₆ O ₁₂
Formula weight	507.39	1630.10	1510.20
Temperature (K)	100 (2)	100 K	100 K
Wavelength (Å)	0.71073	0.71073	0.71073
Crystal system	Orthorhombic	Monoclinic	Monoclinic
<i>a</i> /Å	13.008(3)	13.609(1)	12.9561(2)
<i>b</i> /Å	21.879(7)	18.818(2)	18.569(3)
<i>c</i> /Å	8.675(2)	16.017(1)	15.747(2)
α /°	90.0	90.0	90.0
β /°	90.0	102.670(1)	98.670(2)
γ /°	90.0	90.0	90.0
Space group	<i>Aba</i> 2	<i>P</i> 2 ₁ / <i>c</i>	<i>P</i> 2 ₁ / <i>c</i>
Volume (Å ³)	2469.0(1)	4002(6)	3745.2(9)
<i>Z</i>	4	2	2
Calculated density (g cm ⁻³)	1.365	1.353	1.339
Absorption coefficient (mm ⁻¹)	0.731	0.536	0.565
<i>F</i> ₀₀₀	1044	1687.4	1554
θ range for data collection (°)	2.43 to 28.30	1.53 to 28.40	1.71 to 28.21
Miller index ranges	-17 ≤ <i>h</i> ≤ 17, -27 ≤ <i>k</i> ≤ 26, -11 ≤ <i>l</i> ≤ 6	-17 ≤ <i>h</i> ≤ 18, -24 ≤ <i>k</i> ≤ 24, -20 ≤ <i>l</i> ≤ 20	-14 ≤ <i>h</i> ≤ 17, -23 ≤ <i>k</i> ≤ 19, -20 ≤ <i>l</i> ≤ 19
Reflections collected	7334	108314	22420
Independent reflections	2361	19485	8601
Completeness to θ_{\max} (%)	77.0	0.97	93.2
Max. and min. transmission	0.9141, 0.8083	0.943, 0.907	0.8764, 0.7942
Refinement method	Full-matrix least-squares on <i>F</i> ²	Full-matrix least-squares on <i>F</i> ²	Full-matrix least-squares on <i>F</i> ²
Data / restraints / parameters	1966/ 1/ 159	1766017/1124	7063/ 0/ 475
Goodness-of-fit on <i>F</i> ²	1.086	1.058	1.024
Final <i>R</i> indices [<i>I</i> > 2σ(<i>I</i>)]	<i>RI</i> = 0.0453 and <i>WR2</i> = 0.112	<i>RI</i> = 0.0422 and <i>WR2</i> = 0.1022	<i>RI</i> = 0.036 and <i>WR2</i> = 0.083

3.7 References

- 1 A. V. Gutov, E. B. Rusanov, L. V. Chepeleva, S. G. Garasevich, A. B. Ryabitskii, A. N. Chernega, *Russ. J. Gen. Chem.*, **2009**, *79*, 1513.
- 2 P. Nguyen, Z. Yuan, L. Agocs, G. Lesley, T. B. Marder, *Inorg. Chim. Acta.*, **1994**, *220*, 289.
- 3 F.-L. Yang, M.-G. Chen, X.-L. Li, J. Tao, R.-B. Huang, L. -S. Zheng, *Eur. J. Inorg. Chem.*, **2013**, *24*, 4234.
- 4 N. S. Oxtoby, A. J. Blake, N. R. Champness, C. Wilson, *CrystEngComm.*, **2003**, *5*, 82.
- 5 Barbour, L. J., *Chem. Commun.*, **2006**, 1163.
- 6 M. Y. Masoomi, K. C. Stylianou, A. Morsali, P. Retailleau, D. Maspoch, *Cryst. Growth Des.*, **2014**, *14*, 2092.
- 7 J. Li, H. Liang, Y. Yu, B. Xin, G. Li, Z. Shi, S. Feng, *Eur. J. Inorg. Chem.*, **2011**, 2712.
- 8 M. K. Sharma, P. Lama, P. K. Bharadwaj, *Cryst. Growth Des.*, **2011**, *1*, 1411.

CHAPTER **IV****Tuning MOF sequestration and storage**

Petrochemical and commodity chemical industries have been powering many aspects of modern living since the rise of the industrial revolution in the 18th century - the molecules generated by these industries are both beneficial and detrimental.¹ Examples of this include the combustion oxidation of hydrogen, methane and light hydrocarbons as a source of energy, which sustains various aspects of human society but a by-product of which is the formation of anthropogenic CO₂, a key factor in greenhouse gas emissions.² Despite the established nature of the industry, there is still a tremendous need for improved separation and sequestration technologies. Conventional separation methods such as condensation and distillation no longer present viable options due to their high-energy (thus high cost) and environmentally unfriendly processes (leeching heavy metals into the ground and contaminating water sources). MOFs (metal-organic frameworks) have certain unique features not encountered in conventional porous materials such as zeolites, which include, channels that can be rationally tuned, functional sites that can be readily immobilised and framework dynamism (transformations include bond breaking and forming,³ dimensionality increasing and decreasing,⁴ unit cell volume expansion and contraction,⁵ layer slipping⁶ and interpenetrated network shifting⁷). As a result, recent years have seen the rapid development of MOFs due to their potential applications in gas storage, separation and catalysis.^{8,9,10,11,12,13,14}

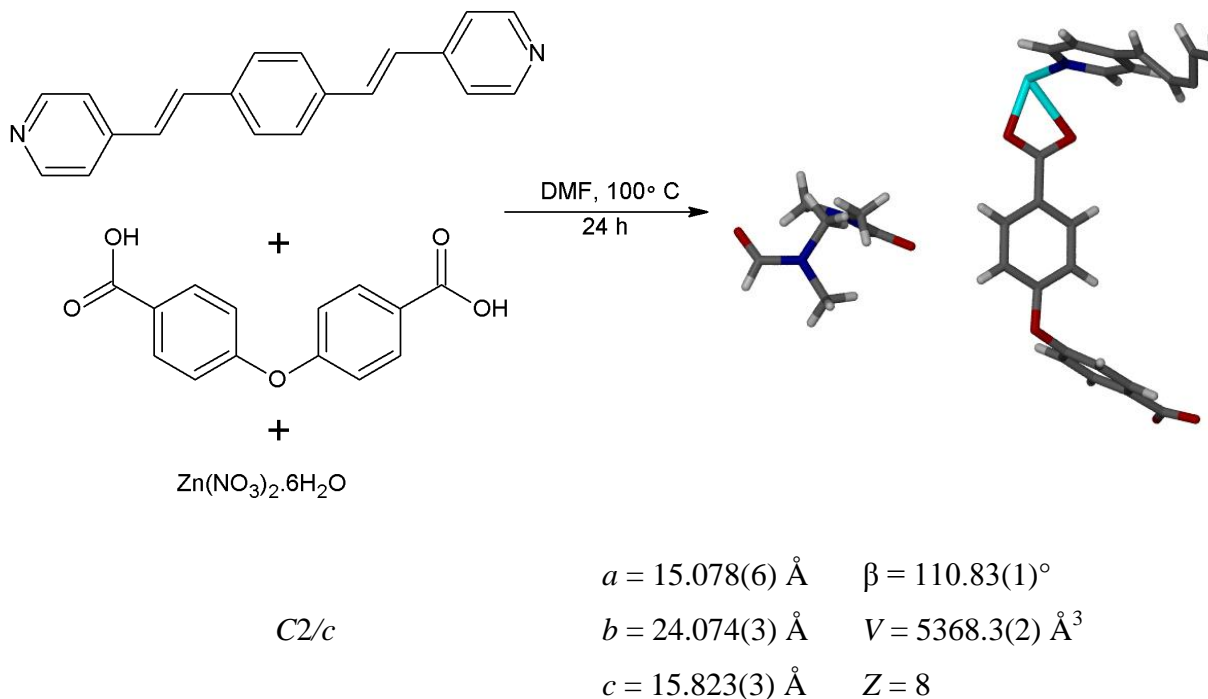
During the course of the work described in the previous chapter, it was discovered that the combination of ligand **L1** with **OBA** and either zinc or cobalt nitrate hexahydrate under highly specific conditions yielded two interesting isostructural MOFs. This chapter reports the characterisation of these two frameworks, an in-depth analysis of their sequestration capabilities as well as their role in tuneable solid-solution framework formation and epitaxial crystal growth.

In 2013 Vittal *et al.*¹⁵ reported the solid-state structure of the framework known in this study as **HC1** (honeycomb 1) with a description of the conformational possibilities of the **L1** ligand. Although the framework is the same as that presented here, the work carried out in this chapter focuses on a completely different aspect to that presented in Vittal's publication. It is, however, important to note, that the published work triggered the idea for the work described in, ChapterV.

CHAPTER IV: TUNING MOF SEQUESTRATION AND STORAGE

4.1 $\{[\text{Zn}(\text{L1})_{0.5}\text{OBA}]\cdot\text{DMF}\}_n$ or **HC1**

HC1 is formed from the reaction of **L1**, **OBA** and Zn(II) nitrate hexahydrate under solvothermal conditions (100 °C, DMF) (**Scheme 4.1**). **HC1** crystallises in the monoclinic space group $C2/c$. The asymmetric unit consists of one zinc cation, one **OBA** ligand, half an **L1** ligand in the *anti* conformation and one DMF molecule disordered over two positions.



Scheme 4.1 Synthesis of **HC1** from the solvothermal reaction of **L1**, **OBA** and zinc(II) nitrate in DMF at 100 °C, with selected crystallographic information.

The framework presents a highly unusual ‘half paddlewheel’ dinuclear zinc carboxylate unit $[\text{Zn}_2(\text{COO})_4]$ (**Figure 4.1a**). The dinuclear zinc centres are bridged by the **OBA** ligands to form a 2D network. The 2D nets stack on top of one another and are further linked into a 3D network by bridging **L1** ligands in the *anti* conformation (**Figure 4.1b**). The structure is threefold interpenetrated and contains large honeycomb-like hexagonal channels along $[1\ 0\ 1]$. These channels are occupied by DMF guest molecules arranged in a sinusoidal manner (**Figures 4.1c 4.2**).

CHAPTER IV: TUNING MOF SEQUESTRATION AND STORAGE

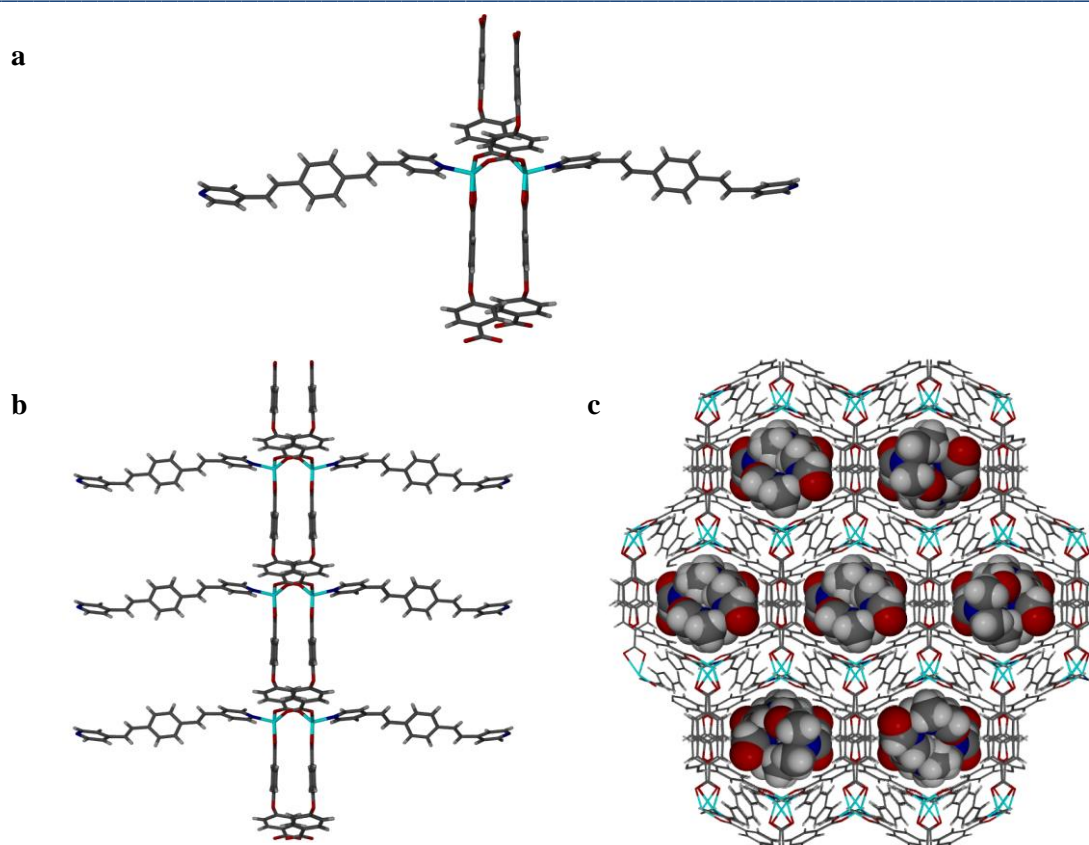


Figure 4.1 a) Unusual ‘half paddlewheel’ moiety in **HC1**. b) 2D network as viewed along the *a* axis. c) Solvent-filled honeycomb channels.

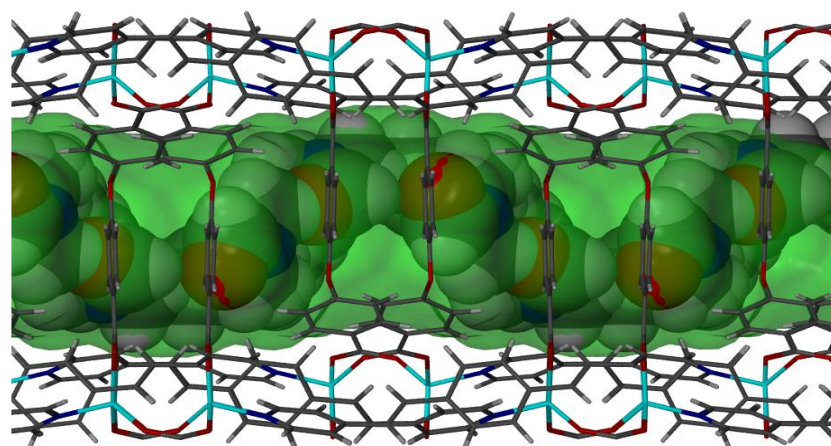


Figure 4.2 Space-filled DMF solvent molecules located in the guest-accessible channel of **HC1** as viewed along $[1\ 0\ 0]$.

One DMF molecule is disordered over two positions with site occupancy of 47% and 53%. The TGA thermogram (**Figure 4.3**) shows a 15% weight loss occurring in the temperature range 30 - 200 °C, which corresponds to one DMF molecule per ASU. Decomposition of the framework commences at 340 °C.

CHAPTER IV: TUNING MOF SEQUESTRATION AND STORAGE

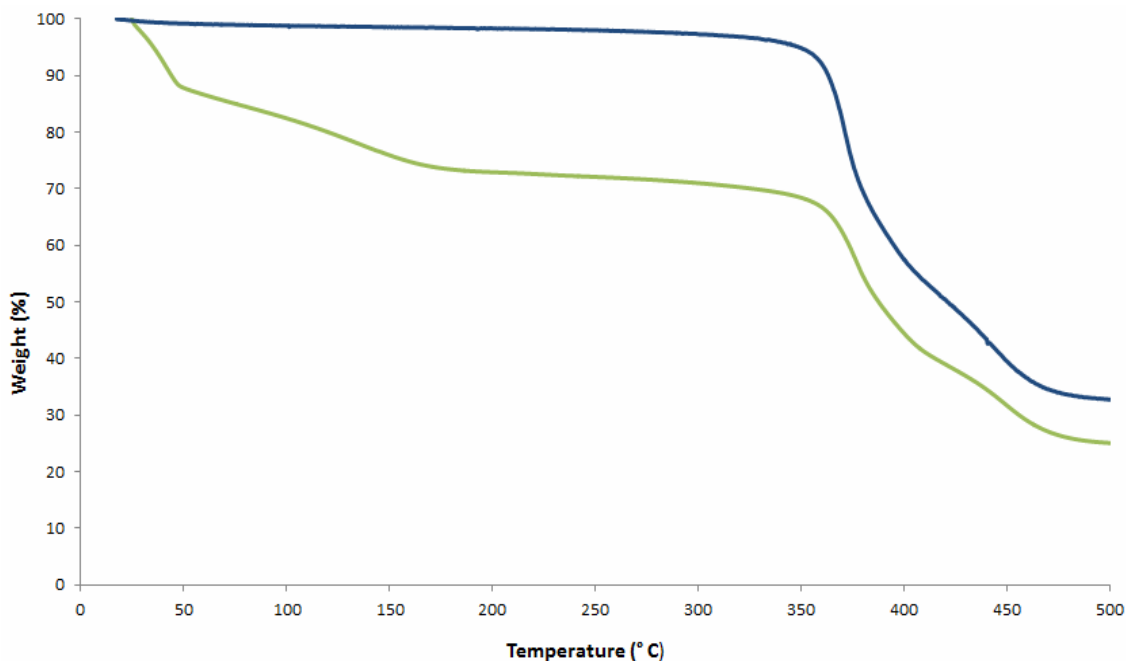


Figure 4.3 TGA of the as-synthesised and the evacuated phases of **HC1** (green and blue lines, respectively).

The apohost form (**HC1'**) is generated by placing the solvate in supercritical CO₂ for 24 hours. Due to the robust nature of the framework, this occurs as a SC-SC transformation. The cell parameters undergo a slight change (**Figure 4.4**). However, it is known that the framework of the empty phase remains the same as that of the synthesised phase with the **L1** ligand in the *anti* conformation. The apohost framework contains 1672 Å³ of solvent accessible space per unit cell.

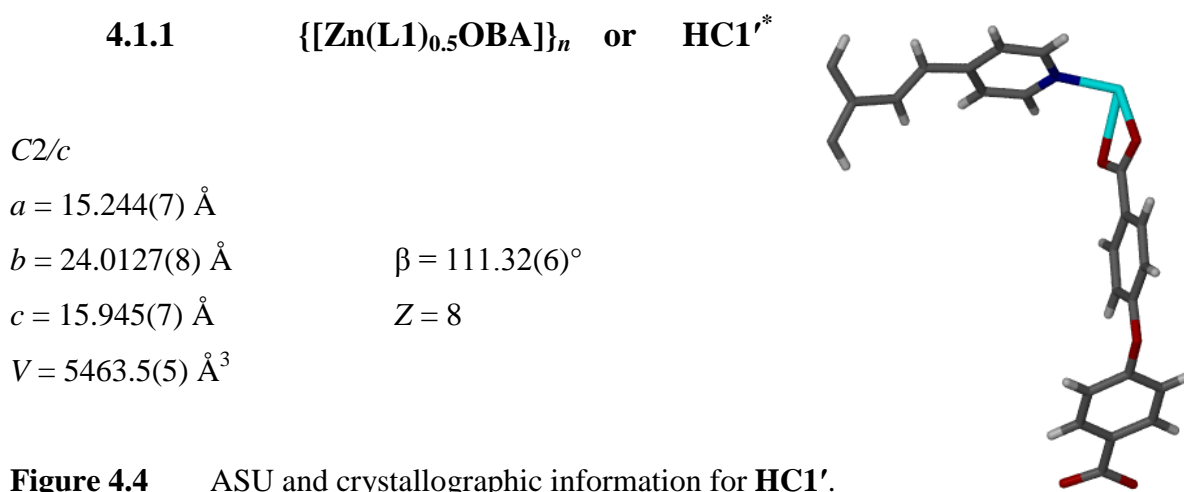


Figure 4.4 ASU and crystallographic information for **HC1'**.

* Prime denotes activation.

4.2 SC-SC guest exchange experiments with HC1

A series of SC-SC guest exchange experiments were carried out using *ortho*-, *meta*- and *para*-xylene (*oxy*, *mxy* and *pxy*) as well as dioxane. X-ray crystal structures were determined for all exchanges. Although the framework undergoes guest exchange, it is important to note that in each case the conformation of **L1** remains fixed in the *anti* conformation.

4.2.1 $\{[\text{Zn}(\text{L1})_{0.5}\text{OBA}]\cdot\text{oxy}\}_n$ or **HC1**·*oxy*

Crystals of **HC1** were immersed in a solution of *ortho*-xylene and allowed to equilibrate over two days. The structure of **HC1**·*oxy* reveals complete exchange of the DMF molecules for *ortho*-xylene (**Figure 4.5**).

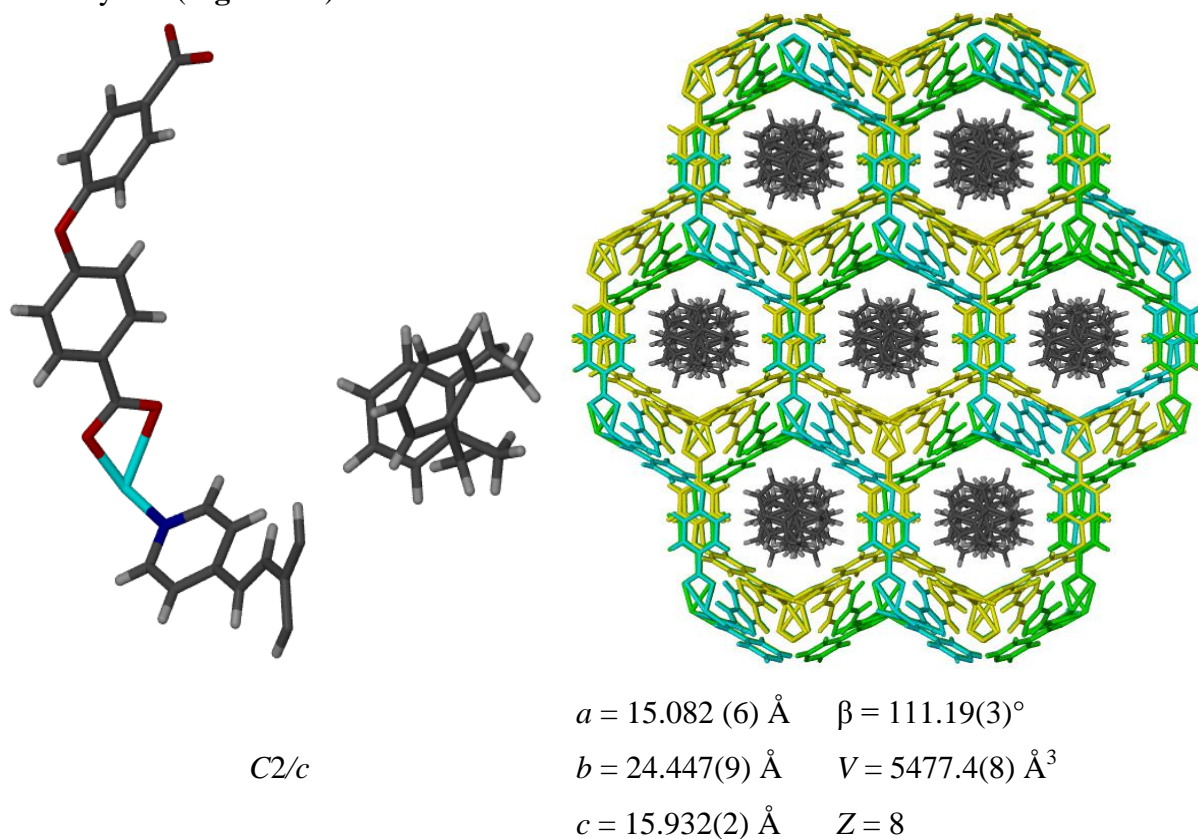


Figure 4.5 The ASU and packing diagram of **HC1**·*oxy* viewed along [1 0 1]. The *oxy* molecules occupy the channels previously filled by the DMF molecules.*

* TGA thermograms for solvent exchanges are given in the supplementary information.

CHAPTER IV: TUNING MOF SEQUESTRATION AND STORAGE

There are no significant differences between the unit cell parameters of the as-synthesised crystals and those of **HC1·oxy**. The ASU consists of one zinc cation, one complete **OBA** ligand, half an **L1** ligand and one *ortho*-xylene molecule disordered over two positions (63:37 site occupancy). The SQUEEZE¹⁶ results are in agreement with the crystallographic model.

4.2.2 $\{[\text{Zn}(\text{L1})_{0.5}\text{OBA}] \cdot mxy\}_n$ or **HC1·mxy**

HC1 was immersed in *meta*-xylene and allowed to equilibrate over two days. The structure of **HC1·mxy** reveals complete exchange of the DMF molecules for *meta*-xylene (Figure 4.6).

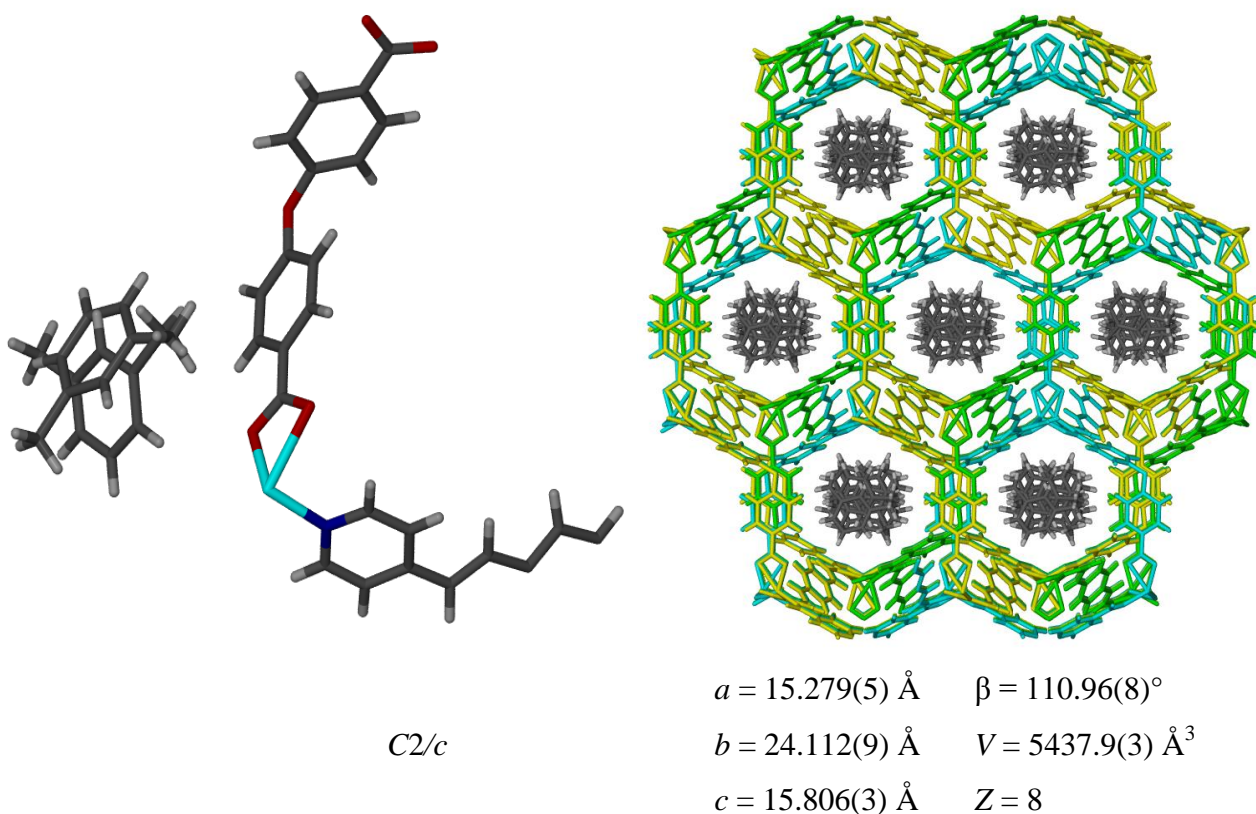


Figure 4.6 The ASU and packing diagram of **HC1·mxy** viewed along [1 0 1]. The disordered *mxy* molecules occupy the channels previously filled by the DMF molecules.

There are no significant differences between the unit cell parameters of the as-synthesised crystals and those of **HC1·mxy**. The ASU consists of one zinc cation, one complete **OBA** ligand, half an **L1** ligand and one *meta*-xylene molecule disordered over two positions with 54% and 46% site occupancy.

4.2.3 $\{[\text{Zn}(\text{L1})_{0.5}\text{OBA}] \cdot \text{pxy}\}_n$ or **HC1**·*pxy*

The crystals of **HC1** were immersed in a solution of *para*-xylene and allowed to equilibrate over two days. The structure of **HC1**·*pxy* reveals complete exchange of the DMF molecules for *para*-xylene (Figure 4.7).

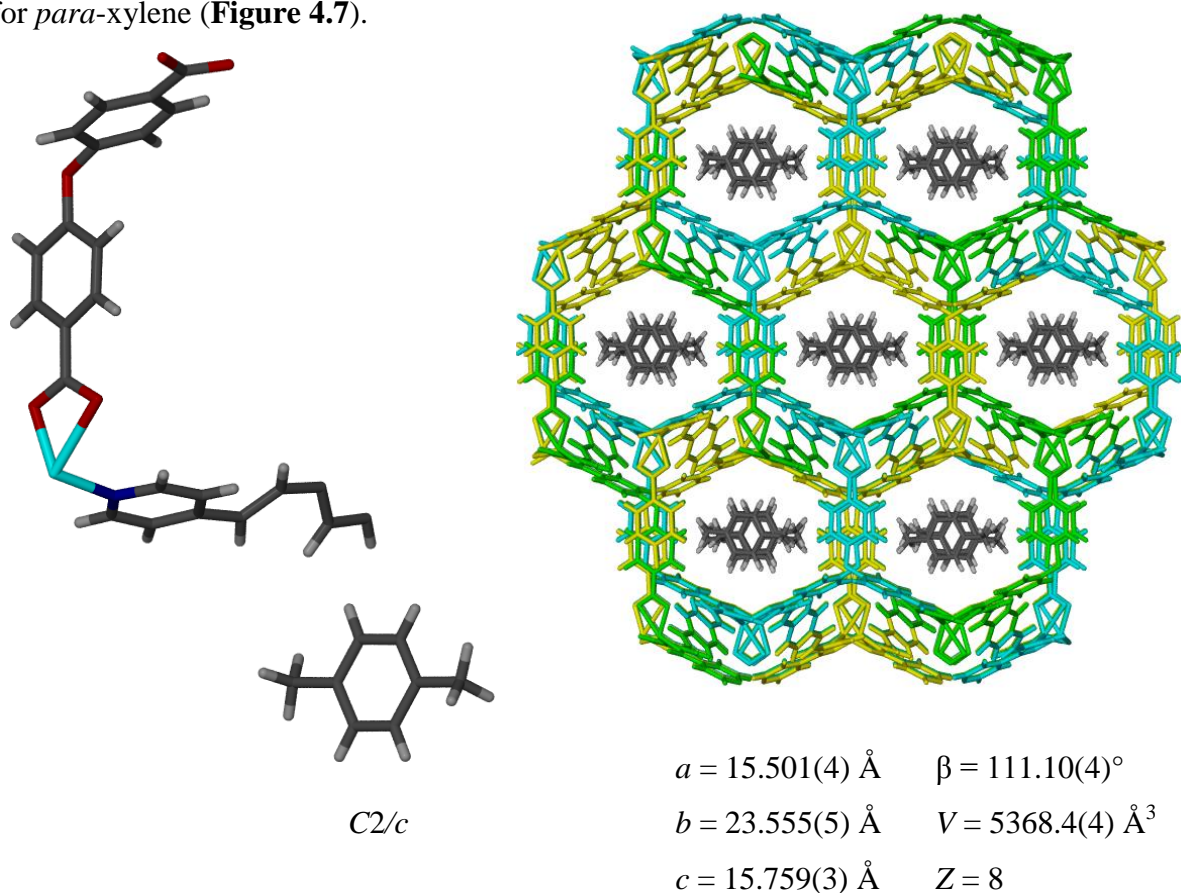


Figure 4.7 The ASU and packing diagram of **HC1**·*pxy* viewed along [1 0 1]. The *pxy* molecules occupy the channels previously filled by the DMF molecules.

There are no significant differences between the unit cell parameters of the as-synthesised crystals and those of **HC1**·*pxy*. The ASU consists of one zinc cation, one complete **OBA** ligand, half an **L1** ligand and one full occupancy *para*-xylene molecule. The extended structure shows the *para*-xylene molecules to be oriented with their methyl groups perpendicular to the channel axis.

4.2.4 $\{[\text{Zn}(\text{L1})_{0.5}\text{OBA}]\cdot\text{dioxane}\}_n$ or **HC1**·dioxane*

The crystals of **HC1** were immersed in dioxane and allowed to equilibrate over two days. The structure of **HC1**·dioxane reveals complete exchange of the DMF molecules for dioxane (Figure 4.8).

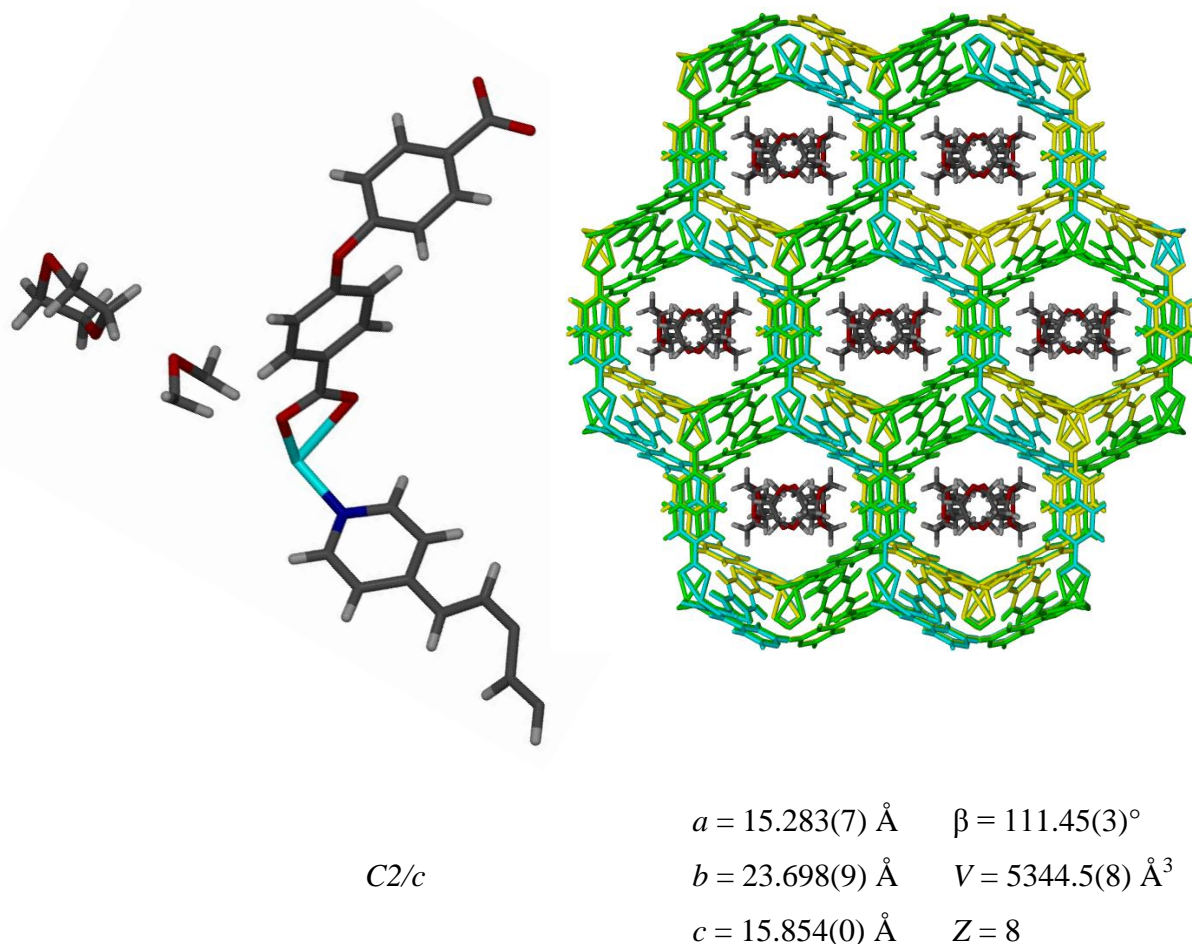


Figure 4.8 The ASU and packing diagram of **HC1**·dioxane viewed along [1 0 1]. The dioxane molecules occupy the channels previously filled by the DMF molecules.

There are no significant differences between the unit cell parameters of the as-synthesised crystals and those of **HC1**·dioxane. The ASU consists of one zinc cation, one complete **OBA** ligand, half an **L1** ligand and half a dioxane molecule disordered over two positions. One of the positions of the dioxane molecule is located on a centre of inversion.

* Despite the large voids, all exchanges exhibited low occupancy, which did not alter with prolonged exposure.

4.3 GC-analysed selectivity testing of HC1

Due to the nature of the pore, **HC1** can accommodate all three of the xylene isomers with differences in the orientation of the guest. It was therefore postulated that the material might exhibit some selectivity. A selectivity study was undertaken using gas chromatography in order to determine whether the material exhibited any preferential uptake of the xylene isomers which are notoriously difficult to separate. A set amount of apohost crystals **HC1'** were submerged overnight in set mixtures of the xylene isomers (**Table 4.1**). The crystals were then removed, dried to remove any surface solvent, washed briefly with hexane (to further remove surface solvent) and then transferred to a fresh solution of hexane, which was kept overnight in a refrigerator. The xylene guest was exchanged for hexane and the supernatant hexane solution was used for analysis (all experiments were performed in triplicate).

From the data in **Table 4.1** it is clear that when presented with an equimolar mixture of all three xylenes, the framework selectively takes up approximately twice as much *ortho* xylene as either *meta* or *para*. A further study using only the *meta* and *para* isomers showed negligible selectivity.*

Table 4.1 Gas chromatographic data for **HC1** and the separation of the xylene isomers.

	Competition Experiment				
	<i>oxy</i> : <i>mxy</i> : <i>pxy</i>			<i>mxy</i> : <i>pxy</i>	
Ratio in solution	1:1:1			1:1	
Peak Area	404203	236980	173039	3851369	3277661
% present	50	29	21	54	46
ESDS	0.13	0.21	0.11	0.16	0.12

* *mxy* : *oxy* and *pxy* : *oxy* experiments may be found in the supplementary information.

4.4 Gravimetric gas sorption by HC1 using CO₂ and alkanes

To further understand the porosity of the desolvated phase of **HC1**, its gas sorption properties were measured at 25 °C using CO₂, methane, ethane, propane and butane (**Figure 4.9**). **HC1** shows conventional Type I sorption behaviour for all selected guests, absorbing approximately two molecules of CO₂ (17.8 wt%), one molecule of methane (4.0 wt%) or ethane (6.7 wt %), half a propane molecule (4.2 wt%) or a very small amount of butane, (*i.e.* ± 0.25 molecules or 2.8 wt%) per ASU. All gases attain full occupancy.*

It is interesting to compare desorption isotherms. Although CO₂ appears to be the preferred guest, unlike for all the alkanes, the CO₂ isotherm shows negligible hysteresis. This presents a potentially interesting means of selectively removing CO₂ from a mixture of CO₂ and alkanes. If, for example, the material is exposed to a gaseous mixture, it would selectively absorb carbon dioxide. Transfer of the material from the gaseous mixture chamber to an empty chamber would enable release of the CO₂, leaving a higher percentage of CO₂ in one chamber relative to the mixture of the CO₂ and alkanes in another. Breakthrough (selectivity) experiments would need to be conducted to verify this hypothesis.

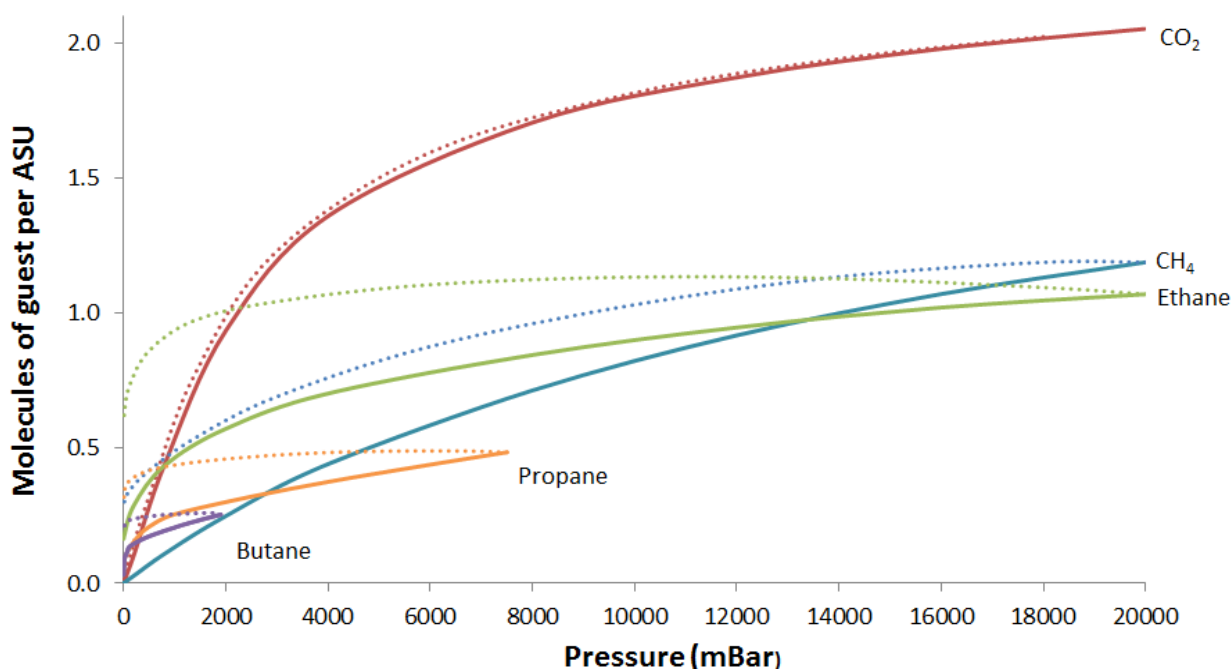
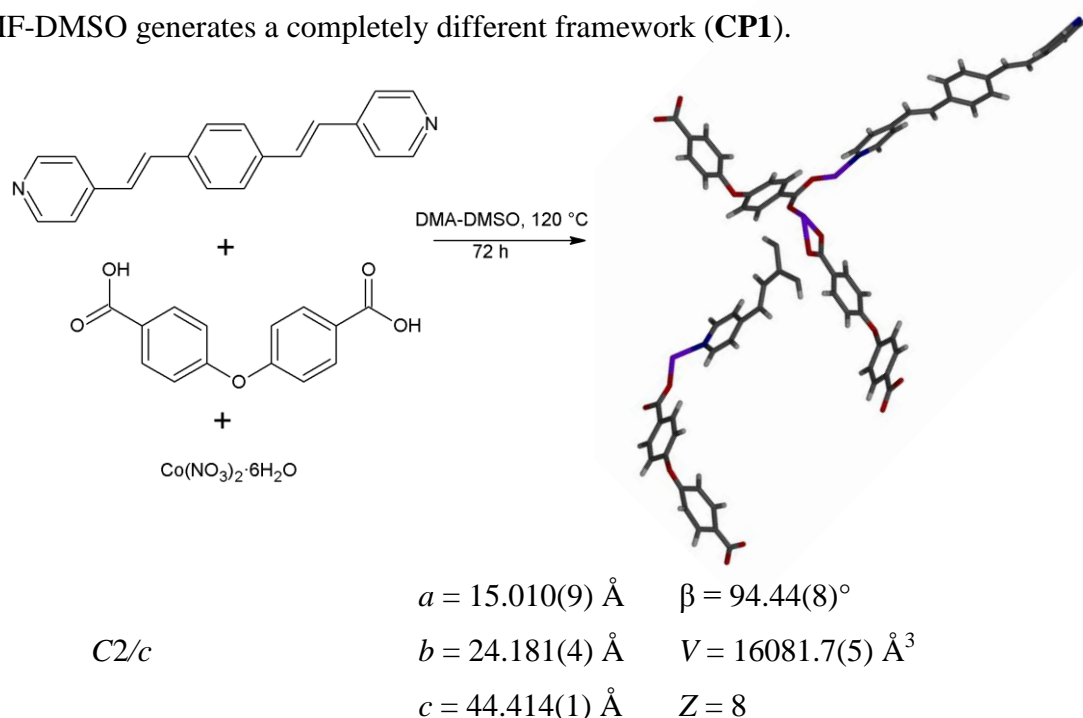


Figure 4.9 CO₂ and selected alkane sorption and desorption isotherms for **HC1** at 25 °C. Solid lines represent sorption and dashed lines represent desorption.

* Maximum gas uptake as indicated by a plateau in the sorption isotherm.

4.5 $\{[\text{Co}_3(\text{L1})_{1.5}\text{OBA}_3]\cdot\text{DMA}\}_n$ or **HC2**

The reaction of **L1**, **OBA** and Co(II) nitrate hexahydrate under particular solvothermal conditions (120 °C, DMA-DMSO) (**Scheme 4.2**) yields **HC2**, a framework which is isostructural to that of **HC1**.^{*} It should be noted that although crystals of **HC2** appear suitable for SCD analysis, numerous data collections revealed the material to be non-merohedrally twinned. Multiple attempts at indexing the reflections were unsuccessful. Twinning appears to be guest-induced, as activation or solvent exchange removes this problem. Similar to **HC1**, **HC2** crystallises in the monoclinic space group $C2/c$. The ASU comprises three cobalt cations, three **OBA** ligands and one and a half **L1** ligands. The solvent could not be modelled but, according to SQUEEZE, one DMA molecule is present in the ASU. This “tripling” of the c axis, volume and components is a symmetry-induced crystallographic artefact of the twinning. In reality this structure is the same as that of **HC1**. It is important to note that, although dimethyl sulphoxide is present during crystallisation, it is not present in the resulting framework. Furthermore, from the information presented in the previous chapter it is also evident that the DMA-DMSO combination is necessary for **HC2** to form as the use of DMF-DMSO generates a completely different framework (**CP1**).



Scheme 4.2 Synthesis of **HC2** from the solvothermal reaction of **L1**, **OBA** and cobalt nitrate in a DMA-DMSO solution at 120 °C, with selected crystallographic information.

^{*} A least-squares overlay of the two structures was performed in Mercury yielding an RMS value of 0.

CHAPTER IV: TUNING MOF SEQUESTRATION AND STORAGE

Thermogravimetric analysis (**Figure 4.10**) shows that **HC2** undergoes an initial loss of 20 wt% (one DMA molecule per ASU) in the 0 - 80 °C range and that the framework then remains stable until decomposition, which sets in at 375 °C.

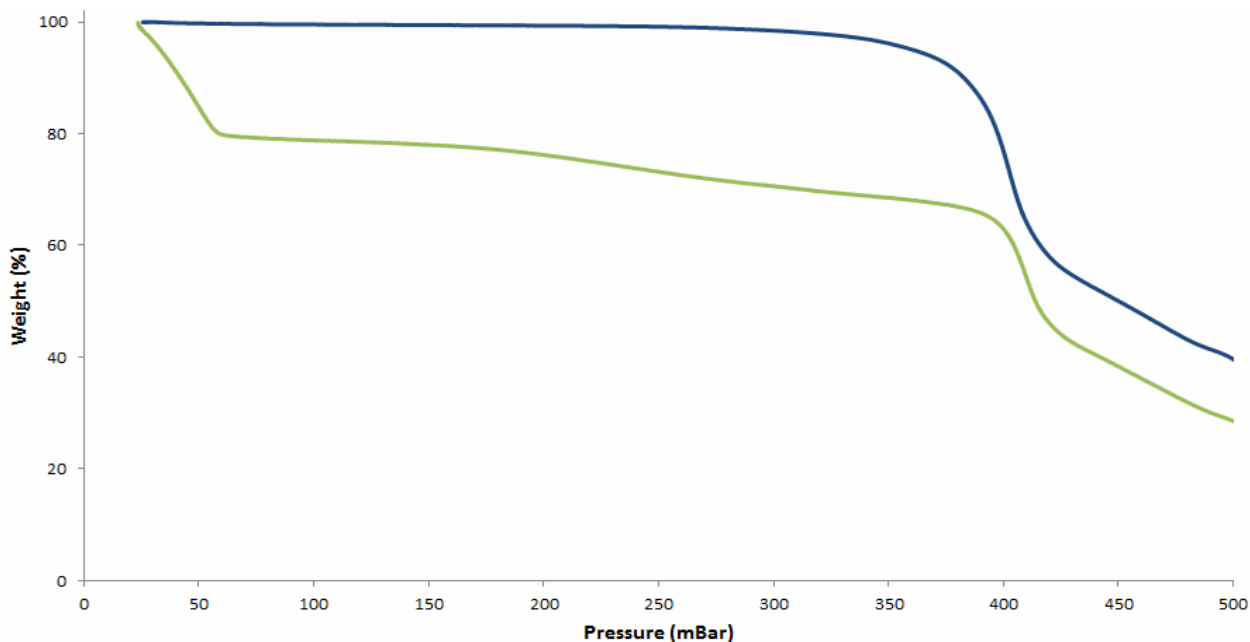


Figure 4.10 TGA of the as-synthesised as well as the evacuated phases of **HC2** (green and blue lines, respectively).

Similar to **HC1**, **HC2** can be activated (**HC2'**) in a SC-SC manner by heating the solvate at 100 °C under reduced pressure for 24 h. The activated form shows negligible change in the unit cell parameters *a* and *b* (**Figure 4.11**). Owing to the elimination of guest-induced twinning the *c* axis experiences a threefold reduction. The apohost framework contains 1629 Å³ of solvent accessible space per unit cell.

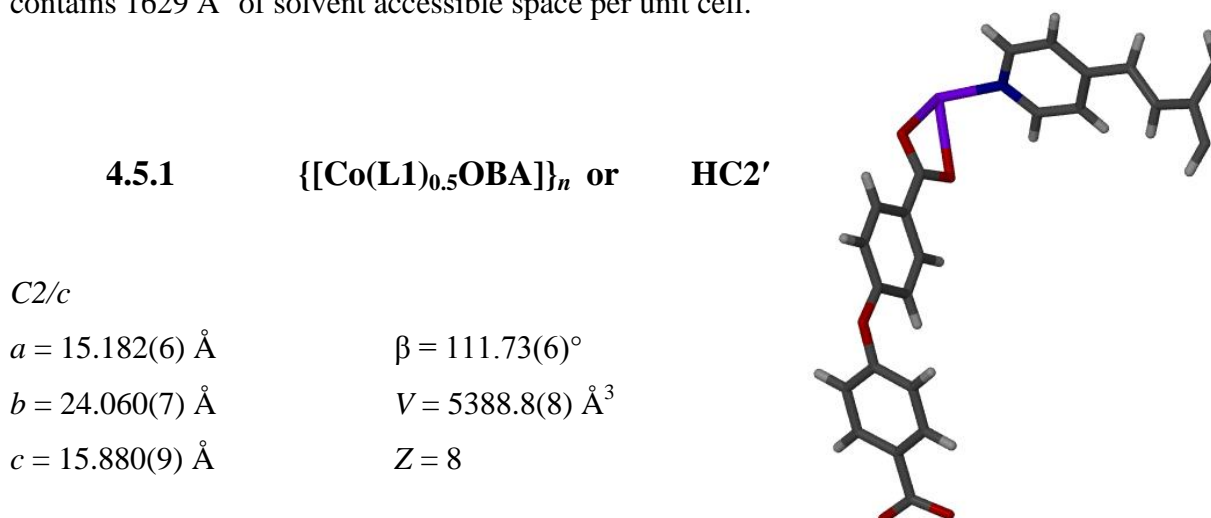


Figure 4.11 ASU and crystallographic information for **HC2'**.

4.6 GC-analysed selectivity testing of HC2

Since **HC2** is isostructural to **HC1**, the separation/selectivity study involving xylene isomers was repeated in order to determine whether the substitution of zinc for cobalt resulted in any change in selectivity. The material was treated in exactly the same manner as **HC1**. From the data presented in **Table 4.2**, two observations can be made. The first is that the peak areas are substantially smaller than those in **Table 4.1** implying very low xylene uptake and that the framework exhibits no substantial selectivity toward any of the three xylene isomers.

Table 4.2 Gas Chromatography data for **HC2** and the separation of the xylene isomers.*

	Competition Experiment		
	<i>oxy : mxy : pxy</i>		
Ratio	1:1:1		
Peak Area	4680	3603	3177
% present	41	31	28
ESDS	0.11	0.14	0.13

It is surprising and currently unclear why metal substitution (in which the two metals are very similar and the experimental conditions were identical) would induce such a dramatic change in uptake. Suggested future work would involve further experiments such as using other first row transition metals able to form similar frameworks and studying their selectivity behaviour in order to establish any notable trends.

* It should be noted that all competition experiments were performed in triplicate.

4.7 Gravimetric gas sorption of CO₂ and alkanes by HC2

Having established deviation in the xylene selectivity behaviour of the two isostructural MOFs **HC1** and **HC2**, the gas sorption properties of **HC2** were measured using CO₂, methane, ethane, propane and butane (**Figure 4.12**). **HC2** also shows Type I sorption behaviour, absorbing approximately one molecule each of CO₂ (9.0 wt%), methane (3.6 wt%), ethane (4.5 wt%), half a molecule of propane (5.1 wt%), or a small amount of butane (*i.e.* ± 0.38 molecules or 4.2 wt%) per ASU. Ethane, propane and butane are the only gases to attain full occupancy. Since the CO₂ and methane isotherms have not plateaued, **HC2** could potentially accommodate more of each of these guests. Although CO₂ is taken up and released with no hysteresis (as for **HC1**), it is not the preferred guest at 20 bar. Surprisingly, **HC2** shows a slight preference for methane, with the isotherm showing substantial hysteresis (0.6 molecules of CO₂ are retained post desorption) indicating a host-guest interaction. The ethane isotherm also shows no hysteresis. It is believed that this material has the potential to act as a filter. For example, if the material were exposed to the gaseous mixture, it could selectively take up methane and CO₂ but retain the methane and release the CO₂. Stimuli induced activation would ensure the release of methane. If the material was then exposed to the residual mixture, it could one again selectively absorb ethane and release it (into a separate container), leaving propane and butane. Once again breakthrough experiments would be required to further investigate this potential scenario.

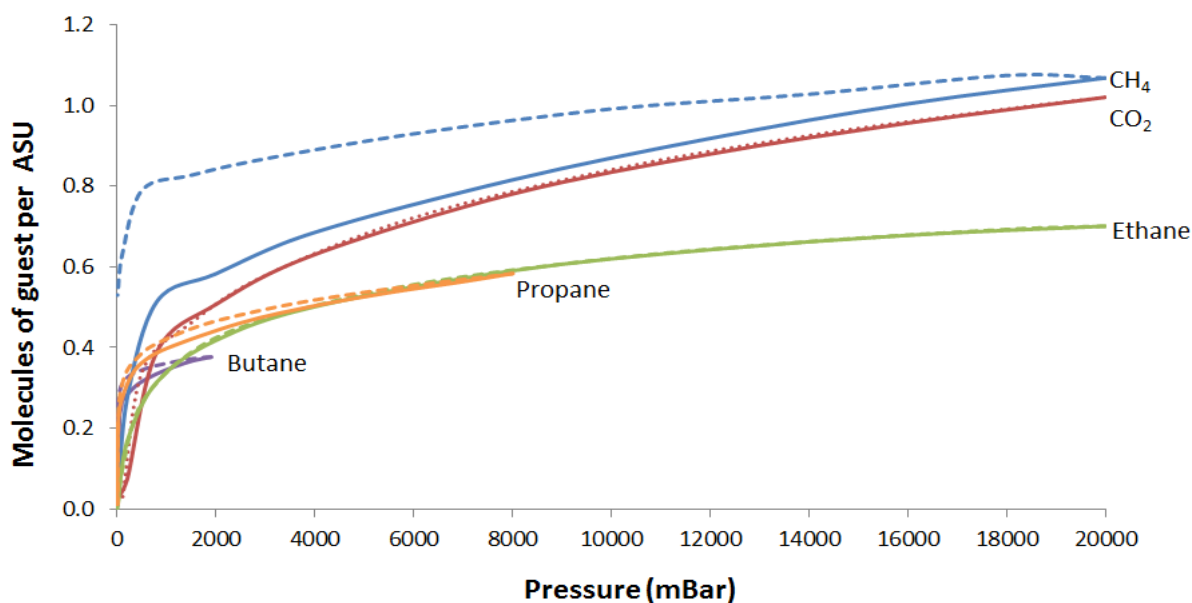


Figure 4.12 CO₂ and selected alkane sorption and desorption isotherms for **HC2** at 25 °C. Solid lines represent sorption and dashed lines represent desorption.

4.8 Pleochroism

Pleochroism is the ability of an anisotropic material to absorb different wavelengths of transmitted light depending upon its crystallographic orientations. As light emerges from a doubly refracting crystal, the beam is split into two polarised light rays, each vibrating in planes at right angles to one another and appearing to differ in colour. "Dichroism" (from the Greek word *dikhroos*, meaning "two-coloured") is when two colours are perceived from two different directions. Minerals in the hexagonal, tetragonal, and trigonal crystal systems are dichroic, and can only show two colours. Although **HC1** and **HC2** are isostuctural, they are not isomorphous as the crystals differ in morphology. The difference in colour (**HC1** is monochromic while **HC2** is pleochroic) is attributed to the electronic properties of the coordinating metals as both complexes exhibit octahedral geometry with the metal in the +2 oxidation state. Complexes synthesised from +2 zinc salts are generally colourless, while those containing hydrated +2 cobalt salts tend to be pink. In the case of **HC1**, the crystals are pale yellow (**L1** is yellow so it is believed that this is what colours the crystals) and petal-shaped while the crystals of **HC2** are pleochroic* and rhombus-shaped (**Figure 4.13**). Depending on the orientation and angle of plane-polarised light, the crystals of **HC2** exhibit two independent colours and can be described as dichroic. At 0° (relative to the direction of polarisation) the crystals appear deep purple while rotation through 90° causes them to appear red. The differences in colours observed in **HC1** and **HC2** are solvent independent as the activated forms of both these crystals exhibit the same phenomenon. Thus the effect is thought to originate from a MLCT (metal to ligand charge transfer) interaction between the octahedral cobalt(II) and **L1**.

* Crystals appear to have different colours at different angles of rotation under plane polarised light.

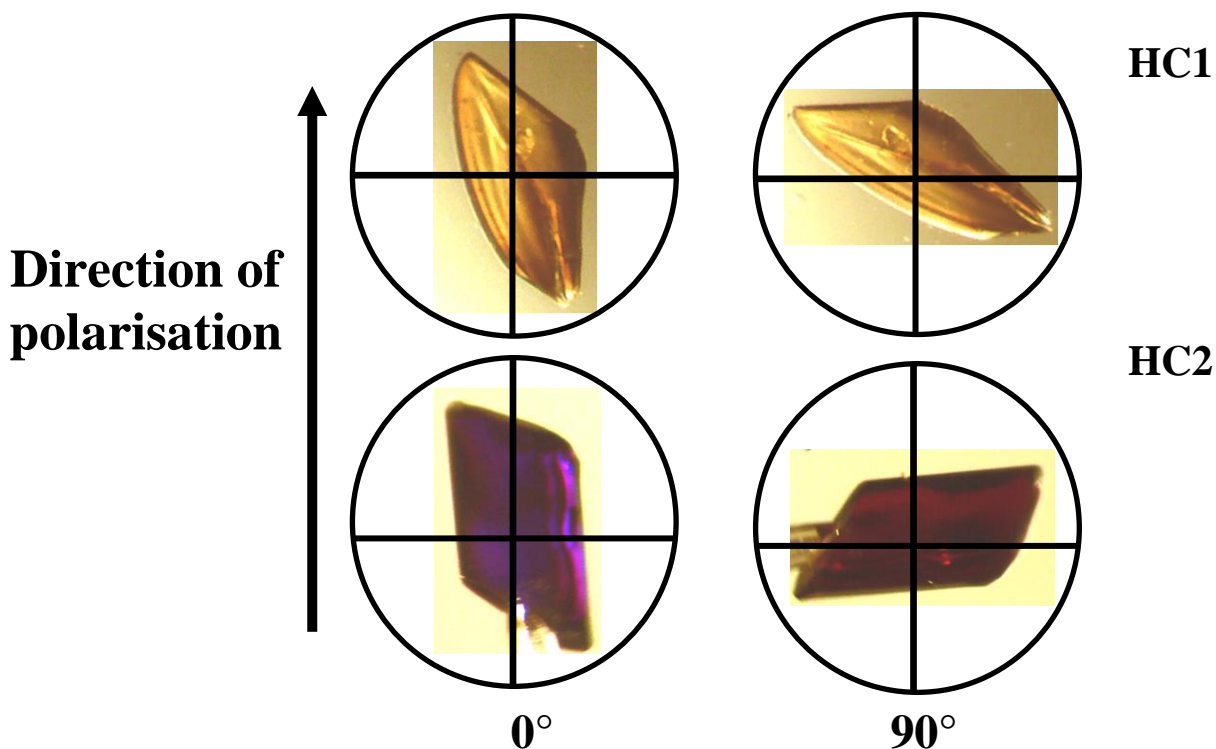


Figure 4.13 Photographs of **HC1** and **HC2** crystals with **HC2** exhibiting pleochroism.

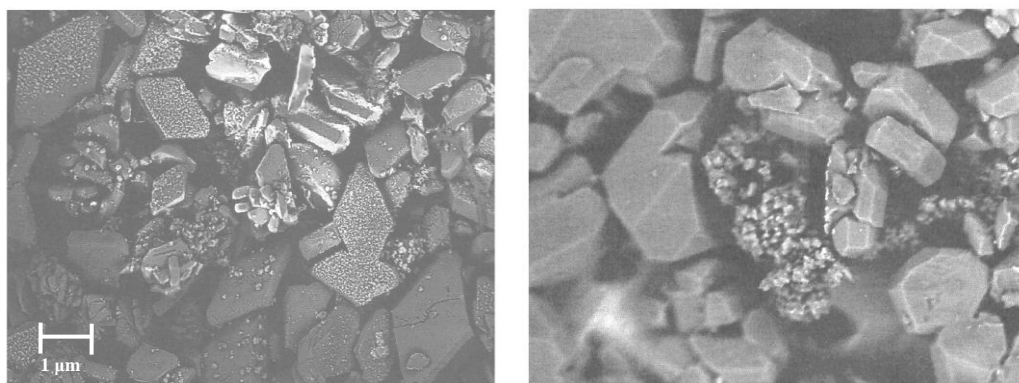
4.9 Solid solutions

The difference in crystal colour for **HC1** and **HC2** prompted crystallisation experiments in which both the zinc and the cobalt salts were present simultaneously to determine if a mechanical mixture or if a solid solution would form. Once solid solution formation was ascertained using energy-dispersive X-ray spectroscopy (EDX) experiments, the metal ratios were varied to further determine whether there was any inherent selectivity for one metal over the other. **Table 4.3** shows the unit cell parameters for the two solid solution MOFs obtained, wherein the Zn:Co ratio was 1:1 and 1:3. Although marginally different, the two frameworks (**HC3** and **HC4**) may be described as isostructural to both **HC1** and **HC2**. **Figure 4.14** shows high-resolution scanning electron microscope (SEM) micrographs of the two solid solutions.

CHAPTER IV: TUNING MOF SEQUESTRATION AND STORAGE

Table 4.3 Cell parameters of isostructural solid solutions **HC3** and **HC4**.

	HC3 Zn:Co = 1:1 (in soln)	HC4 [*] Zn:Co = 1:3 (in soln)	HC5 [†] Zn:Co:Ni = 1:1:1 (in soln)
SG	<i>C2/c</i>	<i>C2/c</i>	Polycrystalline material - thus could not collect a SC data set
a	15.177(3) Å	15.04(3) Å	
b	23.970(5) Å	24.15(7) Å	
c	15.730(5) Å	15.77(2) Å	
β	110.64(9)°	110.9(3)°	
V	5355.1(2) Å ³	5353(4) Å ³	

**Figure 4.14** SEM micrographs of the equimolar solid solutions of **HC3** and **HC4** showing the difference in morphology (scale bar is in micrometers).

Examination of an **HC3** crystal obtained from the vial containing equimolar amounts of zinc and cobalt yielded diamond-shaped trichroic crystals (**Figure 4.15**). When the dominant face (face with largest surface area) of the crystal is at 0° (relative to the plane of polarisation) it appears light purple. As the crystal is rotated through 90° it changes to red. This was also observed for the original **HC2** material. Furthermore, when the crystal is turned on its side, at 0° the crystal appears blue but rotation through 45° causes the red colour to appear. This implies the presence of an additional plane not present in **HC2**.

* A full data set was not collected, hence the decrease in cell parameter accuracy.

† The reason for the nickel-included experiment will be explained further along.

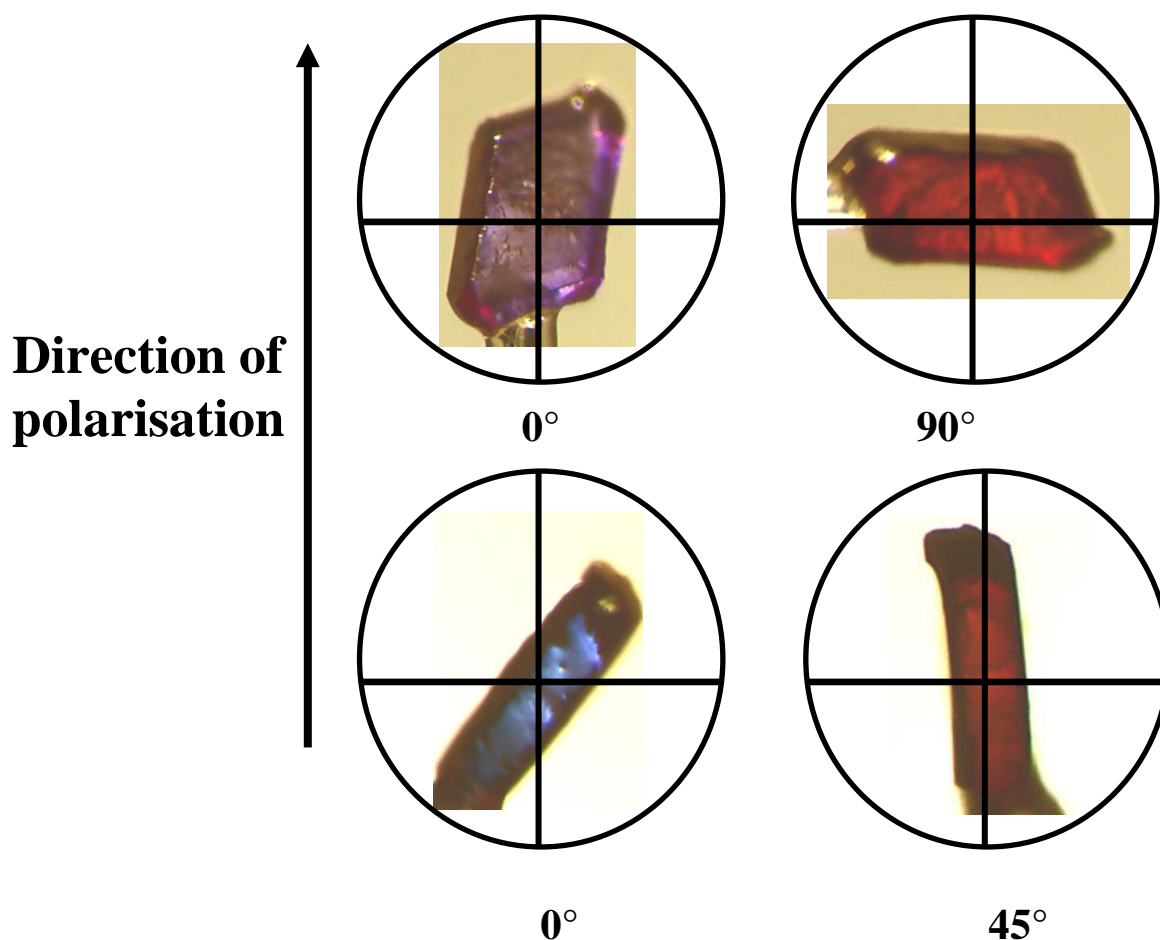


Figure 4.15 Photographs of the **HC3** solid solution showing trichroism.

When the cobalt:zinc ratio was tripled, pleochroic crystals (**HC4**) were once again obtained (**Figure 4.16**). However the shade was paler than that of the crystals obtained from the 1:1 solution. At 0° the dominant face is a very pale violet. Rotation through 90° produces an orange hue. This was an unexpected observation since the cobalt metal is believed to be responsible for the dominant colour and an increase in the amount of cobalt was expected to result in the appearance of a deeper, more intense colour.

CHAPTER IV: TUNING MOF SEQUESTRATION AND STORAGE

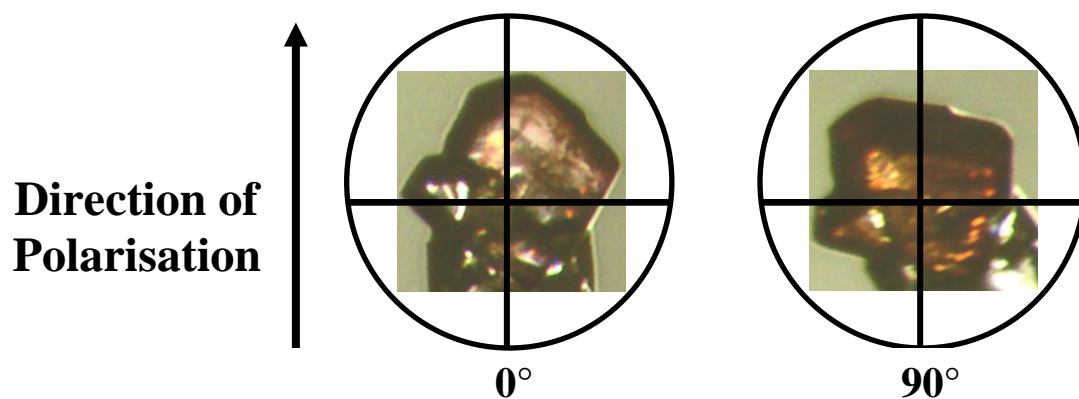


Figure 4.16 Photographs of HC4 solid solution showing pale violet and orange colours.

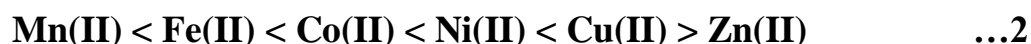
Energy dispersive X-ray spectroscopy experiments (EDX) were carried out and the data are presented in **Table 4.4**. The table shows average values obtained from a random selection of eight separate single crystals per solid solution. When both metals are present in equal amounts during crystallisation, the framework assembles in such a manner as to incorporate three times more zinc than cobalt. If the amount of cobalt is tripled, the framework assembles with six times more zinc than cobalt. This is in accordance with the aforementioned crystal colours. The framework seems to exhibit preferential incorporation of zinc over cobalt even when the crystallisation conditions offer more cobalt than zinc.

Table 4.4 EDX molar ratios of three solid solutions.

Ratio of (Zn:Co: Ni) in vial	Carbon	Nitrogen	Oxygen	Zinc	Cobalt	Nickel	ESDs
1 : 1 : 0 HC3	7.61	1.67	2.96	3.03	0.89	0	0.009
1 : 3 : 0 HC4	7.51	1.38	3.58	2.78	0.56	0	0.013
1 : 1 : 1 HC5	7.70	0.063	4.00	3.89	1.57	0.98	0.012

CHAPTER IV: TUNING MOF SEQUESTRATION AND STORAGE

The trend (zinc preferred over cobalt) is in accordance with the well-known Irving-Williams series.¹⁷



As one moves across the periodic table the ionic radius decreases, resulting in an increase in the relative stabilities of complexes formed. Furthermore, the Crystal Field Stabilisation Energy (CFSE) also increases across the period, with nickel having the highest value. The CFSE value for zinc is zero. A high CFSE value ensures increased stability. Since **HC3** and **HC4** both contain more zinc than cobalt but the CFSE values of the two metals are very similar, there must be additional interactions at play.

In an effort to definitively establish whether the experimentally observed “selectivity” is merely an artefact of a well-known phenomenon, or whether some additional interaction occurs between the ligand and the metals, an additional metal salt was incorporated into the crystallisation conditions. Nickel(II) nitrate hexahydrate was selected owing to its higher CFSE when compared to zinc and cobalt.* The hypothesis was that if the framework behaves according to the Irving-Williams series then the EDX experiments would show a higher percentage of nickel relative to cobalt or zinc. In contrast to the previously well-formed single crystals, incorporation of nickel yielded a polycrystalline material. Although the crystal quality was poor, EDX experiments revealed that, even in the presence of what should be a more stable metal, the framework still assembles with a higher percentage of zinc than cobalt, with nickel being present in the smallest amount. Since zinc is a d^{10} metal ion, the d-orbital involvement in M-L bonding is negligible thus this metal has no particular geometry preference whereas Co(II) and is more likely to exhibit strong geometry preferences.

* Crystallisations involving copper was also attempted but yielded no solid material.

4.10 Epitaxial crystal growth

Having obtained two isostructural MOFs (**HC1** and **HC2**) and observed that one can further obtain isostructural solid solution crystals of the two frameworks (**HC3** and **HC4**), crystallisation of a homoepitaxial* crystal was attempted. Crystals of **HC1** were submerged for 24 h in the crystallisation medium known to produce **HC2** and crystals of **HC2** were immersed for 24 h in the crystallisation medium known to produce **HC1**. Inspection of the original **HC1** crystals revealed the formation of homoepitaxial crystals (**HC6**) while crystals of **HC2** remained unaffected. **Figure 4.17** shows the epitaxial **HC6** crystals: instead of growing on the dominant[†] surface of the **HC1** seed crystal, the **HC2** layer grows around the edges (the smallest *i.e.* the fastest growing surface). Rotation of **HC6** indicates that it too possesses the dichroic tendencies exhibited by the parent compound **HC2**.

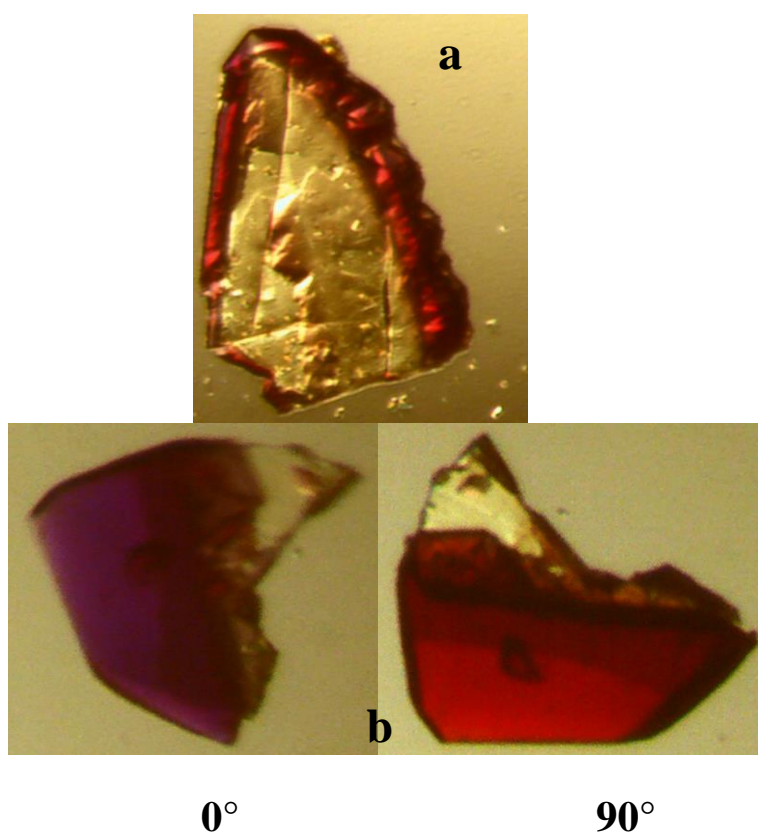


Figure 4.17 Photographs of homoepitaxial crystals of **HC6** showing a) how **HC2** grows around the periphery of **HC1**. b) Dichroism of **HC6**.

* The use of the surface of one crystal to seed the growth of a second isostructural form.

[†] Face with the largest surface area.

4.11 Conclusion

Two isostructural MOFs (one containing zinc, **HC1**, the other containing cobalt, **HC2**) may be readily synthesised using DMF and DMA-DMSO, respectively. A series of SC-SC solvent exchange experiments yielded **HC1** with each of the three xylene isomers and dioxane included into the cavity. The guest exchanges had negligible effects on the cell parameters. In spite of the lack of dynamism exhibited by the host, the similarly-shaped guests orient themselves in various ways within the host, thus prompting the decision to study the potential selectivity of the host for the three xylene guests.

HC1 shows slight selectivity toward *ortho*-xylene, while **HC2** has no discernible preference for any of the xylene isomers. **HC1** crystals are monochromic and the framework shows potential selectivity for CO₂ over a selection of linear hydrocarbons, while **HC2** crystals are pleochromic and show selectivity toward methane, CO₂ and ethane. If the components of the two frameworks are combined, a solid solution is formed. Crystals isolated from this solution are trichroic and the colours observed may potentially be ‘fine-tuned’ by modifying the ratio of zinc to cobalt (**HC3** and **HC4**). EDX experiments indicated that even when cobalt is in excess, the framework still preferentially includes more zinc. At first, this was thought to be due to the Irving-Williams series. However, this was disproved when nickel was added to the crystallisation conditions in equal amounts to zinc and cobalt, with the framework still taking up Zn > Co > Ni, despite nickel having the strongest CFSE.

A homoepitaxial crystal (**HC6**) was grown by immersing crystals of **HC1** in the crystallisation medium of **HC2**. Growth occurred along the perimeter of the original crystal rather than on the major surface of the crystal. The reason for this is currently unknown.

Although **HC1** and **HC2** are isostructural, each framework exhibited different selectivity capabilities thus these properties could potentially be harnessed by combining both metals and varying the composition of the solid solutions to induce the desired selectivity.

4.12 Synthesis of metal organic frameworks HC1 – HC6

HC1: A mixture of $\text{Zn}(\text{NO}_3)_2 \cdot 6\text{H}_2\text{O}$ (15 mg, 0.05 mmol), **OBA** (13 mg, 0.05 mmol) and **L1** (8.5 mg, 0.03 mmol) in 5 mL DMF was heated to 100 °C in a sintered glass vial for 24 h. Yellow petal-shaped crystals were obtained.

HC2: A mixture of $\text{Co}(\text{NO}_3)_2 \cdot 6\text{H}_2\text{O}$ (15 mg, 0.05 mmol), **OBA** (13 mg, 0.05 mmol) and **L1** (8.5 mg, 0.03 mmol) in a 5 mL (1:1 v/v) solution of DMA-DMSO was heated to 100 °C in a sintered glass vial for 24 h. Purple-red rectangular crystals were obtained.

HC3: A mixture of $\text{Zn}(\text{NO}_3)_2 \cdot 6\text{H}_2\text{O}$ (7.5 mg, 0.025 mmol), $\text{Co}(\text{NO}_3)_2 \cdot 6\text{H}_2\text{O}$ (7.5 mg, 0.025 mmol), **OBA** (13 mg, 0.05 mmol) and **L1** (8.5 mg, 0.03 mmol) in a 5 mL (1:1 v/v) solution of DMA-DMSO was heated to 100 °C in a sintered glass vial for 24 h. Purple-red-blue diamond-shaped crystals were obtained.

HC4: A mixture of $\text{Zn}(\text{NO}_3)_2 \cdot 6\text{H}_2\text{O}$ (11 mg, 0.04 mmol), $\text{Co}(\text{NO}_3)_2 \cdot 6\text{H}_2\text{O}$ (3 mg, 0.01 mmol), **OBA** (13 mg, 0.05 mmol) and **L1** (8.5 mg, 0.03 mmol) in a 5 mL (1:1 v/v) solution of DMA-DMSO was heated to 100 °C in a sintered glass vial for 24 h. Pale purple-orange diamond-shaped crystals were obtained.

HC5: A mixture of $\text{Zn}(\text{NO}_3)_2 \cdot 6\text{H}_2\text{O}$ (5 mg, 0.017 mmol), $\text{Co}(\text{NO}_3)_2 \cdot 6\text{H}_2\text{O}$ (5 mg, 0.02 mmol), $\text{Ni}(\text{NO}_3)_2 \cdot 6\text{H}_2\text{O}$ (5 mg, 0.027 mmol), **OBA** (13 mg, 0.05 mmol) and **L1** (8.5 mg, 0.03 mmol) in a 5 mL (1:1 v/v) solution of DMA-DMSO was heated to 100 °C in a sintered glass vial for 24 h. A polycrystalline powder was obtained.

HC6: Crystals of **HC1** were submerged in a mixture of $\text{Co}(\text{NO}_3)_2 \cdot 6\text{H}_2\text{O}$ (15 mg, 0.05 mmol), **OBA** (13 mg, 0.05 mmol) and **L1** (8.5 mg, 0.03 mmol) in a 5 mL (1:1 v/v) solution of DMA-DMSO was heated to 100 °C in a sintered glass vial for 24 h. Homoepitaxial crystals were obtained.

CHAPTER IV: TUNING MOF SEQUESTRATION AND STORAGE

	HC1	HC1'	HC1-oxy
Empirical formula	C ₂₆ H ₂₁ N ₂ O ₆ Zn	C ₂₄ H ₁₆ N O ₅ Zn	C ₃₂ H ₂₆ N O ₅ Zn
Formula weight	514.06	463.77	569.93
Temperature (K)	100(0)	100(0)	100(0)
Wavelength (Å)	Monoclinic	Monoclinic	Monoclinic
Crystal system	0.71073	0.71073	0.71073
<i>a</i> /Å	15.078(6)	15.216(3)	15.083(1)
<i>b</i> /Å	24.074(1)	24.138(4)	24.451(2)
<i>c</i> /Å	15.823(6)	15.905(3)	15.932(2)
α /°	90.0	90.0	90.0
β /°	110.830(7)	111.251(2)	111.193(1)
γ /°	90.0	90.0	90.0
Space group	<i>C2/c</i>	<i>C2/c</i>	<i>C2/c</i>
Volume (Å ³)	5368(4)	5444.4(2)	5478(9)
<i>Z</i>	8	8	8
Calculated density (g cm ⁻³)	1.272	1.132	1.382
Absorption coefficient (mm ⁻¹)	0.952	0.930	0.938
<i>F</i> ₀₀₀	2116.2	1896	2360.0
θ range for data collection (°)	1.67 to 27.81	1.69 to 28.41	1.67 to 28.62
Miller index ranges	-19 ≤ <i>h</i> ≤ 16, -31 ≤ <i>k</i> ≤ 26, -20 ≤ <i>l</i> ≤ 20	-20 ≤ <i>h</i> ≤ 15, -30 ≤ <i>k</i> ≤ 31, -21 ≤ <i>l</i> ≤ 20	-18 ≤ <i>h</i> ≤ 20, -26 ≤ <i>k</i> ≤ 31, -21 ≤ <i>l</i> ≤ 21
Reflections collected	16610	16755	16687
Independent reflections	6063	6238	6270
Completeness to θ_{\max} (%)	94.7	91.1	94.5
Max. and min. transmission	0.895, 0.692	0.830, 0.469	0.881, 0.724
Refinement method	Full-matrix least-squares on <i>F</i> ²	Full-matrix least-squares on <i>F</i> ²	Full-matrix least-squares on <i>F</i> ²
Data / restraints / parameters	3070/350/375	5116/0/287	2776/6/316
Goodness-of-fit on <i>F</i> ²	1.102	1.061	0.991
Final <i>R</i> indices [<i>I</i> > 2 σ (<i>I</i>)]	<i>R</i> 1 = 0.0947, <i>WR</i> 2 = 0.2637	<i>R</i> 1 = 0.0371, <i>WR</i> 2 = 0.1035	<i>R</i> 1 = 0.0991, <i>WR</i> 2 = 0.1994

CHAPTER IV: TUNING MOF SEQUESTRATION AND STORAGE

	HC1·mxy	HC1·pxy	HC1-dioxane
Empirical formula	C ₃₂ H ₂₆ N O ₅ Zn	C ₃₂ H ₂₆ N O ₅ Zn	C ₂₆ H ₁₉ N O ₆ Zn
Formula weight	569.93	563.77	496.81
Temperature (K)	100(0)	100(0)	100(0)
Wavelength (Å)	0.71073	0.71073	0.71073
Crystal system	Monoclinic	Monoclinic	Monoclinic
<i>a</i> /Å	15.281(2)	15.501(1)	15.284(7)
<i>b</i> /Å	24.113(3)	23.562(2)	23.699(1)
<i>c</i> /Å	15.814(2)	15.761(2)	15.854(1)
α /°	90.0	90.0	90.0
β /°	110.968(2)	111.104(9)	111.453(4)
γ /°	90.0	90.0	90.0
Space group	<i>C2/c</i>	<i>C2/c</i>	<i>C2/c</i>
Volume (Å ³)	5439(1)	5370(1)	5345(5)
<i>Z</i>	8	8	8
Calculated density (g cm ⁻³)	1.392	1.395	1.235
Absorption coefficient (mm ⁻¹)	0.945	0.957	0.954
<i>F</i> ₀₀₀	2360.0	2333.1	2040.0
θ range for data collection (°)	1.66 to 28.18	1.65 to 28.12	1.67 to 28.29
Miller index ranges	-13 ≤ <i>h</i> ≤ 19, -23 ≤ <i>k</i> ≤ 30, -19 ≤ <i>l</i> ≤ 20	-20 ≤ <i>h</i> ≤ 19, -29 ≤ <i>k</i> ≤ 30, -15 ≤ <i>l</i> ≤ 20	-19 ≤ <i>h</i> ≤ 20, -25 ≤ <i>k</i> ≤ 30, -20 ≤ <i>l</i> ≤ 14
Reflections collected	11298	15775	14969
Independent reflections	6109	6142	6063
Completeness to θ_{\max} (%)	91.5	93.5	91.2
Max. and min. transmission	0.883,0.813	0.928, 0.806	0.895,0.692
Refinement method	Full-matrix least-squares on <i>F</i> ²	Full-matrix least-squares on <i>F</i> ²	Full-matrix least-squares on <i>F</i> ²
Data / restraints / parameters	2666/0/423	3180/0/356	3066/0/317
Goodness-of-fit on <i>F</i> ²	0.918	0.954	0.986
Final <i>R</i> indices [<i>I</i> > 2 σ (<i>I</i>)]	<i>R</i> 1 = 0.0786, <i>WR</i> 2 = 0.1466	<i>R</i> 1 = 0.0693, <i>WR</i> 2 = 0.1401	<i>R</i> 1 = 0.0909, <i>WR</i> 2 = 0.2326

CHAPTER IV: TUNING MOF SEQUESTRATION AND STORAGE

	HC2	HC2'	HC3
Empirical formula	C ₇₂ H ₄₈ Co ₃ N ₃ O ₁₅	C ₂₄ H ₁₆ CoN ₅ O ₅	C ₂₄ H ₁₆ N ₅ O ₅ Zn _{0.80} Co _{0.20}
Formula weight	1371.92	457.31	462.48
Temperature (K)	100(0)	100(0)	100(0)
Wavelength (Å)	0.71073	0.71073	0.71073
Crystal system	Monoclinic	Monoclinic	Monoclinic
<i>a</i> /Å	15.019(9)	15.183(5)	15.056(3)
<i>b</i> /Å	24.181(9)	24.061(8)	24.231(5)
<i>c</i> /Å	44.410(2)	15.881(7)	15.788(3)
α /°	90.0	90.0	90.0
β /°	94.448(9)	111.736(4)	110.886(3)
γ /°	90.0	90.0	90.0
Space group	<i>C2/c</i>	<i>C2/c</i>	<i>C2/c</i>
Volume (Å ³)	16080(1)	5389(3)	5381.3
<i>Z</i>	8	8	8
Calculated density (g cm ⁻³)	1.133	1.127	1.142
Absorption coefficient (mm ⁻¹)	0.668	0.665	0.886
<i>F</i> ₀₀₀	5616.0	1872.0	1891.2
θ range for data collection (°)	0.92 to 28.44	1.67 to 28.45	1.67 to 28.29
Miller index ranges	-19 ≤ <i>h</i> ≤ 19, -32 ≤ <i>k</i> ≤ 31, -57 ≤ <i>l</i> ≤ 56	-18 ≤ <i>h</i> ≤ 20, -27 ≤ <i>k</i> ≤ 31, -21 ≤ <i>l</i> ≤ 20	-19 ≤ <i>h</i> ≤ 13, -25 ≤ <i>k</i> ≤ 31, -20 ≤ <i>l</i> ≤ 20
Reflections collected	85928	16499	16811
Independent reflections	18869	6238	6229
Completeness to θ_{\max} (%)	93.2	91.7	93.3
Max. and min. transmission	0.957, 0.802	0.910, 0.738	0.911, 0.854
Refinement method	Full-matrix least-squares on <i>F</i> ²	Full-matrix least-squares on <i>F</i> ²	Full-matrix least-squares on <i>F</i> ²
Data / restraints / parameters	9419/2/767	4014/267/280	3148/0/291
Goodness-of-fit on <i>F</i> ²	1.776	1.049	1.002
Final <i>R</i> indices [<i>I</i> > 2 σ (<i>I</i>)]	<i>R</i> 1 = 0.2620, <i>WR</i> 2 = 0.5283	<i>R</i> 1 = 0.1035, <i>WR</i> 2 = 0.2824	<i>R</i> 1 = 0.0983, <i>WR</i> 2 = 0.2781

4.14 References

- 1 http://www.fe.doe.gov/education/energylessons/coal/coal_history.html accessed 18.03.15.
- 2 <http://www.epa.gov/climatechange/ghgemissions/gases/co2.html> accessed 18.03.15.
- 3 B. Xiao, P. J. Byrne, P. S. Wheatley, D. S. Wragg, X. B. Zhao, A. J. Fletcher, K. M. Thomas, L. Peters, J. S. O. Evans, J. E. Warren, W. Z. Zhou, R. E. Morris, *Nat. Chem.*, **2009**, *1*, 289.
- 4 Z. M. Duan, Y. Zhang, B. Zhang, D. B. Zhu, *J. Am. Chem. Soc.*, **2009**, *131*, 6934.
- 5 C. Serre, C. Mellot-Draznieks, S. Surble, N. Audebrand, Y. Filinchuk, G. Ferey, *Science*, **2007**, *315*, 1828.
- 6 J. Seo, C. Bonneau, R. Matsuda, M. Takata, S. Kitagawa, *J. Am. Chem. Soc.* **2011**, *133*, 9005.
- 7 B. Chen, C. Liang, J. Yang, D. S. Contreras, Y. L. Clancy, E. B. Lobkovsky, O. M. Yaghi, S. Dai, *Angew. Chem., Int. Ed.*, **2006**, *45*, 1390.
- 8 R. B. Getman, Y. -S. Bae, C. E. Wilmer, R. Q. Snurr, *Chem. Rev.*, **2012**, *112*, 703.
- 9 K. Sumida, D. L. Rogow, J. A. Mason, T. M. McDonald, E. D. Bloch, Z. R. Herm, T. -H. Bae, J. R. Long, *Chem. Rev.*, **2012**, *112*, 724.
- 10 S. Horike, Y. Inubushi, T. Hori, T. Fukushima, S. Kitagawa, *Chem. Sci.*, **2012**, *3*, 116.
- 11 H. -C. Zhou, J. R. Long, O. M. Yaghi, *Chem. Rev.*, **2012**, *112*, 673.
- 12 H. -S. Lu, L. Bai, W. -W. Xiong, P. Li, J. Ding, G. Zhang, T. Wu, Y. Zhao, J. Lee, Y. Yang, B. Geng, Q. Zhang, *Inorg. Chem.*, **2014**, *53*, 8529.
- 13 J. Gao, K. Ye, L. Yang, W. -W. Xiong, L. Ye, Y. Wang, Q. Zhang, *Inorg. Chem.*, **2014**, *53*, 691.
- 14 a) J. Gao, M. He, Z. Y. Lee, W. Cao, W. -W. Xiong, Y. Li, R. Ganguly, T. Wu, Q. Zhang, *Dalton Trans.*, **2013**, *42*, 11367.; b) I. -H. Park, S. S. Lee, J. J. Vittal, *Chem. Eur. J.*, **2013**, *19*, 2695.
- 15 I. -H. Park, S. S. Lee, J. J. Vittal, *Chem. Eur. J.*, **2013**, *19*, 2695.
- 16 P. Van Der Sluis, A. L. Spek, *Acta Crystallogr., Sect. A*, **1990**, *46*, 194.
- 17 H. M. N. H. Irving, R. J. P. Williams, *J. Chem. Soc.*, **1953**, 637, 3192.

Guest-induced motion in soft porous crystals

MOFs with permanent porosity possess either one-, two- or three-dimensional channels that allow unhindered guest transport. Flexible coordination polymers in which guest transport triggers structural changes within the host are deemed *soft* porous crystals. This study describes novel third generation *soft* porous materials that undergo a pedal-type motion. This motion has been shown to take place in various types of molecules including (*E*)-stilbenes, azobenzenes, *N*-benzylideneanilines, and 1,2-dipyridylethenes.¹ Although not uncommon, this phenomenon is usually misidentified and, as a result, its significance is often overlooked. Pedal motion has been shown to play important roles in solid-state reactions and should always be considered when interpreting the dynamic properties of crystals containing such molecules. In crystals containing 1,2-dipyridylethenes, the two pyridyl rings of the molecule can be thought of as pedals of a bicycle (**Figure 5.1a**). Each pyridyl ring is attached to a central ethene bond by a C-Py bond and can rotate around it.¹ The pedal motion may be regarded as the simultaneous rotation of the two pyridyl rings in opposite directions and the overall molecular rotation coupled to them.¹ Such motion enables the molecule to undergo a conformational change from the *anti*- to the *syn* conformer and back again.¹

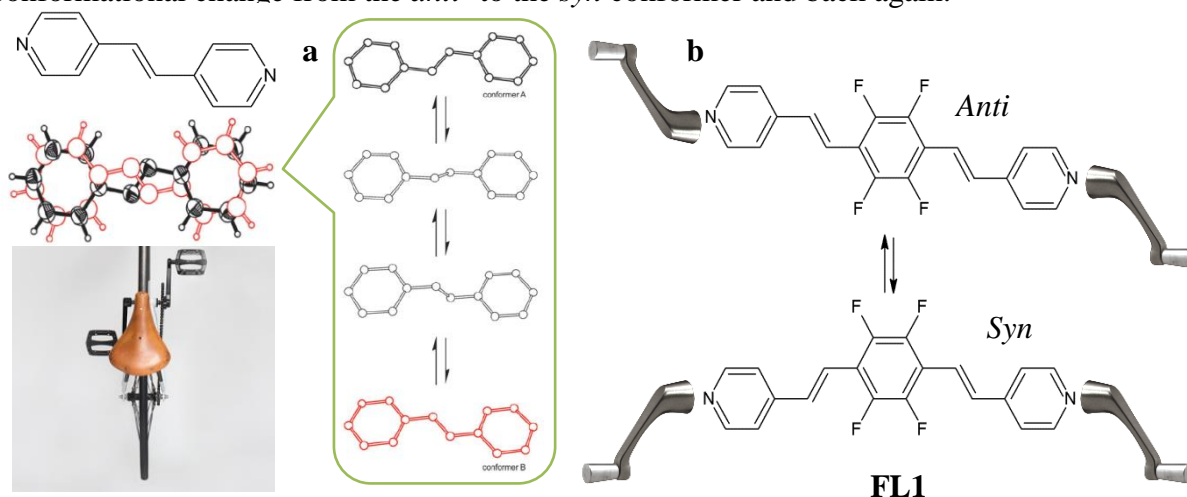


Figure 5.1 a) Conventional pedal motion. b) Crank-handle motion possible in FL1.

Although the term pedal motion has previously been used to describe motion in ligands very similar to FL1² (**Figure 5.1b**) we believe that this analogy breaks down for a system of higher complexity and that “crank-handle” motion is a more accurate term. In the both conformers, the two rings are parallel to each other like two independent crank-handles.

CHAPTER V: GUEST-INDUCED MOTION IN SOFT POROUS CRYSTALS

As the crank-handle motion occurs, the planes of the pyridyl rings do not largely change their orientations and remain parallel to each other. The quaternary carbon-carbon (QCC) bond on the other hand experiences dramatic changes in its orientation. The dihedral angles between the pyridyl rings and the QCC bond increases to reach almost 90° at the transition state. Eventually the QCC bond rotates 180° and the whole molecule adopts a different orientation (*syn* conformer). Since the molecules experience only minor alterations of their shape and volume, such changes are able to occur in a SC-SC manner. When the crank-handle motion and the concomitant conformational interconversion take place in the crystal, the two alternating conformers may be randomly distributed and thus observed as disorder in the crystal structure.¹ Such materials may be ‘tuned’ depending on the nature and type of stimulus applied and have potential applications in the dynamic switching of optical, electric, magnetic and gas uptake properties.^{3,4,5,6,7,8}

It is important to note that not all ligands containing such pedal- or crank-handle moieties show disorder. This is not to say that such motion cannot occur in these structures but rather that such a material might fall into one of two categories. The first involves the inhibition of the conformational interconversion due to a high energy barrier to the pedal- or crank-handle motion. If the activation energy of the motion is very large in the crystal, the rate of the conformational interconversion is greatly reduced and the populations of the conformers can no longer obey the Boltzmann distribution. As a result, only one conformer exists in the crystal and no disorder appears in the observed structure. Alternatively, one could explain this in terms of the low stability of the minor conformer. When the energy difference between the two conformers is large, pedal- or crank-handle motion does not result in any detectable disorder because the Boltzmann distribution predicts that there will be a small to negligible population of the minor conformer.^{1,9}

In addition to crank-handle motion, dipyriddyethene and its derivatives have been shown to undergo [2 + 2] cycloaddition reactions.¹⁰ The probability of the ligand **FL1** undergoing such a reaction is increased by its incorporation into a MOF. Di-coordination to a metal (especially cadmium +2 which has a tendency to form SBUs conducive to layered motif formations)¹¹ fixes the ligands in place and enables the alignment of one ligand on top of another in a ladder-like fashion. This coupled with the presence of electron withdrawing fluorine substituents on the central phenyl ring (which promote contraction of the distance between successive ligands due to offset π - π and electrostatic interactions) creates an optimum environment for [2 + 2] cycloaddition.¹²

CHAPTER V: GUEST-INDUCED MOTION IN SOFT POROUS CRYSTALS

Two groups of soft porous compounds (**SPC1** and **SPC2**) are described in this chapter. Both are extremely robust, possess 1D channels and were synthesised using 1,4'-bis-(pyridyl-ethenyl)-tetrafluorobenzene (**FL1**) (**Figure 5.1**). This fluorinated version of the **L1** ligand described in Chapter IV (fluorine was selected owing to its small size, ensuring minimum steric interference but maximum electrostatic modification) was combined with the flexible **OBA** carboxylic acid ligand and either zinc nitrate hexahydrate or cadmium nitrate tetrahydrate salts. The resulting MOFs undergo guest exchange via a series of SC-SC transformations and exhibit interesting gas sorption properties. In addition, **SPC1** and **SPC2** undergo unique conformational conversions that can be altered by guest inclusion.

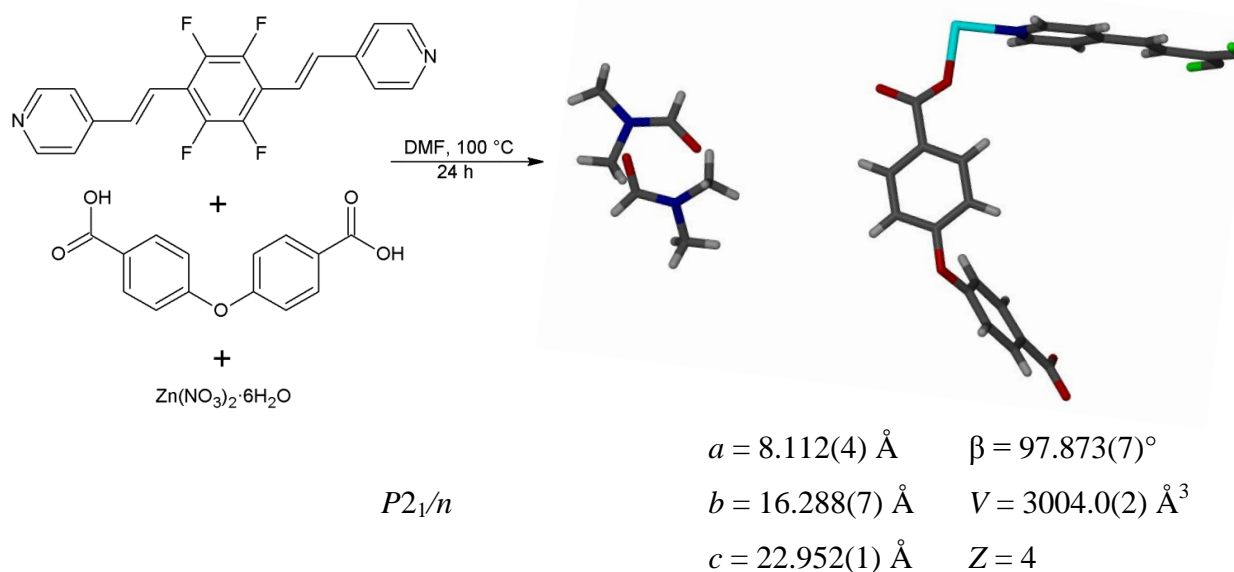
5.1 MOFs prepared using FL1

FL1 was designed to extend the work already carried out with **L1**. It was rationalised that the introduction of fluorine substituents to the central phenyl ring would result in even greater framework interaction with guest molecules such as CO₂ (fluorine atoms are small, highly electronegative atoms which would interact strongly with the carbon atom of CO₂).¹³ Functionalisation of the central phenyl ring ensures that **FL1** behaves very differently when compared to its parent compound **L1** and this is particularly evident with the frameworks obtained (fluorine atoms are electron-withdrawing and would thus greatly alter the electrostatic as well as steric nature of the ligand). Crystallisation of **FL1** with zinc and cadmium nitrate salts results in several 3D frameworks. The zinc-containing MOF (**SPC1**) shows reversible, highly guest specific transformations while the cadmium-containing MOF (**SPC2**) differs in that it contains more rigid void space, which is discussed in-depth below.

CHAPTER V: GUEST-INDUCED MOTION IN SOFT POROUS CRYSTALS

5.1.1 $\{[\text{Zn}(\text{FL1})_{0.5}(\text{OBA})]\cdot\text{DMF}\}_n$ or **SPC1a**

SPC1a was formed from the reaction of **FL1**, **OBA** and Zn(II) nitrate hexahydrate under solvothermal conditions (100 °C, DMF) (Scheme 5.1). **SPC1a** crystallises in the monoclinic space group $P2_1/n$. The ASU consists of one zinc cation, one **OBA** ligand, half an **FL1** ligand (located on an inversion centre) and one DMF molecule disordered over two positions (60:40 site occupancy).



Scheme 5.1 Synthesis of **SPC1a** from the solvothermal reaction of **FL1**, **OBA** and zinc nitrate in DMF at 100 °C, with selected crystallographic information.

Unlike the parent framework **HC1**, this framework contains a typical paddlewheel dinuclear zinc carboxylate unit $[\text{Zn}_2(\text{COO})_4]$ (Figure 5.2a). The metal centres are bridged by the **OBA** ligands to form a 2D network. The 2D nets stack on top of one another and are further linked into a 3D network by bridging **FL1** ligands in the *anti* conformation. The structure is twofold interpenetrated and contains large ‘triangular’ corrugated channels along $[1\ 0\ 0]$ that are occupied by DMF molecules (Figure 5.2b). Figure 5.2c shows the **OBA** molecules aligned down the b axis in a uniform manner (central oxygen atoms of neighbouring **OBA** ligands are displaced from one another by 8.24 Å).

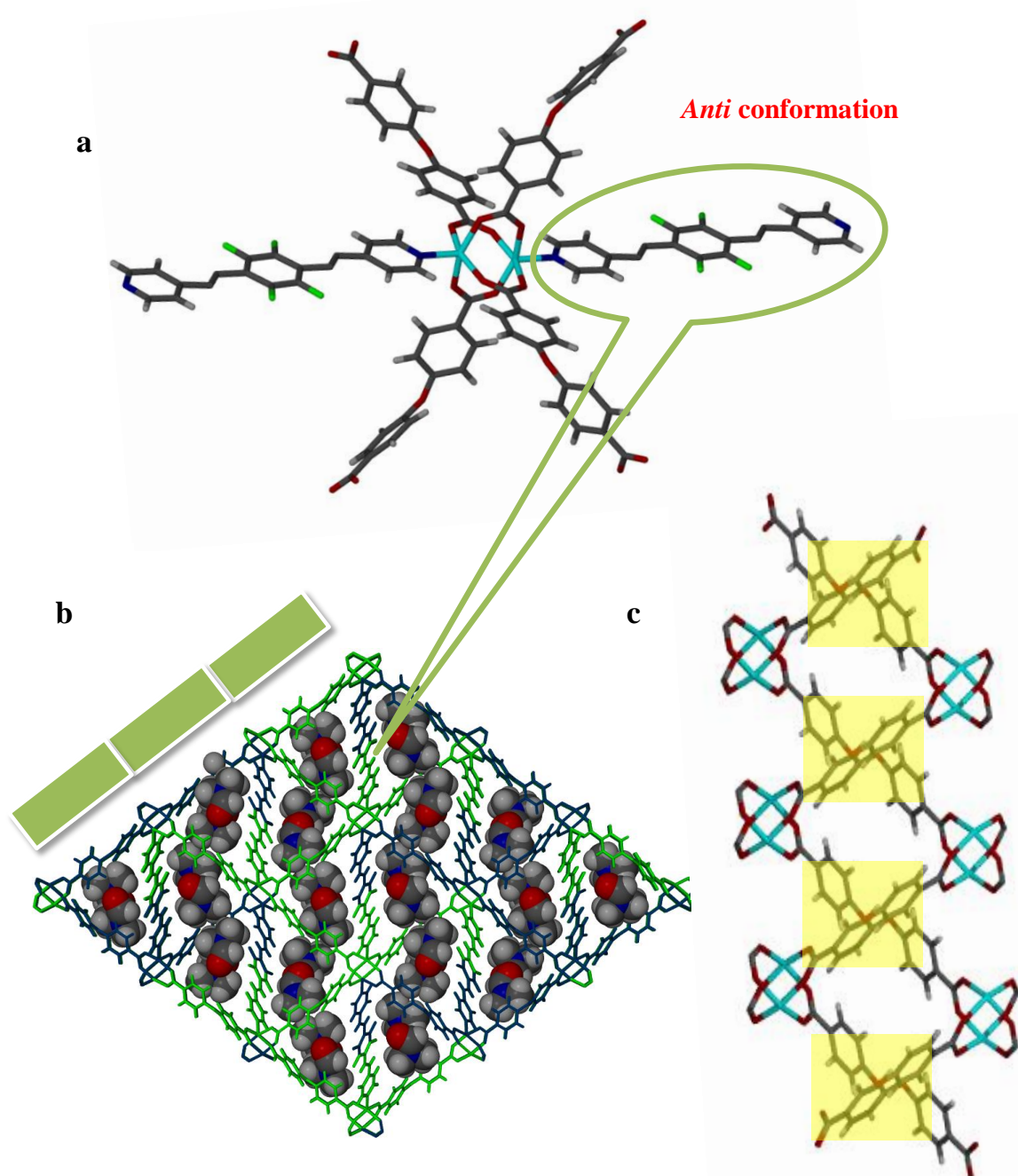


Figure 5.2 a) Paddlewheel moiety of SPC1a with FL1 in the *anti* conformation. b) Solvent-filled channels viewed along the *a* axis. c) OBA ligands viewed down the *b* axis with uniform (yellow) alignment.

The TGA thermogram (**Figure 5.3**) shows mass loss from 30 - 150 °C. Unfortunately it was not possible to deconvolute the thermogram to distinguish residual surface solvent from guest removal. SQUEEZE¹⁴ corroborated the single DMF molecule modelled per formula unit. The framework appears to be stable until decomposition sets in at 350 °C.

CHAPTER V: GUEST-INDUCED MOTION IN SOFT POROUS CRYSTALS

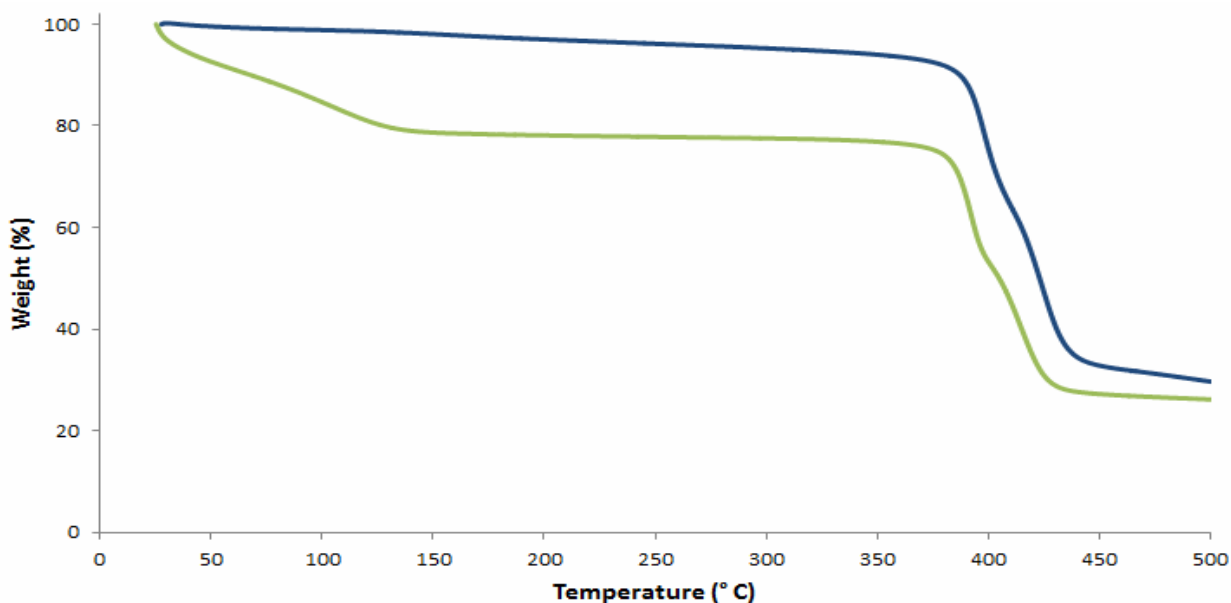


Figure 5.3 TGA of the as-synthesised as well as the evacuated phases of **SPC1a** (green and blue lines, respectively).

The apohost form (**SPC1a'**) may be generated by heating the solvate at 150 °C under reduced pressure for 24 h. Due to the robust nature of the framework, this occurs as a SC-SC transformation. The cell parameters undergo some change (**Figure 5.4**) but the conformation of ligand **FL1** is of particular interest. The ASU comprises one zinc ion, one **OBA** ligand and one **FL1** ligand located on a centre of inversion. In place of the previously observed *anti* conformation, both fragments now possess the *syn* conformation (**Figure 5.5**). The solvated form **SPC1a** may be regenerated by simply immersing the **SPC1a'** crystals in DMF.

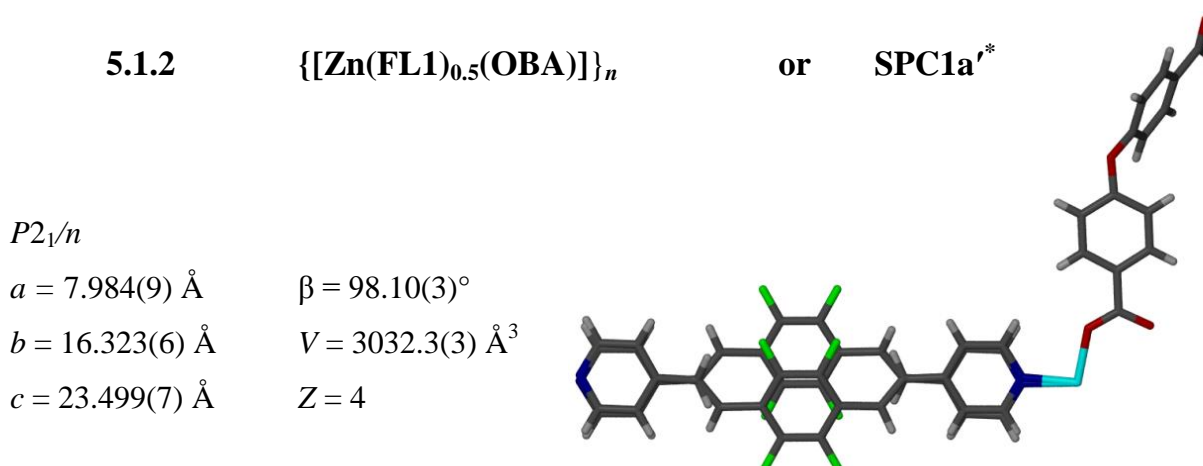


Figure 5.4 Crystallographic information for **SPC1a'** with the ASU showing the fluorinated ring and ethene bonds of **FL1** disordered over two positions.

* Prime denotes activation.

CHAPTER V: GUEST-INDUCED MOTION IN SOFT POROUS CRYSTALS

Figure 5.5a shows the extended structure of **SPC1a'** with the **OBA** ligands adopting a sinusoidal arrangement not observed in the solvate **SPC1a**. **Figure 5.5b** shows the **OBA** molecules viewed down the *b* axis aligned in a different but none the less uniform manner (central oxygen atoms from adjacent **OBA** ligands are displaced from one another by 8.46 Å). The porous structure possesses 138 Å³ of solvent-accessible space per unit cell.

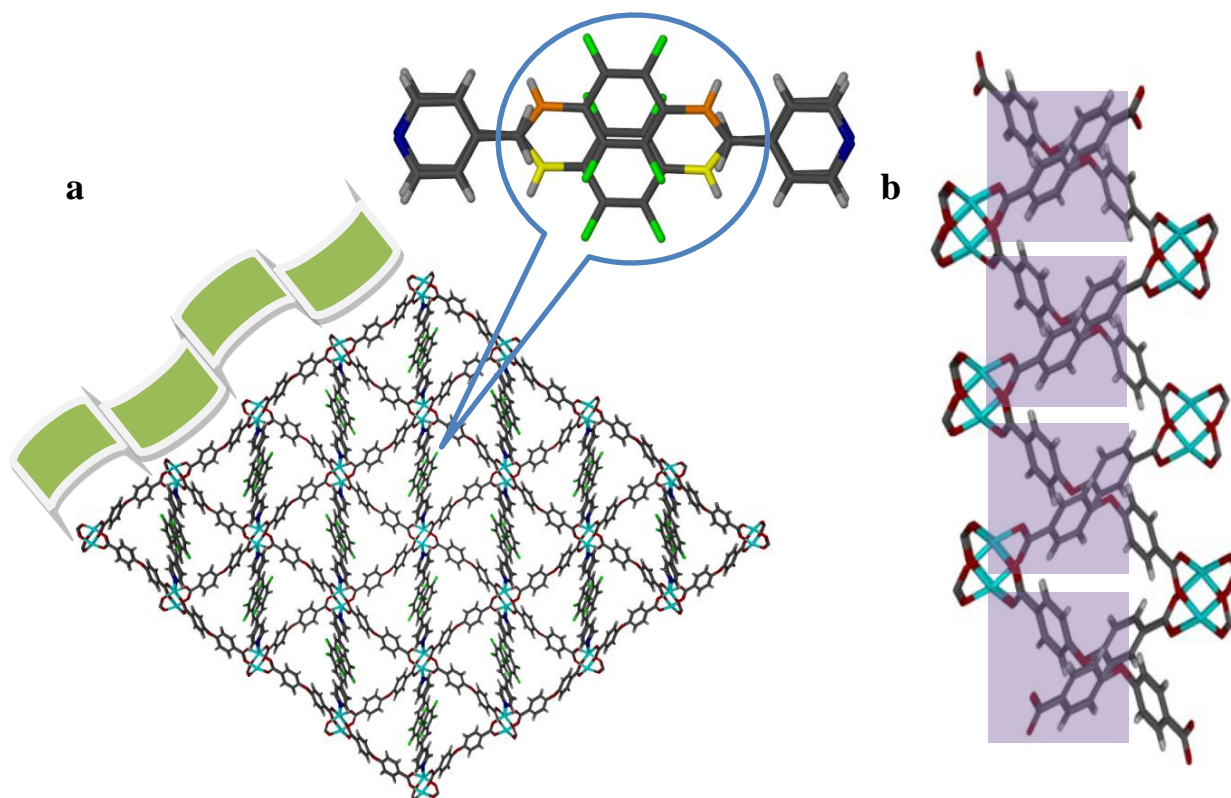


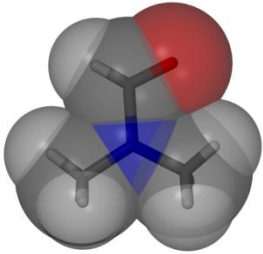
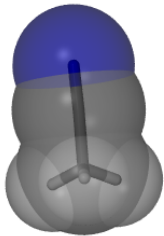
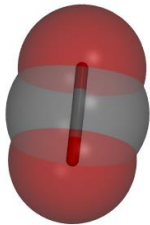
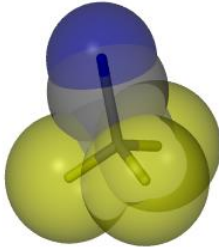
Figure 5.5 a) **FL1** ligand showing disordered fluorinated ring with both fragments in the *syn* conformation and sinusoidal propagation of the **OBA** ligands. b) **OBA** ligands viewed down the *b* axis (purple alignment).

5.2 SC-SC guest exchange experiments in **SPC1a**

Having observed that simple activation induces crank-handle motion within the ligand **FL1**, several SC-SC guest exchange experiments were carried out in the hope of establishing whether this transformation is guest-dependent. If so, this material could be classified as a guest-triggered switch. Crystals of **SPC1a** were exposed to a selection of guests including acetonitrile, supercritical CO₂ and trichloroacetonitrile. In all instances the DMF molecules were replaced by the target guest. **Table 5.1** presents the relevant crystallographic data obtained from the exchanges.

CHAPTER V: GUEST-INDUCED MOTION IN SOFT POROUS CRYSTALS

Table 5.1 Crystallographic data for SC-SC solvent-exchange experiments with **SPC1a**.*

$P2_1/n$			$P2_1/c$
			
SPC1a	SPC1a·ACN	SPC1a·CO₂[†]	SPC1a·Cl₃ACN
$a = 8.118(8) \text{ \AA}$	$a = 15.917(3) \text{ \AA}$	$a = 8.208(5) \text{ \AA}$	$a = 16.103(4) \text{ \AA}$
$b = 16.197(1) \text{ \AA}$	$b = 16.433(2) \text{ \AA}$	$b = 16.018(3) \text{ \AA}$	$b = 16.246(3) \text{ \AA}$
$c = 23.073(8) \text{ \AA}$	$c = 23.289(7) \text{ \AA}$	$c = 24.089(4) \text{ \AA}$	$c = 23.764(5) \text{ \AA}$
$\beta = 97.98(1)^\circ$	$\beta = 102.99(2)^\circ$	$\beta = 98.99(4)^\circ$	$\beta = 103.70(3)^\circ$
$V = 3004.8(4) \text{ \AA}^3$	$V = 5961.4(8) \text{ \AA}^3$	$V = 3128.4(8) \text{ \AA}^3$	$V = 6040.3(2) \text{ \AA}^3$
One DMF molecule disordered over two positions	Six full occupancy acetonitrile molecules	IR confirmed stretch at 2340 cm^{-1}	Three trichloroacetonitrile molecules (two of which are disordered) and one DMF molecule

The SC-SC guest exchange experiments produced several interesting results. As previously mentioned, the DMF solvate (**SPC1a**) contains the **FL1** ligand in the *anti* conformation. Exposure of this material to acetonitrile (**SPC1a·ACN**) results doubling of the *a* axis.

The ASU contains double the number of components as the original **SPC1a** with two crystallographically independent **FL1** ligand halves. This crystallographic artefact arises from two independent **FL1** ligands assuming different conformations, thus altering the periodicity of the structure. One of the **FL1** ligands is in the *syn* conformation with the fluorinated ring disordered over two positions while the second **FL1** ligand is in the *anti* conformation.

* Thermogravimetric data for these experiments as well as the IR spectrum showing the CO₂ stretch are located in the supplementary data.

[†] Data for eight different unit cells was collected with no evidence of cell parameter change thus no full data set was recorded.

CHAPTER V: GUEST-INDUCED MOTION IN SOFT POROUS CRYSTALS

It is clear that the changes observed in the cell parameters of **SPC1a·ACN** are due to a structural change, and not simply a loss of symmetry due to a guest change.

In light of the interesting result with acetonitrile, a molecule of similar size and shape (CO_2) was selected in the hope of establishing whether steric or electrostatic forces are responsible for the partial conversion. The **SPC1a·CO₂** unit cell shows some parameter changes, but there is no doubling of any parameters. In an attempt to further understand the potential electrostatic effect observed in **SPC1a·ACN**, an acetonitrile derivative (trichloroacetonitrile) was selected (it has the same core electrostatic properties with large additional contributions from the chloride ions). The cell parameters of **SPC1a·Cl₃ACN** are similar to those of the **SPC1a·ACN** structure. The ASU contains the same number of components as the acetonitrile structure but unlike the acetonitrile structure or the original solvate, the **SPC1a·Cl₃ACN** ASU contains one full **FL1** ligand in the *syn* conformation disordered over two positions. It is important to note that all exchanges are reproducible and reversible. Owing to their anomalous behaviour the **SPC1a·ACN** and **SPC1a·Cl₃ACN** structures will now be discussed in greater detail.

5.2.1 $\{[\text{Zn}_2(\text{FL1})(\text{OBA})_2] \cdot 6\text{ACN}\}_n$ or **SPC1a·ACN**

In spite of unit cell doubling, **SPC1a·ACN** remains in the monoclinic space group $P2_1/n$. The ASU contains two zinc ions, two **OBA** ligands and two crystallographically independent halves of the ligand **FL1**. **Figure 5.6** shows the two conformations present with the *syn* conformer disordered over two positions. The ASU also contains six acetonitrile guest molecules, five of which are involved in electrostatic guest-guest interactions with the sixth experiencing an offset π - π host-guest interaction (**Figure 5.7**).

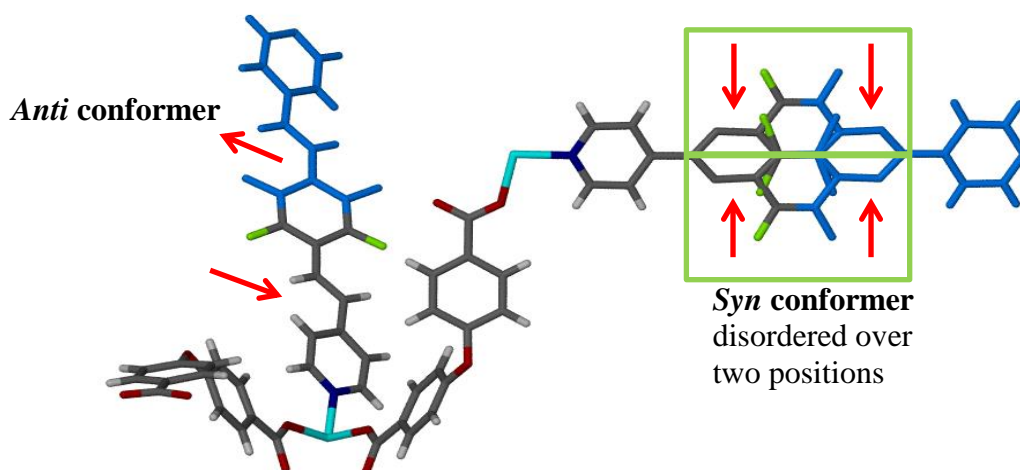


Figure 5.6 ASU of **SPC1a·ACN** with additional atoms coloured blue to show the two conformations of the **FL1** ligand. Solvent molecules have been omitted for clarity.

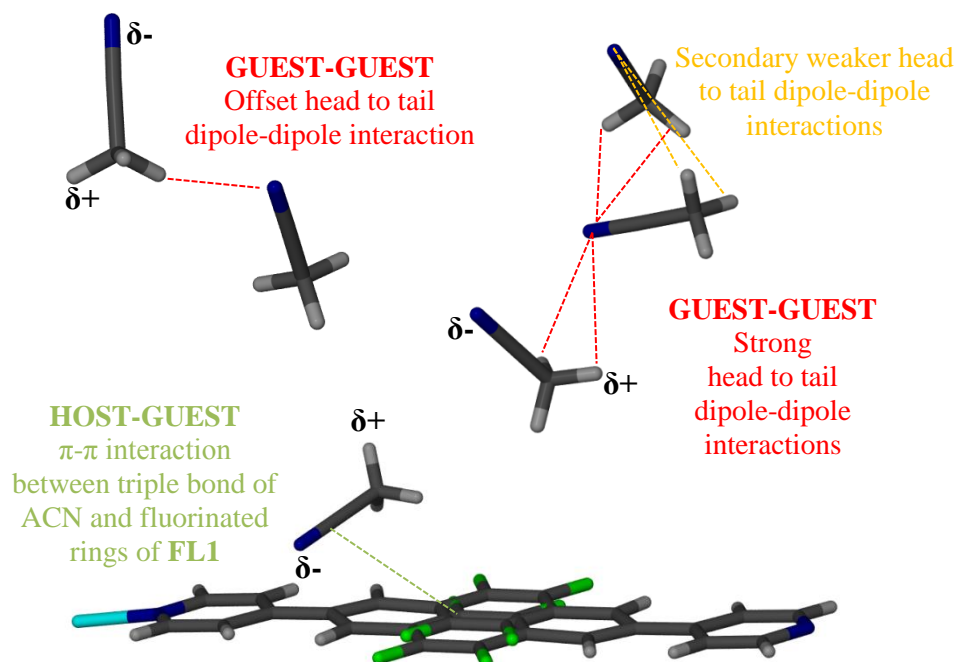


Figure 5.7 Types of interactions experienced by the six ACN guest molecules in **SPC1a**.

Figure 5.8 shows the densely packed acetonitrile molecules located within the corrugated channels of **SPC1a·ACN**. Omission of these molecules from the figure gives a better idea of the acid and pyridyl ligand conformations. The two independent **FL1** ligands align one over another with the ligand in the *anti* conformation approximately perpendicular (fluorine atoms of *anti*- point toward phenyl ring of *syn*-) to the disordered *syn* conformer (**Figure 5.9a**). The **OBA** ligands are not eclipsed one over another but rather arrange in a clam-shell manner (**Figure 5.9a**). When viewed down the *b* axis, the **OBA** ligands adopt an **AB** arrangement in which the oxygen atoms of adjacent **OBA** ligands lie in an alternating, aligned or displaced manner by 8.69 Å (**Figure 5.9b**) relative to one another.

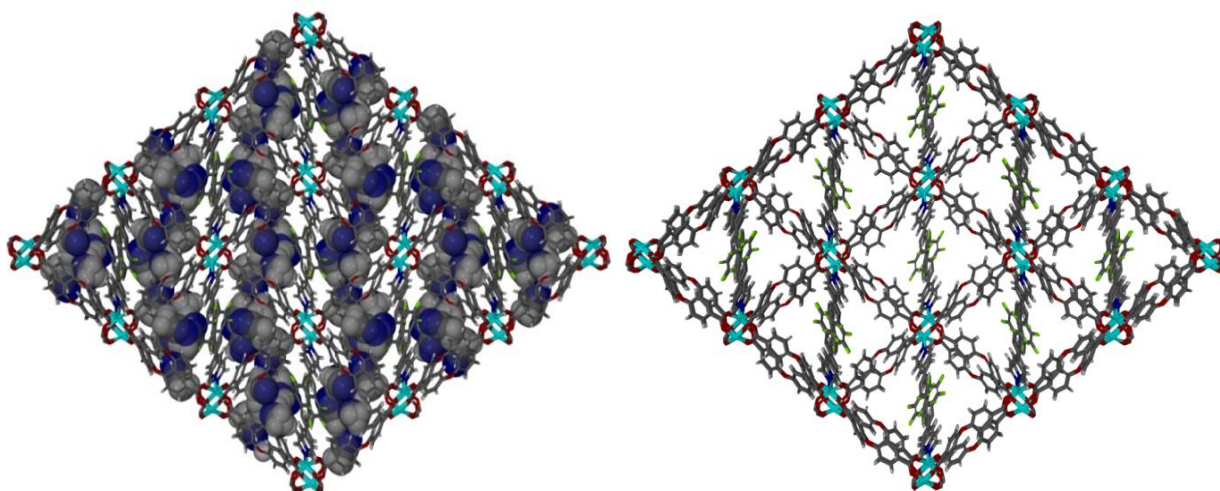


Figure 5.8 SPC1a·ACN viewed down the *a* axis shown with space-filled acetonitrile guest molecules (left) and with the solvent hidden (right).

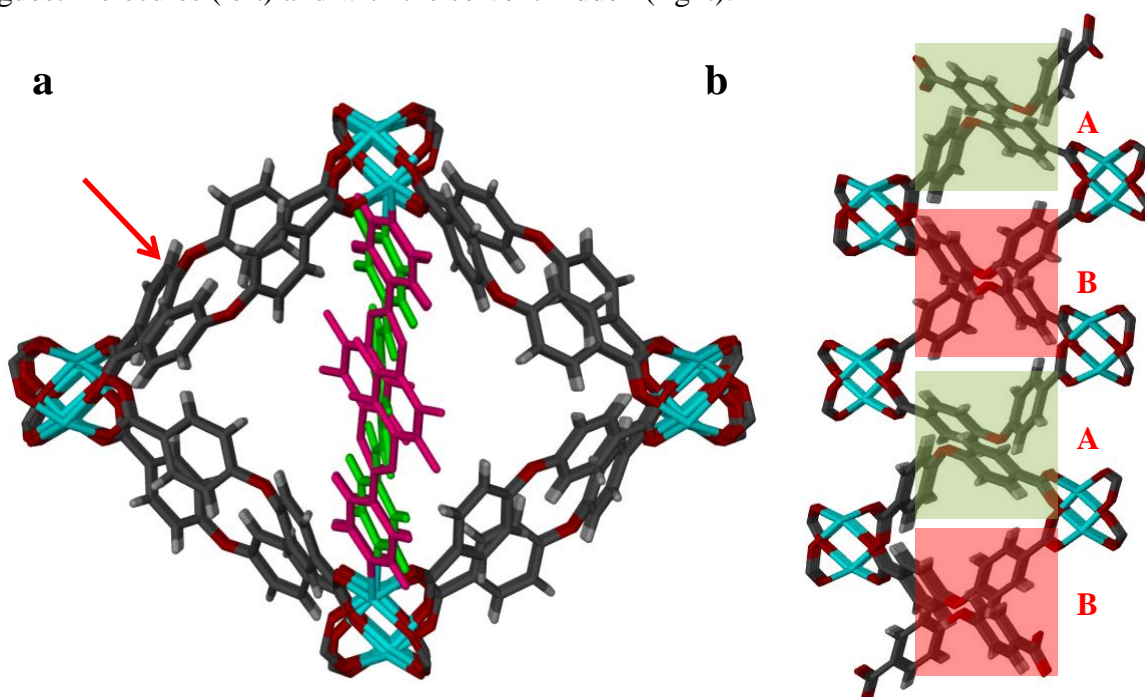


Figure 5.9 a) Portion of SPC1a·ACN with solvent hidden to show orientations of ligands. b) OBA packing viewed down the *b* axis with AB (green-red) arrangement.

5.2.2 $\{[\text{Zn}_2(\text{FL1})(\text{OBA})_2] \cdot 3\text{Cl}_3\text{ACN} \cdot \text{DMF}\}_n$ or SPC1a·Cl₃ACN

SPC1a·Cl₃ACN crystallises in the space group $P2_1/c$. The ASU contains two metal centres, two OBA ligands, and one FL1 ligand in the *syn* conformation disordered over two positions (52:48 site occupancy) as shown in **Figure 5.10**.

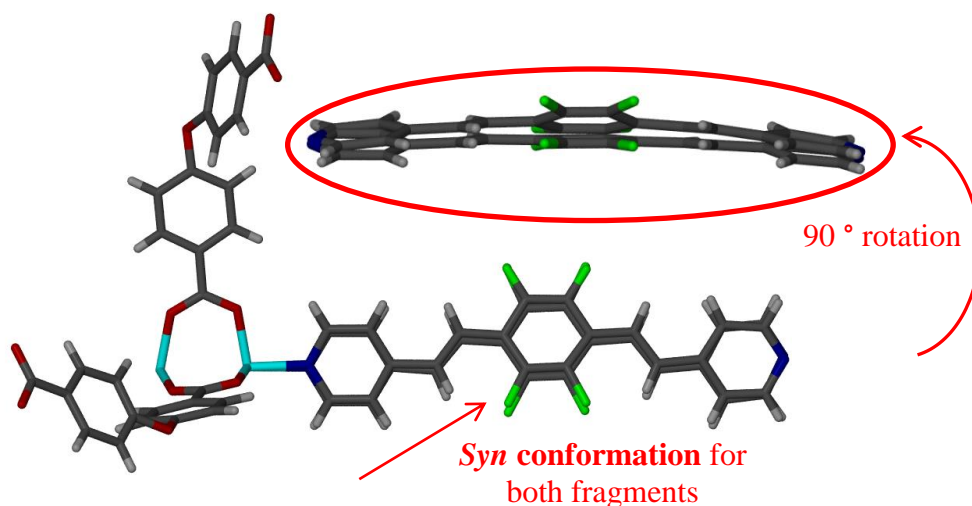


Figure 5.10 ASU of $\text{SPC1a}\cdot\text{Cl}_3\text{ACN}$ showing both disordered fragments of the **FL1** ligand in the *syn* conformation. Solvent molecules have been omitted for clarity.

The ASU also contains three trichloroacetonitrile guest molecules, two of which are disordered over two positions (57:43 site occupancy) and one DMF molecule (residual solvent from guest exchange). One disordered Cl_3ACN is involved in a guest to guest interaction with another Cl_3ACN while the second disordered Cl_3ACN is involved in a host-guest interaction with the **FL1** ligand (**Figure 5.11**).

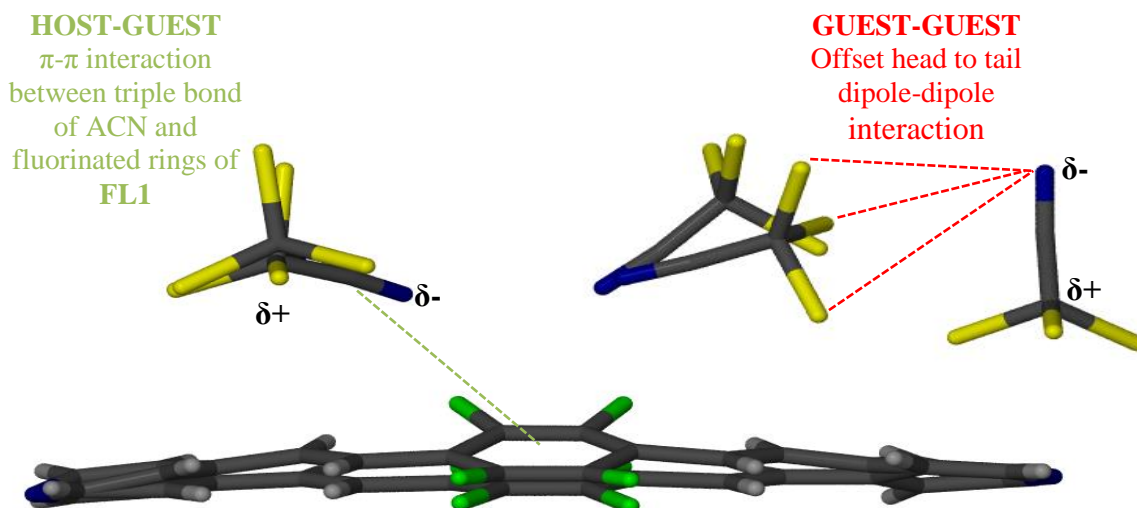


Figure 5.11 Types of interactions experienced by the Cl_3ACN guest molecules in $\text{SPC1a}\cdot\text{Cl}_3\text{ACN}$.

Figure 5.12 shows trichloroacetonitrile molecules tightly packed within the channels of $\text{SPC1a}\cdot\text{Cl}_3\text{ACN}$. When the guest molecules are hidden, the fluorinated rings of **FL1** ligands can clearly be seen to lie on top of another perpendicular to the paddlewheel (**Figure 5.13a**).

CHAPTER V: GUEST-INDUCED MOTION IN SOFT POROUS CRYSTALS

Figure 5.13a also shows the **OBA** ligands aligned in an eclipsed arrangement. When viewed down the *b* axis (**Figure 5.13b**), the ligands adopt an **AB** arrangement in which the oxygen atoms of adjacent **OBA** ligands lie displaced from one another by 8.52 or 8.35 Å.

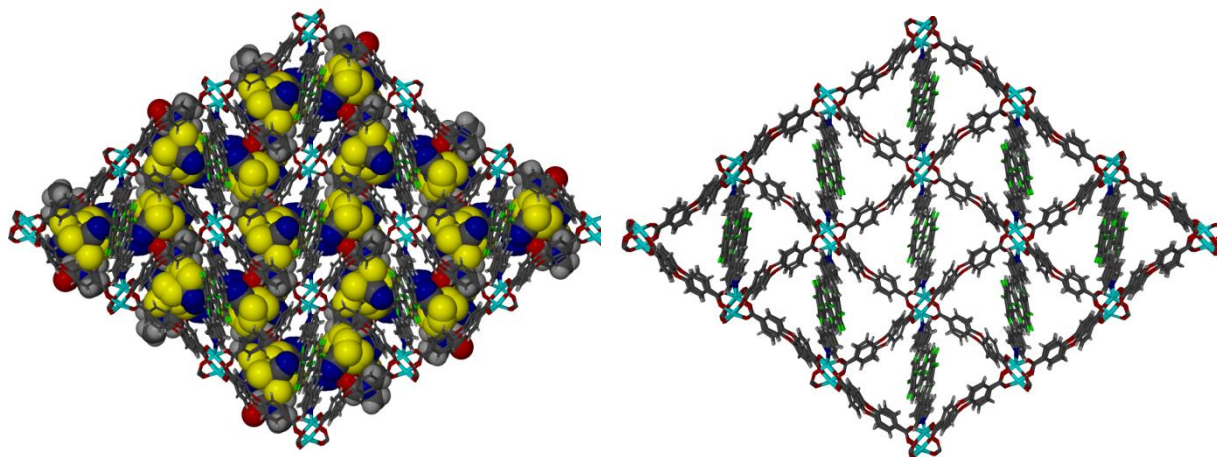


Figure 5.12 **SPC1a·Cl₃ACN** viewed down the *a* axis with space-filled trichloroacetonitrile and DMF molecules (left) and with the solvent molecules hidden (right).

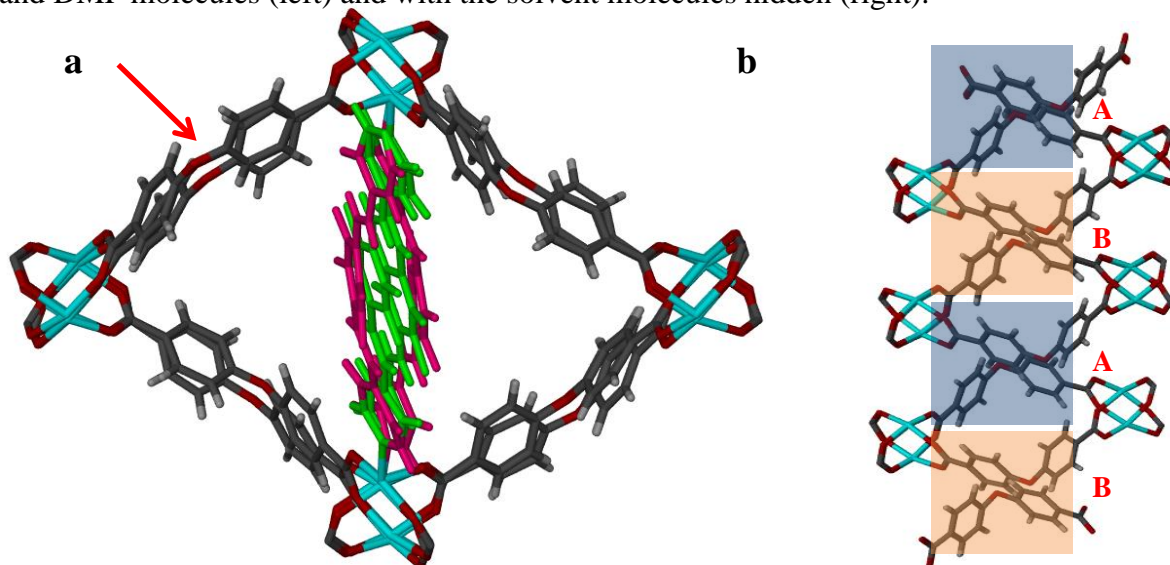


Figure 5.13 **a)** Extended structure of **SPC1a·Cl₃ACN** with solvent hidden to show the orientations of the ligands. **b)** **OBA** arrangement viewed down *b* with **AB** (blue-orange) stacking.

The crank-handle motion experienced by **SPC1a** appears to be highly solvent specific. It is believed that due to the ability of acetonitrile and trichloroacetonitrile to act as a collective rather than as individual molecules (both capable of forming infinite dipole-dipole dimers) their guest-guest electrostatic interactions have a larger effect on the host. For this to be verified, extensive computational studies would need to be performed.

5.3 Gravimetric gas sorption for SPC1a' using CO₂ and a series of linear alkanes

The gas sorption properties of **SPC1a'** were measured at 25 °C using CO₂, methane, ethane, propane and butane (**Figure 5.14**). **SPC1a'** shows Type I sorption behaviour for all selected guests, absorbing approximately one molecule of CO₂ (3.8 wt% at 20 bar), half a molecule of methane (1.7 wt% at 20 bar), ethane (3.9 wt% at 20 bar), propane (4.5 wt% at 8 bar) or a very small amount of butane, (*i.e.* ± 0.22 molecules or 2.6 wt% at 2 bar) per ASU. None of the gases attain full occupancy at 20 bar with the material absorbing only one of four possible CO₂ molecules (determined from the molecular volume of guest divided by solvent accessible space of the host)*. ¹⁵ It is thus possible that the framework could potentially accommodate more guest molecules. The potential selectivity trend is as follows: CO₂ > ethane > methane = propane > butane. Methane is the only gas showing negligible hysteresis.

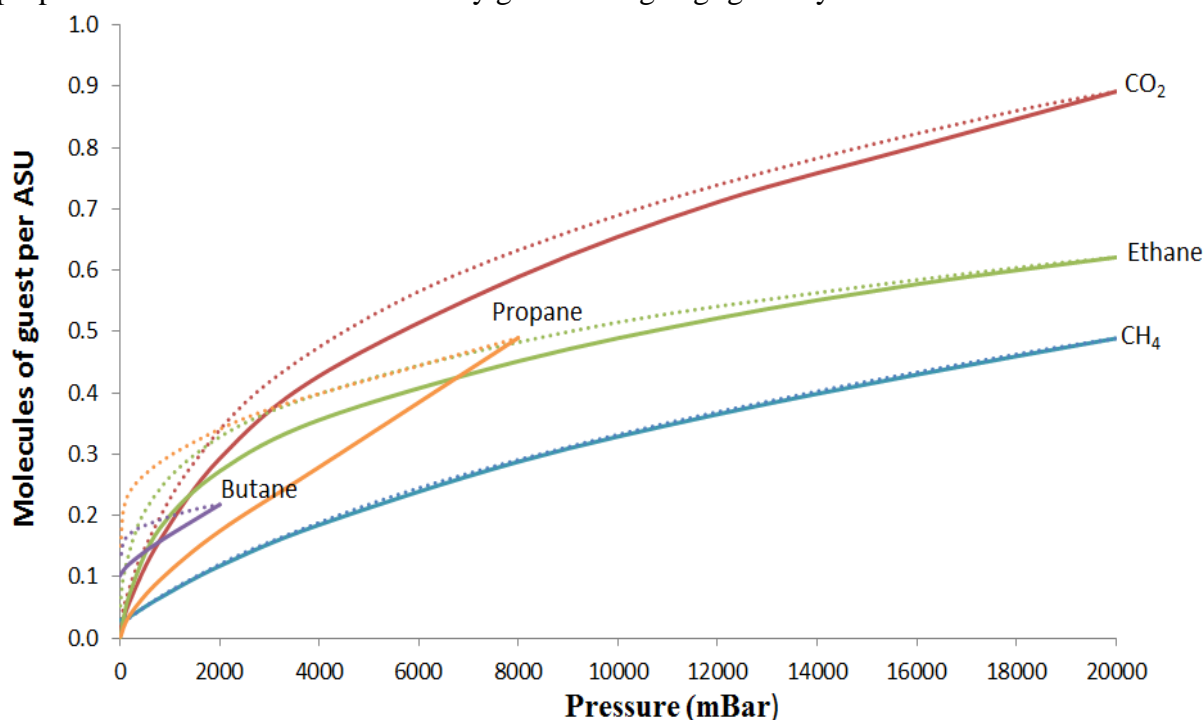


Figure 5.14 CO₂ and selected alkane sorption and desorption isotherms of **SPC1a'** at 25 °C. Solid lines represent sorption and dashed lines represent desorption.[†]

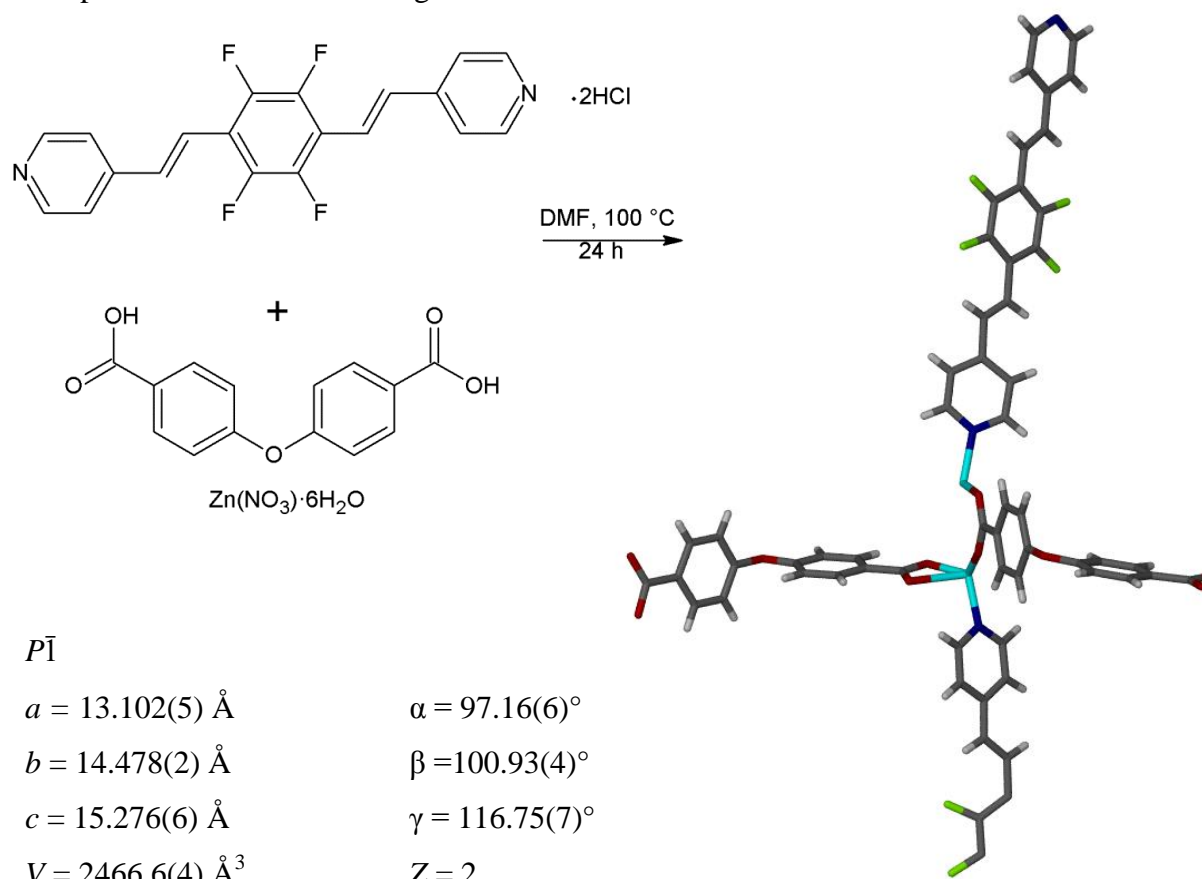
* According to Rebek *et al.* occupancy calculated this way is almost never actually obtained thus good theoretical occupancy is considered to fall in the range 0.55 ± 0.09 with larger packing coefficients of 0.70 only occurring in systems stabilised by strong intermolecular interactions.

[†] The butane and propane isotherms only reach 2 and 8 bar, respectively (*i.e.* the maximum pressure that each gas can attain at 25 °C).

CHAPTER V: GUEST-INDUCED MOTION IN SOFT POROUS CRYSTALS

5.4 $\{[\text{Zn}_2(\text{FL1})_{1.5}(\text{OBA})_2]\}_n$ or **SPC1b**

When the ligand **FL1** was replaced with the **FL1**·2HCl salt (a precursor of the synthetic product) and the crystallisation process repeated, (**Scheme 5.2**) a completely different material was obtained. The material, **SPC1b**, crystallises in the triclinic space group $P\bar{1}$, with the ASU comprising two zinc ions, two **OBA** ligands and one and a half **FL1** ligands, both independent instances of the ligand in the *anti* conformation.



Scheme 5.2 Synthesis of **SPC1b** from the solvothermal reaction of **FL1**·2HCl, **OBA** and zinc nitrate in DMF at 100 °C, with selected crystallographic parameters.

Expansion of the ASU shows that the material contains the unusual but previously described half paddlewheel moiety observed for the **FL1** predecessor **L1**, described in Chapter IV. Further examination of the structure reveals that the reason for the presence of 1.5 **FL1** ligands is that one is di-coordinated, possessing a centre of inversion, while the other is only mono-coordinated.

CHAPTER V: GUEST-INDUCED MOTION IN SOFT POROUS CRYSTALS

The packing diagram shown in **Figure 5.15** is reminiscent of the honeycomb MOF **HC1**.^{*} However, in **SPC1b** the mono-coordinated **FL1** ligands protrude into what was previously empty space, ensuring that the framework has no solvent-accessible voids, as verified by Mercury and SQUEEZE. Since only one of the two **FL1** ligands is fully coordinated, the framework is unable to grow in a uniform manner to form interpenetrated layers and thus an interdigitated structure is formed instead (**Figure 5.16**).

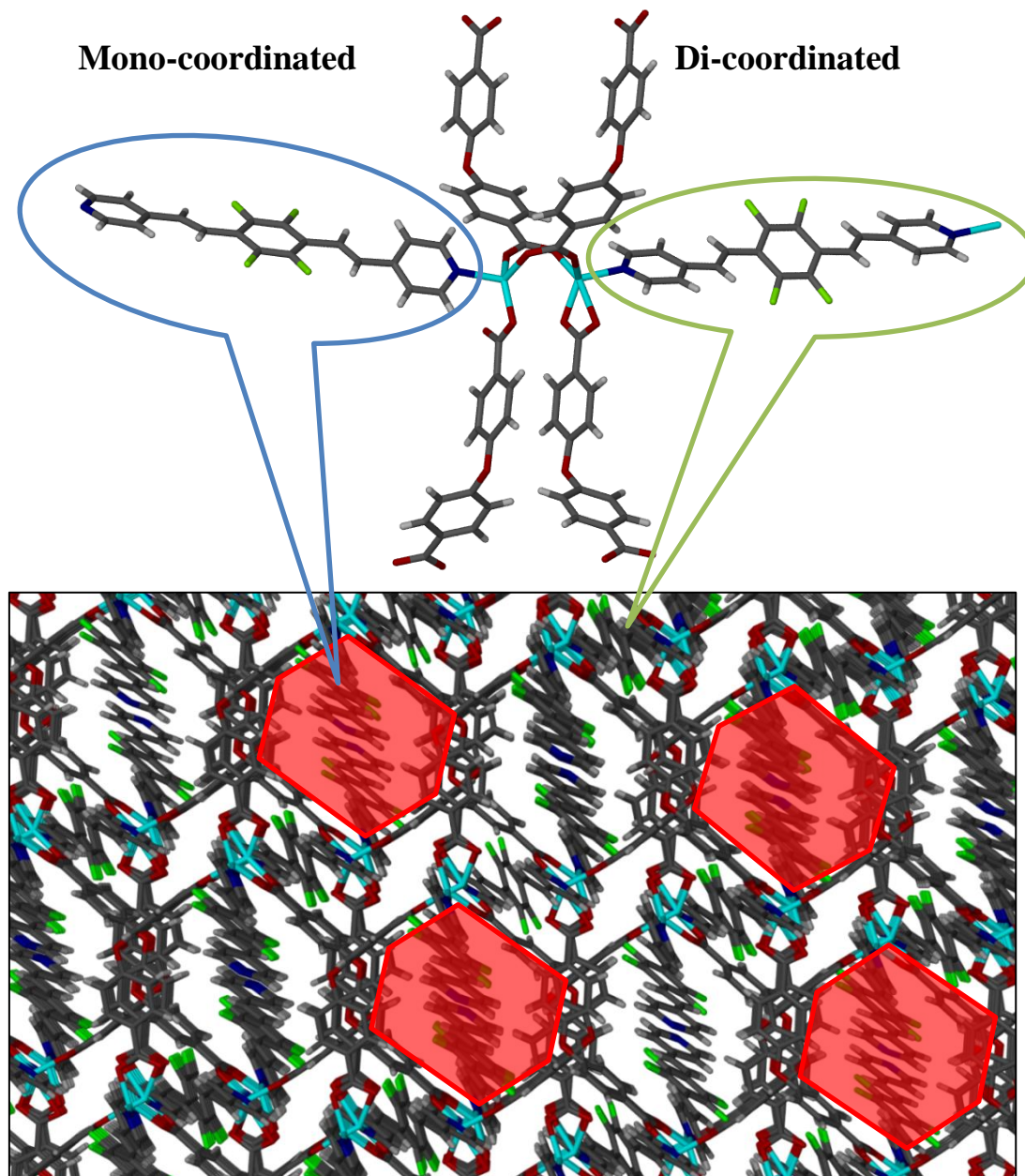


Figure 5.15 Half paddlewheel moiety (top) and an extended view of the **SPC1b** structure projected along $[1\ 0\ 1]$ showing the dual nature of the **FL1** ligand and the honeycomb motif.

^{*} Page 84

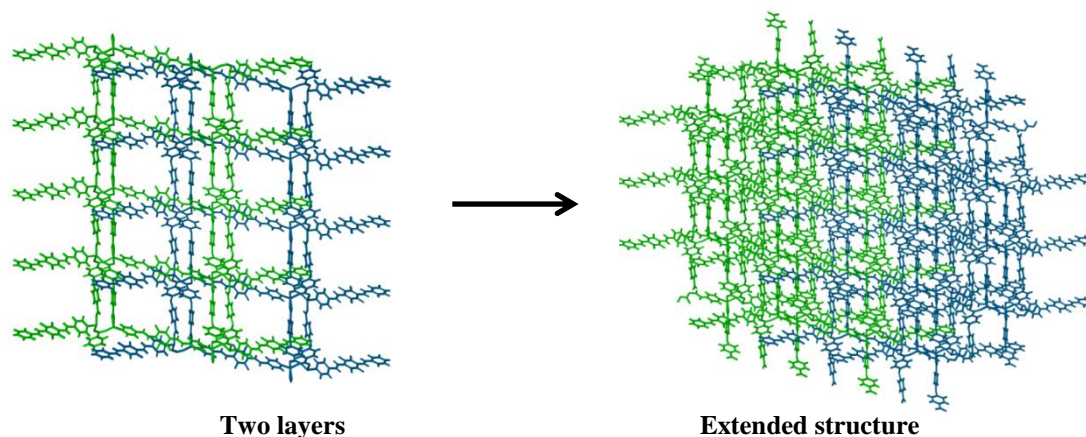


Figure 5.16 View down the a axis of **SPC1b**, showing interdigitation of the layers.

Attempts to coordinate the second pyridyl moiety by immersing crystals of **SPC1b** in a solution of the components proved unsuccessful. The C-N-C angle for the fully coordinated **FL1** ligand is 117.3° while it is 115.6° in the non-coordinated part of the mono-coordinated ligand. A search of the CSD shows these to be the typical angles of neutral molecules. It remains unclear whether it is the alteration of the pH or the presence of the small counter-ion (not located in the crystal structure) that enables the formation of such a structure.

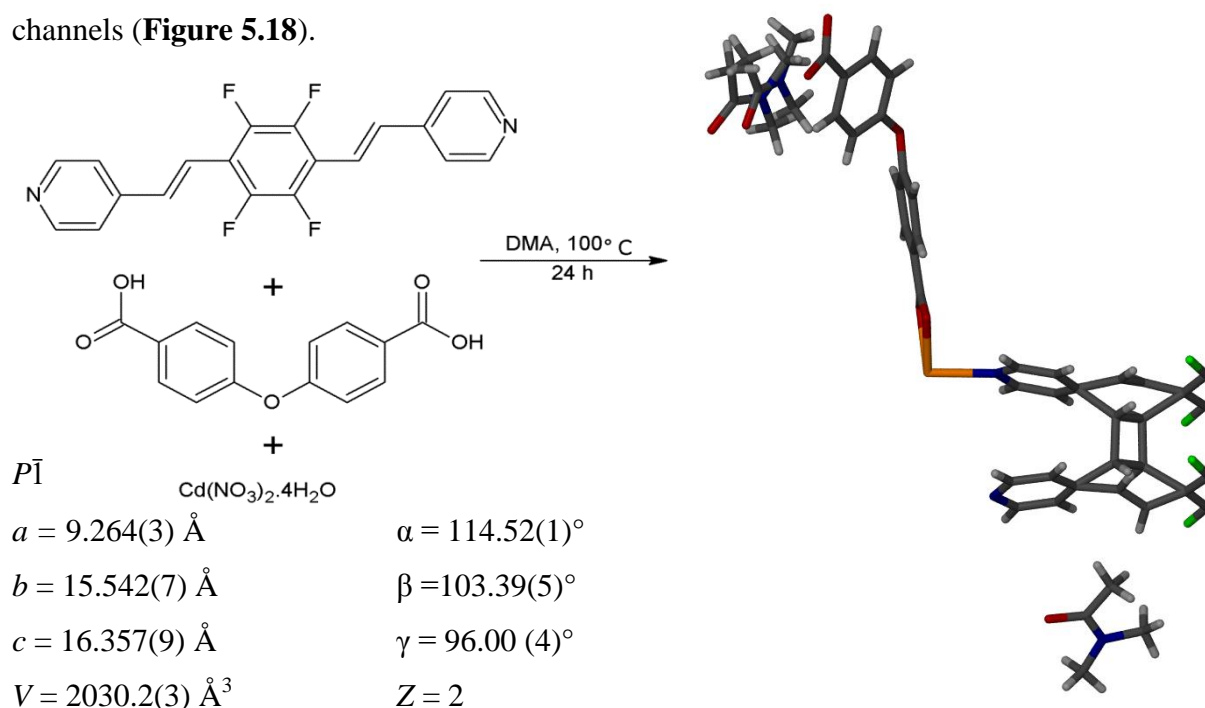
Having obtained an interesting series of zinc frameworks, cadmium, a metal very similar to zinc but possessing its own unique properties and coordination motifs was selected in the hope of attaining further understanding of **FL1** coordination polymers.

5.5 $\{[\text{Cd}(\text{FL1})(\text{OBA})]\cdot 2\text{DMA}\}_n$ or **SPC2a**

SPC2a was formed using a similar solvothermal reaction to that for **SPC1a** but the zinc salt was replaced by Cd(II) nitrate tetrahydrate and the DMF solvent by DMA (**Scheme 5.3**). **SPC2a** crystallises in the triclinic space group $P\bar{1}$. The ASU consists of one cadmium cation, one **OBA** ligand, one **FL1** ligand (disordered over two positions and located on a centre of inversion) and two DMA molecule (one of which is disordered over two positions, 67:33 site occupancy). The **FL1** ligand is disordered over two positions with both fragments in the *anti* conformation. The reason for the disorder, and what makes this structure highly unusual, is that the **FL1** ligand appears to have undergone a partial [2 + 2] cycloaddition reaction. Expansion of the ASU shows the presence of a typical cadmium SBU composed of two cadmium ions, four **OBA** ligands and four **FL1** ligands, with each pair of ligands having undergone partial [2 + 2] addition at each of the ethene bonds (**Figure 5.17**).

CHAPTER V: GUEST-INDUCED MOTION IN SOFT POROUS CRYSTALS

Of the four carboxylate oxygen atoms, two are chelating a single metal centre while the other two are bridging two metal centres. These cadmium-based paddlewheels assemble to form a 2D non-interpenetrated ladder-like grid with DMA guest molecules located within the channels (**Figure 5.18**).



Scheme 5.3 Synthesis of **SPC2a** from the solvothermal reaction of **FL1**, **OBA** and cadmium nitrate in DMA at 100 °C, with selected crystallographic information.

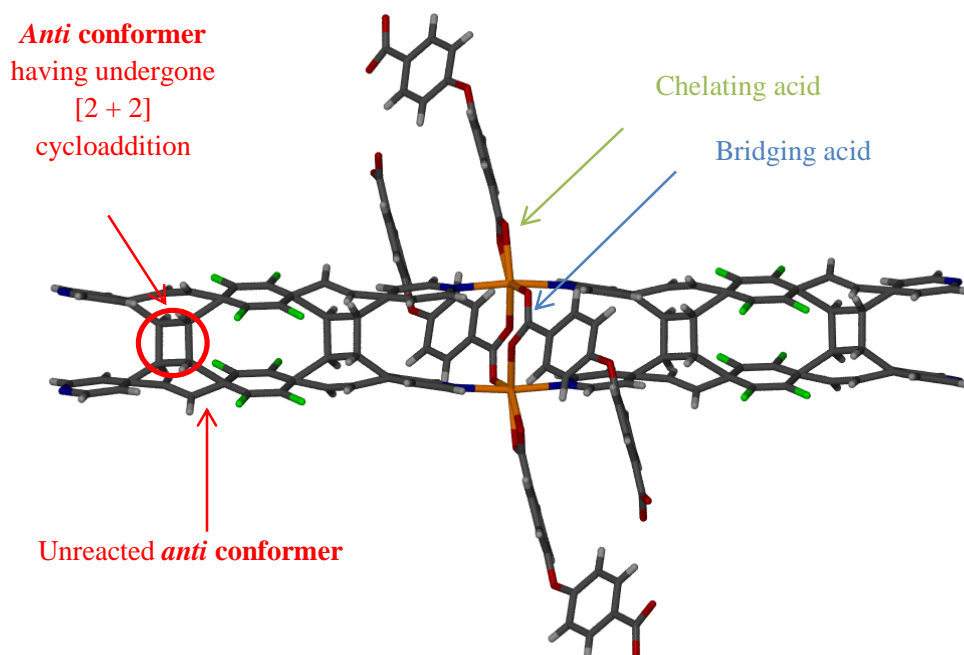


Figure 5.17 Cadmium SBU in **SPC2a** with **FL1** in *anti*-conformation with partial [2 + 2] cycloaddition.

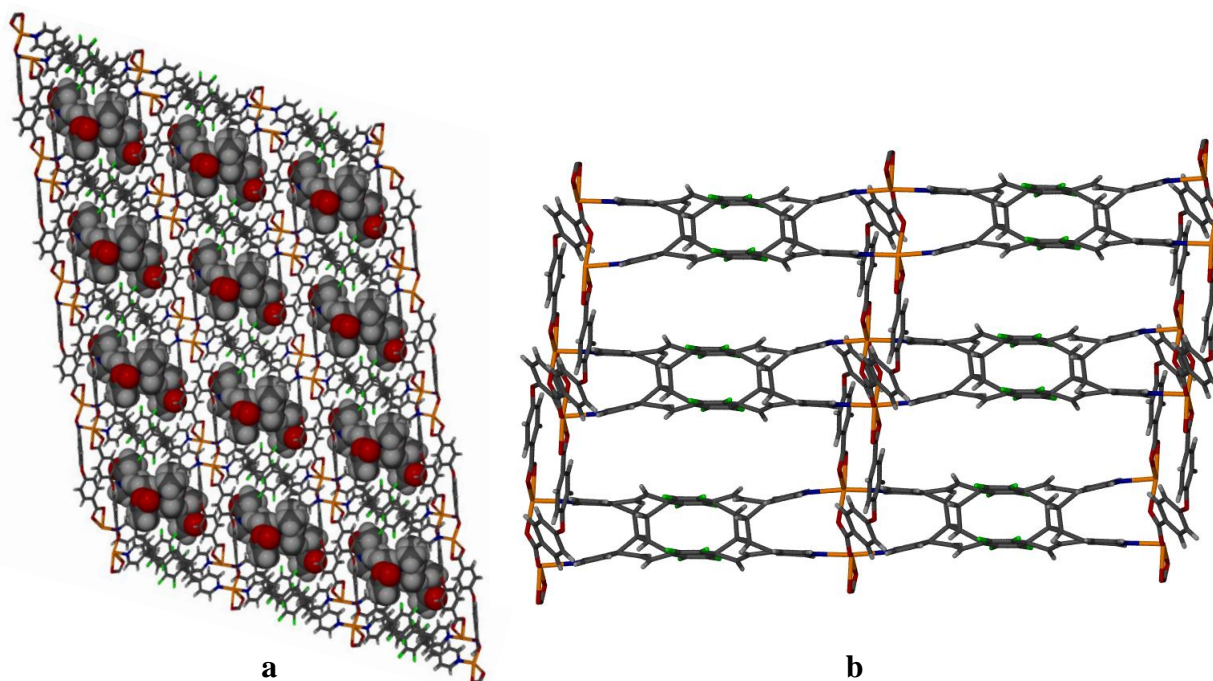


Figure 5.18 a) Solvent filled channels viewed along the *a* axis. b) Packing diagram of **SPC2a** ligands viewed down the *ac* plane showing partial [2 + 2] addition.

As mentioned earlier in this chapter, there are a many literature examples wherein organic molecules are shown to undergo [2 + 2] cycloaddition reactions. Although fewer in number, the literature also contains examples of dipyrindylethene based MOFs undergoing similar cycloadditions.¹⁰ It must however be noted that most of those reactions occur as SC-SC transformations wherein the ‘open-form’ MOF is crystallised and then ring closed using photo irradiation. Heat is then applied to reverse the process. To the best of our knowledge this is the first example of such a ligand being incorporated into a MOF with partial cyclisation having taken place during the crystallisation process. Since such structural transformations normally involve significant rearrangement of molecular components in the form of bond rotation, bending, sliding, shrinking or swelling, it is highly unusual for crystals of such a material to retain their singularity. It is currently unclear whether this reaction is purely heat dependent or whether it is a combination of heat and the use of a particular solvent (in this case, DMA). What is clear is that for [2 + 2] cycloaddition to be possible with this selection of ligands, cadmium is the preferred metal in comparison to zinc, as it allows for the formation of a non-interpenetrated ladder-like arrangement that positions the **FL1** ligands directly one on top of another (**Figure 5.18b**). In addition, the fluorine atoms help alter the electrostatic nature of the central phenyl ring, thus promoting cyclisation.

CHAPTER V: GUEST-INDUCED MOTION IN SOFT POROUS CRYSTALS

Despite having attempted to dry the crystals of surface solvent, the TGA (**Figure 5.19**) shows consistent mass loss from RT with a total mass loss of 21% occurring in the temperature range 25 - 200 °C. This corresponds to the single-crystal and SQUEEZE data as two DMA molecules per formula unit. The framework is then stable until decomposition sets in at 365 °C.

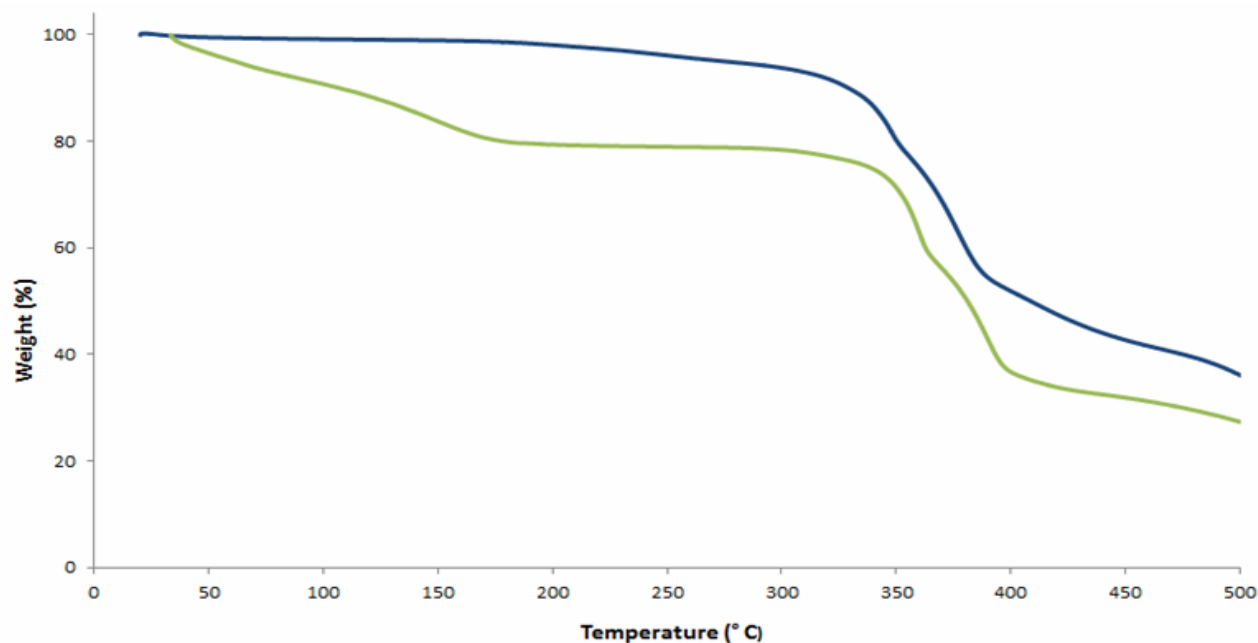


Figure 5.19 TGA of the as-synthesised as well as the evacuated phases of **SPC2a** (green and blue lines, respectively).

SPC2a' (apohost form) may be generated in a SC-SC transformation by heating the solvate at 85 °C under reduced pressure for 24 h or by exposing the sample to supercritical CO₂. The cell parameters undergo some contraction (**Figure 5.20**) but the conformation of the **FL1** ligand remains the same. Furthermore, the partial [2 + 2] cycloaddition persists. The ASU shows one cadmium ion, one **OBA** ligand and one disordered **FL1** ligand in the *anti* conformation. Extension of the ASU (**Figure 5.21**) shows the presence of corrugated channels running along the *a* axis with 250 Å³ of solvent accessible space per unit cell.

CHAPTER V: GUEST-INDUCED MOTION IN SOFT POROUS CRYSTALS

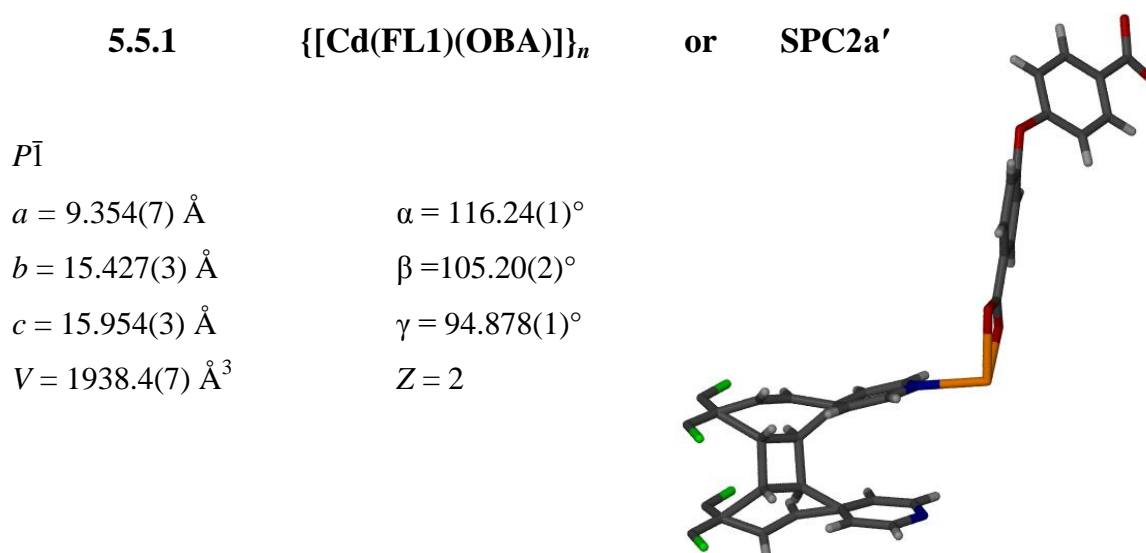


Figure 5.20 Crystallographic information of **SPC1a'**, with the ASU. The **FL1** ligand is in the *anti* conformation.

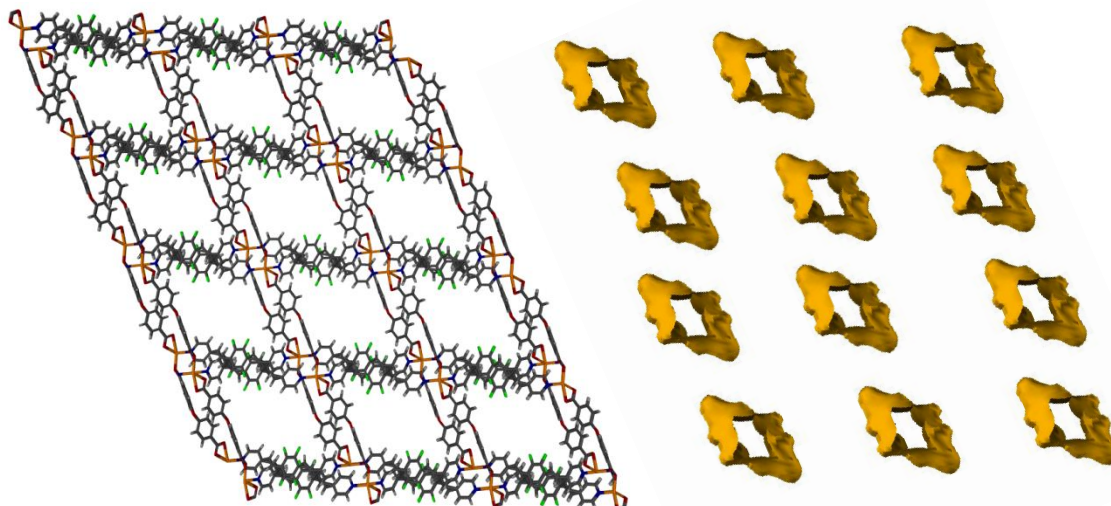


Figure 5.21 a) Packing diagram (left) and corrugated solvent accessible channels (right) of **SPC1a'**, viewed down the *a* axis.

It should be noted that although well-shaped, the crystals of **SPC2a** are inherently striated and that activation both by gradual heating or exposure to supercritical CO_2 dramatically affects crystal diffraction quality.* Since $[2 + 2]$ cyclisation by irradiation is a well-described phenomenon in the literature, a crystal of the solvated form of **SPC2a** was selected for irradiation in the hope that the partially completed $[2 + 2]$ cycloaddition could be pushed to completion in a SC-SC manner. The crystal was irradiated with ultra-violet light at 365 nm for three hours then data were recorded at 100 K.

* **SPC2a** crystals were activated several times with the best data set only possessing 88% completeness.

CHAPTER V: GUEST-INDUCED MOTION IN SOFT POROUS CRYSTALS

5.5.2 Irradiation of SPC2a or SPC2a_Irrad

Upon exposure to ultraviolet light, the previous colourless **SPC2a** crystal appears to fluoresce green. The structure of **SPC2a_irrad** remains triclinic but the cell parameters experience some change (mostly in the length of the *c* axis). Examination of the ASU (**Figure 5.22**) shows that although the [2 + 2] cyclisation has not proceeded to completion, the reaction has progressed with only one of the two ethene arms remaining disordered over the two positions. The ratio of cyclised to non-cyclised ligand has increased from 54:46 to 76:24. Prolonged irradiation did not induce any further conversion.

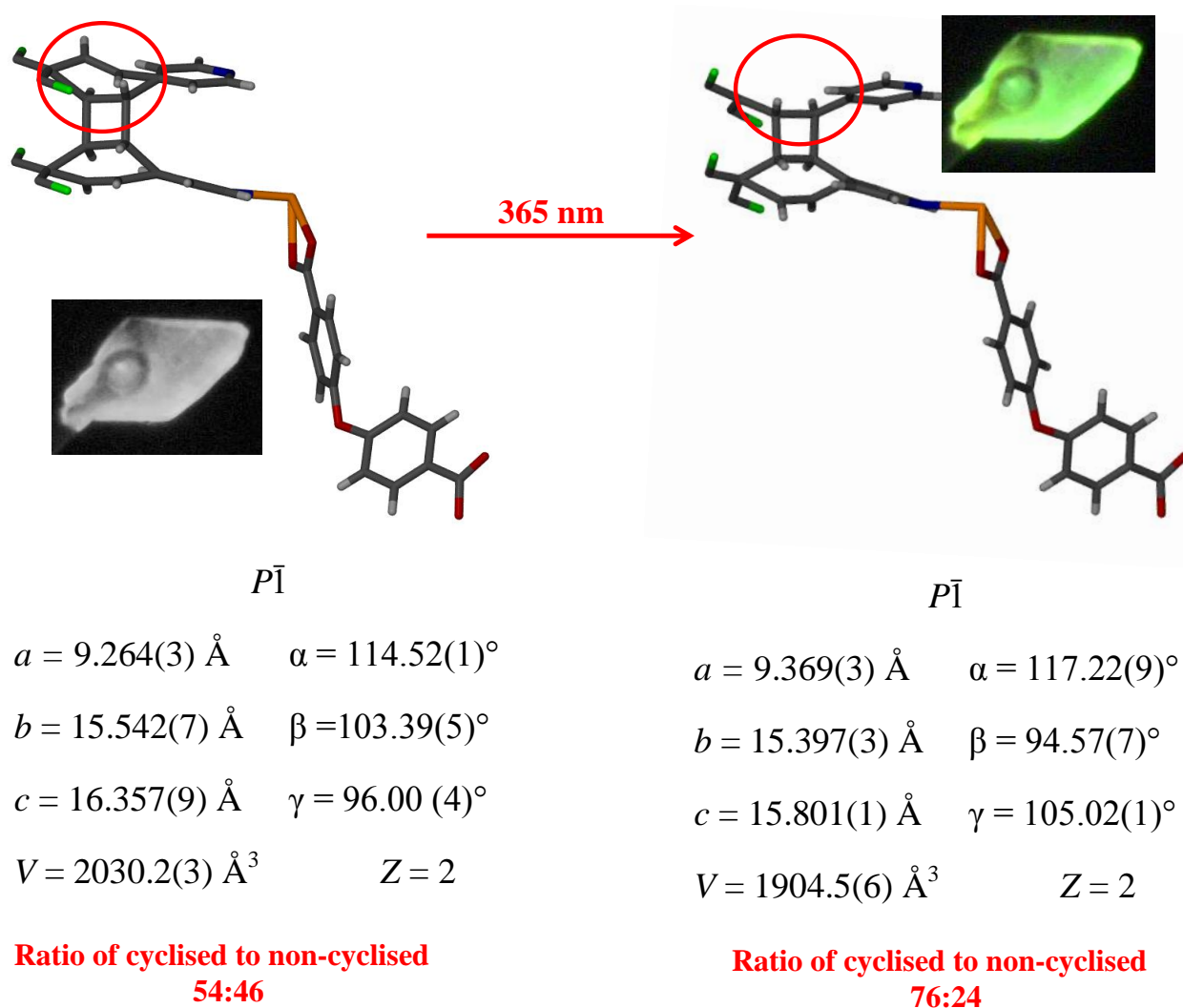
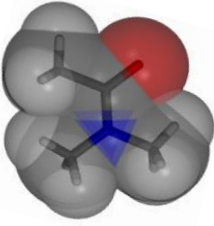
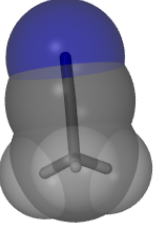
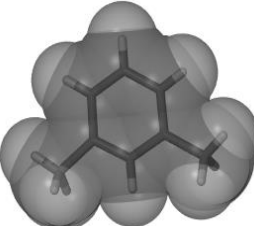
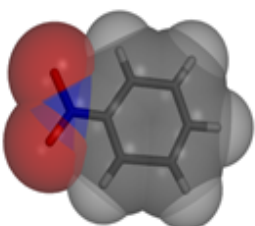


Figure 5.22 Comparison of the ASU and unit cell parameters of **SPC2a** with **SPC2a_Irrad**.

5.6 SC-SC guest exchange experiments in SPC2a

A series of SC-SC guest exchange experiments were carried out to establish whether selected guest molecules would alter the degree of [2 + 2] cycloaddition present. Crystals of **SPC2a**^{*} were exposed to a selection of guests such as acetonitrile, a commercial mixture of xylenes and nitrobenzene. In all instances the DMA molecules were replaced by the relevant guest. **Table 5.4** presents the relevant crystallographic data obtained from the exchanges.

Table 5.4 Crystallographic data for SC-SC solvent exchange experiments with **SPC2a**[†].

<i>P</i> $\bar{1}$			
			
SPC2a	SPC2a·ACN	SPC2a·Xymix	SPC1a·NB
$a = 9.264(3) \text{ \AA}$	$a = 9.656(7) \text{ \AA}$	$a = 9.280(1) \text{ \AA}$	$a = 9.233(2) \text{ \AA}$
$b = 15.542(7) \text{ \AA}$	$b = 16.013(6) \text{ \AA}$	$b = 15.462(7) \text{ \AA}$	$b = 15.375(3) \text{ \AA}$
$c = 16.357(9) \text{ \AA}$	$c = 16.529(7) \text{ \AA}$	$c = 15.961(6) \text{ \AA}$	$c = 16.260(4) \text{ \AA}$
$\alpha = 114.52(1)^\circ$	$\alpha = 116.84(1)^\circ$	$\alpha = 111.90(9)^\circ$	$\alpha = 112.18(8)^\circ$
$\beta = 103.39(5)^\circ$	$\beta = 105.84(1)^\circ$	$\beta = 105.07(3)^\circ$	$\beta = 103.53(9)^\circ$
$\gamma = 96.00(4)^\circ$	$\gamma = 94.56(6)^\circ$	$\gamma = 93.877(2)^\circ$	$\gamma = 93.81(2)^\circ$
$V = 2030.2(3) \text{ \AA}^3$	$V = 2142.1(4) \text{ \AA}^3$	$V = 2016.5(8) \text{ \AA}^3$	$V = 2047.0(8) \text{ \AA}^3$
Two DMA molecules one of which is disordered over two positions (67:33 site occupancy)	Two acetonitrile molecules (one disordered over two positions (58:42 site occupancy)	One <i>meta</i> -xylene molecule disordered over two positions (50:50 site occupancy)	Two nitrobenzene molecules both disordered over two positions (73:27 and 65:35 site occupancy)
54:46 cyclised : uncyclised	57:43 cyclised : uncyclised	76:24 cyclised : uncyclised	51:49 cyclised : uncyclised

^{*} Solvate crystals were selected for exchange as even mild activation induces crystal striation.

[†] Thermogravimetric plots for these guest-exchange experiments may be located in the supplementary data.

CHAPTER V: GUEST-INDUCED MOTION IN SOFT POROUS CRYSTALS

Unlike with **SPC1a**, the guest exchange experiments performed with **SPC2a** showed no crank-handle flipping. As mentioned earlier, the DMA solvate (**SPC2a**) contains the **FL1** ligand in the *anti* conformation with the molecule disordered over two positions, one of which is the [2 + 2] cyclised conformer. Although exposure of this material to acetonitrile yielded some change in the unit cell parameters (attributed to the change in size and shape of the guest) there was no alteration of the conformation of **FL1** as observed in **SPC1a·ACN**. It should however be noted that the ratio of the two conformers shifted to 57:43 (cyclised : uncyclised).

Having been unable to induce crank-handle motion or push the [2 + 2] cyclisation to 100% conversion, two aromatic guest molecules (a commercial xylene mixture and nitrobenzene) were introduced. It was postulated that π -stacking, increased hydrogen bonding and the presence of a bulky electronegative nitro substituent would facilitate 100% conversion to the cyclised [2 + 2] conformer. Immersion of the material in a commercial xylene mixture resulted in only *meta*-xylene being included in the crystal structure. Thus future work could entail detailed selectivity studies. In the context of the current scope, although the unit cell parameters underwent some change, neither the *meta*-xylene containing structure (**SPC2a·Xymix**) nor the structure containing nitrobenzene (**SPC1a·NB**) showed any conformational alteration, with the ligand **FL1** remaining in the disordered *anti* conformation in both structures. Although no structural change was observed, the ratio of cyclised conformer relative to non-cyclised conformer was observed to increase for *meta*-xylene from 54:46 ratio to 76:24. These preliminary studies suggest that the degree of cyclisation in **SPC2a** may be fine-tuned through guest inclusion.

Three potentially interesting future studies would involve: (i) performing variable temperature SCD experiments on both **SPC1a'** and **SPC2a'** to determine what effect temperature would have on crank-handle motion as well as on the [2 + 2] cycloaddition; (ii) perform crystallisations at various temperatures in an attempt to modulate the degree of [2 + 2] cyclisation obtained in **SPC2a**; (iii) irradiate the *meta*-xylene containing crystals of **SPC2a·Xymix** to determine if they would undergo complete cyclisation.

5.7 Gravimetric gas sorption for SPC2a' using CO₂ and a series of linear alkanes

The gas sorption properties of **SPC2a'** were measured at 25 °C using CO₂, methane, ethane, propane and butane (**Figure 5.23**). **SPC2a'** also shows Type I sorption behaviour for all selected guests but, unlike **SPC1a'**, this material absorbs substantial amounts of all five gases. **SPC2a'** absorbs approximately five molecules of CO₂ (54.0 wt% at 20 bar), three molecules of methane (14.3 wt% at 20 bar), ethane (22.3 wt% at 20 bar), propane (36.9 wt% at 8 bar) or two molecules of butane, (27.7 wt% at 2 bar) per ASU. Although none of the gases attain full occupancy at 20 bar, the material absorbs five of seven CO₂ molecules* that could theoretically be accommodated within the MOF (the only material in the entire thesis to attain such high occupancy). The potential selectivity trend is as follows: CO₂ > propane > methane > butane > ethane. All isotherms show hysteresis, with inflections present in both the sorption and desorption isotherms for ethane. This is interesting as it implies the presence of possible interactions between the **SPC2a'** host and the ethane guest or a structural change. It is believed that both the increased uptake and sorption stepping stem from the material being partially cyclised. Future experiments could involve detailed gas-cell work to better understand the exact nature of the interaction. Of all the materials discussed thus far, this is by far the most promising candidate for breakthrough experiments and potential industrial use.

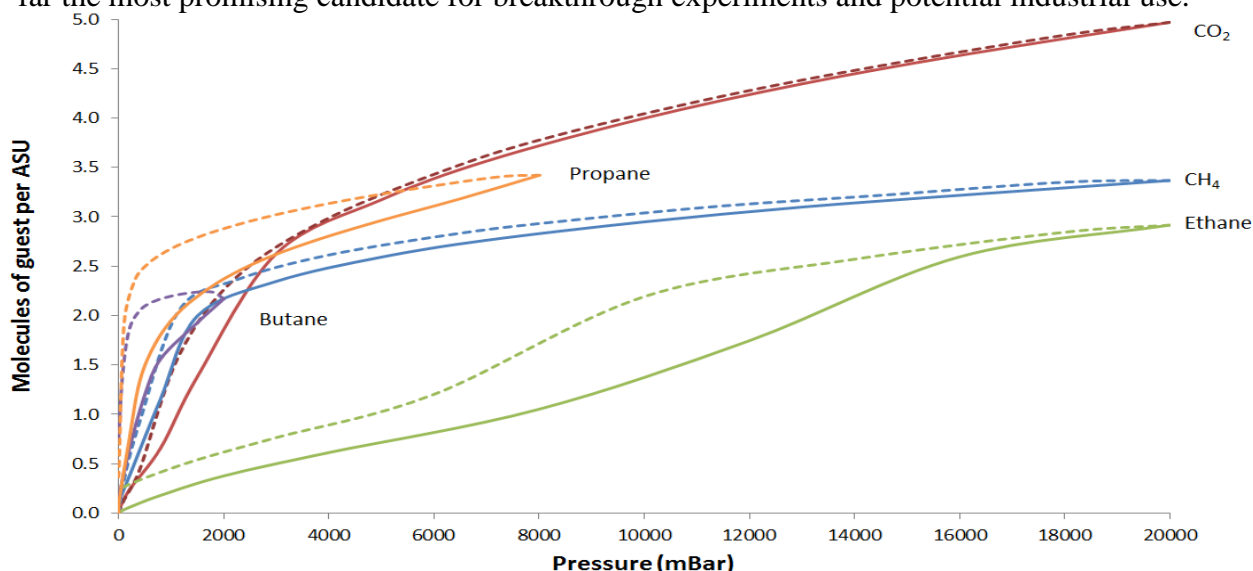


Figure 5.23 CO₂ and selected alkane sorption and desorption isotherms of **SPC2a'** at 25 °C. The solid lines represent sorption and dashed lines represent desorption.

* This coincides with the theory proposed by Rebek *et al.* of strong intermolecular interactions being present.

5.8 $\{[\text{Cd}(\text{FL1})(\text{OBA})]\cdot\text{X}^*\}_n$ or **SPC2b**

In addition to the MOFs experiencing dynamic crank-handle motion, two isoskeletal structures of a third MOF containing cadmium, **OBA** and the **FL1** were independently obtained through modification of the solvent medium. If the components are combined in DMF alone, the MOF **SPC2b1** may be obtained while addition of these components to a DMF-DMSO mixture yields **SPC2b2**.

Both materials possess the same ASU comprised of one cadmium ion, one **OBA** ligand and one **FL1** ligand in the *syn* conformation (**Figure 5.24**). In **SPC2b1**, the fluorinated ring is disordered over two positions (63:37 site occupancy). The **FL1** ligand in **SPC2b2** remains ordered but is slightly twisted in comparison to the **FL1** ligand in **SPC2b1**. The **SPC2b1** structure contains two disordered DMF molecules (one DMF is disordered over two positions 55:45 while the second is disordered over three positions 56:24:20 site occupancy). According to SQUEEZE the **SPC2b2** structure has three DMF molecules, of which only two could be modelled (one of which is also disordered over three positions, 47:27:26 site occupancy) and one water molecule. These two structures differ from **SPC2a** in the orientation of the **FL1** ligand as well as the solvent present.

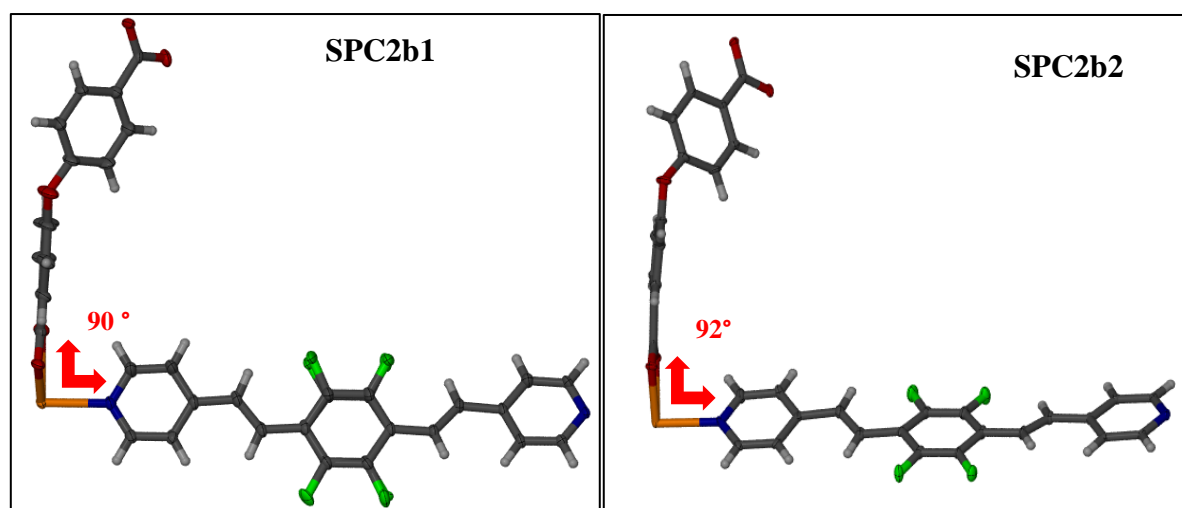


Figure 5.24 ASU of the two **SPC2b** isoskeletal structures showing the *syn* conformation of the **FL1** ligand (the solvent has been omitted for clarity).

* Since the two isoskeletal compounds are discussed together X denotes the solvent. There are two molecules of DMF for **SPC2b1** and three molecules of DMF and one water molecule for **SPC2b2**.

CHAPTER V: GUEST-INDUCED MOTION IN SOFT POROUS CRYSTALS

A comparison of the extended ASU of **SPC2a** with **SPC2b** (**SPC2b1** and **SPC2b2** are the same) shows the two materials to be completely different (**Figure 5.25**). As previously mentioned, **SPC2a** was grown from DMA with the **FL1** ligand in the *anti* conformation. This conformation is believed to be critical for [2 + 2] addition as growth from DMF or DMF-DMSO causes the **FL1** ligand in **SPC2b** to adopt a *syn* conformation, thus preventing the possibility of [2 + 2] cycloaddition.

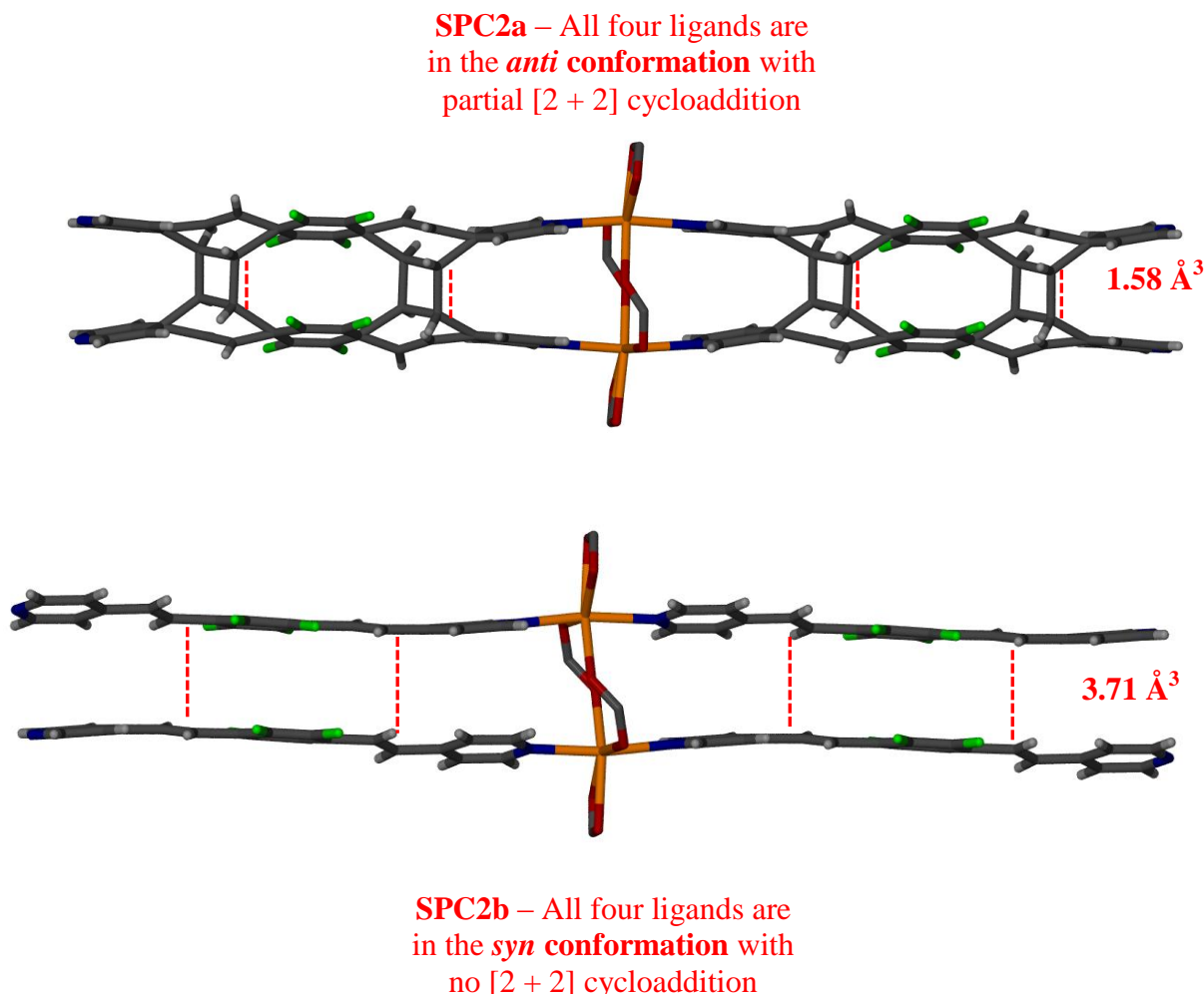


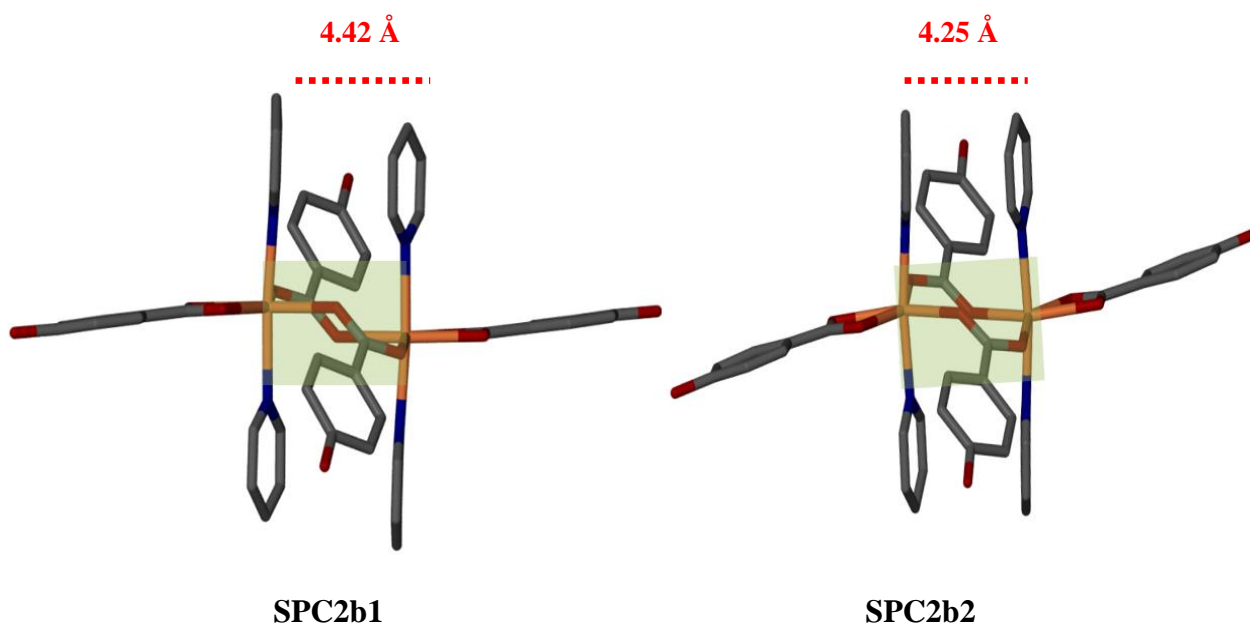
Figure 5.25 Comparison of the distance separating **FL1** ligands in **SPC2a** and **SPC2b**.

In spite of the presence of DMSO during crystallisation of **SPC2b2**, no DMSO molecules are present in the structure. Examination of the crystallographic data presented in **Table 5.5** indicates a substantial deviation in unit cell dimensions and volume. This difference is not due to crank-handle motion of the **FL1** ligand as both remain in the same conformation. The question then arises: could the minor difference in the amount of solvent present in each structure really have such an effect on the cell parameters, or are there additional factors at play?

Table 5.5 Crystallographic parameters for the two **SPC2b** MOFs.

SPC2b1 (DMF) 2 DMF guest molecules	SPC2b2 (DMF-DMSO) 3 DMF and one water guest molecules
$P\bar{1}$	$P\bar{1}$
$a = 9.740(6) \text{ \AA}$	$a = 9.566(2) \text{ \AA}$
$b = 15.291(6) \text{ \AA}$	$b = 15.342(6) \text{ \AA}$
$c = 15.421(9) \text{ \AA}$	$c = 15.794(2) \text{ \AA}$
$\alpha = 116.25(7)^\circ$	$\alpha = 107.50(3)^\circ$
$\beta = 97.09(1)^\circ$	$\beta = 106.91(5)^\circ$
$\gamma = 107.99(7)^\circ$	$\gamma = 94.07(3)^\circ$
$V = 1958.8(9) \text{ \AA}^3$	$V = 2082.9(2) \text{ \AA}^3$

A comparison of the paddlewheels based on cadmium metal centres in **Figure 5.26** shows that the **SPC2b1** SBU contains the **OBA** ligands in a stepped orientation with an internal Cd-O-C-O torsion angle of 105.6° , while the **SPC2b2** SBU is more linear with an internal torsion angle of 92.3° . The distance between the two cadmium centres also differs, with a distance of 4.42 \AA for **SPC2b1** and 4.25 \AA for **SPC2b2**.

**Figure 5.26** Cadmium SBUs of **SPC2b1** and **SPC2b2**.

CHAPTER V: GUEST-INDUCED MOTION IN SOFT POROUS CRYSTALS

Examination of the extended structures of **SPC2b1** and **SPC2b2** reveals the effect these changes have on the overall structures. When **SPC2b1** is viewed down the a axis, the rectangular pores (previously seen with **SPC2**) are slanted and rhombic in shape while the corresponding view in **SPC2b2** shows the pores to be more rectangular (**Figure 5.27**).

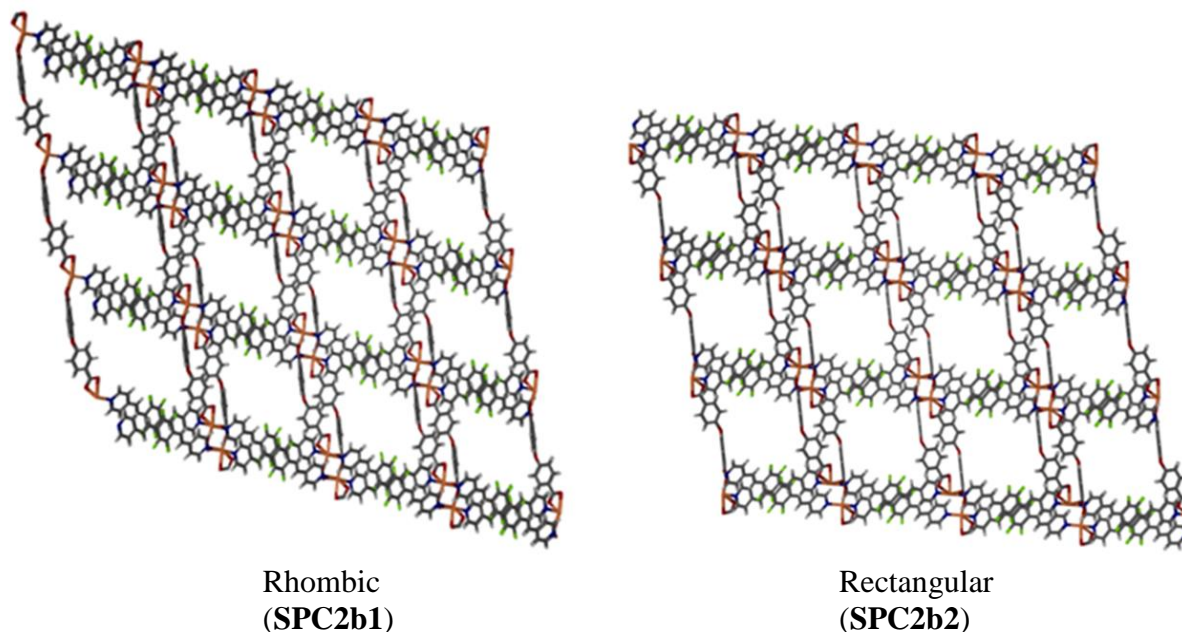


Figure 5.27 View down the a axis showing the pore shapes for the two isoskeletal structures **SPC2b1** and **SPC2b2**.

From the crystallographic data presented in **Table 5.5** it is clear that the a axis is not the only dimension to differ substantially. The c axis also increases from 15.42 Å in **SPC2b1** to 15.79 Å in **SPC2b2**. Closer inspection of the structures viewed down this axis (**Figure 5.28**) reveals that, in the case of **SPC2b1**, the **OBA** ligands stack one on top of another with a repeat distance of 4.41 Å separating adjacent oxygen atoms. Examination of a space-filled diagram shows no solvent-accessible space per unit cell. However, using a probe radius of 1.4 Å, the structure possesses 12% solvent-accessible space. The structure of **SPC2b2** differs in that the **OBA** ligands are arranged to allow the oxygen atoms not only to align but to overlap (**Figure 5.28**). This minor contraction causes the channels to distend, increasing the solvent-accessible space to 14%.

CHAPTER V: GUEST-INDUCED MOTION IN SOFT POROUS CRYSTALS

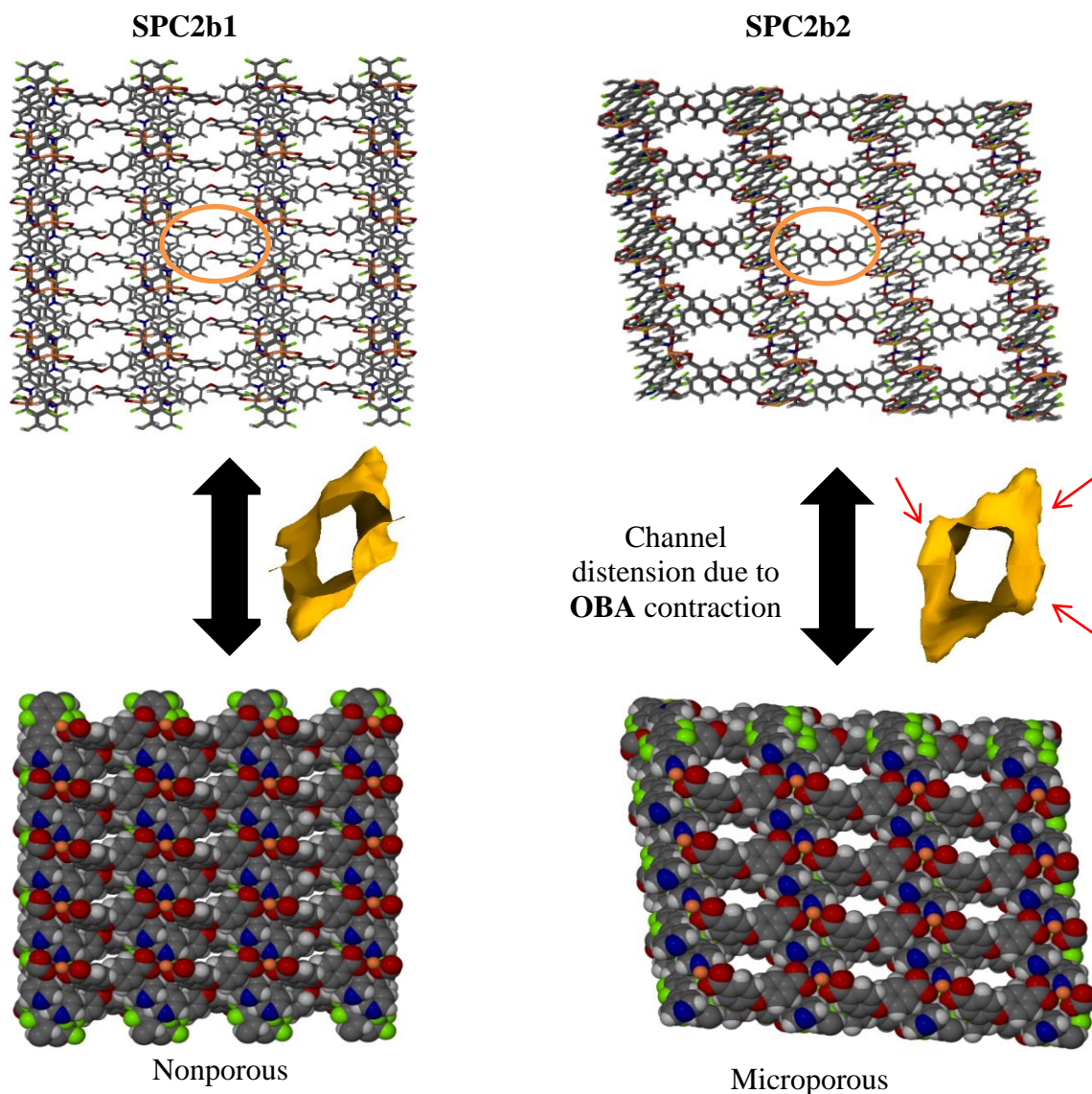


Figure 5.28 View down the c axis of the isoskeletal structures of **SPC2b1** and **SPC2b2** showing the deviation in **OBA** orientation and the effect this has on the pore size and shape.

It seems unlikely that the cause of the differences is due to one additional DMF and water molecule being present in the ASU. In all likelihood the difference in the amount of solvent encapsulated is a result of the amount of void space present. Since the only difference between the two structures was the growth medium, it is proposed that the DMSO solvent acts as a templating solvent, promoting framework formation while simultaneously affecting the coordination abilities of the **OBA** ligand (acid coordination dictates SBU formation). It is important to note that immersing crystals of **SPC2b1** in a DMF-DMSO solution does not yield **SPC2b2** and placing **SPC2b2** crystals in DMF does not yield **SPC2b1**. This implies that this phenomenon occurs pre-crystallisation, and that once the paddlewheel is formed it cannot be easily altered.

5.9 Conclusion

Fluorination of the **L1** ligand (**FL1**) induces dramatic variations in the frameworks obtained. **SPC1a** is composed of zinc, **OBA** and **FL1** and is a twofold interpenetrated 3D structure containing solvent molecules in triangular crenelated channels. This material appears to be very susceptible to crank-handle motion, undergoing conformational changes with activation and upon the incorporation of various guest molecules such as acetonitrile, carbon dioxide and trichloroacetonitrile. Particular attention is drawn to the inclusion of acetonitrile and its derivative trichloroacetonitrile which induce anomalous crank-handle motion as a result of what is believed to be host-guest and guest-guest electrostatic interactions. Future work could involve an in-depth computational study to better understand this phenomenon. The activated material exhibited some selectivity toward CO₂ over a series of linear alkanes.

Repetition of the crystallisation process replacing the **FL1** ligand with the **FL1·2HCl** salt yielded the unusual interdigitated MOF **SPC1b** wherein one of the two **FL1** ligands is mono-coordinated, ensuring the formation of a non-porous material somewhat reminiscent of the MOF **HC1** described in chapter IV.

Substitution of the zinc salt with cadmium nitrate in the presence of DMA yielded the MOF **SPC2a**. This material is constructed from 2D layers that stack in such a manner as to create rectangular corrugated channels that contain solvent, with the **FL1** ligand present in the *anti* conformation but disordered over two positions, one of which is the [2 + 2] cyclised conformer. The material may be activated with no alteration of the ligand conformation or the degree of [2 + 2] cycloaddition observed. Photoirradiation and guest exchange were shown to play a role in driving the degree of [2 + 2] observed. Exposure of the activated material to CO₂ and a series of linear alkanes results in dramatic selectivity properties. CO₂ appears to be preferred over the hydrocarbons and an interesting stepped ethane sorption isotherm was obtained. This material is an excellent candidate for breakthrough experiments. In addition to these two MOFs, alteration of the solvent medium to DMF or DMF-DMSO produces two isoskeletal structures (**SPC2b1** and **SPC2b2**) of a third material. Both structures have the same conformation of **FL1** (*syn* conformer) with no [2 + 2] addition but differ in their paddlewheel conformation and, as a result, in the solvent-accessible space present. This difference is attributed to the inclusion of DMSO in the crystallisation conditions, thus changing the SBU formed.

5.10 Synthesis of metal-organic frameworks SPC1-SPC2

SPC1a: A mixture of $\text{Zn}(\text{NO}_3)_2 \cdot 6\text{H}_2\text{O}$ (15 mg, 0.025 mmol), **OBA** (13 mg, 0.05 mmol) and **FL1** (11 mg, 0.03 mmol) in a 5 mL solution of DMF was heated to 100 °C in a sintered glass vial for 24 h. Yellow lozenge-shaped crystals were obtained.

SPC1b: Synthesis was carried out using the same procedure described for **SPC1a** but the HCl salt of the **FL1** was used in place of just **FL1**. Pale yellow diamond-shaped crystals were obtained after 24 h.

SPC2a: A mixture of $\text{Cd}(\text{NO}_3)_2 \cdot 4\text{H}_2\text{O}$ (9 mg, 0.05 mmol), **OBA** (13 mg, 0.05 mmol) and **FL1** (11 mg, 0.03 mmol) in a 5 mL solution of DMA was heated to 100 °C in a sintered glass vial for 24 h. Pale yellow diamond-shaped crystals were obtained after 24 h.

SPC2b1: Synthesis was carried out using the same procedure described for **SPC2a** but using 5 ml of DMF. Colourless lozenge-shaped crystals were obtained.

SPC2b2: Synthesis was carried out using the same procedure described for **SPC2a** but using DMF-DMSO (4:1 v/v) as the solvent mixture. Colourless crystals were obtained after 24 h.

CHAPTER V: GUEST-INDUCED MOTION IN SOFT POROUS CRYSTALS

	SPC1a	SPC1a'	SPC1a-ACN
Empirical formula	C ₂₇ H ₂₁ F ₂ N ₂ O ₆ Zn	C ₂₄ H ₁₄ F ₂ N ₁ O ₅ Zn	C ₆₀ H ₄₅ F ₄ N ₈ O ₁₀ Zn ₂
Formula weight	572.85	493.70	1245.42
Temperature (K)	100(0)	100(0)	100(0)
Wavelength (Å)	0.71073	0.71073	0.71073
Crystal system	<i>P</i> 2 ₁ / <i>n</i>	<i>P</i> 2 ₁ / <i>n</i>	<i>P</i> 2 ₁ / <i>n</i>
<i>a</i> /Å	8.112(4)	7.9849(2)	15.917(3)
<i>b</i> /Å	16.288(7)	16.3226(5)	16.433(2)
<i>c</i> /Å	22.952(1)	23.4990(7)	23.389(5)
α /°	90.0	90.0	90.0
β /°	97.983(7)	98.103(2)	102.992(3)
γ /°	90.0	90.0	90.0
Space group	Monoclinic	Monoclinic	Monoclinic
Volume (Å ³)	3004(2)	3032.34(2)	5961(2)
<i>Z</i>	4	4	4
Calculated density (g cm ⁻³)	1.267	1.081	1.388
Absorption coefficient (mm ⁻¹)	0.868	0.847	0.881
<i>F</i> ₀₀₀	1172	999.6	2549.2
θ range for data collection (°)	1.54 to 28.26	3.05 to 28.30	1.41 to 28.31
Miller index ranges	-9 ≤ <i>h</i> ≤ 10, -18 ≤ <i>k</i> ≤ 20, -25 ≤ <i>l</i> ≤ 30	-10 ≤ <i>h</i> ≤ 10, -21 ≤ <i>k</i> ≤ 21, -31 ≤ <i>l</i> ≤ 31	-11 ≤ <i>h</i> ≤ 21, -20 ≤ <i>k</i> ≤ 21, -30 ≤ <i>l</i> ≤ 25
Reflections collected	18682	94058	36035
Independent reflections	6982	7533	13829
Completeness to θ_{\max} (%)	93.9	99.8	93.2
Max. and min. transmission	0.886, 0.806	0.865, 0.834	0.868, 0.700
Refinement method	Full-matrix least-squares on <i>F</i> ²	Full-matrix least-squares on <i>F</i> ²	Full-matrix least-squares on <i>F</i> ²
Data / restraints / parameters	4560/8/378	6654/502/359	9017/1/781
Goodness-of-fit on <i>F</i> ²	1.027	1.103	1.025
Final <i>R</i> indices [<i>I</i> > 2 σ (<i>I</i>)]	<i>R</i> 1 = 0.0879, <i>wR</i> 2 = 0.2609	<i>R</i> 1 = 0.0491, <i>wR</i> 2 = 0.1411	<i>R</i> 1 = 0.0721, <i>wR</i> 2 = 0.1735

CHAPTER V: GUEST-INDUCED MOTION IN SOFT POROUS CRYSTALS

	SPC1a-Cl₃ACN	SPC1b	SPC2a
Empirical formula	C ₅₅ H ₃₀ C ₁₈ F ₄ N ₅ O ₁₀ Zn ₂	C ₅₈ H ₃₄ F ₆ N ₃ O ₁₁ Zn ₂	C ₄₂ H ₃₈ CdF ₄ N ₄ O ₉
Formula weight	1420.00	1193.66	931.17
Temperature (K)	100(0)	100(0)	100(0)
Wavelength (Å)	0.71073	0.71073	0.71073
Crystal system	<i>P</i> 2 ₁ / <i>c</i>	<i>P</i> $\bar{1}$	<i>P</i> $\bar{1}$
<i>a</i> /Å	16.103(3)	13.102(3)	9.264(5)
<i>b</i> /Å	16.246(3)	14.478(3)	15.543(8)
<i>c</i> /Å	23.764(4)	15.277(3)	16.357(9)
α /°	90.0	97.166(2)	114.521(6)
β /°	103.703(3)	100.934(2)	103.395(6)
γ /°	90.0	116.757(2)	96.004(6)
Space group	Monoclinic	Triclinic	Triclinic
Volume (Å ³)	6043.73	2466.6(8)	2030.2(2)
<i>Z</i>	4	2	2
Calculated density (g cm ⁻³)	1.562	1.607	1.523
Absorption coefficient (mm ⁻¹)	1.232	1.065	0.617
<i>F</i> ₀₀₀	2846.6	1210	948.0
θ range for data collection (°)	1.30 to 28.27	1.75 to 28.30	1.44 to 28.38
Miller index ranges	-16 ≤ <i>h</i> ≤ 21, -20 ≤ <i>k</i> ≤ 21, -30 ≤ <i>l</i> ≤ 31	-16 ≤ <i>h</i> ≤ 17, -18 ≤ <i>k</i> ≤ 19, -20 ≤ <i>l</i> ≤ 19	-12 ≤ <i>h</i> ≤ 12, -19 ≤ <i>k</i> ≤ 20, -21 ≤ <i>l</i> ≤ 20
Reflections collected	36879	28799	19081
Independent reflections	13957	11349 [Rint = 0.0530]	9085
Completeness to θ_{\max} (%)	93.1	92.4	89.3
Max. and min. transmission	0.799, 0.485	0.8757, 0.7590	0.899, 0.669
Refinement method	Full-matrix least-squares on <i>F</i> ²	Full-matrix least-squares on <i>F</i> ²	Full-matrix least-squares on <i>F</i> ²
Data / restraints / parameters	8341/54/713	7527/ 0/ 716	7615/17/455
Goodness-of-fit on <i>F</i> ²	1.473	1.071	1.212
Final <i>R</i> indices [<i>I</i> > 2 σ (<i>I</i>)]	<i>R</i> 1 = 0.1299, <i>wR</i> 2 = 0.3925	<i>R</i> 1 = 0.058, <i>wR</i> 2 = 0.129	<i>R</i> 1 = 0.0859, <i>wR</i> 2 = 0.2246

CHAPTER V: GUEST-INDUCED MOTION IN SOFT POROUS CRYSTALS

	SPC2a'	SPC2a_Irrad	SPC2a-ACN
Empirical formula	C ₃₄ H ₂₀ CdF ₄ N ₂ O ₅	C ₆₇ H ₃₉ Cd ₂ F ₈ N ₄ O ₁₀	C ₃₈ H ₂₆ CdF ₄ N ₄ O ₅
Formula weight	724.92	1436.79	811.20
Temperature (K)	100(0)	100(0)	100(0)
Wavelength (Å)	0.71073	0.71073	0.71073
Crystal system	<i>P</i> $\bar{1}$	<i>P</i> $\bar{1}$	<i>P</i> $\bar{1}$
<i>a</i> /Å	9.355(2)	9.369(7)	9.657(2)
<i>b</i> /Å	15.427(4)	15.397(1)	16.010(3)
<i>c</i> /Å	15.954(4)	15.800(1)	16.530(3)
α /°	116.241(3)	117.229(6)	116.841(1)
β /°	105.202(4)	105.021(7)	105.189(1)
γ /°	94.878(3)	94.577(6)	94.566(1)
Space group	Triclinic	Triclinic	Triclinic
Volume (Å ³)	1938.5(8)	1905(2)	2142(7)
<i>Z</i>	2	2	2
Calculated density (g cm ⁻³)	1.242	1.252	1.258
Absorption coefficient (mm ⁻¹)	0.618	0.628	0.568
<i>F</i> ₀₀₀	724.0	717.0	816.2
θ range for data collection (°)	2.30 to 28.47	1.53 to 28.43	1.46 to 27.51
Miller index ranges	-12 ≤ <i>h</i> ≤ 12, -20 ≤ <i>k</i> ≤ 20, -21 ≤ <i>l</i> ≤ 21	-11 ≤ <i>h</i> ≤ 11, -20 ≤ <i>k</i> ≤ 20, -20 ≤ <i>l</i> ≤ 20	-11 ≤ <i>h</i> ≤ 12, -20 ≤ <i>k</i> ≤ 14, -21 ≤ <i>l</i> ≤ 20
Reflections collected	16321	15980	9937
Independent reflections	8233	8395	7669
Completeness to θ_{\max} (%)	83.9	87.4	78.0
Max. and min. transmission	0.956, 0.806	0.917, 0.718	0.943, 0.846
Refinement method	Full-matrix least-squares on <i>F</i> ²	Full-matrix least-squares on <i>F</i> ²	Full-matrix least-squares on <i>F</i> ²
Data / restraints / parameters	6010/4/428	4863/4/434	3728/0/245
Goodness-of-fit on <i>F</i> ²	1.048	1.000	1.361
Final <i>R</i> indices [<i>I</i> > 2 σ (<i>I</i>)]	<i>R</i> 1 = 0.0786, <i>wR</i> 2 = 0.2030	<i>R</i> 1 = 0.0921, <i>wR</i> 2 = 0.2481	<i>R</i> 1 = 0.1412, <i>wR</i> 2 = 0.2971

	SPC2a-Xymix	SPC2a-NB	SPC2b1
Empirical formula	C ₄₂ H ₃₀ Cd F ₄ N ₂ O ₅	C ₄₄ H ₃₀ Cd F ₄ N ₄ O ₈	C ₄₀ H ₃₄ Cd F ₄ N ₄ O ₇
Formula weight	831.09	935.99	871.12
Temperature (K)	100(0)	100(0)	100(0)
Wavelength (Å)	0.71073	0.71073	0.71073
Crystal system	<i>P</i> $\bar{1}$	<i>P</i> $\bar{1}$	<i>P</i> $\bar{1}$
<i>a</i> /Å	9.2801(2)	9.233(2)	9.7406(6)
<i>b</i> /Å	15.460(3)	15.375(3)	15.2916(1)
<i>c</i> /Å	15.962(3)	16.260(4)	15.4210(9)
α /°	111.909(2)	112.188(3)	63.743(3)
β /°	105.073(2)	103.539(3)	82.909(3)
γ /°	93.877(2)	93.812(3)	72.000(3)
Space group	Triclinic	Triclinic	Triclinic
Volume (Å ³)	2016.6(6)	2046.9(8)	1958.9(2)
<i>Z</i>	2	2	2
Calculated density (g cm ⁻³)	1.369	1.519	1.477
Absorption coefficient (mm ⁻¹)	0.604	0.612	0.630
<i>F</i> ₀₀₀	840.0	944.5	884.0
θ range for data collection (°)	1.58 to 28.12	1.41 to 28.24	2.20 to 28.37
Miller index ranges	-12 ≤ <i>h</i> ≤ 12, -19 ≤ <i>k</i> ≤ 20, -20 ≤ <i>l</i> ≤ 21	-12 ≤ <i>h</i> ≤ 12, -20 ≤ <i>k</i> ≤ 20, -21 ≤ <i>l</i> ≤ 21	-12 ≤ <i>h</i> ≤ 12, -19 ≤ <i>k</i> ≤ 20, -20 ≤ <i>l</i> ≤ 20
Reflections collected	24532	49604	49999
Independent reflections	9295	10060	8782
Completeness to θ_{\max} (%)	94.3	99.2	89.6
Max. and min. transmission	0.961, 0.774	0.936, 0.775	0.919, 0.778
Refinement method	Full-matrix least-squares on <i>F</i> ²	Full-matrix least-squares on <i>F</i> ²	Full-matrix least-squares on <i>F</i> ²
Data / restraints / parameters	7846/4/517	8705/21/512	6906/41/432
Goodness-of-fit on <i>F</i> ²	1.044	1.038	1.107
Final <i>R</i> indices [<i>I</i> > 2σ(<i>I</i>)]	<i>R</i> 1 = 0.0611, <i>wR</i> 2 = 0.1684	<i>R</i> 1 = 0.0623, <i>wR</i> 2 = 0.1674	<i>R</i> 1 = 0.0595, <i>wR</i> 2 = 0.1403

SPC2b2	
Empirical formula	C ₄₀ H ₃₄ CdF ₄ N ₄ O ₈
Formula weight	887.12
Temperature (K)	100(0)
Wavelength (Å)	0.71073
Crystal system	<i>P</i> $\bar{1}$
<i>a</i> /Å	9.566(2)
<i>b</i> /Å	15.343(4)
<i>c</i> /Å	15.794(4)
α /°	107.503(2)
β /°	106.915(2)
γ /°	94.075(3)
Space group	Triclinic
Volume (Å ³)	2083.0(9)
<i>Z</i>	2
Calculated density (g cm ⁻³)	1.414
Absorption coefficient (mm ⁻¹)	0.596
<i>F</i> ₀₀₀	900.0
θ range for data collection (°)	1.64 to 28.49
Miller index ranges	-12 ≤ <i>h</i> ≤ 12, -19 ≤ <i>k</i> ≤ 20, -21 ≤ <i>l</i> ≤ 21
Reflections collected	22428
Independent reflections	9533
Completeness to θ_{\max} (%)	90.4
Max. and min. transmission	0.951, 0.800
Refinement method	Full-matrix least-squares on <i>F</i> ²
Data / restraints / parameters	7789/24/527
Goodness-of-fit on <i>F</i> ²	1.076
Final <i>R</i> indices [<i>I</i> > 2σ(<i>I</i>)]	<i>R</i> 1 = 0.0853, <i>wR</i> 2 = 0.2397

5.12 References

- 1 J. Harada, K. Ogawa, *Chem. Soc. Rev.*, **2009**, 38, 2244.
- 2 I.-H. Park, S. S. Lee, J. J. Vittal, *Chem. Eur. J.*, **2013**, 19, 2695.
- 3 J. Lee, O. K. Farha, J. Roberts, K. A. Scheidt, S. T. Nguyen, J. T. Hupp, *Chem. Soc. Rev.*, **2009**, 38, 1450
- 4 J. L. Rowsell, O. M. Yaghi, *Angew. Chem., Int. Ed.*, **2005**, 44, 4670.
- 5 Q.-R. Fang, G.-S. Zhu, Y.-Y. Ji, J.-W. Ye, M. Xue, H. Yang, Y. Wang, S.-L. Qiu, *Angew. Chem., Int. Ed.*, **2007**, 46, 6638.
- 6 J.-R. Li, R. J. Kuppler, H.-C. Zhou, *Chem. Soc. Rev.*, **2009**, 38, 1477.
- 7 C. N. R. Rao, A. K. Cheetham, A. Thirumurugan, *J. Phys. Condens. Matter.*, **2008**, 20, 083202.
- 8 G. Ferey, *Chem. Soc. Rev.*, **2008**, 37, 191.
- 9 a) N. W. Ashcroft, N. D. Mermin, *Solid State Physics*; Holt, Rinehart & Winston: **1976**.; b) D. Das, T. Jacobs, L. J. Barbour, *Nat. Mater.*, **2010**, 9, 36.
- 10 a) L. R. MacGillivray, J. L. Atwood, *J. Am. Chem. Soc.*, **1997**, 119, 6931.; b) L. R. MacGillivray, J. L. Reid, J. A. Ripmeester, *J. Am. Chem. Soc.*, **2000**, 122, 7817.; b) J. Hu, L. J. Barbour, G. W. Gokel, *New J. Chem.* **2004**, 28, 907.; c) G. W. Gokel, *Chem. Commun.*, **2003**, 23, 3251.; d) J. A. R. P. Sarma, G. R. Desiraju, G. R. *J. Chem. Soc., Chem. Commun.*, **1984**, 145.; e) K. Vishnumurthy, T. N. G. Row, K. Venkatesan, *J. Chem. Soc., Perkin Trans. 2*, **1997**, 615.; f) G. R. Desiraju, R. Kamala, B. H. Kumari, J. A. R. P. Sarma, *J. Chem. Soc., Perkin Trans. 2* **1984**, 181.; g) C. V. K. Sharma, K. Panneerselvam, L. Shimoni, H. Katz, H. L. Carrell, G. R. Desiraju, *Chem. Mater.* **1994**, 6, 1282.; h) I. G. Georgiev, L. R. MacGillivray, *Chem. Soc. Rev.*, **2007**, 36, 1239.
- 11 H.-J. Cheng, M. Yu, H.-X. Li, C.-N. Lu, D.-X. LI, M.-M. Chen, Z.-G. Ren, J.-P. Lang, *J. Coord. Chem.*, **2013**, 66, 2335.
- 12 G. W. Coates, A. R. Dunn, L.M. Henling, J.W. Ziller, E. B. Lobkovsky, R. H. Grubbs, *J. Am. Chem. Soc.*, **1998**, 120, 15, 3641.

CHAPTER V: GUEST-INDUCED MOTION IN SOFT POROUS CRYSTALS

- 13 a) P. Pachfule, R. Das, P. Poddar, R. Banerjee, *CrystGrowth Des.*, **2011**, 11, 1215.;
b) Z. Hulvey, D. A. Sava, J. Eckert, A. K, *Inorg. Chem.*, **2010**, 50, 403.; c) P.
Pachfule, R. Das, P. Poddar, R. Banerjee, *Inorg. Chem.*, **2011**, 50, 3855.; d)
P. Pachfule, Y. Chen, J. Jiang, R. Banerjee R., *Chem. Eur. J.*, **2012**, 18, 688.; e) Y-S.
Bae, O. K. Farha, J. T. Hupp, R. Q. Snurr, *J. Mater. Chem.*, **2009**, 19, 2131.;
f) A. Demessence, D. M. D'Alessandro, M. L. Foo J. R. Long, *J. Am. Chem.
Soc.*, **2009**, 131, 8784.
- 14 P. Van Der Sluis, A. L. Spek, *Acta Crystallogr., Sect. A*, **1990**, 46, 194.
- 15 S. Mecozzi, J. Rebek, Jr, *Chem. Eur. J.*, **1998**, 4, 1016.

Photochromic Compounds

Although the underlying theme (probing MOF properties) remains the same, the pyridyl ligands employed in this study are of a completely different nature (varying in structure, reactivity and colour). The reason for this work was to further explore stimuli responsive behaviour in MOFs by including photochemistry. In order to do this, ligands possessing photo-responsive moieties were utilized.

6.1 Introduction

Of all known photochromic compounds, the diarylethenes are considered the most promising owing to their impressive quantum yield, high fatigue resistance and photo-stationary state.¹ Such molecules transform by means of a 6- π Woodward-Hoffman electrocyclic reaction.² The thermal analogue (parallel conformation) of a diarylethene is unable to undergo such a conversion due to steric hindrance (**Figure 6.1**).¹ Both ring-open forms are colourless, with the *anti*-parallel conformer turning blue upon exposure to ultraviolet light.

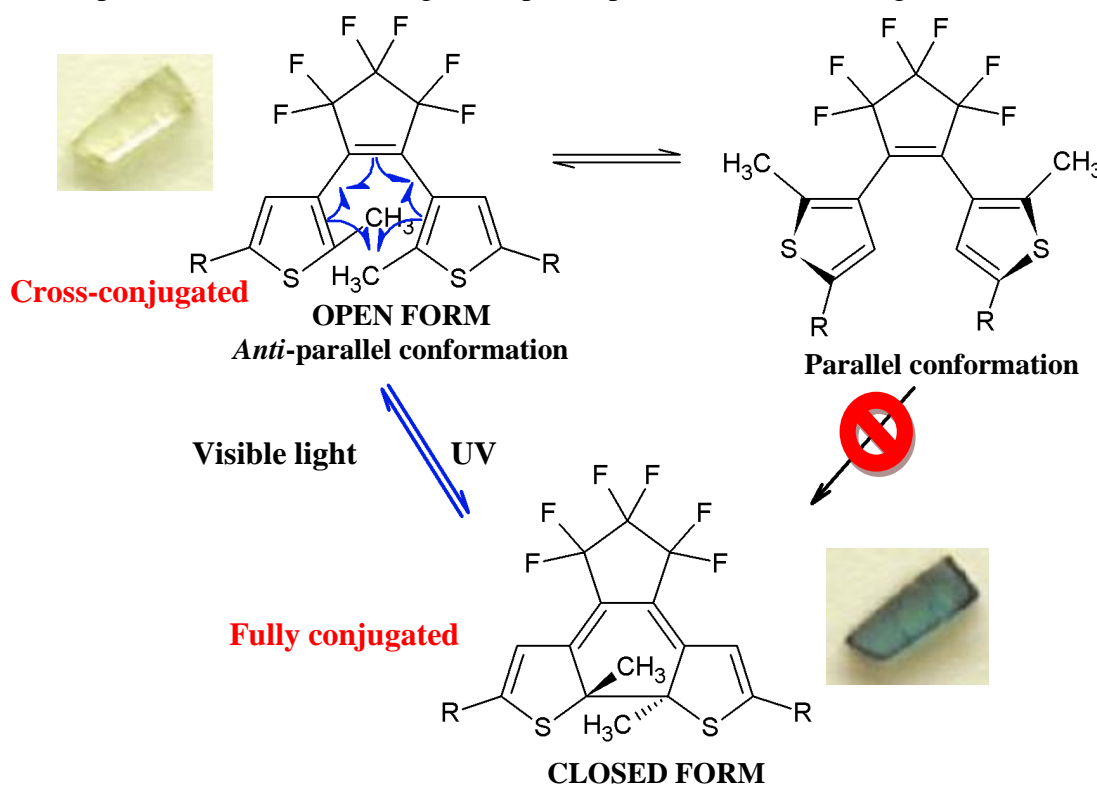


Figure 6.1 Conformation of a simple diarylethene and the photochromic reaction mechanism.²

CHAPTER VI: PHOTOCROMIC COMPOUNDS

The differences in colour stem from the differences in the electronic properties of the molecules. In the ring-open isomers, the aryl and ethene groups can rotate freely, enabling their electron systems to separate in a non-planar cross-conjugated manner. The nearly planar structure of the closed form with the asymmetrically arranged carbon atoms and the conjugation that extends throughout the whole molecule are the reasons for the shift of absorbance to longer wavelengths.

Substitution of the thiophene rings can further affect the degree of absorbance. Substituents that allow extension of the conjugated system or create a donor-acceptor pattern ensure that absorbance of the closed form occurs at higher wavelengths (800 nm).³ Since diarylethenes experience only small changes in shape upon isomerisation, these photochromic compounds are ideal for solid-state SC-SC analysis as structural changes have the potential to occur without the loss of crystal singularity. The literature contains many examples of photocyclised diarylethenes with various substituents situated on either the 2' or the 3' positions of the thiophene rings; a search of the CSD (Version 1.17) produced 147 hits. Of these examples, there are only four structures with R = Ph (all published by Irie *et al.*^{4,5}) showing photo-induced ring closure (interestingly all of these structures show the ring-closed conformer as the minor species) and all employ an ethyl substituted phenyl thiophene. The most notable example was published in *Nature* in 2007 wherein Irie showed not only the SC-SC light induced ring closure of a P-type* 1,2-bis(2-ethyl-5-phenyl-3-thienyl)perfluorocyclopentene but also the dramatic reversible shape and colour change exhibited by crystals of such materials (**Figure 6.2**).⁵ According to Irie, there are two principal requirements for ring closure to occur: (i) the reactive carbon-carbon distance must be 4 Å or shorter in the open-ring conformer and (ii) the molecular packing of the open-ring conformer must be conducive to ring closure.^{6,3d}

* Photochemically reversible type where the isomers are stable and may be converted to their original form photochemically but not thermally.

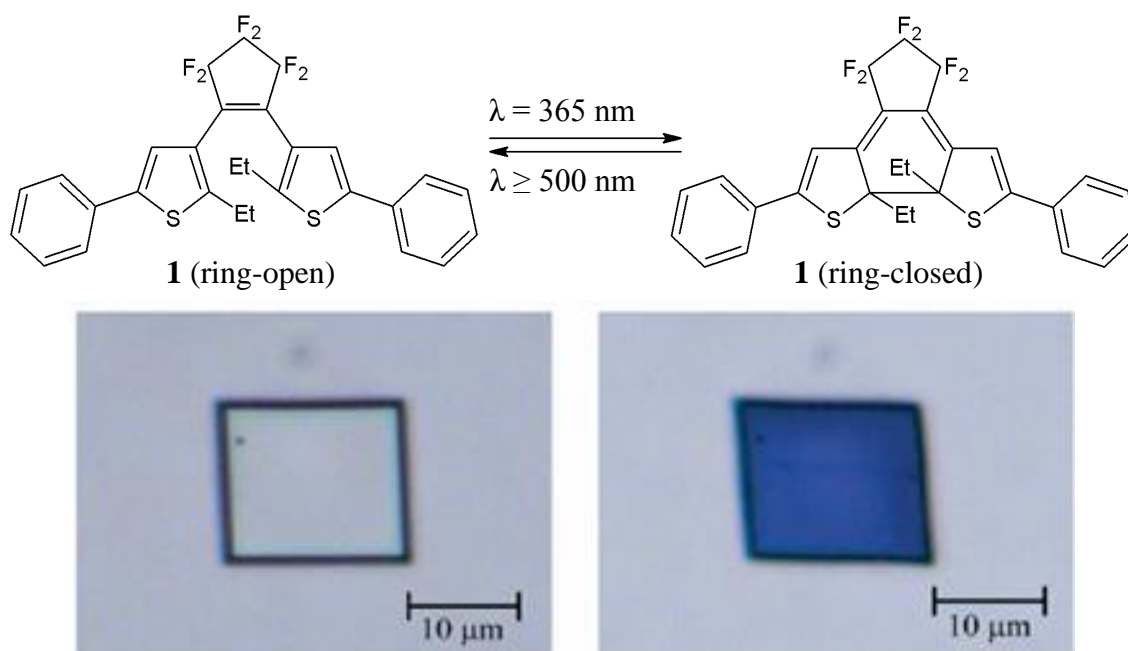


Figure 6.2 Reversible colour and shape change of a P-type 1,2-bis(2-ethyl-5-phenyl-3-thienyl)perfluorocyclopentene upon irradiation with ultraviolet or white light.⁵

Although metal-organic frameworks show enormous potential for gas storage and separation, they require changes in pressure and/or temperature in order to absorb or desorb a guest. Such operations are energy intensive and thus, on an industrial scale, cost inefficient. One way to circumvent such problems would be to incorporate photosensitive ligands into MOF membranes thus enabling remote control of properties (depending on the intensity and wavelength of the light employed, the material could be switched ‘on’ or ‘off’ at will). This is by no means a novel concept. However, all previous examples of photo-switchable coordination materials were comprised of rigid stimuli-unresponsive ligand backbones with appended mono-coordinated azobenzene groups or photo-switchable guest molecules included into framework channels.⁷

Following on Irie’s success with phenyl-substituted diarylethenes and with the goal of MOF formation in mind, two hexafluorinated diarylethene ligands containing coordinating pyridyl moieties at both ends were synthesised by Dr Simon Herbert. **Figure 6.3** shows 1,2-bis[2-methyl-5-(4-pyridyl)-3-thienyl]perfluorocyclopentene **DL1** (a ligand previously described in the literature²) and 1,2-bis[2-ethyl-5-(4-pyridyl)-3-thienyl]perfluorocyclopentene **DL2** (a new ligand).

Before discussing the MOFs obtained, attention is drawn to the ligands themselves.

CHAPTER VI: PHOTOCROMIC COMPOUNDS

Although previous reports⁸ described photocyclisation reactions of the methyl-substituted diarylethene (**DL1**) coordinated to various metal ions, little mention was made of the photocyclisation capabilities of the pure ligand. Crystal structures of both materials were obtained with **DL1** crystallising in the triclinic space group $P\bar{1}$ with two molecules in the ASU while **DL2** crystallises in the monoclinic space group $P2_1/n$ with one molecule (which contains one ethyl group disordered over two positions) in the ASU. Both ligands crystallise as the open form conformer with reactive carbon-carbon atom distances of 3.56 and 3.53 Å in **DL1** and 3.64 Å in **DL2**.

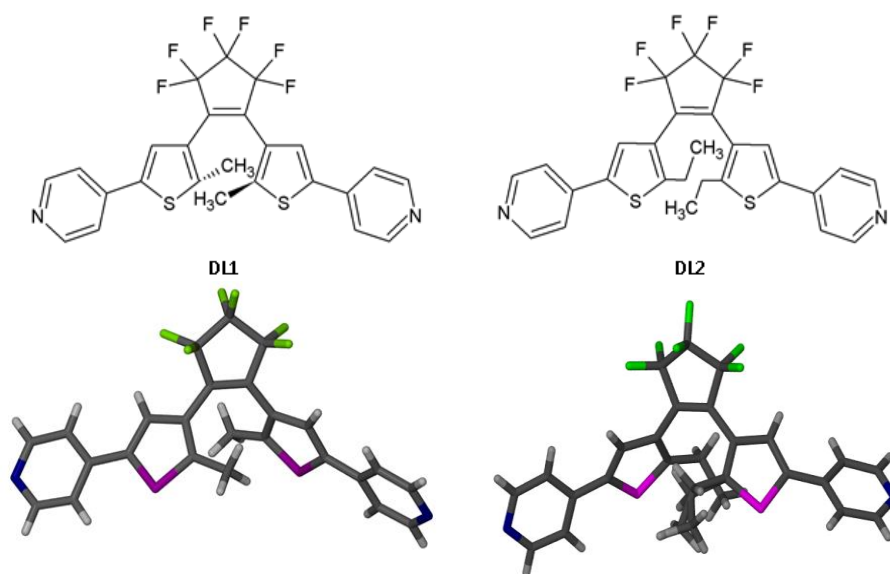


Figure 6.3 Solid-state structures of diarylethenes **DL1** and **DL2** (showing disordered ethyl arm) used in this study.

The crystals of **DL1** and **DL2**^{*} were consistent with similar literature examples^{3,4} in that the initially colourless crystals immediately turned a uniform dark blue colour upon exposure to ultraviolet light (365 nm). Unlike the phenyl-substituted diarylethene,⁵ irradiation did not induce any discernible shape change in either **DL1** or **DL2**. Owing to the location[†] of the irradiation source (**Figure 6.4**), it was not possible to irradiate and collect low temperature diffraction data simultaneously (source positioned directly beneath the cryostream).⁹

^{*} Synthetic procedures may be found in the supplementary information.

[†] A detailed description of which is presented in Chapter II.

CHAPTER VI: PHOTOCROMIC COMPOUNDS

In the context of structure determination of irradiated crystals for all materials described in this chapter, “continuous” refers to the collection of diffraction data *during* UV irradiation at room temperature while “intermittent” refers to UV irradiation at room temperature *followed by* diffraction data collection at 100 K. Despite numerous data collections, examination of the **DL1** and **DL2** structures showed no electron density peaks in the region of interest and thus no discernible ring closure.



Figure 6.4 Photographs of a) continuous* and b) intermittent irradiation experimental configurations using a 365 nm UV light source.

If a crystal of either ligand is left in paratone oil under UV light, it appears to “bleed”, with a blue halo forming around its perimeter. If the crystal is removed, the blue halo remains, implying slight solubility of the ligand in the oil. Examination of the packing arrangements of both ligands provides a potential explanation of why the ethyl-substituted thiophene could be more likely to undergo ring closure when compared to the methyl-substituted thiophene. As **Figure 6.5** shows the packing of the **DL1** ligands is poorly suited for ring closure as it involves the partial insertion of one pyridyl ring from one **DL1** into the V-shaped cavity of another. This is not the case with the **DL2** ligand as the V-shaped ligands orient away from one another.† The additional energy required to move the **DL1** ligands far enough apart to facilitate ring-closure combined with the short alkyl arm may impede ring closure in **DL1**.

In an attempt to gain further insight, the ligands were dissolved in deuterated acetone and ^1H NMR spectra were recorded pre- and post-irradiation.

* Several different assemblies were considered, including a simplified version of Raithby’s light-emitting diode.⁸ None of these setups provided the required irradiation intensity needed for conversion, hence the decision to devise our own configuration.

† It is important to note that although differing in *para*-position substituents, **DL1** and **DL2** are isostructural to the examples found in the CSD and pack in a similar manner (**Figure 6.5**).

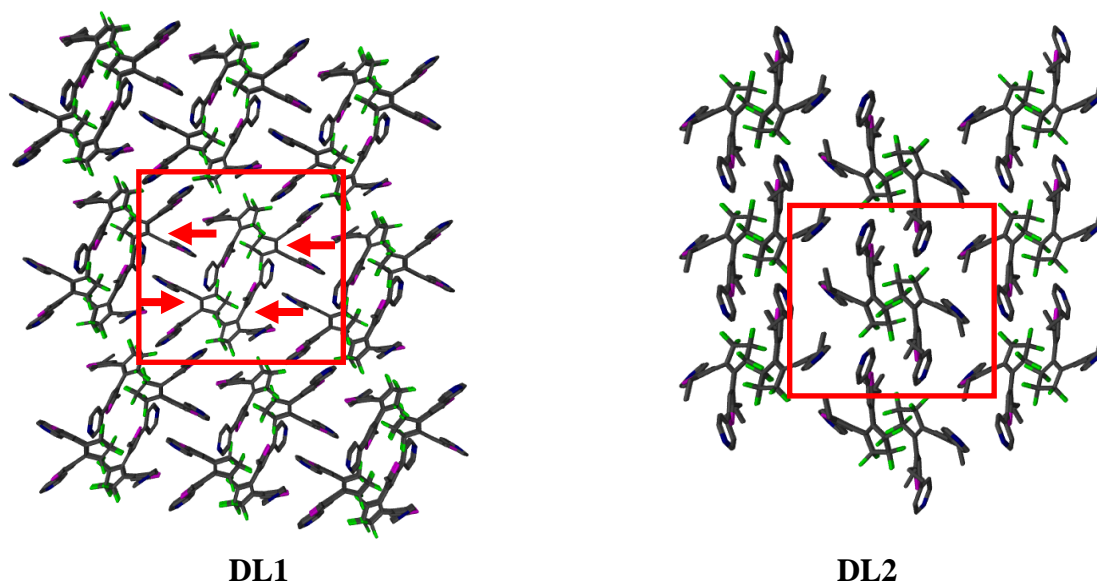


Figure 6.5 Packing diagrams of **DL1**^{*} and **DL2** with hydrogen atoms omitted for clarity.

The first blue spectrum (from the bottom) in **Figure 6.6a** shows the three unique proton signals for the thiophene and the pyridyl rings. After exposure of the material to high intensity UV light (365 nm), a second set of similar but much lower intensity peaks was observed, indicating the appearance of a second species in solution. Particular attention is drawn to the peaks labelled 2 and 2' as this thiophene proton experiences a large shift (7.78 to 7.18 ppm) as a result of ring closure. Continuous irradiation increases the ratio of the closed to open forms until equilibrium is reached; after 40 hours of irradiation only a quarter of the molecules had converted to the closed form.

^{*}Single-crystal variable-temperature and gas cell experiments (using various pressures of CO₂) were performed in the hope that the external stimuli would alter the internal packing, thus enabling irradiation induced ring closure to occur. Unfortunately, this did not happen.

CHAPTER VI: PHOTOCROMIC COMPOUNDS

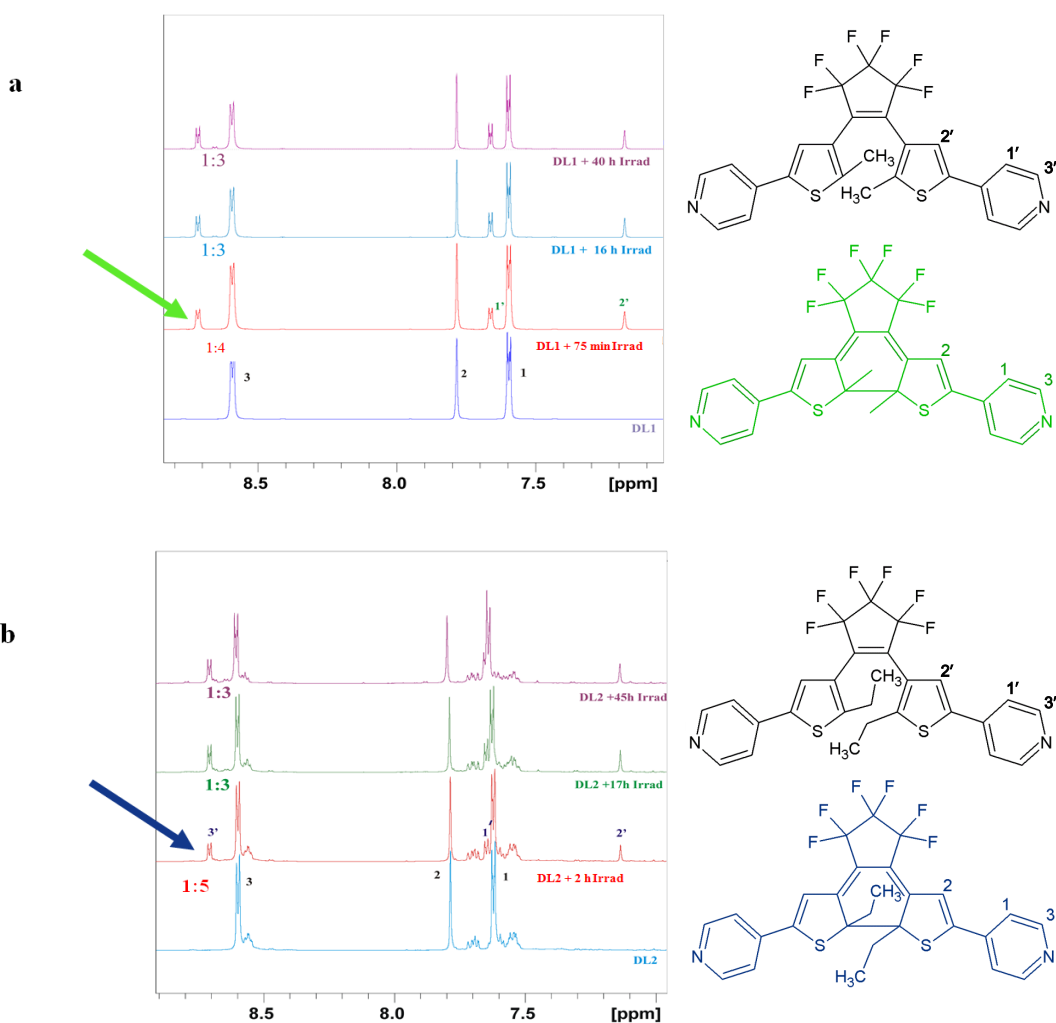


Figure 6.6 Variable time UV irradiation ^1H NMR spectra of the a) **DL1** and b) **DL2** ligands pre- and post-irradiation.

Although the **DL2** ligand sample (**Figure 6.6b**) has a few impurities (synthesis of this ligand is more difficult due to the larger alkyl group), it behaves in a similar manner to its methyl analogue, with the thiophene proton once again experiencing a substantial shift (7.78 to 7.13 ppm) upon irradiation. As with **DL1**, the **DL2** ligand proceeds to a 3:1 open to closed ratio after which the reaction ceases.

Since NMR showed ring closure takes place in solution, it is proposed that molecular packing restrictions may well be responsible for impeding methyl-substituted ring-closure. However, this does not account for why the **DL2** ligand does not undergo ring-closure in the solid-state. Although unexpected, it is believed that the incorporation of a single nitrogen heteroatom alters the electrostatic nature of the ligand sufficiently to impede photocyclisation.

CHAPTER VI: PHOTOCROMIC COMPOUNDS

In spite of the poor conversion exhibited by the uncoordinated diarylethene ligands, there are reports in the literature showing that **DL1** when coordinated to a metal, can undergo ring closure.⁷ As a result, a series of rationally designed MOFs were prepared in the hope that the addition of the metal ions as well as diacid ligands would alter the photochromic behaviour of the diarylethene ligands as well as the properties of the overall material. Four commercially available carboxylic acid ligands (one short, one rigid, one flexible and one with its own photochromic potential) were selected; terephthalic acid (**TPA**), 4,4'-biphenyl-dicarboxylic acid (**BPDC**), 4,4'-oxybisbenzoic acid (**OBA**) and 4,4'-azobenzene-dicarboxylic acid (**AZDC**) (**Figure 6.7**).

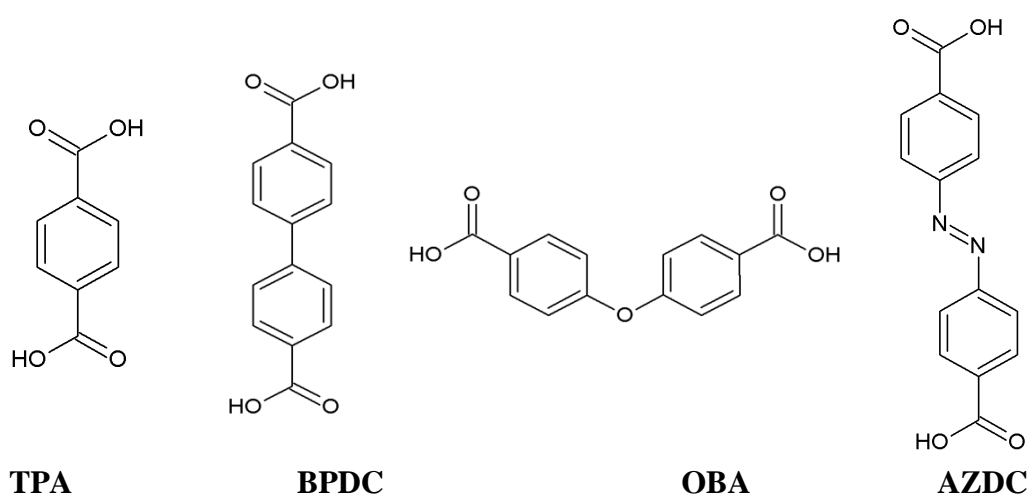


Figure 6.7 Four commercially available carboxylic acids used as ligands in this study.

6.2 Solvothermal crystallisation conditions

Optimal* conditions for framework formation in this study involved the dissolution of the diarylethene ligand (0.015 mmol), the carboxylate ligand (0.025 mmol) and the zinc[†] nitrate salt (0.025 mmol) in a 2 mL (1:1 v/v) solution of DMF and EtOH. The solution was heated in a sintered glass vial at 100 °C for 24 h and then cooled to room temperature.

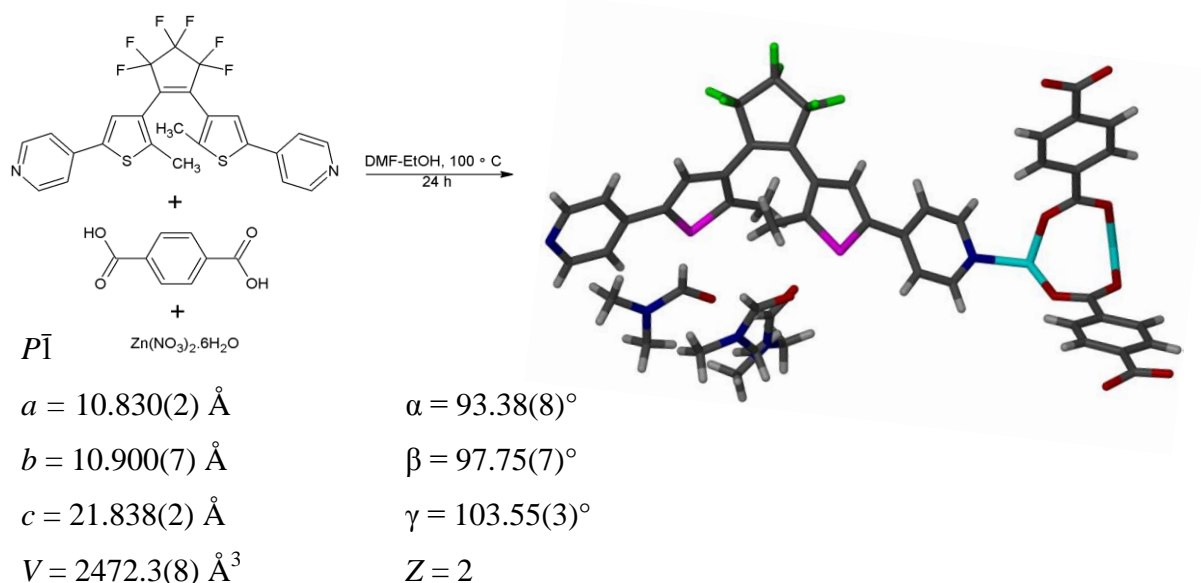
* Several methods, including layering, slow evaporation and diffusion were attempted.

[†] Zinc was selected due to its low cost, stable binding tendencies and ability to yield colourless complexes (coloured metals could potentially affect ring closure visibility).

6.3 Resultant MOFs

6.3.1 $\{[\text{Zn}_2(\text{DL1})\text{TPA}_2]\cdot 2\text{DMF}\}_n$ or PCCP_1

PCCP_1 was formed from the reaction of **DL1**, **TPA** and Zn(II) nitrate hexahydrate under solvothermal conditions (100 °C, DMF-EtOH) (**Scheme 6.1**) and crystallises in the triclinic space group $P\bar{1}$. The ASU consists of two zinc cations, one **DL1** ligand in the ring-open conformation with the fluorine ring disordered over two positions*, two **TPA** ligands and two DMF guest molecules of which one is disordered over two positions.



Scheme 6.1 Synthesis of **PCCP_1** from the solvothermal reaction of **DL1**, **TPA** and zinc nitrate in a DMF-EtOH mixture at 100 °C with selected crystallographic information.

PCCP_1 contains a zinc paddlewheel composed of four **OBA** ligands coordinated in an equatorial manner to two metal ions with two **DL1** ligands located in the axial positions. The distance between the two carbon atoms involved in ring closure is 3.49 Å (**Figure 6.8a**). The **DL1** ligands are oriented in a stepped manner with the paddlewheel moieties stacking directly one on top of another (**Figure 6.8b**) to form a three dimensional (3D) net.

* The three apex carbon atoms and the associated fluorine atoms on the **DL2** ligand are disordered over two positions. This has been hidden for visual clarity.

Figure 6.8c shows the twofold interpenetrated nature of the extended structure with discrete voids occupied by disordered DMF molecules.

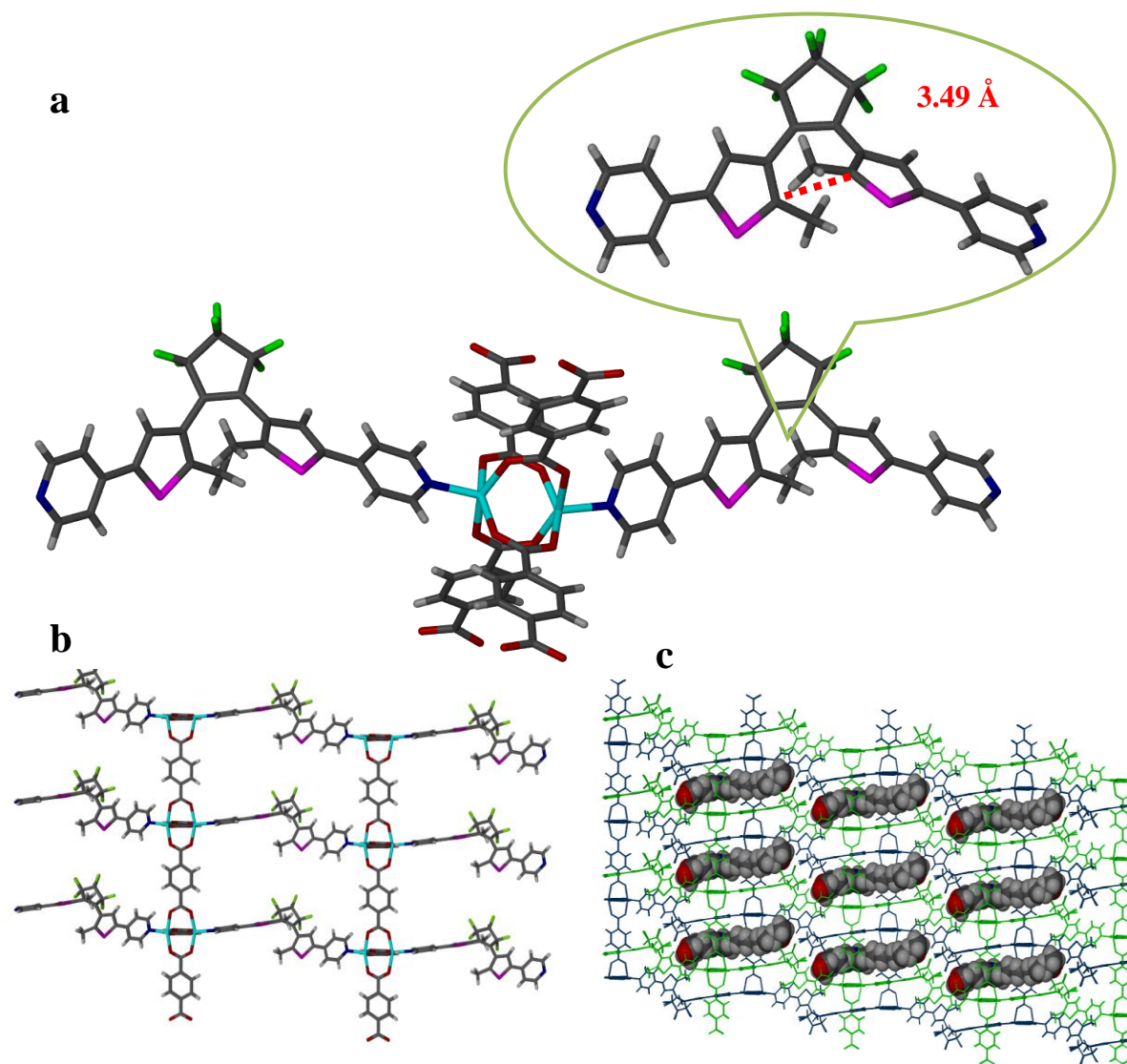


Figure 6.8 a) Paddlewheel geometry in **PCCP_1**. b) View down the *a* axis showing stepped orientation of **DL1** ligand in one layer of **PCCP_1**. c) View along crystallographic *a* axis showing twofold interpenetration and DMF-filled solvent channels.

Of the two DMF molecules present, one has full occupancy while the other is disordered over two positions with site occupancy values of 55% and 45%. TGA analysis (**Figure 6.9**) shows minor surface solvent loss followed by a 13% weight loss occurring in the temperature range of 35 - 150 °C, corresponding to the crystallographic data as two DMF molecules per formula unit. The material is then stable until framework decomposition commences at 350 °C. The very thin plate-like crystals could not be activated with retention of crystal singularity.

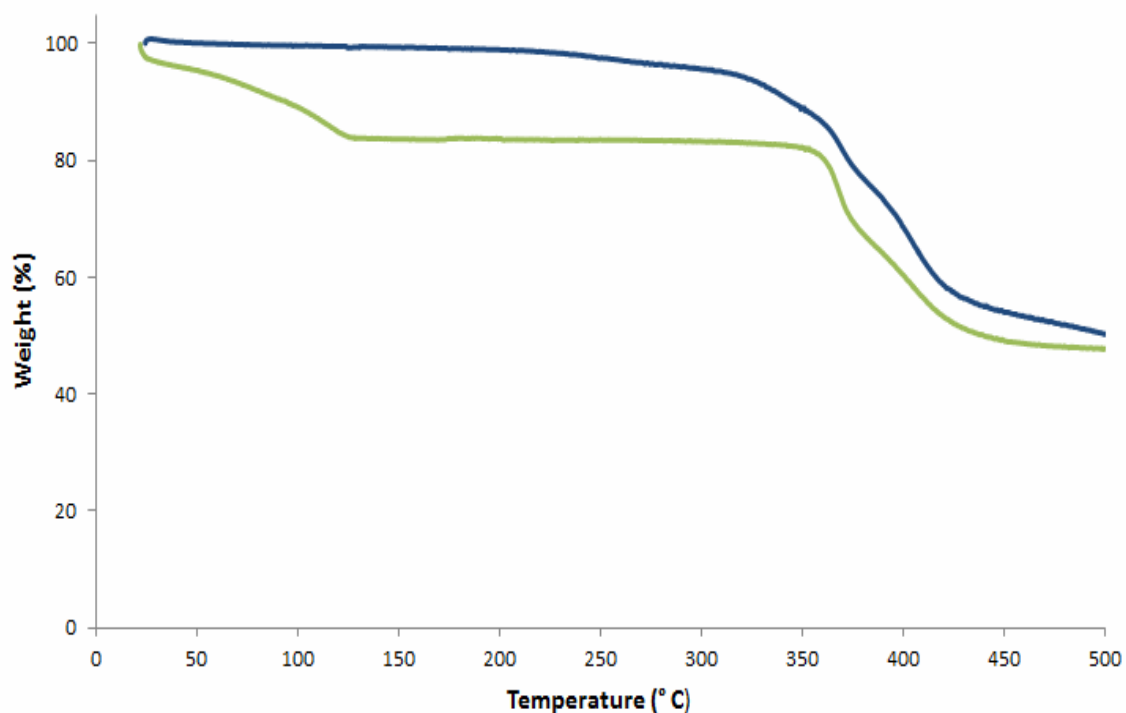


Figure 6.9 TGA of the as-synthesised as well as the evacuated phases of **PCCP_1** (green and blue lines, respectively).

6.3.1.1 PCCP_1 Irradiation Experiments

Exposure of **PCCP_1** crystals to ultraviolet light (365 nm) induces a dramatic colour change (**Figure 6.10**). Initially colourless crystals turn reddish-brown. This process is reversible and shows excellent fatigue resistance (colour change can be induced ≥ 50 cycles).

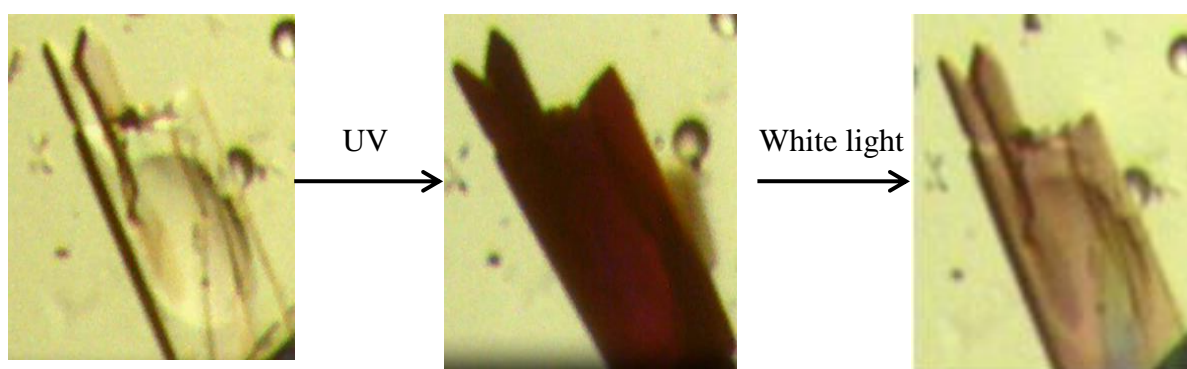


Figure 6.10 Photographic evidence of a **PCCP_1** crystal undergoing a reversible colour change when exposed to ultraviolet and visible light.

CHAPTER VI: PHOTOCROMIC COMPOUNDS

As previously mentioned, the literature^{3,4} contains many examples of diarylethenes both coordinated and not, undergoing similar colour changes when irradiated with ultraviolet light. The dramatic colour change is ascribed to ring closure and the formation of a fully conjugated ring system (**Figure 6.11**). In uncoordinated ligands this change elicits only a minor reduction of cell parameters, however it is anticipated that when incorporated into a MOF, ring closure would result in a more significant reduction of cell parameters.

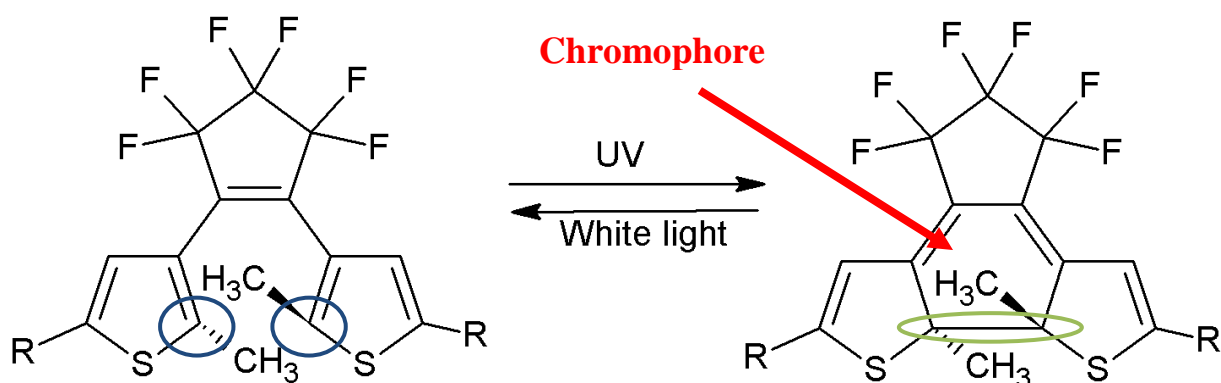


Figure 6.11 Well established conversion between the open and closed forms of diarylethenes upon irradiation.

6.3.1.2 Solid-state UV-visible spectroscopy

A series of solid-state UV-visible spectra were recorded in an attempt to ascertain whether ring closure had indeed occurred.* After recording the spectrum for a sample of **PCCP_1** the same sample was then irradiated for one minute (365 nm) and the spectrum rerecorded. **Figure 6.12** shows that the original form contains two bands, one at 354 and one at 433 nm. These bands compare favourably with previous reports^{10,11,12,13} for other diarylethene ligands and can be attributed to π - π^* transitions in the ligand and metal-to-ligand charge transfer of the divalent zinc to the π^* orbital of the bridging ligand. The spectrum of the irradiated sample exhibits a broad maximum in the green spectral range, which is responsible for the red colour observed.

* A common approach in the literature for confirming ring closure.

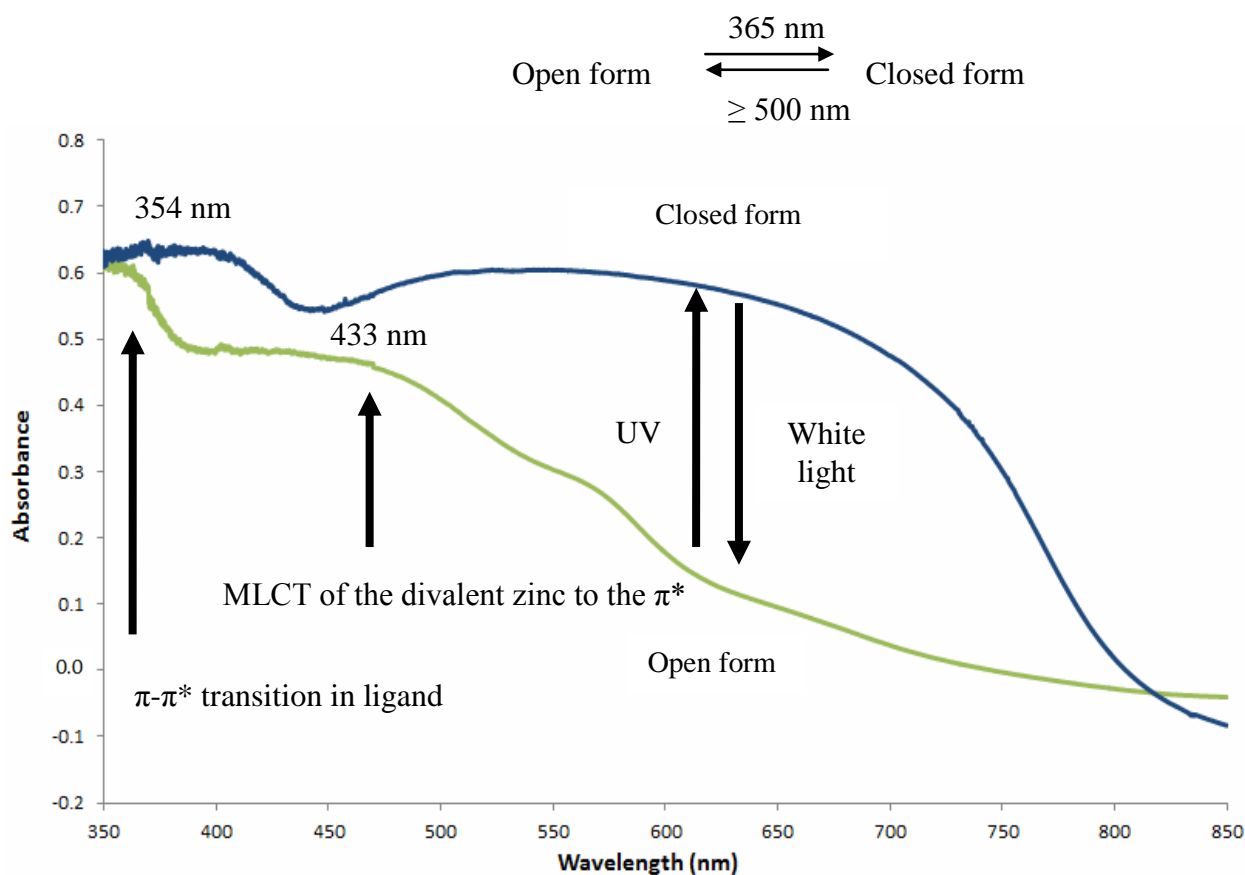


Figure 6.12 Solid-state UV-Vis spectra of the original (green) and irradiated (blue) forms of **PCCP_1**.

In conjunction with the previously mentioned change in colour, **PCCP_1** crystals also experience a change in shape. **Figure 6.13** shows how extended irradiation causes a crystal of **PCCP_1** to gradually widen, eventually resulting in crystal splitting. Further irradiation induced contraction to a slightly smaller version of the original shape. It is believed that a structural change occurs as the crystal changes colour. As each diarylethene molecule undergoes ring closure it stimulates its neighbour to undergo a similar reaction thus creating a ‘domino-effect’ which propagates through the crystal, culminating in a uniform structure of a single ring-closed conformer with an even dark colour.

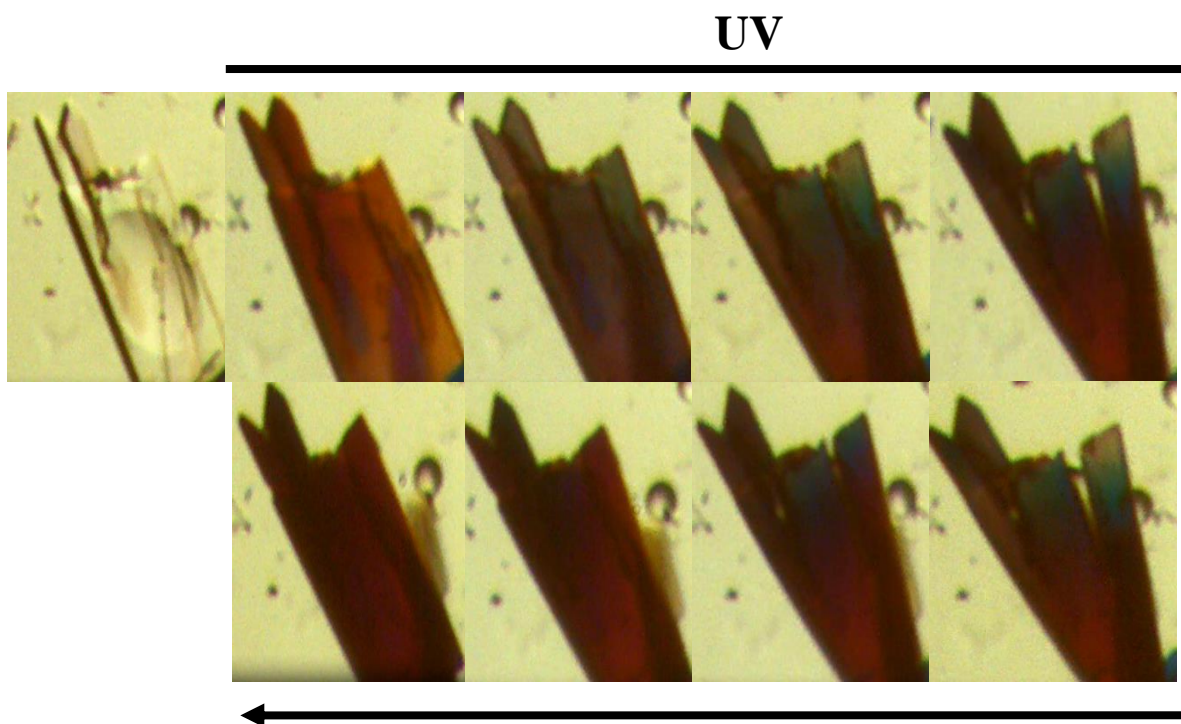


Figure 6.13 Consecutive photographs showing UV-irradiation induced shape alteration experienced by **PCCP_1**.

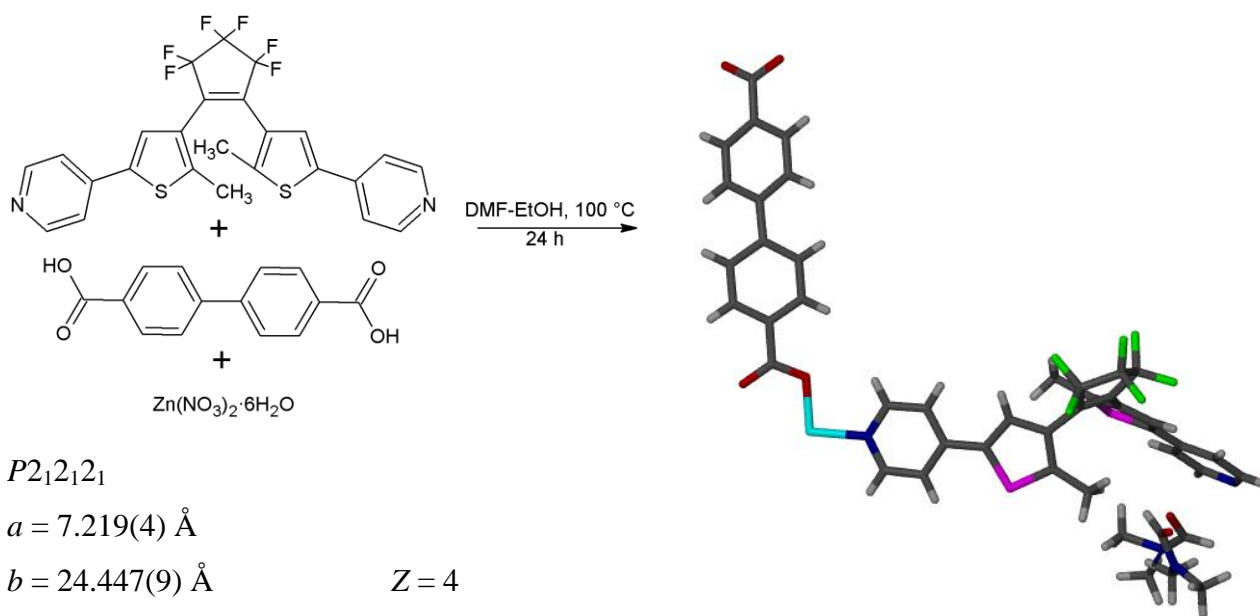
Figure 6.13 shows that UV-irradiation induces substantial mechanical transformation of the crystal. SC-SC experiments were thus undertaken in an attempt to understand the reasons for the transformation. Despite minimal visible crystal deterioration, irradiated crystals dramatically decreased in diffraction quality. Although a crystallographically rigorous diffraction dataset could not be recorded, three unit cells were determined. **Table 6.1** shows the effect of various levels of UV and white light irradiation on the unit cell parameters for a single crystal of **PCCP_1**. The unit cell for **PCCP_1** was first determined at 100 K under ambient light, after which the temperature was raised slowly to 22 °C. The unit cell was then redetermined (**PCCP_1I**) at room temperature during continuous irradiation of the crystal with 365 nm UV light. A marked decrease in all of the unit cell parameters was observed (vastly overshadowing any differences that might be due to thermal effects), implying that ring closure had occurred. Finally, the UV lamp was removed and the crystal was irradiated with white light during cooling back to 100 K over a period of 15 minutes. The unit cell was again recorded (**PCCP_1PI**), yielding parameters similar to those of the original form **PCCP_1**. The crystal remained coloured, implying that a small fraction of molecules remained ring-closed.

Table 6.1 Unit cell parameters for **PCCP_1** under white, UV and post UV white light.

	PCCP_1 White light (100 K)	PCCP_1I UV irradiation (RT)	PCCP_1PI White light post UV irradiation (100 K)
a	10.83 Å	10.01 Å	10.89 Å
b	10.92 Å	10.19 Å	10.99 Å
c	22.07 Å	20.06 Å	21.62 Å
α	98.17°	96.91°	90.73°
β	92.52°	94.44°	99.75°
γ	98.92°	103.62°	103.22°
V	2545 Å ³	1962 Å ³	2479 Å ³

6.3.2 $\{[\text{Zn}(\text{DL1})\text{BPDC}] \cdot 2\text{DMF}\}_n$ or **PCCP_2**

PCCP_2 was formed by the reaction of **DL1**, **BPDC** and Zn(II) nitrate hexahydrate under solvothermal conditions (100 °C, DMF-EtOH) (**Scheme 6.2**). **PCCP_2** crystallises in the orthorhombic space group $P2_12_12_1$. The ASU consists of one zinc cation, one **DL1** ligand, one **BPDC** ligand and one DMF molecule disordered over two positions (the second DMF molecule is to diffuse to model but was corroborated by TGA).



Scheme 6.2 Synthesis of **PCCP_2** from the solvothermal reaction of **DL1**, **BPDC** and zinc nitrate in a DMF-EtOH mixture at 100 °C, with selected crystallographic information.

CHAPTER VI: PHOTOCROMIC COMPOUNDS

Each metal centre possesses tetrahedral coordination geometry (**Figure 6.14a**) comprised of two **DL1** ligands and two **BPDC** ligands. The **DL1** ligands adopt a sigmoidal arrangement and are present in the ring-open form (**Figure 6.14b**) with the distance between carbon atoms associated with ring closure being 3.65 Å. Although the 3D network is fivefold interpenetrated, there are large corrugated channels running along the *a* axis. **Figure 6.14c** shows dimethylformamide molecules occupying these channels.

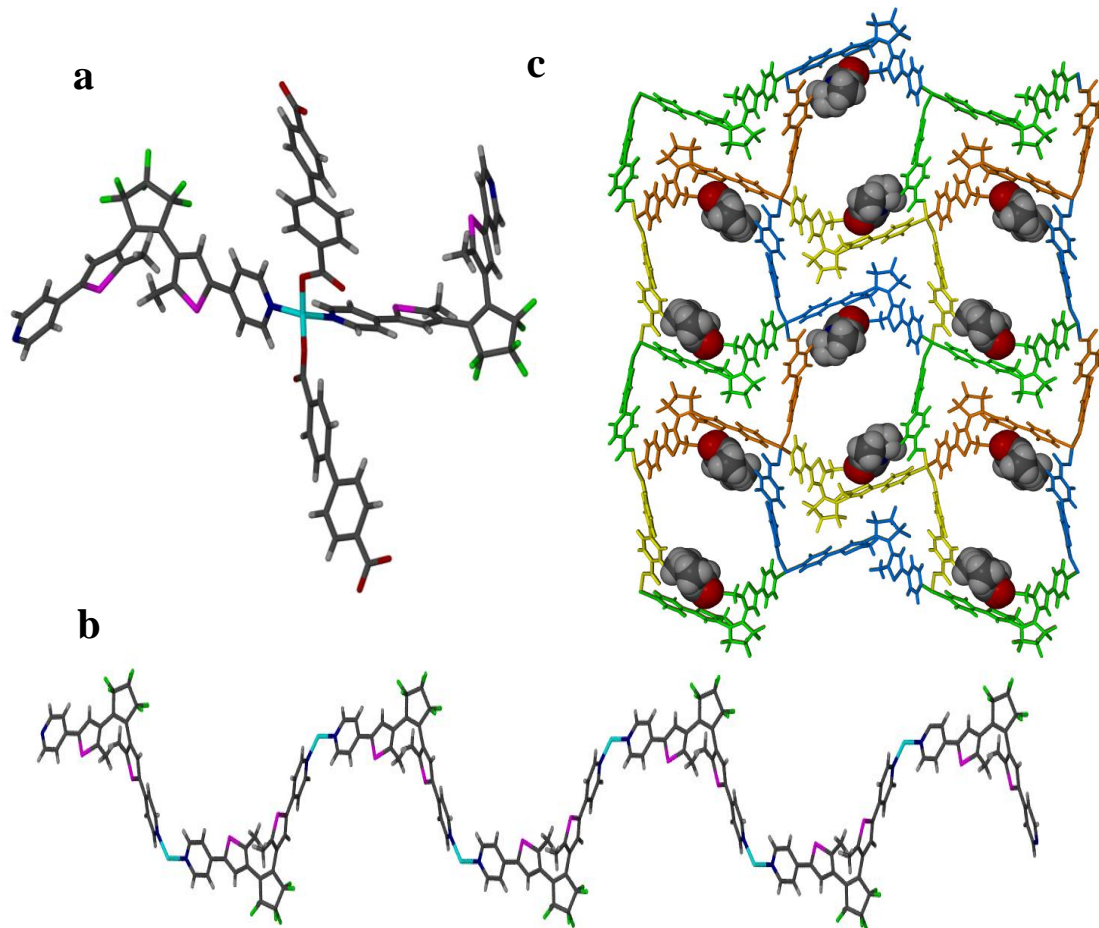


Figure 6.14 a) Tetrahedral geometry in **PCCP_2**. b) Sigmoidal chain of **DL1** ligand. c) View along the crystallographic *a* axis showing fivefold interpenetration and DMF filled solvent channels.

One DMF molecule is disordered over two positions with 63% and 37% site occupancy. TGA analysis (**Figure 6.15**) shows some initial mass loss attributed to surface solvent with an additional 20% mass loss occurring in the temperature range of 50 - 175 °C. This corresponds to the SQUEEZE data as two DMF molecules per formula unit. Due to diffuse electron density this second DMF molecules could not be modelled. Decomposition of the framework begins at 325 °C.

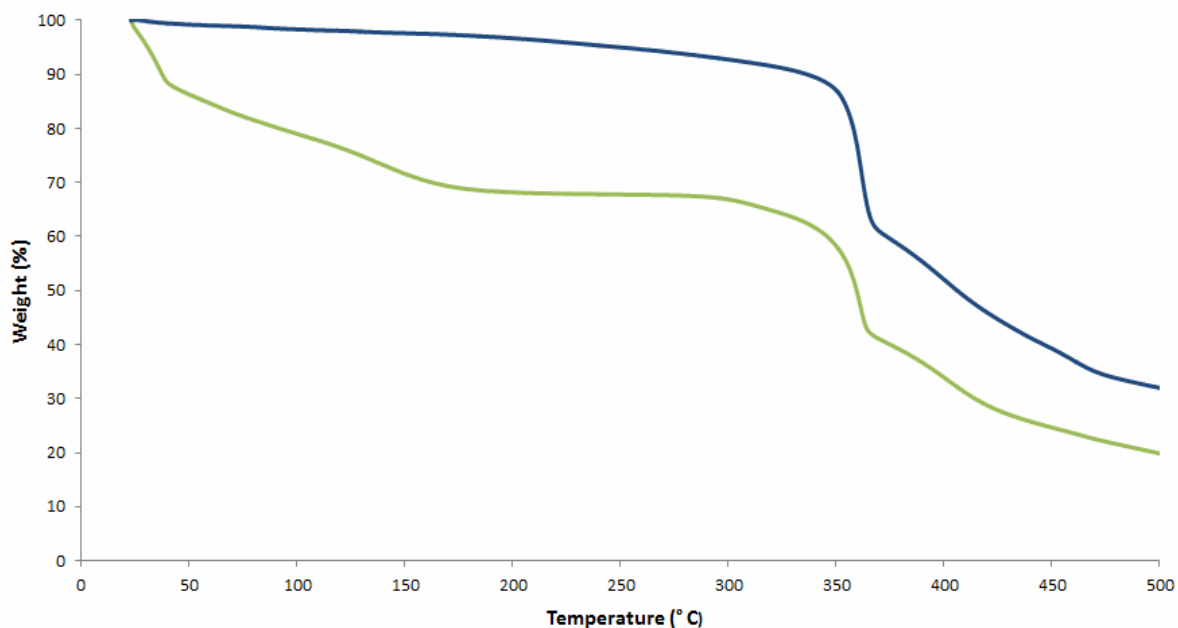


Figure 6.15 TGA of the as-synthesised as well as the evacuated phases of **PCCP_2** (green and blue lines).

6.3.2.1 $\{[\text{Zn}(\text{DL1})\text{BPDC}]\}_n$ or **PCCP_2'**

The apohost form (**PCCP_2'**) may be generated by heating the solvate at 100 °C under reduced pressure for 24 h. Due to the robust nature of the framework, this occurs as a SC-SC transformation. The cell parameters undergo a slight change (**Figure 6.16**). In spite of this, the host framework of the empty phase remains the same as that of the as-synthesised phase.

$P2_12_12_1$

$a = 7.156(2) \text{ \AA}$

$b = 24.666(9) \text{ \AA}$

$c = 29.109(1) \text{ \AA}$ $Z = 4$

$V = 5138.3(0) \text{ \AA}^3$

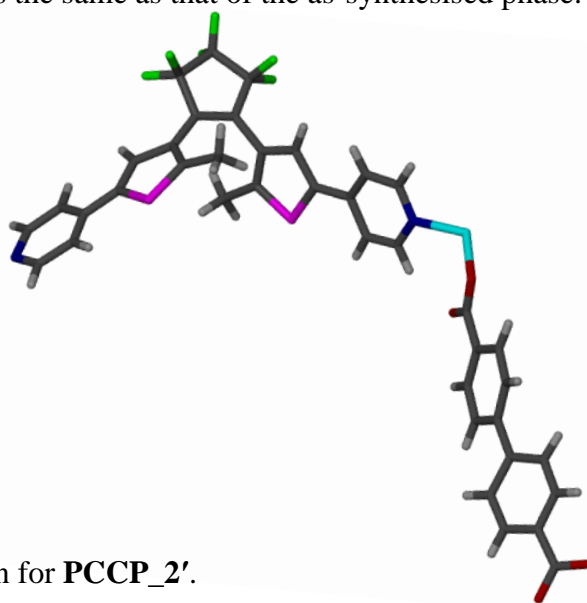


Figure 6.16 Crystallographic information for **PCCP_2'**.

Examination of the extended structure shows the previously described corrugated channels with the framework now possessing 1026 \AA^3 of solvent accessible space per unit cell (**Figure 6.17**).

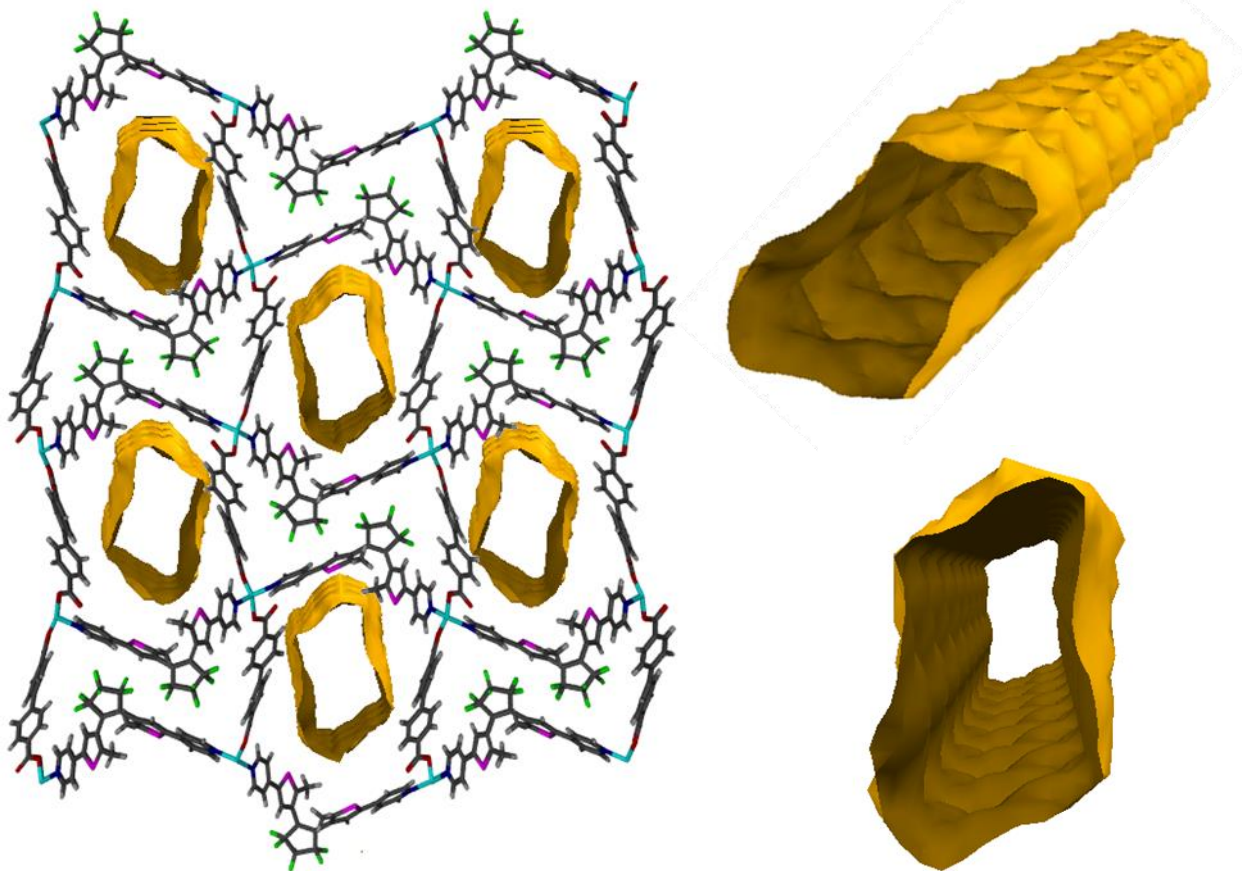



Figure 6.17 PCCP_2' viewed along the crystallographic *a* axis showing solvent-accessible voids.

Having successfully activated **PCCP_2'** and retained crystal quality, a series of diffraction experiments under a selection of temperatures were undertaken. A single crystal of **PCCP_2'** was selected, glued onto a glass fibre and successive data collections were recorded at 100, 298, 308, 318, 328 and 338 K. **Table 6.1** provides the crystallographic data obtained from these experiments as well as the calculated linear thermal expansion coefficients.

CHAPTER VI: PHOTOCROMIC COMPOUNDS

Table 6.1 Crystallographic data as a function of temperature for **PCCP_2'**.

Temperature					
					
<i>P</i>2₁2₁2₁					
100 K	298 K	308 K	318 K	328 K	338 K
<i>a</i> = 7.095(4) Å	<i>a</i> = 7.182(2) Å	<i>a</i> = 7.177(9) Å	<i>a</i> = 7.182(5) Å	<i>a</i> = 7.186(0) Å	<i>a</i> = 7.183(7) Å
<i>b</i> = 24.676(4) Å	<i>b</i> = 24.631(2) Å	<i>b</i> = 24.604(2) Å	<i>b</i> = 24.601(3) Å	<i>b</i> = 24.607(6) Å	<i>b</i> = 24.613(5) Å
<i>c</i> = 29.162(4) Å	<i>c</i> = 29.345(3) Å	<i>c</i> = 29.333(3) Å	<i>c</i> = 29.352(5) Å	<i>c</i> = 29.369(6) Å	<i>c</i> = 29.345(8) Å
<i>V</i> = 5106.01 Å ³	<i>V</i> = 5191.27 Å ³	<i>V</i> = 5180.45 Å ³	<i>V</i> = 5186.55 Å ³	<i>V</i> = 5193.43 Å ³	<i>V</i> = 5188.81 Å ³
$\alpha_a = 52 \quad \alpha_b = 11 \quad \alpha_c = 26$					

Thermal expansion is due to an increase in kinetic energy of every atom within a material (bond-bending and bond-stretching vibrations) and, consequently, an increase in the collective molecular motion.¹⁴ Thermal expansion or contraction may be defined as the ability of an object to change in size as a response to a change in temperature. The linear expansion coefficient is a measure of the fractional change in size per degree change in temperature at a constant pressure. These values are calculated as follows:

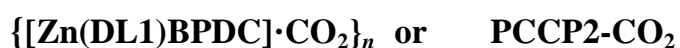
$$\alpha = \frac{\Delta L}{L_0 \Delta T} \quad \dots 1$$

α represents the linear thermal expansion coefficient as the change in length (ΔL) divided by the product of the initial length (L_0) and the overall temperature difference (ΔT). Previous studies have shown that certain materials exhibit anomalous thermal expansion behaviour and such materials may be categorised into one of three types: remarkably large positive thermal expansion (PTE), zero thermal expansion (ZTE) and negative thermal expansion (NTE).¹⁵

Despite a continuous increase in temperature, none of the cell parameters in **PCCP_2'** show any significant thermal expansion. The expansion coefficients were determined to be $\alpha_a = 52$, $\alpha_b = 11$, $\alpha_c = 26$. This low thermal expansion is unusual for such a porous material and implies that **PCCP_2** is a rigid material undergoing minimal motion even when subjected to elevated temperatures.

6.3.2.2 Supercritical CO₂ experiment

Crystals of **PCCP_2** were subjected to a solution of supercritical carbon dioxide for 24 hours as an alternate means of obtaining the apohost structure. Instead, **PCCP2-CO₂** was obtained (**Figure 6.18**). According to SQUEEZE, there should be four CO₂ guest molecules per asymmetric unit. Unfortunately, it was only possible to model one carbon dioxide molecule, with 45% occupancy. The reason behind the presence of CO₂ is an electrostatic interaction between the oxygen atom on the CO₂ guest molecule and the sulphur atoms on the diarylethene ligands (**Figure 6.19**).



$P2_12_12_1$

$a = 7.100(0) \text{ \AA}$

$b = 24.677(0) \text{ \AA} \quad Z = 4$

$c = 24.283(4) \text{ \AA}$

$V = 5130.6(5) \text{ \AA}^3$

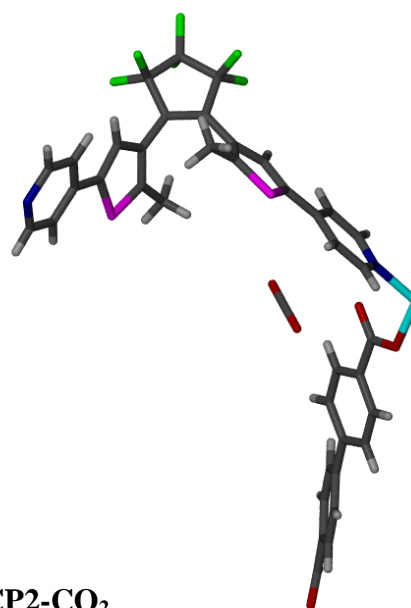


Figure 6.18 Crystallographic information and ASU of **PCCP2-CO₂**

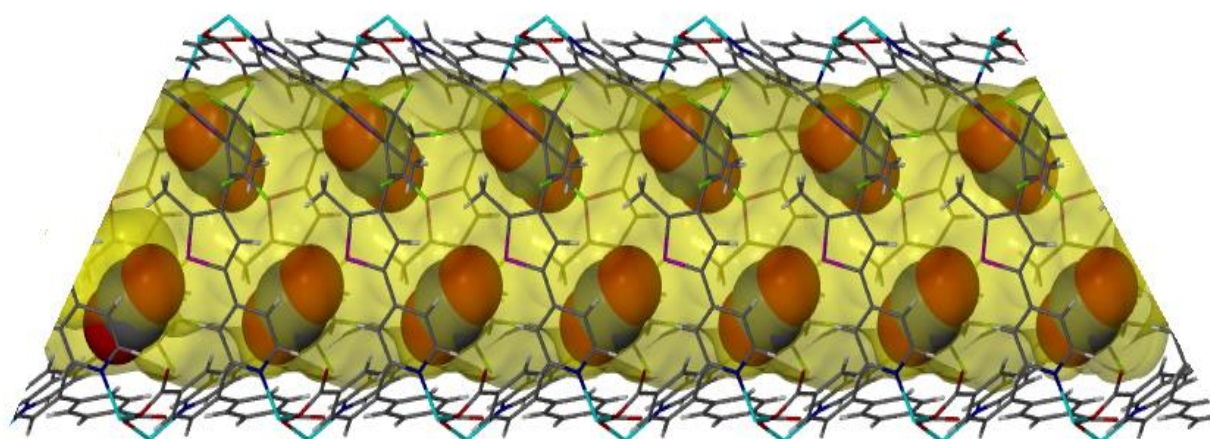


Figure 6.19 CO₂ molecules located in the corrugated guest accessible contact surface channels of **PCCP2-CO₂** viewed along a .

CHAPTER VI: PHOTOCROMIC COMPOUNDS

IR spectra were recorded to further verify the presence of carbon dioxide. A comparison of the apohost and the sample exposed to supercritical carbon dioxide highlights the presence of a distinct peak at 2340 cm^{-1} (**Figure 6.20**). This is consistent with the literature value for an asymmetric carbon dioxide stretch.¹⁶ Furthermore, other variations in the region associated with the host material ($500 - 1500\text{ cm}^{-1}$) indicate possible interactions between the guest molecules and the host framework.

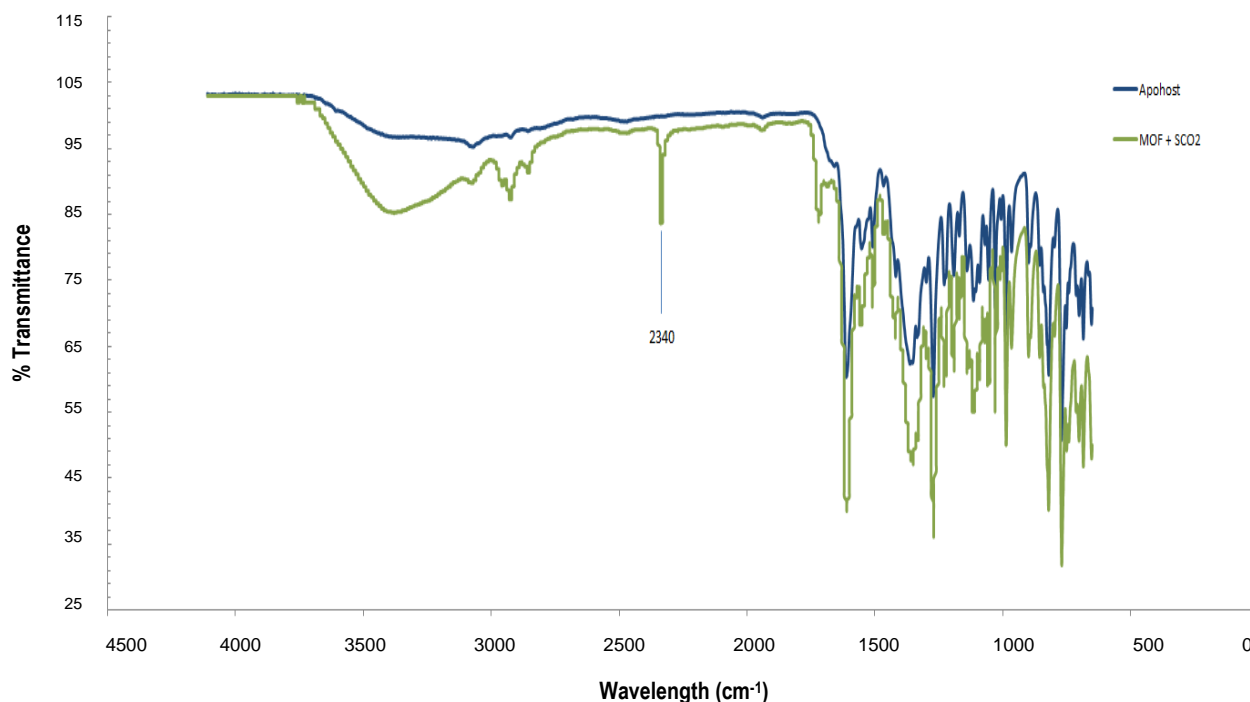


Figure 6.20 Overlaid IR spectra of PCCP_2' and PCCP2-CO₂.

6.3.2.3 PCCP_2 Irradiation Experiments

As observed with PCCP_1, exposure of PCCP_2 crystals to ultraviolet light (365 nm) induced a colour change (**Figure 6.21**). Initially colourless crystals transformed to dark blue. Unlike PCCP_1, PCCP_2 displayed no visible change in shape. This process is reversible and shows excellent fatigue resistance (the colour change could be induced ≥ 100 cycles).



Figure 6.21 Photographic evidence of a **PCCP_2** crystal undergoing a reversible colour change when exposed to visible and ultraviolet light

6.3.2.4 PCCP_2 Solid-state UV-visible spectroscopy

A UV-visible spectrum of the apohost of **PCCP_2** was recorded. The same sample was then irradiated for one minute and the spectrum rerecorded. **Figure 6.22** shows that the original form contains two bands, one at 353 nm and one at 425 nm. These bands are once again attributed to π - π^* transitions in the ligand and metal-to-ligand charge transfer of the divalent zinc to the π^* orbital of the bridging ligand. An examination of the irradiated spectrum shows a broad peak maximizing at 614 nm. In **Figure 6.22** the absorption maximum is in the orange region of the spectrum and thus the transmitted colour is blue.

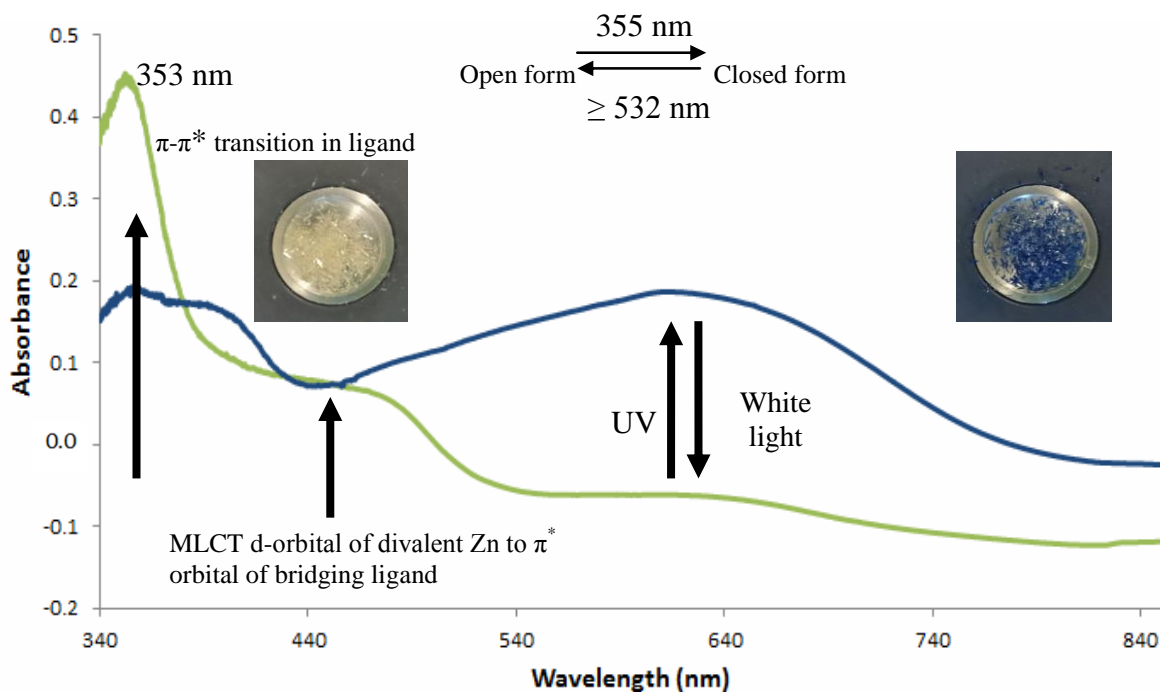


Figure 6.22 Solid-state UV-visible spectra of **PCCP_2**, which had been exposed to white and ultraviolet light.

CHAPTER VI: PHOTOCROMIC COMPOUNDS

During the course of this study Guo *et al.*¹⁷ published a communication wherein they presented **PCCP_2** as a structure labelled **DMOF**. They described this framework as the first example of a diarylethene containing MOF, wherein the entire ligand was able to undergo photochromic switching. The authors presented single-crystal data of the open form, thermogravimetric analysis and solid-state UV spectra which showed a reversible colour change that was ascribed to the structural transformation of the **DL1** ligand from the open-to the ring-closed conformation. The study was completed with low pressure CO₂ sorption experiments (0 - 1 bar, erroneously reported as $P/P_o = 0 - 1$ at 25 °C) of the non-irradiated and irradiated forms showing a marked difference in the uptake and release capabilities of the material (5.0 cm³g⁻¹ for white light and 20.1 cm³g⁻¹ under UV).

Figure 6.21 shows that irradiation did not diminish the quality of the crystals and SC-SC transformation experiments were thus undertaken in an attempt to verify the hypothesis proposed by Guo *et al.*¹⁷ Despite the vivid colour change and numerous data collections with varying degrees of exposure to UV irradiation, **PCCP_2** did not exhibit any discernible unit cell change, structural change or electron density peaks in the area believed to be undergoing ring closure. Furthermore, the distance between the two carbons involved in ring closure (**Figure 6.11**) remains 3.68 Å regardless of guest or colour change. It is believed that, although a partial conversion from the open to closed form is occurring at the crystal surface (hence the colour change), the extent of this conversion is so minor (the framework is not dynamic enough) that the average bulk structure remains unchanged. An examination of the UV spectra under varying degrees of exposure to UV irradiation (**Figure 6.23**) revealed that the band associated with π - π^* and MLCT transitions at 375 nm increased while the band attributed to ring closure at 625 nm decreased with extended exposure. Thus, **PCCP_2** seems to undergo a minor conversion to the ring closed form upon initial exposure to UV irradiation, however as the exposure continues, no more material is converted to the closed form. In fact, a cycloreversion reaction is believed to be occurring (heat generated by extended UV irradiation causes the rings to reopen).

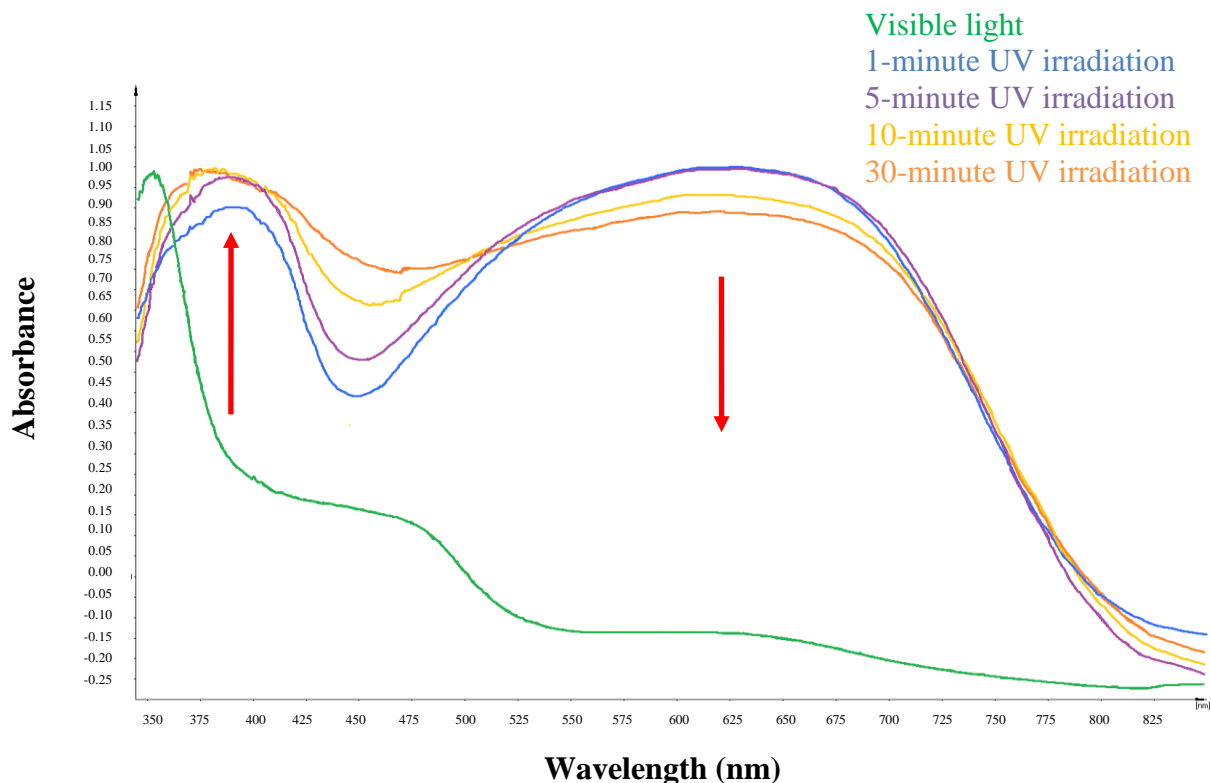


Figure 6.23 Solid-state UV-visible spectra of PCCP_2 recorded post irradiation exposure.

In an attempt to establish at what point the material displayed its highest turnover, powder patterns of the irradiated sample were collected over a period of three days.

5.3.2.5 PCCP_2 Variable time Irradiation PXRD

In order to perform variable irradiation experiments (sample was exposed to one wavelength for varying periods of time), the beam knife was removed from the powder diffractometer and in its place, a light source (365 nm) was attached (**Figure 6.24**). The sample remained under continuous irradiation with powder patterns collected at specific time intervals.

CHAPTER VI: PHOTOCROMIC COMPOUNDS

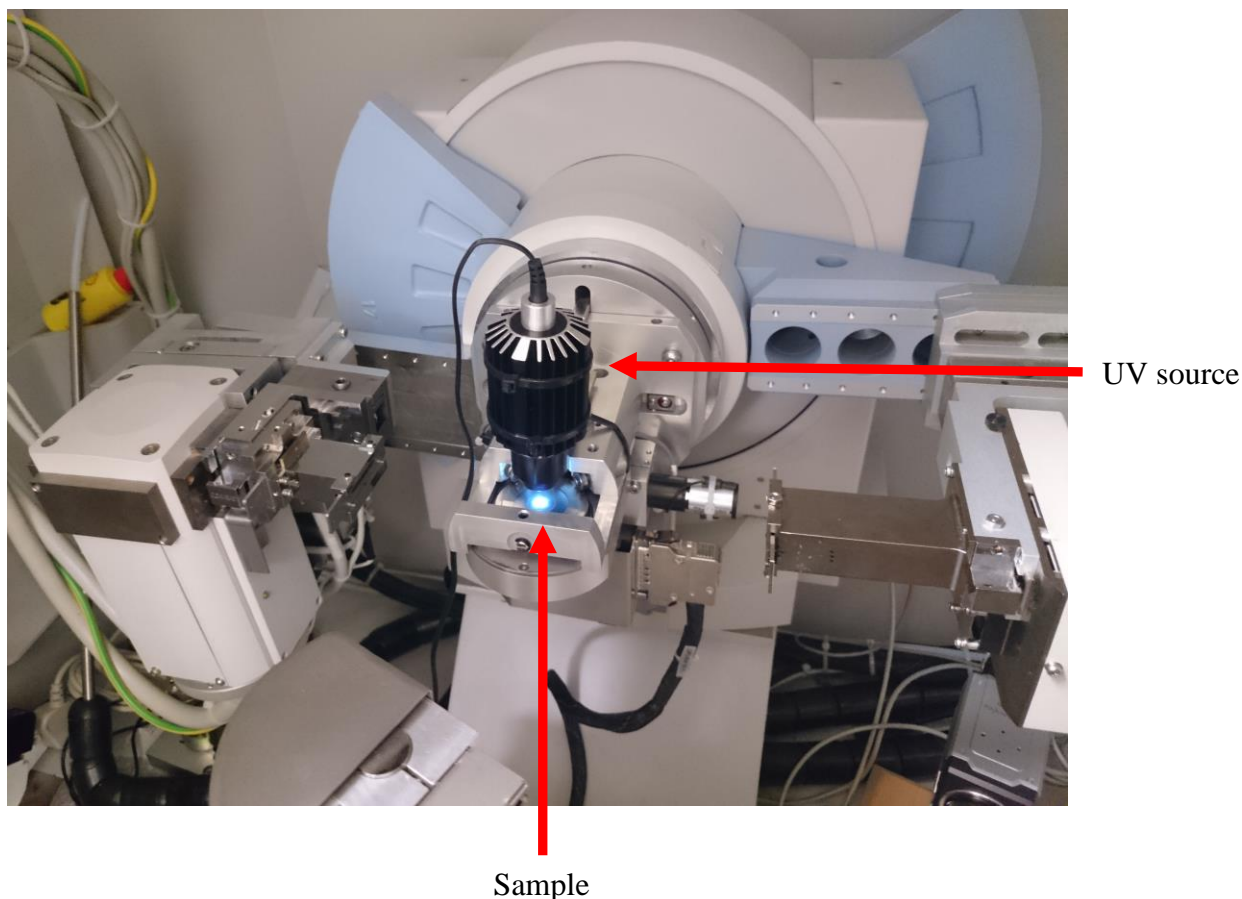


Figure 6.24 Photograph showing instrument setup for recording PXRD data for a sample under continuous UV irradiation.

Figure 6.25 shows stacked PXRD patterns for **PCCP_2** recorded at varying intervals of exposure. The initially colourless sample undergoes an immediate colour change but little to no pattern change with continued exposure to UV light (a structural change such as ring closure would be clearly observed in the PXRD). After approximately 30 hours of exposure, the PXRD pattern sharpens, indicating that the material may have undergone a cycloreversion, with the PXRD pattern now beginning to resemble the original non-irradiated powder pattern. Further irradiation causes the material to once again undergo changes. An examination of the material after the experiment indicated the blue sample had become light brown. It is believed that when initially exposed to UV-light **PCCP_2** undergoes a low percentage conversion to the ring-closed form and, due to the intense colour of this form, it is observed as a very distinct colour change. Further irradiation does not promote greater conversion; in fact, it is believed that the heat generated from prolonged irradiation has the opposite effect with whatever small amount already converted to the closed form beginning to reopen.

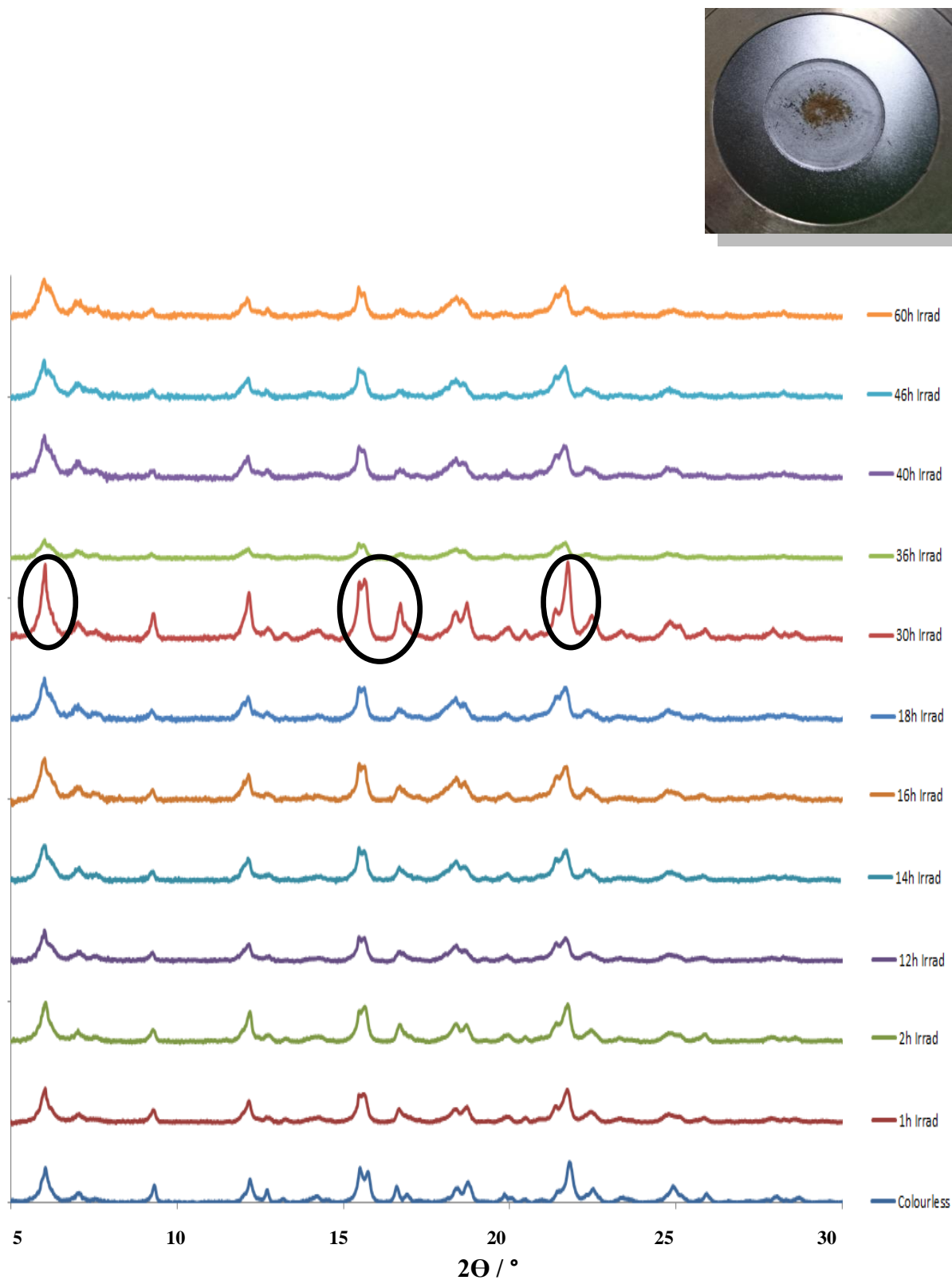


Figure 6.25 Stacked PXRD patterns of **PCCP_2** exposed to variable degrees of UV irradiation.

5.3.2.6 Gravimetric gas sorption by PCCP_2 using CO₂

Unable to attain solid-state (single-crystal or PXRD) evidence that **PCCP_2** is indeed undergoing complete ring closure, extended versions of the sorption experiments reported by Guo *et al.*¹⁷ were attempted in the hope of gaining further insight. **PCCP_2** shows conventional Type I sorption behaviour (no hysteresis), absorbing approximately one and a half molecules of CO₂ (7.4 wt %) per ASU (**Figure 6.26**). At 20 bar, full occupancy was not attained and, as a result, **PCCP_2** could potentially accommodate more guest molecules. A comparison of this isotherm to that published indicated a good correlation; however, it is important to note that at 1 bar, the occupancy reported ($5.0 \text{ cm}^3 \text{ g}^{-1}$) is equivalent to 0.15 molecules per ASU (within standard deviation). Owing to the fact that the IGA sample chamber is constructed from steel, continuous UV irradiation could not be performed. Thus the activated form of **PCCP_2** was irradiated for an hour and then loaded in the dark. The isotherm recorded for the irradiated form showed negligible uptake and release of the guest by the **PCCP_2** host.

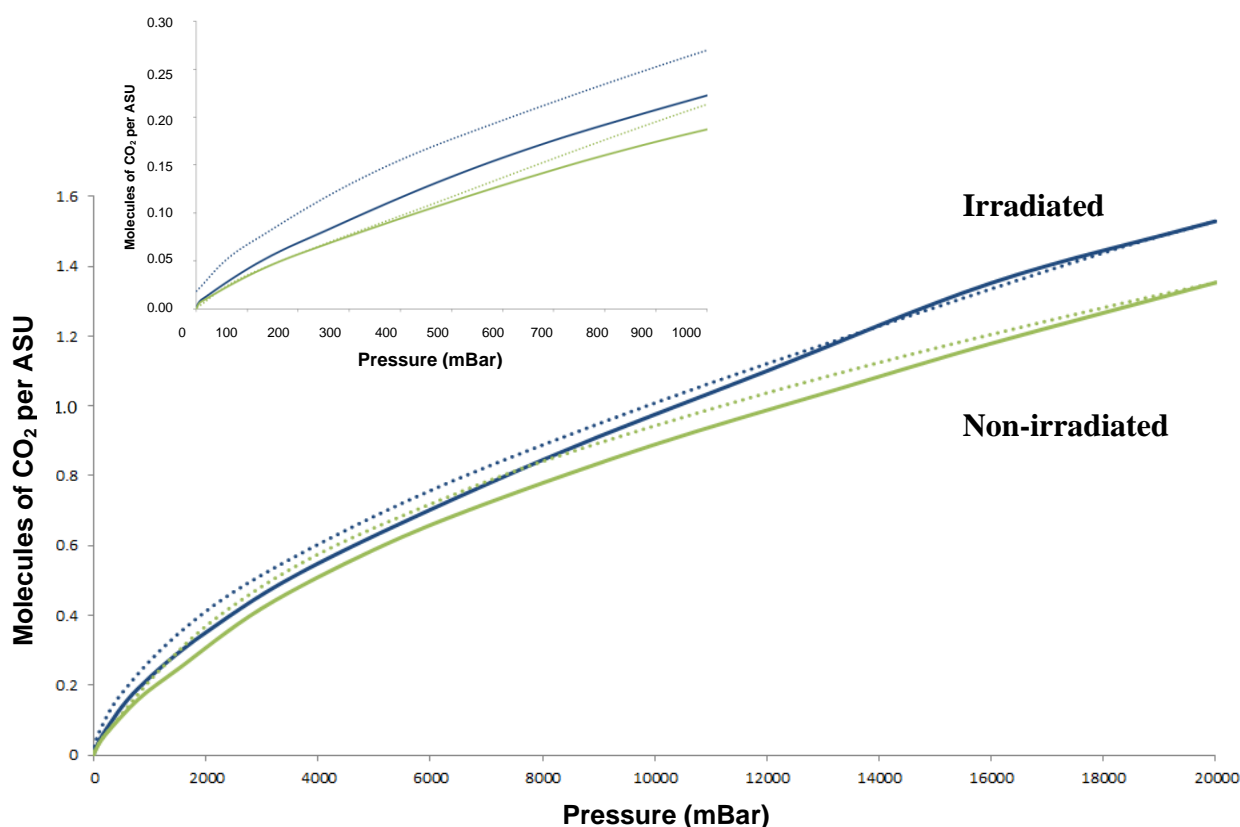


Figure 6.26 CO₂ sorption and desorption isotherms at 25 °C for the non-irradiated and irradiated forms of **PCCP_2**. Solid lines represent sorption while dashed lines represent desorption.

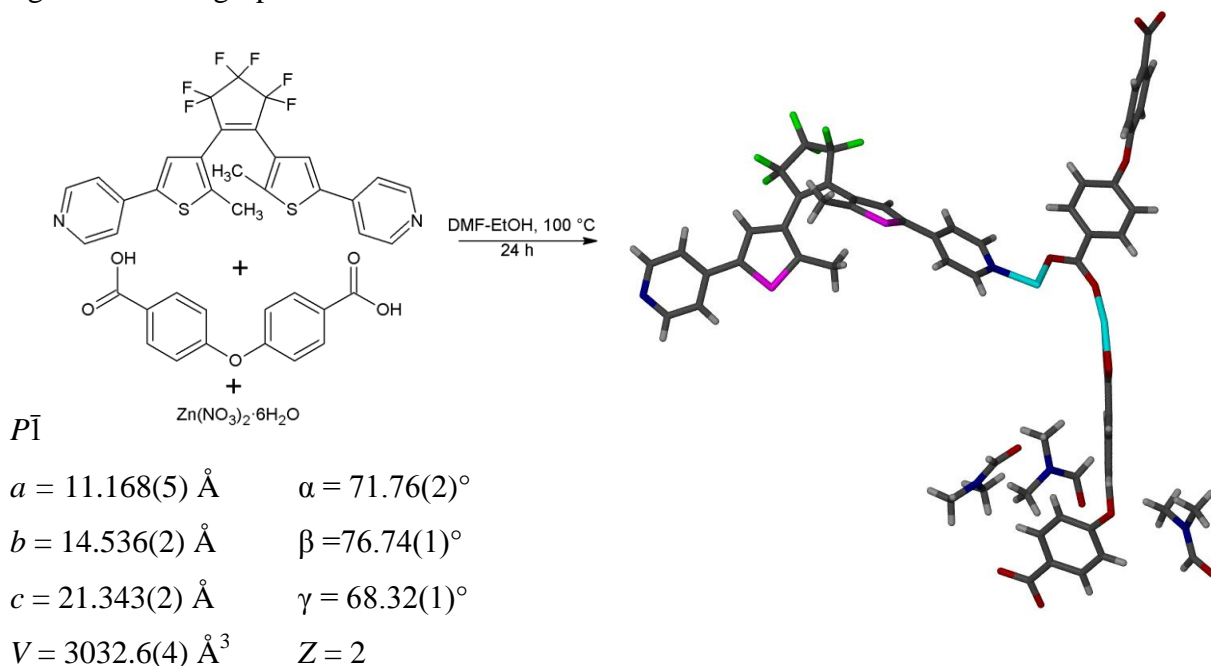
CHAPTER VI: PHOTOCROMIC COMPOUNDS

The results published by Guo *et al.*¹⁷ could not be reproduced. It is believed that although **PCCP_2*** does undergo some ring closure (hence the distinct colour change), it is incapable of undergoing high turnover ring closure in the solid state. An extension of the sorption study indicated no change in uptake capabilities between the two forms with the framework exhibiting insufficient uptake in the 0-1 bar range for definitive conclusions to be drawn.

Having observed some success with a short linker (**PCCP_1**) compared to that of the long rigid linker in **PCCP_2**, crystallisations involving the previously utilised flexible **OBA** ligand were attempted in the hope that this would impart a greater degree of dynamism to the MOFs formed and thus promote ring closure.

6.3.3 {[Zn₂(DL1)OBA₂]**3**DMF}_n or **PCCP_3**

PCCP_3 was formed by the reaction of **DL1**, **OBA** and Zn(II) nitrate hexahydrate under solvothermal conditions (100 °C, DMF-EtOH) (**Scheme 6.3**). **PCCP_3** crystallises in the triclinic space group $P\bar{1}$. The ASU consists of two zinc cations, two **OBA** ligands, one **DL1** ligand in the ring-open conformation and three DMF molecules.



Scheme 6.3 Synthesis of **PCCP_3** from the solvothermal reaction of **DL1**, **OBA** and zinc nitrate in a DMF-EtOH mixture at 100 °C with selected crystallographic information.

* Repetition of the crystallisation process substituting the **DL1** ligand with the **DL2** ligand induces the formation of an isostructural MOF. This material behaves in a manner very similar to that of **PCCP-2** and is thus not included in this discussion.

CHAPTER VI: PHOTOCROMIC COMPOUNDS

As with previous examples* of MOFs involving zinc and the **OBA** ligand, **PCCP_3** contains a distorted version of the half “paddlewheel” dinuclear zinc carboxylate unit $[\text{Zn}_2(\text{COO})_4]$ (**Figure 6.27a**). The dinuclear zinc centres are bridged by **OBA** ligands to form a 2D grid. The 2D nets stack on top of one another and are further linked into a 3D network by bridging **DL1** ligands (**Figure 6.27b**). The reactive carbon-carbon atom distance is 3.88 Å. The structure is twofold interpenetrated and contains channels along $[0\ 1\ 0]$, which are occupied by DMF molecules (**Figure 6.27c**).

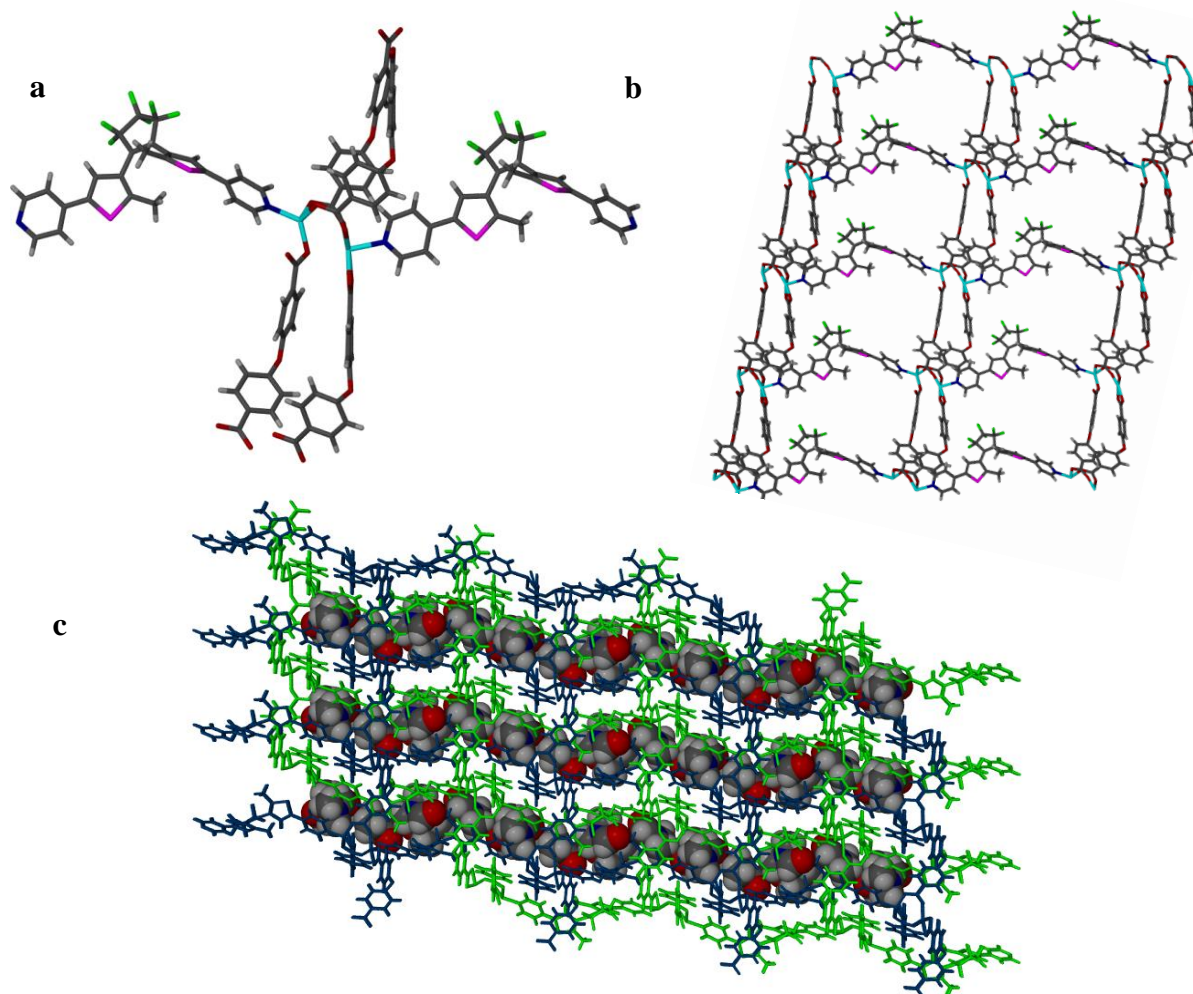


Figure 6.27 a) Half paddlewheel moiety in **PCCP_3**. b) Single net showing staggered extended structure. c) Solvent filled channels viewed along $[0\ 1\ 0]$.

All DMF molecules were modelled at full occupancy. TGA analysis (**Figure 6.28**) indicates a 16% mass loss occurring in the temperature range 0 - 125 °C, which corresponds to the SC model and SQUEEZE data as three DMF molecules per formula unit. Decomposition of the framework commences at 375 °C.

* **CP1** (pg 44), **CP5** (pg 56) and **HC1** (pg 84).

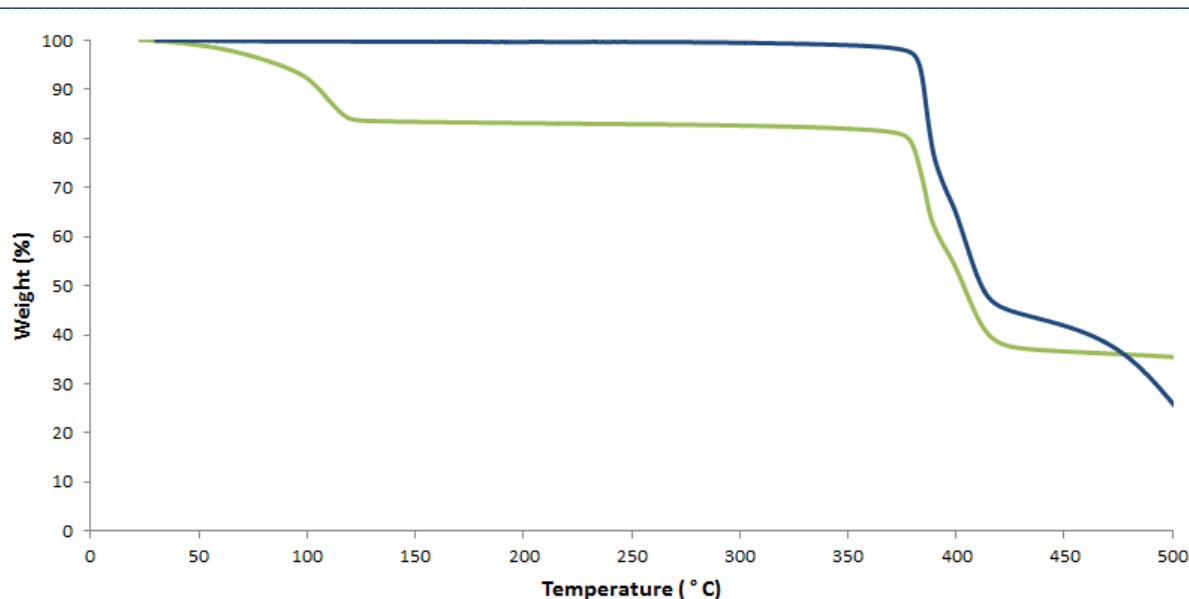


Figure 6.28 TGA of the as-synthesised as well as the evacuated phases of **PCCP_3** (green and blue lines respectively).

Although twofold interpenetrated (thus a higher degree of stability), and with the TGA data showing complete solvent removal at comparatively low temperatures, neither solvent exchange nor the use of supercritical CO₂ could retain **PCCP_3** crystal singularity. Gradual heating did enable the collection of data for the partially desolvated form **PCCP_3a**. This form contains one less DMF molecule than the original. An examination of the cell parameters (**Figure 6.29**) indicates that the material undergoes a structural adjustment upon loss of one of the guest molecules. Despite this, the reactive carbon-carbon atom distance remains 3.89 Å.

6.3.3.1 $\{[\text{Zn}_2(\text{DL1})\text{OBA}_2]\cdot 2\text{DMF}\}_n$ or **PCCP_3a**

$P\bar{1}$

$$a = 11.188(8) \text{ \AA} \quad \alpha = 82.17(1)^\circ$$

$$b = 14.544(6) \text{ \AA} \quad \beta = 76.30(4)^\circ$$

$$c = 21.369(5) \text{ \AA} \quad \gamma = 67.66(6)^\circ$$

$$V = 3024.6(5) \text{ \AA}^3 \quad Z = 2$$

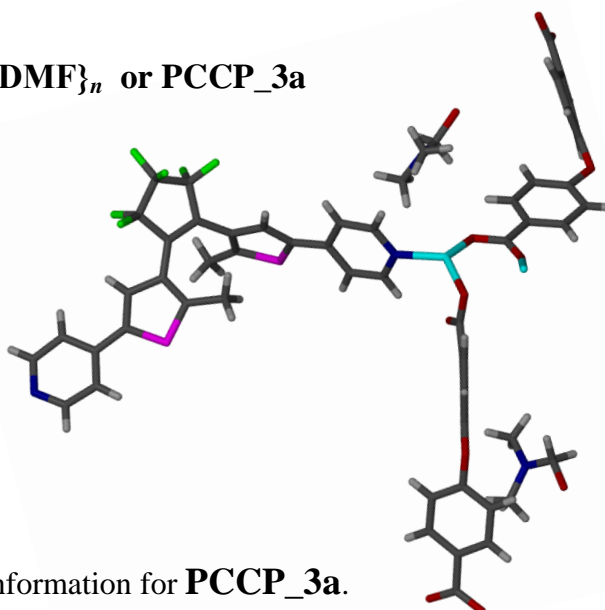


Figure 6.29 ASU and crystallographic information for **PCCP_3a**.

6.3.3.2 PCCP_3 Irradiation Experiments

Exposure of **PCCP_3** crystals to ultraviolet light (365 nm) induced the expected colour change (**Figure 6.30**). Initially colourless block shaped crystals were transformed to violet upon irradiation. This process is reversible and shows good fatigue resistance (the change in colour could be induced ≥ 50 cycles). The distance between the two carbon atoms involved in ring closure is 3.88 Å.

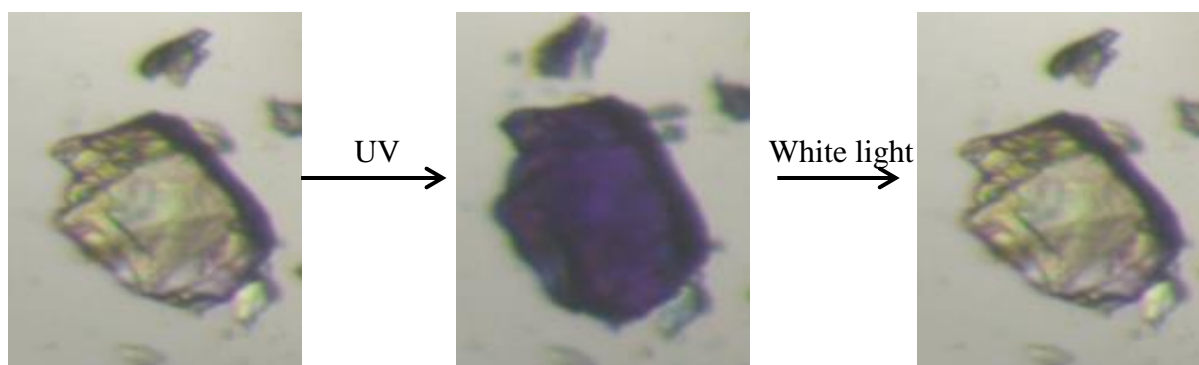


Figure 6.30 Photographs of **PCCP_3** crystals showing a reversible colour change (colourless to violet) when exposed to visible and ultraviolet light.

6.3.3.3 PCCP_3 Solid state UV-visible spectroscopy

A UV-visible spectrum of the original solvate of **PCCP_3** was recorded. The same sample was then irradiated for one minute and the spectrum rerecorded. **Figure 6.31** shows the original form exhibiting two bands, one at 350 and one at 465 nm. These bands are also attributed to π - π^* transitions in the ligand and metal-to-ligand charge transfer of the divalent zinc to the π^* orbital of the bridging ligand, respectively. Examination of the spectrum of the irradiated sample shows a very broad peak. This peak is in the “red” region of the visible spectrum and is associated with the purple-blue colour observed.

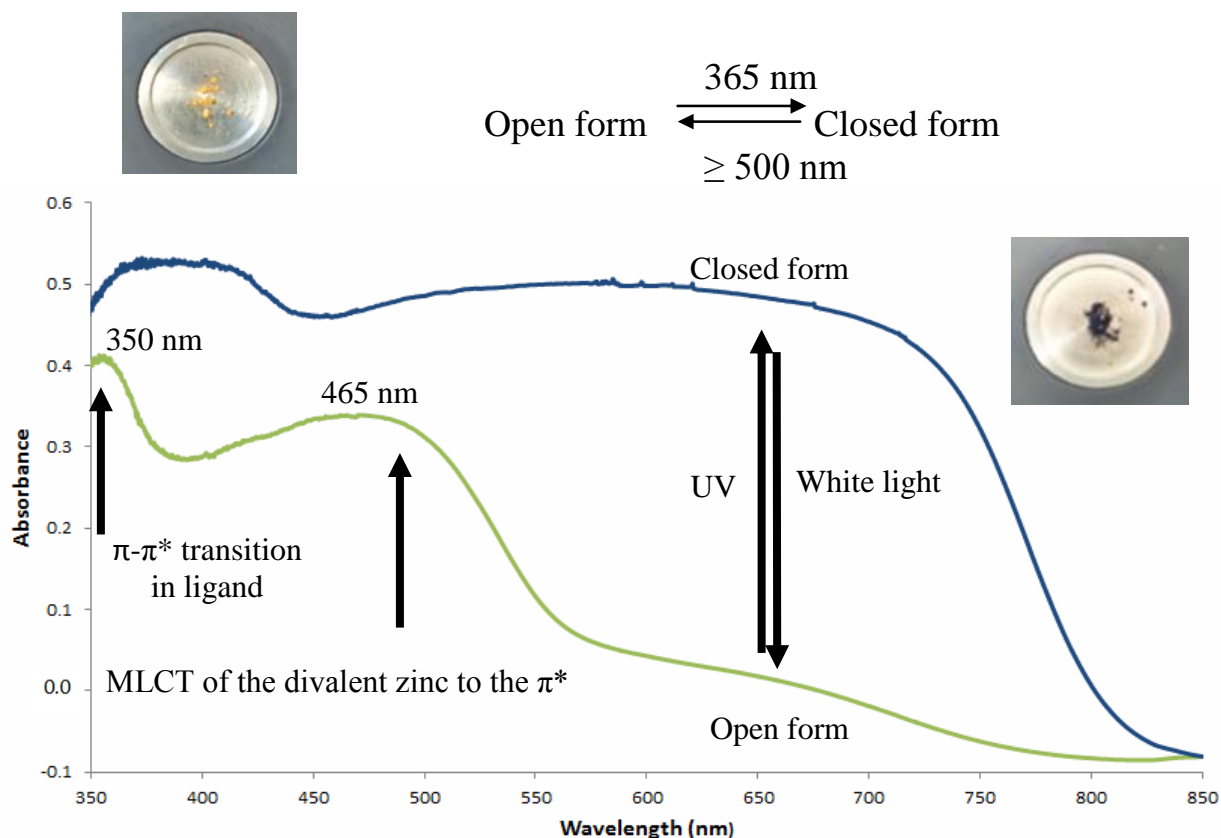
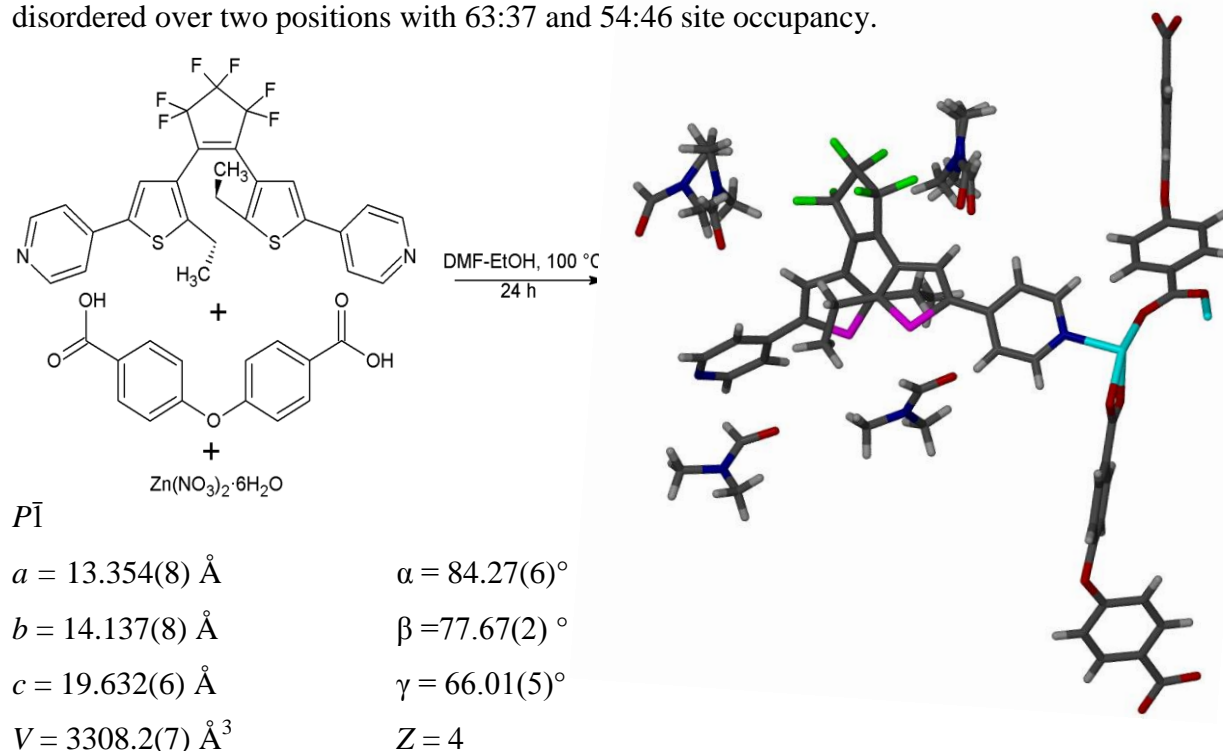


Figure 6.31 Solid-state UV-visible spectra of **PCCP_3**, which has been exposed to white and ultraviolet light with associated sample photographs.

Once again SC irradiation experiments were undertaken in the hope of observing ring closure in the solid state. Although yet another vivid colour change was observed, numerous data collections with varying degrees of UV exposure induced no discernible parameter change and no crystallographic evidence of ring closure. Furthermore, the distance between the two carbon atoms involved in ring closure remains 3.84 Å. This implies that, although a partial conversion from the open to closed form occurs (hence the colour change), the extent of this conversion is so minor (the framework is not dynamic enough) that the overall structure remains unchanged. Unfortunately, experiments to produce the activated form of **PCCP_3** were unsuccessful as crystals lose singularity upon desolvation.

6.3.4 $\{[\text{Zn}_2(\text{DL2})\text{OBA}_2]\cdot 4\text{DMF}\}_n$ or PCCP_4

PCCP_4 forms when DL2, OBA and Zn(II) nitrate hexahydrate are combined under solvothermal conditions (100 °C, DMF-EtOH) (Scheme 6.4). PCCP_4 crystallises in the triclinic space group $P\bar{1}$ with the ASU consisting of two zinc cations, two OBA ligands, one DL2 ligand in the ring-open conformation and four DMF molecules, two of which are disordered over two positions with 63:37 and 54:46 site occupancy.



Scheme 6.4 Synthesis of PCCP_4 from the solvothermal reaction of DL2, OBA and zinc nitrate in a DMF-EtOH mixture at 100 °C with selected crystallographic information.

MOF PCCP_4 is very similar to its methyl counterpart PCCP_3. PCCP_4 also contains a distorted version of the half paddlewheel SBU (Figure 6.32a). One of the pyridyl ligands is twisted such that it is perpendicular to the second. A notable difference between the two structures is the distance separating the two oxygen atoms of adjacent OBA ligands in PCCP_4, which is 4.37 Å. Unlike in PCCP_3, within a single net of PCCP_4 the ethyl substitutes of DL2 are eclipsed rather than staggered (Figure 6.32b). The reactive carbon-carbon distance is 3.73 Å. The structure is twofold interpenetrated and contains channels along $[0\ 1\ 1]$, which are occupied by DMF molecules (Figure 6.32c).

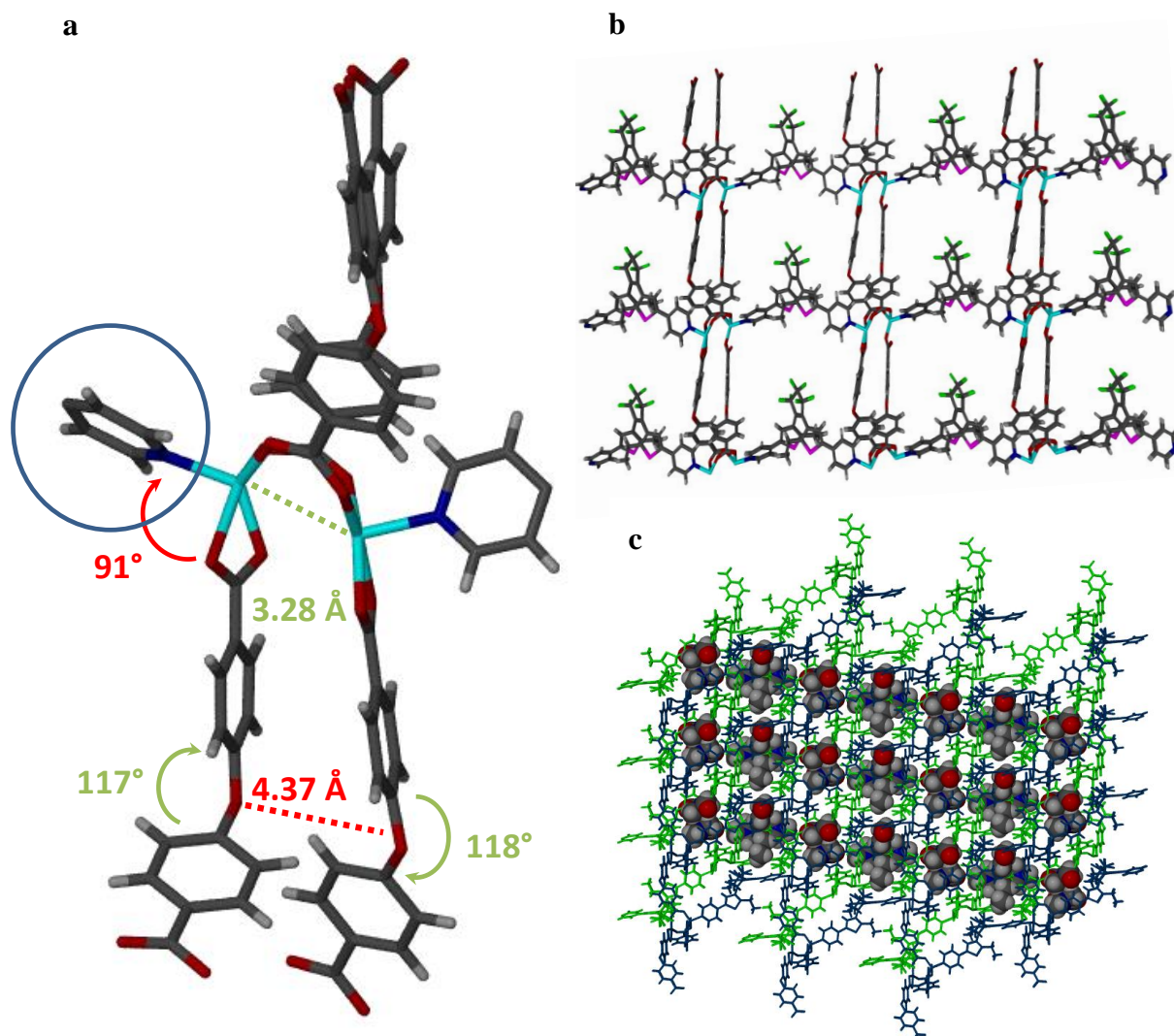


Figure 6.32 a) Simplified PCCP_4 half paddlewheel moiety. b) Single net showing eclipsed extended structure. c) Solvent filled channels viewed along [0 1 0].

Unfortunately, no TGA could be carried out due to an insufficient amount of sample (crystals are very difficult to grow)*. In spite of this, the apohost form (PCCP_4') may be generated by prolonged exposure of the solvate to vacuum at room temperature or to a solution of supercritical CO₂ for 24 h. Although the crystals experienced a certain amount of visible deterioration and striation, the framework is sufficiently robust that activation occurs as a SC-SC transformation. The activated structure exhibits a dramatic change in the cell parameters (Figure 6.33).

* It should be noted, for all the MOFs discussed in this chapter, crystallisations of the closed form (irradiation while crystallising) were attempted but in spite of colour changes, no structures of the closed forms were obtained. This is not surprising, as DL1 and DL2 are believed to obey a P-type mechanism.

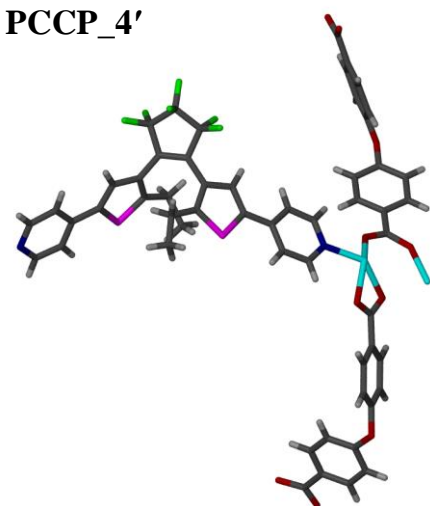
<p>6.3.4.1</p> <p>$P\bar{1}$</p> <p>$a = 13.197(7) \text{ \AA}$</p> <p>$b = 13.606(2) \text{ \AA}$</p> <p>$c = 16.997(2) \text{ \AA}$</p> <p>$V = 2793.2(5) \text{ \AA}^3$</p>	<p>$\{\{\text{Zn}_2(\text{DL2})\text{OBA}_2\}\}_n$ or PCCP_4'</p> <p>$\alpha = 89.87(3)^\circ$</p> <p>$\beta = 89.48(2)^\circ$</p> <p>$\gamma = 66.23(4)^\circ$</p> <p>$Z = 4$</p>	
----------------------------------------------------------------------------------------------------------------------------------------------------------------------------------------------------------------------------------------------	--------------------------------------------------------------------------------------------------------------------------------------------------------------------------------------------------------------------------------------------------	------------------------------------------------------------------------------------

Figure 6.33 Crystallographic information for **PCCP_4'**.*

The reason for the notable change in cell parameters becomes apparent upon examination of the half paddlewheel. **Figure 6.34a** shows the change in the orientation of the **OBA** and pyridyl ligands. Unlike the solvate, the two pyridyl rings in **PCCP_4'** are twisted to the same extent with the distance separating the central oxygen atoms of adjacent **OBA** ligands increasing to 6.07 \AA . Extension of the structure shows the effect this alteration has on the pore size as one net of **PCCP_4'** (**Figure 6.34b**) shows a dramatically reduced pore size. Guest removal induces a concertina effect, resulting in pore contraction.

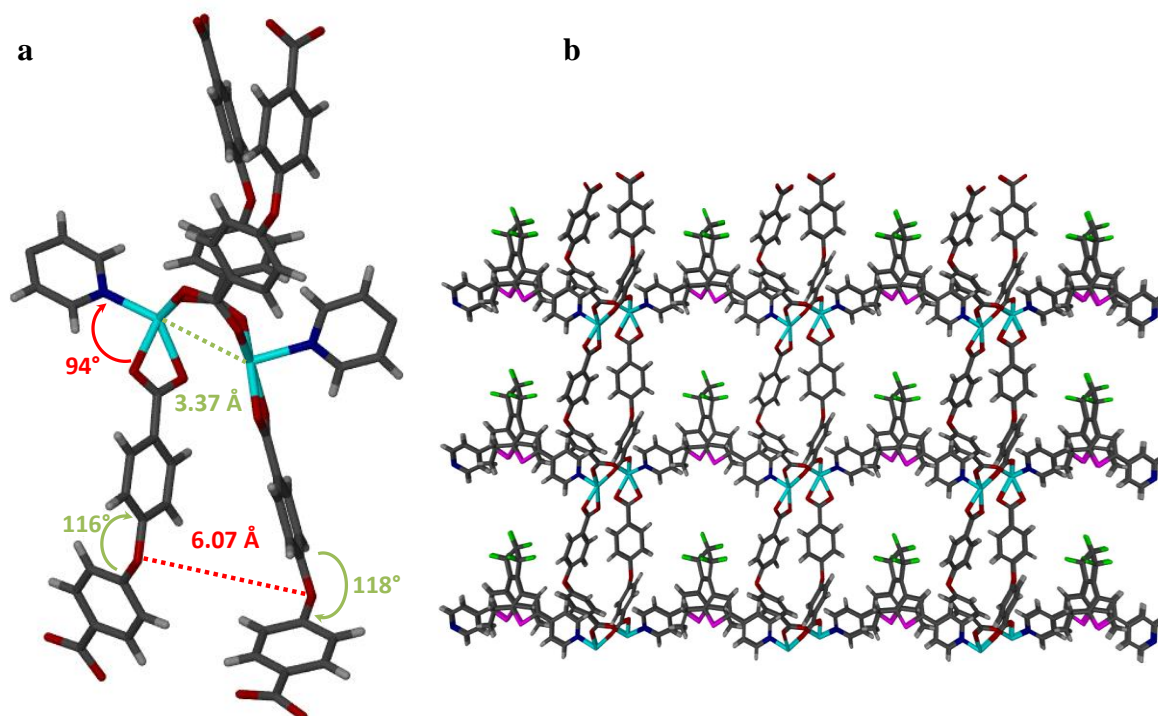


Figure 6.34 a) Half paddlewheel moiety of **PCCP_4'**. b) Single net showing extended structure.

* Structure obtained by exposing crystals to supercritical CO_2 .

CHAPTER VI: PHOTOCROMIC COMPOUNDS

Interestingly the carbon-carbon distance associated with ring closure contracts to 3.46 Å. It was hypothesised that irradiation of this form may yield the closed form structure. Despite the lack of TGA data, SQUEEZE analysis indicated only 23 electrons present in the ASU. This is attributed to one diffuse CO₂ molecule per ASU and, as a result, the structure is considered highly activated. The structure contains 14 Å³ of solvent accessible space per unit cell (using a probe radius of 1.4 Å), which is a staggering 90% reduction from the original PCCP_4 form.

6.3.4.2 Irradiation Experiments

Due to the motion experienced by both the DL2 and OBA ligands upon guest removal and the proximity of the two active carbon atoms, irradiation experiments were performed. Similar to the previous examples, exposure of PCCP_4' crystals to ultraviolet light (365 nm) induced a colour change (Figure 6.35). Initially bright yellow-orange crystals were transformed green. The difference in colour observed between PCCP_1, PCCP_2, PCCP_3 and PCCP_4' is related to electronic interactions between the various components in each ensemble. This process is reversible (upon exposure to white light) and shows good fatigue resistance (the colour change could be induced ≥ 50 cycles).

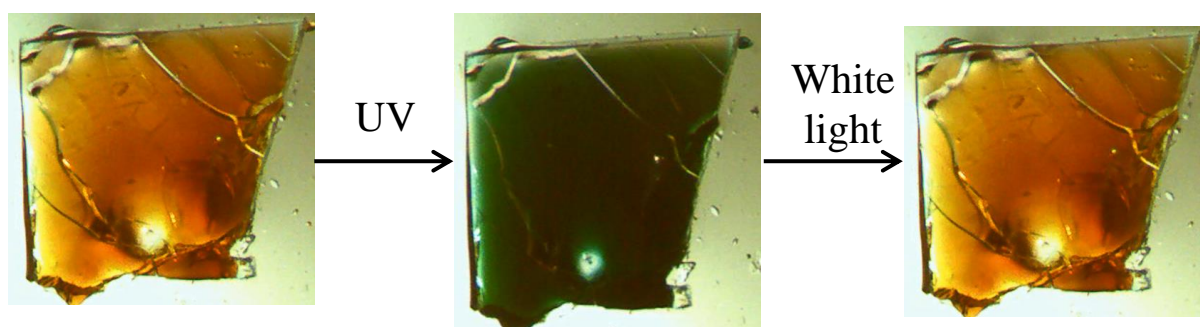


Figure 6.35 Photographic evidence of PCCP_4 crystals showing a reversible colour change (yellow-orange to green) when exposed to visible and ultraviolet light.

6.3.4.3 PCCP_4 Solid state UV-visible spectroscopy

A UV-visible spectrum of the original apohost of **PCCP_4'** was recorded. The same sample was then irradiated for one minute and the spectrum rerecorded. **Figure 6.36** shows that the original form contains two bands, one at 360 and one at 465 nm. An examination of the spectrum of the irradiated sample shows a broad band, which is attributed to the green colour observed.

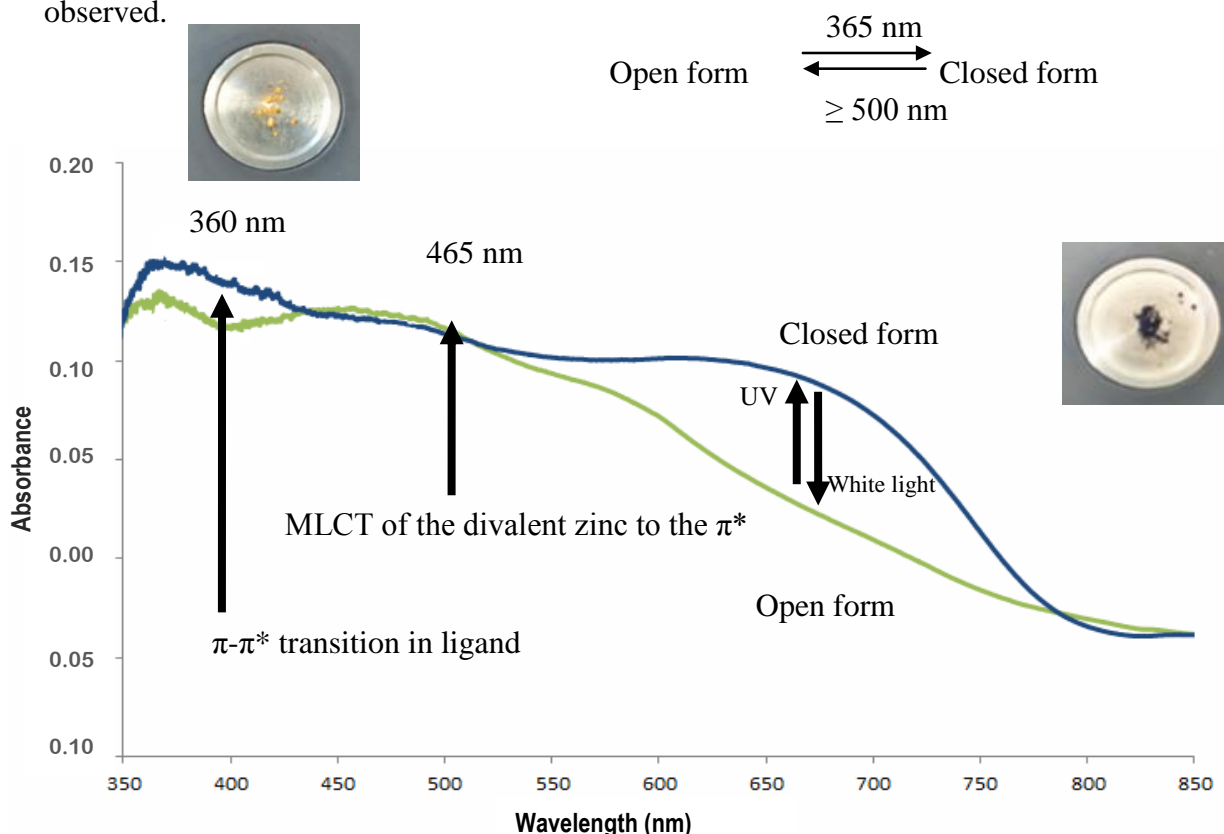


Figure 6.36 Solid-state UV-visible spectra of **PCCP_4'** during white and ultraviolet light.

In order to determine the extent of conversion in the solid state, a SC-SC transformation experiment was carried out. A crystal of **PCCP_4'** was glued to the tip of a glass fibre and irradiated for one hour under 365 nm ultraviolet light. Diffraction data were then recorded for this crystal under constant UV irradiation at room temperature (**Figure 6.4a**). **PCCP_4'-Irrad** (**Figure 6.37**) has the same space group as **PCCP_4'** but exhibited a further reduction in cell parameters and, most importantly, the formation of the ring-closed system. **Figure 6.38a** shows the change in paddlewheel orientation with the distance separating the oxygen atoms of adjacent **OBA** ligands increasing to 6.43 Å. Not surprisingly, a reduction in unit cell parameters led to a further reduction in solvent accessible space (**Figure 6.38**). The structure can be considered to be nonporous.

CHAPTER VI: PHOTOCROMIC COMPOUNDS

The distance between the two carbon atoms involved in ring closure becomes 1.53 Å (a typical value for a C-C single bond). This is the first structurally verified example of light-induced ring closure incorporated into the backbone of a MOF.

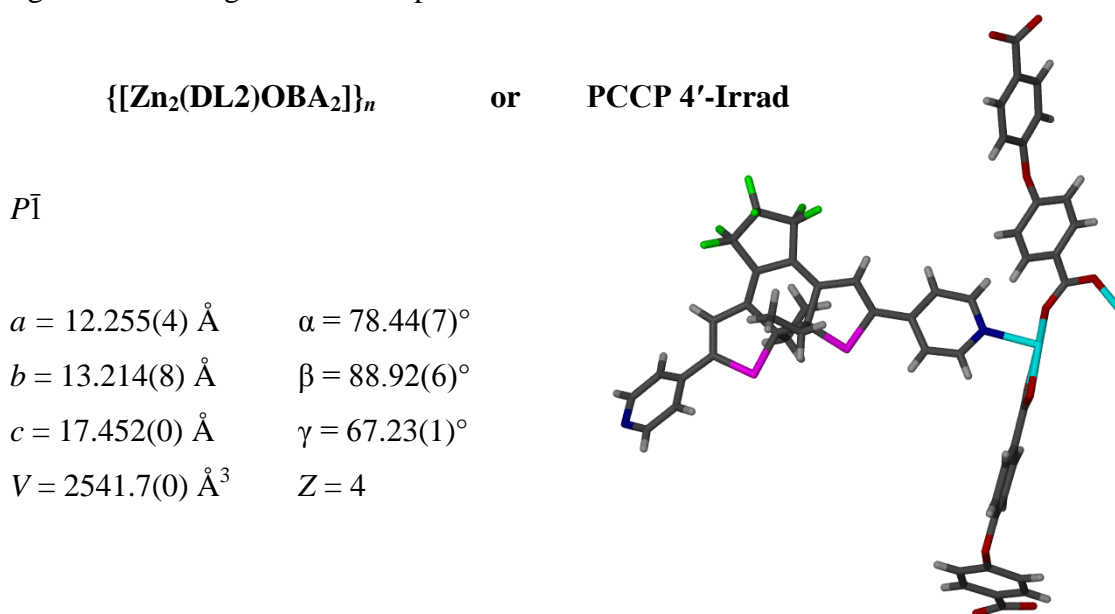


Figure 6.37 Crystallographic information for PCCP4'-Irrad.

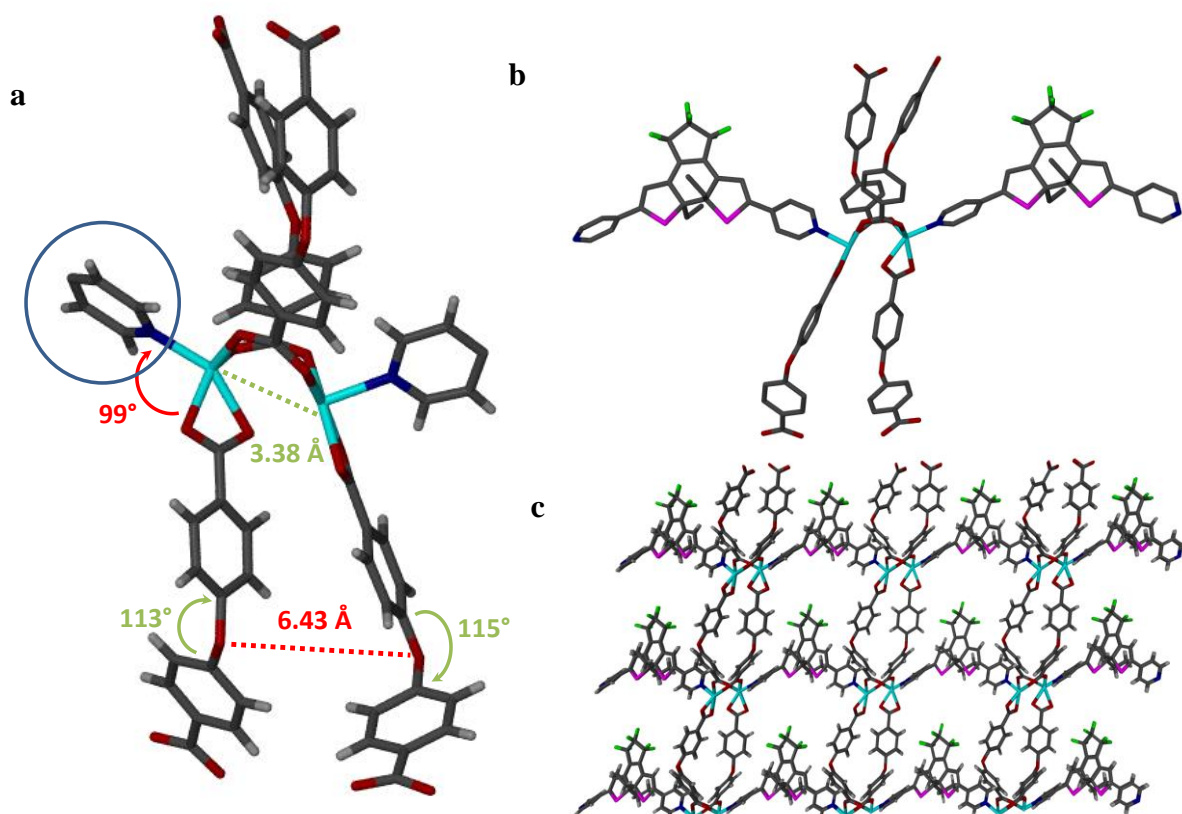


Figure 6.38 a) PCCP4'-Irrad simplified SBU showing ligand motion. b) Paddlewheel moiety with hydrogen atoms hidden in order to clearly show ring closure. c) Single net showing extended structure with further slanted and decreased pore size.

Figure 6.39 shows **PCCP_4** overlaid onto **PCCP4'-Irrad**. This provides the reader with a clear visual understanding of the profound transformations experienced by **PCCP_4** material.

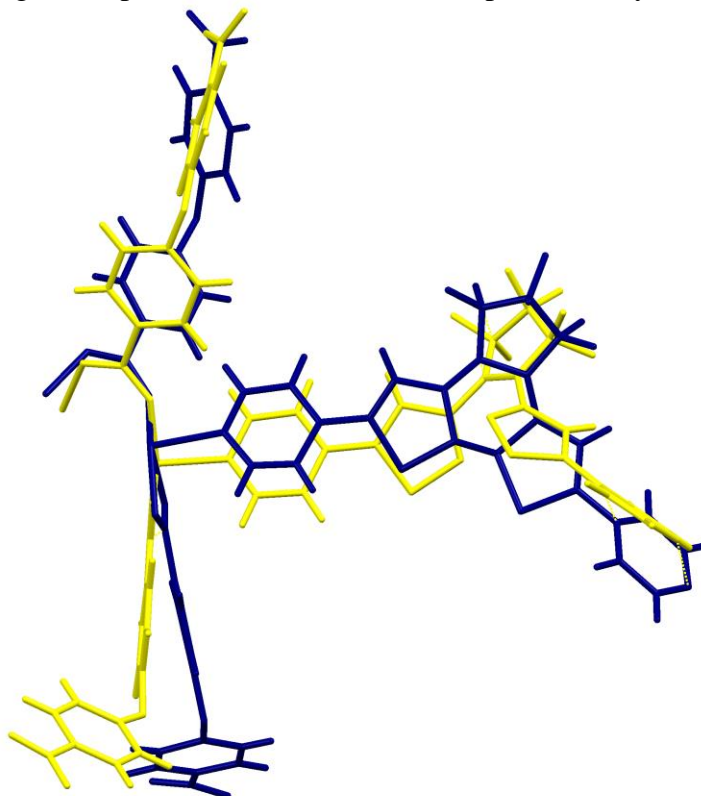


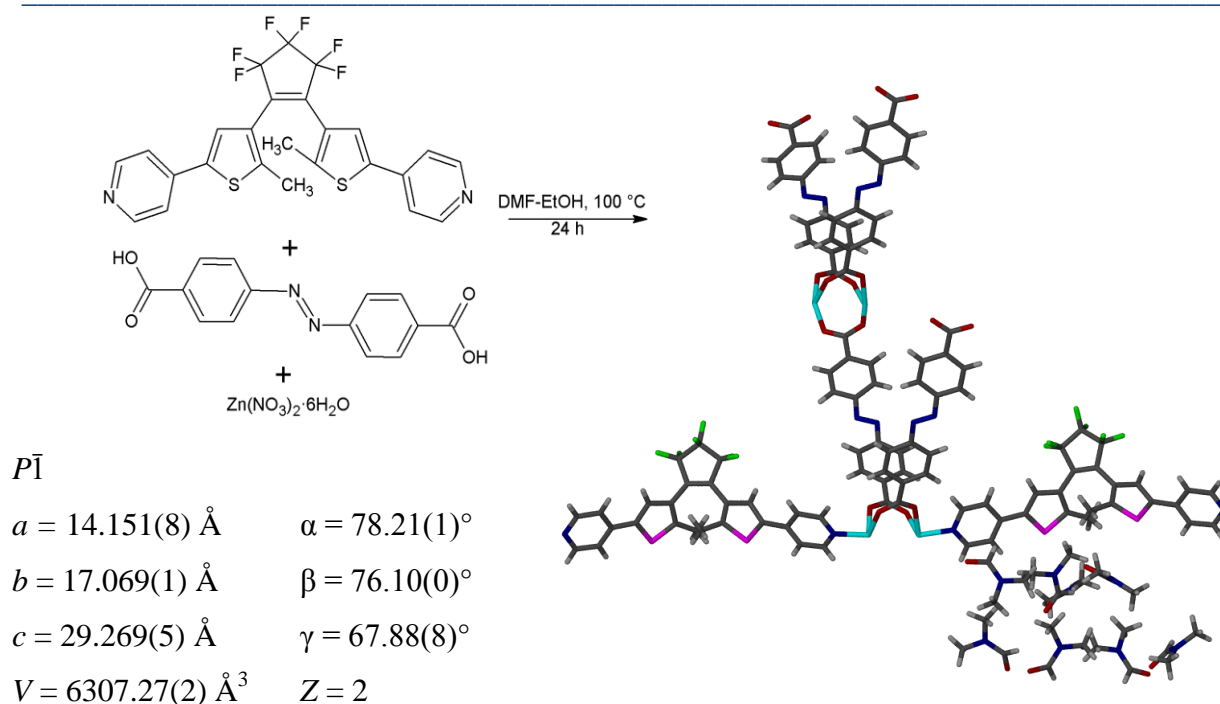
Figure 6.39 Least-squares overlay showing structural transformation of **PCCP_4** (yellow) to **PCCP4'-Irrad** (blue).

Having finally obtained a successful example of light-induced ring closure with **OBA**, an additional MOF was synthesised in an attempt to ascertain whether a carboxylic acid with independent photochromic properties (**AZDC**) could be substituted for **OBA** and whether ring-closure would still occur.

6.3.5 $\{[\text{Zn}_4(\text{DL1})_2\text{AZDC}_4]\cdot 2\text{DMF}\}_n$ or **PCCP_5**

Crystals of **PCCP_5** were grown from the solvothermal reaction of Zn(II) nitrate hexahydrate, **DL1** and **AZDC** at 100 °C (Scheme 6.5). **PCCP_5** crystallises in the triclinic space group $P\bar{1}$. The ASU consists of four zinc cations, two **DL1** ligands*, four **AZDC** ligands and two DMF molecules, each disordered over four positions.

* In one of the **DL1** ligands, the fluorine atoms and three associated para-position carbon atoms of the five-membered ring are disordered over two positions. This has been hidden for clarity.



Scheme 6.5 Synthesis of **PCCP_5** from the solvothermal reaction of **DL1**, **AZDC** and zinc nitrate in a DMF-EtOH mixture at 100 °C with selected crystallographic information.

PCCP_5 has a distorted paddlewheel moiety where two of the four acid groups are twisted (**Figure 6.40**) and the pyridyl rings of the **DL1** ligands align almost orthogonal to one another (one is planar and the other is twisted). The 2D nets stack directly on top of one another and are linked into 3D nets by bridging **DL1** ligands (**Figure 6.41a**). There are two **DL1** ligands present in the ASU; both are in the ring open conformation with C-C atom distances of 3.48 and 3.54 Å. In spite of fourfold interpenetration, the structure possesses channels along the *a* axis that are occupied by the DMF molecules (**Figure 6.41b**).

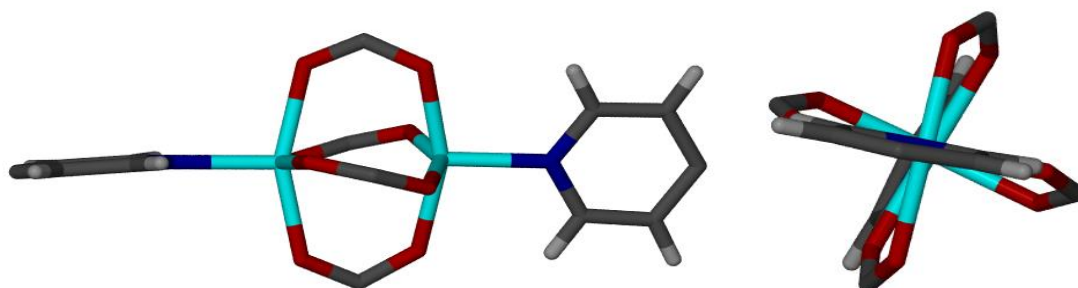


Figure 6.40 Distorted paddlewheel present in **PCCP_5**

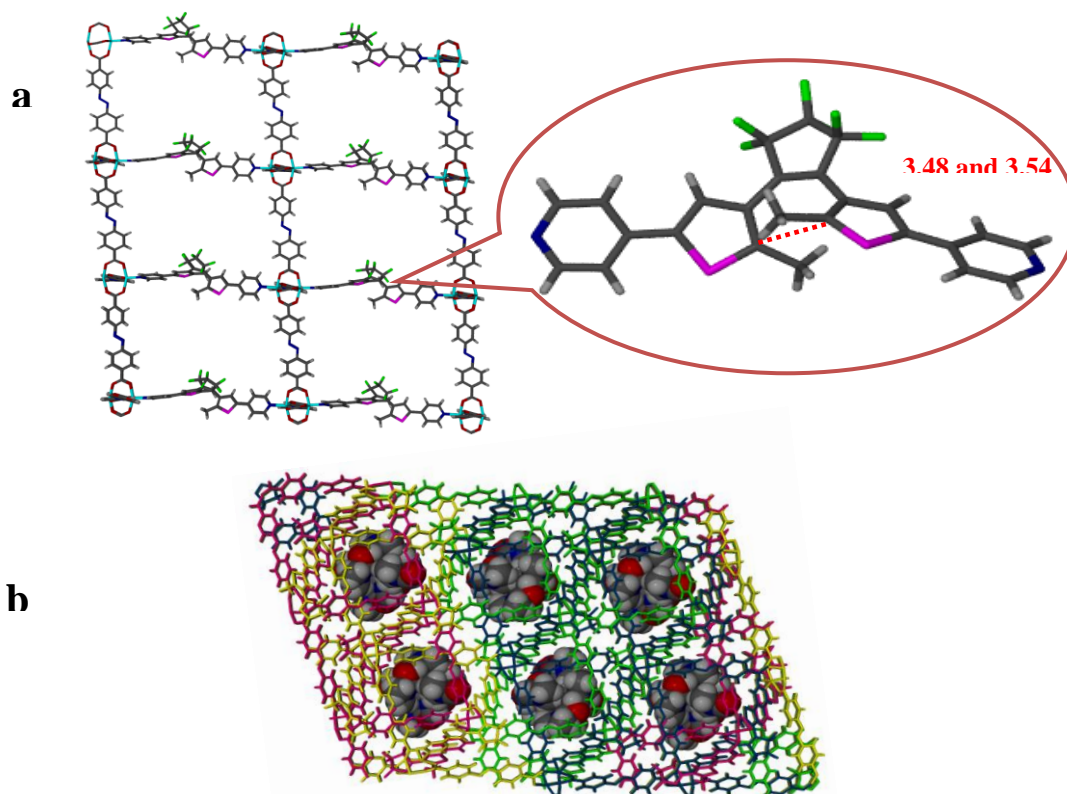


Figure 6.41 a) A single net of PCCP_5 showing reactive C-C distances. b) Fourfold interpenetrated structure, with space-filled DMF guest molecules viewed down the *a* axis.

TGA shows that desolvation starts at room temperature and is complete at approximately 175 °C (**Figure 6.42**). The 13% weight loss corresponds to the loss of two DMF molecules per formula unit. The framework is stable up to 300 °C, after which decomposition commences.

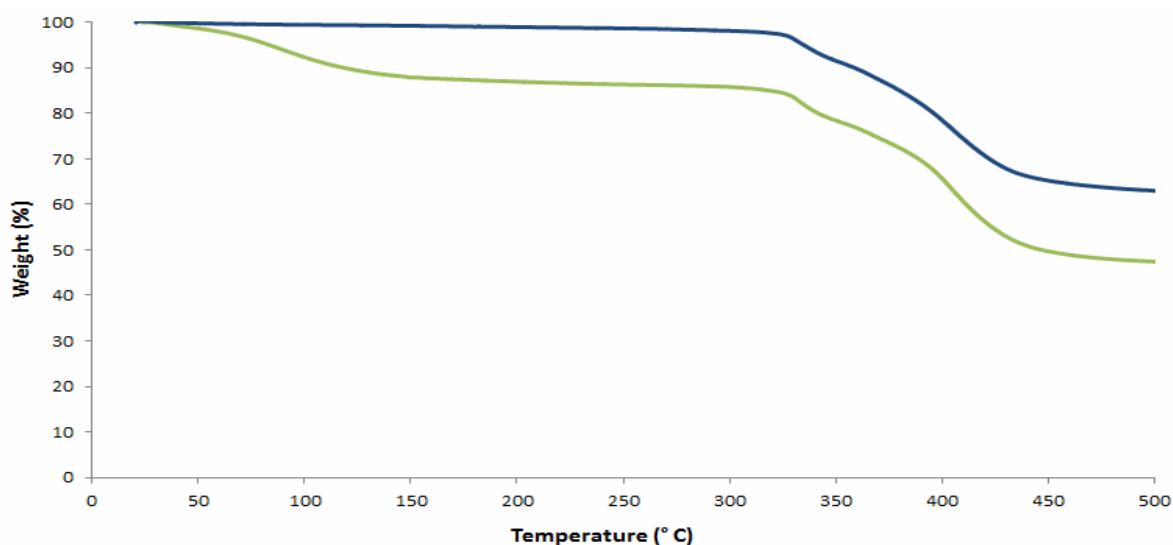


Figure 6.42 TGA of the as-synthesised as well as the evacuated phases of PCCP_5 (green and blue lines).

Having established low temperature activation without loss of crystal singularity, the as-synthesised crystals were heated at 150 °C for 24 h to generate the activated form **PCCP_5'** (Figure 6.43).

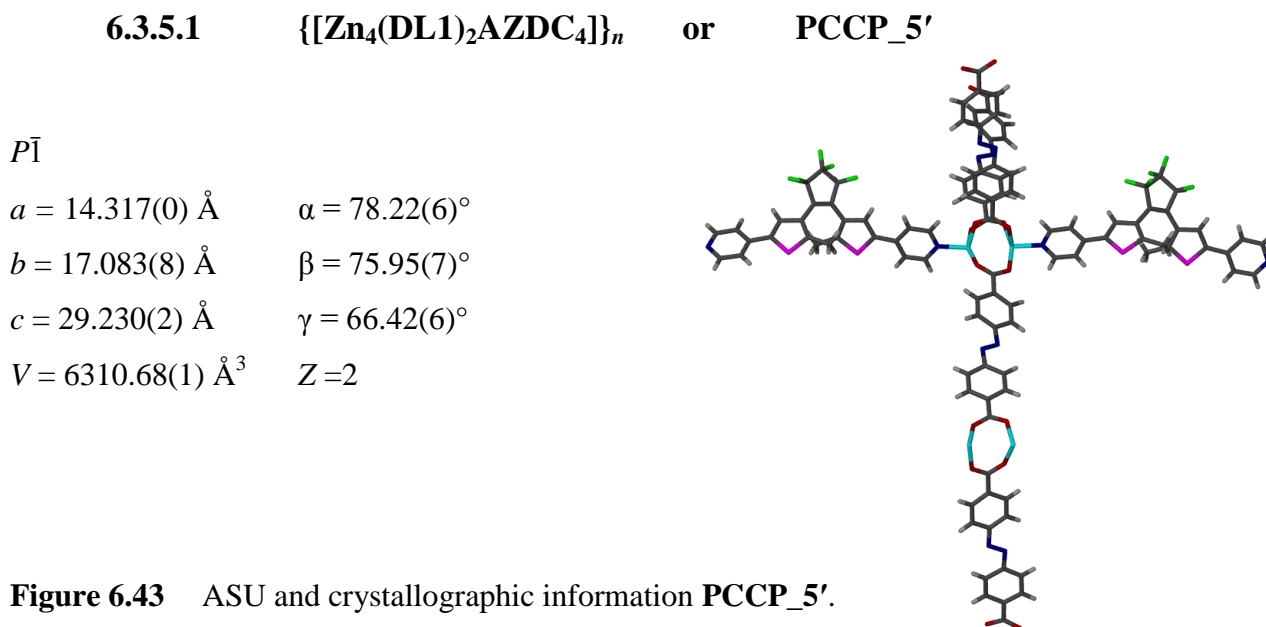


Figure 6.43 ASU and crystallographic information **PCCP_5'**.

The unit cell parameters of **PCCP_5'** experience little change in comparison to the original solvate **PCCP_5** and the overall host structure is considered unchanged by activation. The reactive C-C atom distances remain 3.52 and 3.55 Å for the two diarylethenes. The framework has 548 Å³ of solvent accessible space per unit cell (Figure 6.44) in the form of crenelated channels.

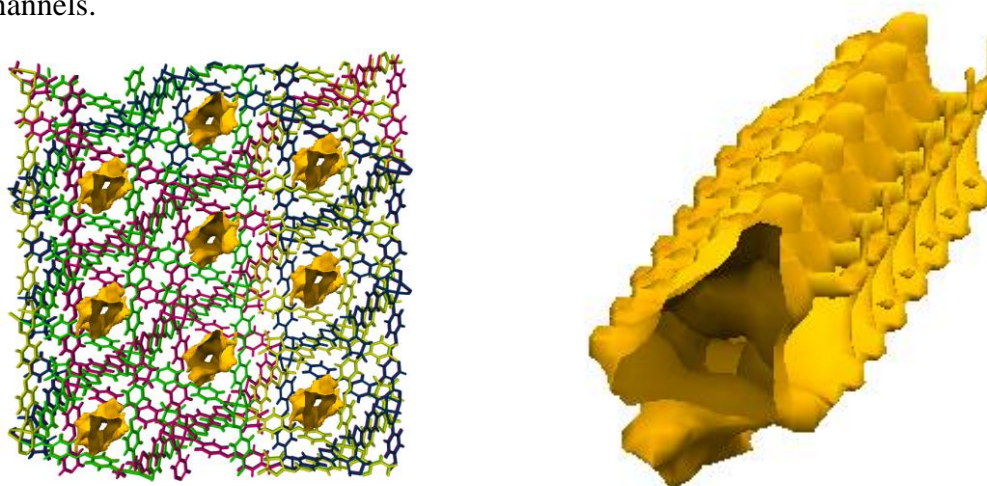


Figure 6.44 View along the crystallographic a axis of **PCCP_5'**, showing solvent accessible voids.

6.3.5.2 Irradiation Experiments

The inherent proximity of the two active carbon atoms, even in the solvated form, makes this material an ideal candidate for ring closure and irradiation experiments were therefore carried out on **PCCP_5'**. Since the **AZDC** ligand is brightly coloured, crystals of **PCCP_5** are deep orange. Exposure of these crystals to ultraviolet light (365 nm) induced no visible colour change (**Figure 6.45**). The initially orange crystals remained uniformly orange regardless of the exposure time.

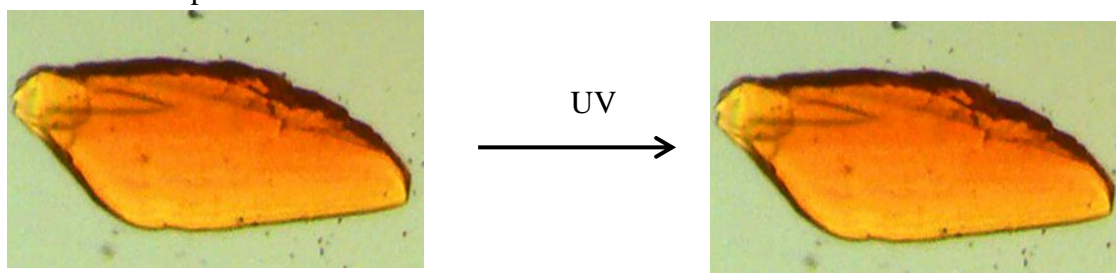


Figure 6.45 Photographic evidence of a **PCCP_5'** crystal showing no discernible colour change pre- and post-exposure to ultraviolet light.

6.3.5.3 Solid state UV-Visible spectroscopy

Despite the lack of a discernible change in colour, UV-visible spectroscopy experiments were carried out anyway. As with the previous examples, a UV-visible spectrum of the original apohost of **PCCP_5'** was recorded. The same sample was then irradiated for one minute and the spectrum rerecorded. **Figure 6.46** shows that the original form contains one very broad band in the range 400 - 570 nm. This band compares favourably with that for previous examples¹⁸⁻¹⁹ of other **AZDC** ligands and can be attributed to the *trans* (*E*) conformation of the ligand. The spectrum of the irradiated sample shows the same **AZDC** broad peak but with an additional broad band at 625 nm. This is believed to be as a result of the closed form isomer of the coordinated **DL1** ligand. However, due to the inherent colour of the **AZDC** ligand, the overall colour of the crystals appears unchanged.

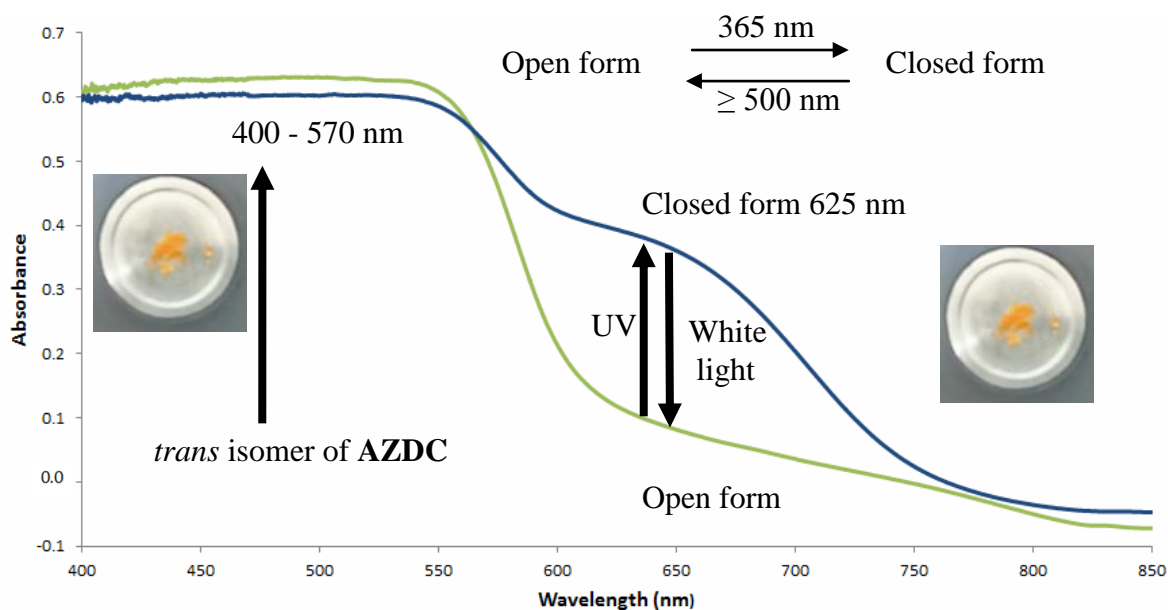


Figure 6.46 Solid-state UV-visible spectra of **PCCP_5** recorded after exposure to white and ultraviolet light.

Having established that the only definitive way to determine the condition of the central ring in a diarylethene molecules is to carry out single-crystal X-ray diffraction analysis, a SC-SC transformation experiment was carried out. A crystal of **PCCP_5'** was glued to the tip of a glass fibre and irradiated for one hour under 365 nm ultraviolet light. A SCD experiment was then performed on this crystal under constant irradiation at room temperature. Despite the distance between the two carbons involved in ring closure decreasing to 3.47 and 3.48 Å (a distance considered very suitable for ring closure), the diarylethene ligands remained in the open form.*

6.4 Conclusion

Since diarylethenes seem the most promising of all known photochromic compounds, and following Irie's tremendous success with the phenyl derivative, two pyridyl functionalised diarylethene ligands (**DL1** and **DL2**) were synthesised and characterised. Unfortunately, despite a dramatic colour change, no ring-closed structures could be obtained.

* As with **PCCP_2**, repetition of the crystallisation process for **PCCP_5** substituting **DL1** with **DL2** induces the formation of an isostructural MOF. This material behaved in a manner very similar to that of **PCCP-5** and is thus not included in this discussion.

CHAPTER VI: PHOTOCROMIC COMPOUNDS

It is believed that the reason for this is twofold. Firstly, the methyl isomer is far less susceptible to ring closure when compared to its ethyl counterpart as a result of the difference in molecular packing (steric hindrance results in the need for higher activation energy thus it is less likely that the methyl diarylethene will ring close when compared to its ethyl counterpart). Furthermore, the incorporation of a heteroatom into the phenyl ring appears to alter the electronic nature of the ligands sufficiently to impede ring-closure. The mechanism for this is as yet unclear and future work would greatly benefit from an in-depth computational study.

The diarylethene photochromic ligands were incorporated into five novel 3D MOFs. The frameworks incorporated variable-length rigid, flexible and photochromic dicarboxylic acid ligands. The materials obtained show different paddlewheel SBUs with the degree of interpenetration varying from two- to fourfold. As with the ligands, the colour change associated with diarylethene ring closure (colourless to blue) and widely reported in the literature is misleading and likely to be a surface effect only as no crystallographic evidence for the ring-closed chromophore is discernible in the single crystal data.

Certain frameworks exhibited dramatic colour changes with no discernible change in cell parameters and no ring closure (**PCCP_2** and **PCCP_3**), while others exhibited a colour change, which happened to coincide with ring closure (**PCCP_1** and **PCCP_4**). In addition no visible colour or structural change was observed for **PCCP_5** upon UV irradiation but solid-state UV indicated some ring closure. This was not observed in the SC. As a result colour changes (visible to the naked eye or through the use of UV-visible spectroscopy) are not a definitive indication of ring closure and should be corroborated using additional techniques.

From the five frameworks developed in this study several conclusions may be drawn. There is no doubt that, despite the colour change observed in photochromic compounds, ring closure in diarylethene molecules or in diarylethene containing MOFs is not a simple reaction and by no means a guaranteed event. More importantly, despite the many literature reports, colour change is highly subjective and not a definitive sign of ring closure. There are certain rules that must be obeyed for such a transformation to occur in the bulk phase solid-state material. It is proposed that the material must possess a low degree of interpenetration (non- or twofold interpenetrated) so that the framework can accommodate the structural change propagating through the lattice as the material is exposed to UV light. This first rule may be amended by the incorporation of highly flexible ligands as these could enable greater motion in spite of a higher degree of interpenetration.

Lastly, it is strongly believed that ring closure requires the distance between the two carbon atoms actively involved in ring closure to be no longer than 3.5 Å. Although no viable molecular switch (capable of fine-tuning sorption properties) was developed, this work serves as a guideline to show that such materials are indeed possible and that photochromic switch formation using MOFs could become an achievable technique.

6.5 Synthesis of photochromic compounds PCCP_1 – PCCP_5

PCCP_1: A mixture of $\text{Zn}(\text{NO}_3)_2 \cdot 6\text{H}_2\text{O}$ (8 mg, 0.025 mmol), **TPA** (4 mg, 0.025 mmol) and **DL1** (8 mg, 0.015 mmol) in a 2 mL solution of DMF-EtOH was heated to 100 °C. Colourless rectangular crystals were obtained after 24 h.

PCCP_2: A mixture of $\text{Zn}(\text{NO}_3)_2 \cdot 6\text{H}_2\text{O}$ (8 mg, 0.025 mmol), **BPDC** (6 mg, 0.025 mmol) and **DL1** (8 mg, 0.015 mmol) in a 2 mL solution of DMF-EtOH was heated to 100 °C. Large colourless plate-like crystals were obtained after 24 h.

PCCP_3: A mixture of $\text{Zn}(\text{NO}_3)_2 \cdot 6\text{H}_2\text{O}$ (8 mg, 0.025 mmol), **OBA** (6.5 mg, 0.025 mmol) and **DL1** (8 mg, 0.015 mmol) in a 2 mL solution of DMF-EtOH was heated to 100 °C. Colourless cuboid crystals were obtained after 24 h.

PCCP_4: A mixture of $\text{Zn}(\text{NO}_3)_2 \cdot 6\text{H}_2\text{O}$ (8 mg, 0.025 mmol), **OBA** (6.5 mg, 0.025 mmol) and **DL2** (8 mg, 0.015 mmol) in a 2 mL solution of DMF-EtOH was heated to 100 °C. Orange diamond crystals were obtained after 24 h.

PCCP_5: A mixture of $\text{Zn}(\text{NO}_3)_2 \cdot 6\text{H}_2\text{O}$ (8 mg, 0.025 mmol), **AZDC** (7 mg, 0.025 mmol) and **DL1** (8 mg, 0.015 mmol) in a 2 mL solution of DMF-EtOH was heated to 100 °C. Orange petal-shaped crystals were obtained after 24 h.

	DL1	DL2	PCCP_1
Empirical formula	C ₅₀ H ₃₂ N ₄ F ₁₂ S ₄	C ₂₇ H ₂₀ F ₆ N ₂ S ₂ C ₂₇ H ₂₀	C ₄₆ H ₃₅ F ₆ N ₄ O ₁₀ S ₂ Zn ₂
Formula weight	1045.07	550.57	1092.85
Temperature (K)	100(0)	100(0)	100(0)
Wavelength (Å)	0.71073	0.71073	0.71073
Crystal system	Triclinic	Monoclinic	Triclinic
<i>a</i> /Å	11.586(1)	11.642(4)	10.830(3)
<i>b</i> /Å	12.857(8)	9.830(3)	10.901(3)
<i>c</i> /Å	15.754(1)	21.519(7)	21.838(6)
α /°	76.892(2)	90.0	93.388(4)
β /°	85.625(2)	96.955(5)	97.757(4)
γ /°	76.935(2)	90.0	103.553(4)
Space group	<i>P</i> $\bar{1}$	<i>P</i> 21/ <i>n</i>	<i>P</i> $\bar{1}$
Volume (Å ³)	2225.8(5)	2444.5(1)	2472.4(1)
<i>Z</i>	2	4	2
Calculated density (g cm ⁻³)	1.559	1.496	1.468
Absorption coefficient (mm ⁻¹)	0.307	0.284	1.134
<i>F</i> ₀₀₀	1064.0	1128.0	1110.0
θ range for data collection (°)	1.67 to 28.28	1.90 to 28.26	1.89 to 28.32
Miller index ranges	-15 ≤ <i>h</i> ≤ 15, -17 ≤ <i>k</i> ≤ 16, -20 ≤ <i>l</i> ≤ 20	-12 ≤ <i>h</i> ≤ 15, -12 ≤ <i>k</i> ≤ 12, -27 ≤ <i>l</i> ≤ 25	-14 ≤ <i>h</i> ≤ 14, -14 ≤ <i>k</i> ≤ 14, -28 ≤ <i>l</i> ≤ 29
Reflections collected	26383	14585	69923
Independent reflections	10254	5769	12128
Completeness to θ_{\max} (%)	92.9	95.0	98.4
Max. and min. transmission	0.9394, 0.8917	0.9832, 0.9454	0.8797, 0.7885
Refinement method	Full-matrix least-squares on <i>F</i> ²	Full-matrix least-squares on <i>F</i> ²	Full-matrix least-squares on <i>F</i> ²
Data / restraints / parameters	8201/ 0/ 630	3668/ 6/ 356	7818/ 780/ 750
Goodness-of-fit on <i>F</i> ²	1.031	0.987	1.019
Final <i>R</i> indices [<i>I</i> > 2 σ (<i>I</i>)]	<i>R</i> 1 = 0.043, <i>wR</i> 2 = 0.096	<i>R</i> 1 = 0.050, <i>wR</i> 2 = 0.110	<i>R</i> 1 = 0.055, <i>wR</i> 2 = 0.121

	PCCP_2	PCCP_2'	PCCP_2' (298K)
Empirical formula	C ₄₂ H ₃₁ F ₆ N ₃ O ₅ S ₂ Zn	C ₃₉ H ₂₄ F ₆ N ₂ O ₄ S ₂ Zn	C ₃₉ H ₂₄ F ₆ N ₂ O ₄ S ₂ Zn
Formula weight	901.21	828.09	828.09
Temperature (K)	100(0)	100(0)	298(0)
Wavelength (Å)	0.71073	0.71073	0.71073
Crystal system	Orthorhombic	Orthorhombic	Orthorhombic
<i>a</i> /Å	7.217(5)	7.156(2)	7.182(3)
<i>b</i> /Å	24.471(3)	24.666(9)	24.631(9)
<i>c</i> /Å	28.683(3)	29.109(1)	29.345(1)
α /°	90.0	90.0	90.0
β /°	90.0	90.0	90.0
γ /°	90.0	90.0	90.0
Space group	<i>P</i> 212121	<i>P</i> 212121	<i>P</i> 212121
Volume (Å ³)	5066(9)	5138(3)	5191(3)
<i>Z</i>	4	4	4
Calculated density (g cm ⁻³)	1.182	1.070	1.060
Absorption coefficient (mm ⁻¹)	0.628	0.612	0.606
<i>F</i> ₀₀₀	1840	1680	1680
θ range for data collection (°)	1.66 to 28.25	1.40 to 28.55	1.39 to 28.54
Miller index ranges	-9 ≤ <i>h</i> ≤ 9, -31 ≤ <i>k</i> ≤ 29, -33 ≤ <i>l</i> ≤ 37	-9 ≤ <i>h</i> ≤ 9, -32 ≤ <i>k</i> ≤ 32, -39 ≤ <i>l</i> ≤ 39	-9 ≤ <i>h</i> ≤ 9, -32 ≤ <i>k</i> ≤ 32, -39 ≤ <i>l</i> ≤ 39
Reflections collected	320320	82388	82574
Independent reflections	11756	12851	12941
Completeness to θ_{\max} (%)	94.0	98.0	98.0
Max. and min. transmission	0.886, 0.904	0.9357, 0.7286	0.9363, 0.7308
Refinement method	Full-matrix least-squares on <i>F</i> ²	Full-matrix least-squares on <i>F</i> ²	Full-matrix least-squares on <i>F</i> ²
Data / restraints / parameters	9181/533/10	7955/ 0/ 489	8096/ 0/ 489
Goodness-of-fit on <i>F</i> ²	1.045	1.043	1.052
Final <i>R</i> indices [<i>I</i> > 2 σ (<i>I</i>)]	<i>R</i> 1 = 0.066, <i>wR</i> 2 = 0.205	<i>R</i> 1 = 0.066, <i>wR</i> 2 = 0.171	<i>R</i> 1 = 0.066, <i>wR</i> 2 = 0.171

	PCCP_2' (308K)	PCCP_2' (318K)	PCCP_2' (328K)
Empirical formula	C ₃₉ H ₂₄ F ₆ N ₂ O ₄ S ₂ Zn	C ₃₉ H ₂₄ F ₆ N ₂ O ₄ S ₂ Zn	C ₃₉ H ₂₄ F ₆ N ₂ O ₄ S ₂ Zn
Formula weight	828.09	828.09	828.09
Temperature (K)	308(2)	318(0)	328(2)
Wavelength (Å)	0.71073	0.71073	0.71073
Crystal system	Orthorhombic	Orthorhombic	Orthorhombic
<i>a</i> /Å	7.178(2)	7.182(2)	7.186(3)
<i>b</i> /Å	24.604(8)	24.601(8)	24.608(9)
<i>c</i> /Å	29.333(9)	29.352(9)	29.370(1)
α /°	90.0	90.0	90.0
β /°	90.0	90.0	90.0
γ /°	90.0	90.0	90.0
Space group	<i>P</i> 212121	<i>P</i> 212121	<i>P</i> 212121
Volume (Å ³)	5180(3)	5187(3)	5193(3)
<i>Z</i>	4	4	4
Calculated density (g cm ⁻³)	1.062	1.060	1.059
Absorption coefficient (mm ⁻¹)	0.607	0.607	0.607
<i>F</i> ₀₀₀	1680.0	1680.0	1680.0
θ range for data collection (°)	1.39 to 28.32	1.39 to 28.30	1.39 to 28.29
Miller index ranges	-9 ≤ <i>h</i> ≤ 9, -32 ≤ <i>k</i> ≤ 32, -39 ≤ <i>l</i> ≤ 39	-9 ≤ <i>h</i> ≤ 9, -32 ≤ <i>k</i> ≤ 32, -39 ≤ <i>l</i> ≤ 39	-9 ≤ <i>h</i> ≤ 9, -32 ≤ <i>k</i> ≤ 32, -39 ≤ <i>l</i> ≤ 39
Reflections collected	82388	82388	82388
Independent reflections	12851	12851	12851
Completeness to θ_{\max} (%)	99.0	100.0	99.0
Max. and min. transmission	0.9362, 0.7304	0.9363, 0.7306	0.9364, 0.7309
Refinement method	Full-matrix least-squares on <i>F</i> ²	Full-matrix least-squares on <i>F</i> ²	Full-matrix least-squares on <i>F</i> ²
Data / restraints / parameters	7956/ 0/ 489	7959/ 0/ 489	7955/ 0/ 489
Goodness-of-fit on <i>F</i> ²	1.039	1.040	1.040
Final <i>R</i> indices [<i>I</i> > 2 σ (<i>I</i>)]	<i>R</i> 1 = 0.066, <i>wR</i> 2 = 0.170	<i>R</i> 1 = 0.066, <i>wR</i> 2 = 0.170	<i>R</i> 1 = 0.066, <i>wR</i> 2 = 0.170

	PCCP_2' (338K)	PCCP_2_SCO₂	PCCP_3
Empirical formula	C ₃₉ H ₂₄ F ₆ N ₂ O ₄ S ₂ Zn	C ₄₀ H ₂₄ F ₆ N ₂ O ₆ S ₂ Zn	C ₆₁ H ₅₃ F ₆ N ₅ O ₁₃ S ₂ Zn ₂
Formula weight	828.09	848.05	1351.05
Temperature (K)	338(2)	100(0)	100(0)
Wavelength (Å)	0.71073	0.71073	0.71073
Crystal system	Orthorhombic	Orthorhombic	Triclinic
<i>a</i> /Å	7.184(4)	7.100(6)	11.169(3)
<i>b</i> /Å	24.614(1)	24.677(2)	14.536(4)
<i>c</i> /Å	29.346(2)	29.283(2)	21.343(6)
α /°	90.0	90.0	71.760(4)
β /°	90.0	90.0	76.741(4)
γ /°	90.0	90.0	68.321(5)
Space group	<i>P</i> 212121	<i>P</i> 212121	<i>P</i> $\bar{1}$
Volume (Å ³)	5189(5)	5130.6(7)	3032.6(15)
<i>Z</i>	4	4	2
Calculated density (g cm ⁻³)	1.060	1.098	1.480
Absorption coefficient (mm ⁻¹)	0.607	0.616	0.944
<i>F</i> ₀₀₀	1680.0	1718.7	1386.1
θ range for data collection (°)	1.39 to 28.31	1.62 to 28.31	1.01 to 28.41
Miller index ranges	-9 ≤ <i>h</i> ≤ 9, -32 ≤ <i>k</i> ≤ 32, -39 ≤ <i>l</i> ≤ 39	-9 ≤ <i>h</i> ≤ 9, -32 ≤ <i>k</i> ≤ 26, -32 ≤ <i>l</i> ≤ 38	-14 ≤ <i>h</i> ≤ 12, -16 ≤ <i>k</i> ≤ 18, -28 ≤ <i>l</i> ≤ 28
Reflections collected	82388	32713	19420
Independent reflections	12851	11923	13518
Completeness to θ_{\max} (%)	99.0	93.0	90.00.8206
Max. and min. transmission	0.9363, 0.7307	0.9220, 0.8421	0.8919,
Refinement method	Full-matrix least-squares on <i>F</i> ²	Full-matrix least-squares on <i>F</i> ²	Full-matrix least-squares on <i>F</i> ²
Data / restraints / parameters	7955/ 0/ 489	7368/ 0/ 517	7368/ 0/ 822
Goodness-of-fit on <i>F</i> ²	1.040	0.812	0.954
Final <i>R</i> indices [<i>I</i> > 2 σ (<i>I</i>)]	<i>R</i> 1 = 0.066, <i>wR</i> 2 = 0.170	<i>R</i> 1 = 0.048, <i>wR</i> 2 = 0.187	<i>R</i> 1 = 0.077, <i>wR</i> 2 = 0.159

	PCCP_3a	PCCP_4	PCCP_4'
Empirical formula	C ₅₈ H ₄₃ F ₆ N ₄ O ₁₂ S ₂ Zn ₂	C ₆₅ H ₆₀ F ₆ N ₅ O ₁₃ S ₂ Zn ₂	C ₅₅ H ₃₆ F ₆ N ₂ O ₁₀ S ₂ Zn ₂
Formula weight	1282.22	1438.49	1193.72
Temperature (K)	100(2)	100(0)	100(2)
Wavelength (Å)	Triclinic	Triclinic	Triclinic
Crystal system	0.71073	0.71073	0.71073
<i>a</i> /Å	11.189(3)	13.354(6)	13.434(2)
<i>b</i> /Å	14.545(3)	14.136(9)	13.602(2)
<i>c</i> /Å	21.369(5)	19.632(7)	17.115(2)
α /°	97.829(2)	84.267(2)	89.100(1)
β /°	103.696(2)	77.664(2)	88.467(1)
γ /°	112.334(2)	66.013(2)	65.633(1)
Space group	<i>P</i> $\bar{1}$	<i>P</i> $\bar{1}$	<i>P</i> $\bar{1}$
Volume (Å ³)	3024(6)	3307(9)	2847(7)
<i>Z</i>	2	2	2
Calculated density (g cm ⁻³)	1.408	1.444	1.392
Absorption coefficient (mm ⁻¹)	0.941	0.872	0.991
<i>F</i> ₀₀₀	1311	1479.5	1212
θ range for data collection (°)	1.56 to 28.28	2.46 to 26.53	1.64 to 28.24
Miller index ranges	-14 ≤ <i>h</i> ≤ 14, -19 ≤ <i>k</i> ≤ 19, -28 ≤ <i>l</i> ≤ 27	-16 ≤ <i>h</i> ≤ 16, -17 ≤ <i>k</i> ≤ 17, -24 ≤ <i>l</i> ≤ 24	-17 ≤ <i>h</i> ≤ 17, -17 ≤ <i>k</i> ≤ 17, -22 ≤ <i>l</i> ≤ 22
Reflections collected	33249	68045	49726
Independent reflections	13868	12866	13279
Completeness to θ_{\max} (%)	92.4	99.5	94.4
Max. and min. transmission	0.8533, 0.7779	0.641, 0.848	0.9170, 0.7513
Refinement method	Full-matrix least-squares on <i>F</i> ²	Full-matrix least-squares on <i>F</i> ²	Full-matrix least-squares on <i>F</i> ²
Data / restraints / parameters	6149/ 738/ 774	11655/910/678	7117/ 796/ 749
Goodness-of-fit on <i>F</i> ²	1.093	1.064	1.084
Final <i>R</i> indices [<i>I</i> > 2 σ (<i>I</i>)]	<i>R</i> 1 = 0.099, <i>wR</i> 2 = 0.247	<i>R</i> 1 = 0.057, <i>wR</i> 2 = 0.174	<i>R</i> 1 = 0.0845, <i>wR</i> 2 = 0.165

	PCCP_4' Irrad	PCCP_5	PCCP_5'
Empirical formula	C ₅₅ H ₃₆ F ₆ N ₂ O ₁₀ S ₂ Zn ₂	C ₁₁₈ H ₉₂ F ₁₂ N ₁₆ O ₂₀ S ₄ Zn ₄	C ₁₀₆ H ₆₄ F ₁₂ N ₁₂ O ₁₆ S ₄ Zn ₄
Formula weight	1189.87	2671.88	2379.49
Temperature (K)	298(2)	100(0)	100(0)
Wavelength (Å)	Triclinic	Triclinic	Triclinic
Crystal system	0.71073	0.71073	0.71073
<i>a</i> /Å	12.260(1)	14.1518(2)	14.3170(2)
<i>b</i> /Å	13.257(2)	17.0691(2)	17.084(2)
<i>c</i> /Å	17.62(2)	29.270(3)	29.230(4)
α /°	78.598(1)	78.211(2)	78.226(2)
β /°	89.230(1)	76.100(2)	75.957(2)
γ /°	67.499(1)	67.888(2)	66.426(2)
Space group	<i>P</i> $\bar{1}$	<i>P</i> $\bar{1}$	<i>P</i> $\bar{1}$
Volume (Å ³)	2587(5)	6307.4(12)	6310.7(14)
<i>Z</i>	2	2	2
Calculated density (g cm ⁻³)	1.527	1.407	1.252
Absorption coefficient (mm ⁻¹)	1.086	0.906	0.894
<i>F</i> ₀₀₀	1190	2728.0	2408.0
θ range for data collection (°)	1.70 to 28.02	1.62 to 28.21	1.57 to 27.62
Miller index ranges	-16 ≤ <i>h</i> ≤ 16, -17 ≤ <i>k</i> ≤ 17, -23 ≤ <i>l</i> ≤ 23	-18 ≤ <i>h</i> ≤ 18, -22 ≤ <i>k</i> ≤ 22, -37 ≤ <i>l</i> ≤ 36	-18 ≤ <i>h</i> ≤ 18, -221 ≤ <i>k</i> ≤ 22, -37 ≤ <i>l</i> ≤ 38
Reflections collected	29822	152227	142463
Independent reflections	12143[Rint = 0.164]	28515	26678
Completeness to θ_{\max} (%)	97.0	99.7	1.00
Max. and min. transmission	0.8964, 0.7922	0.916, 0.789	0.890, 0.861
Refinement method	Full-matrix least-squares on <i>F</i> ²	Full-matrix least-squares on <i>F</i> ²	Full-matrix least-squares on <i>F</i> ²
Data / restraints / parameters	3616/ 0/ 724	17768/1745/3033	16460/1416/1471
Goodness-of-fit on <i>F</i> ²	0.950	1.012	1.027
Final <i>R</i> indices [<i>I</i> > 2 σ (<i>I</i>)]	<i>R</i> 1 = 0.109, <i>wR</i> 2 = 0.243	<i>R</i> 1 = 0.871, <i>wR</i> 2 = 0.247	<i>R</i> 1 = 0.779, <i>wR</i> 2 = 0.230

6.7 References

- 1 H. Tian, S. Yang, *Chem. Soc. Rev.*, **2004**, *33*, 85.
- 2 a) R. B. Woodward, Roald Hoffmann *J. Am. Chem. Soc.*, **1965**, *87*, 395.; b) R. Hoffmann, R. B. Woodward, *J. Am. Chem. Soc.*, **1965**, *87*, 2046.
- 3 S. L. Gilat, S. H. Kawai, J. -M. Lehn, *Chem. Eur. J.*, **1995**, *1*, 275.
- 4 a) M. Morimo, S. Kobatake, M. Irie, *Photochem. Photobiol. Sci.*, **2003**, *2*, 1088.; b) M. Morimoto, M. Irie, *Chem. Commun.*, **2011**, *47*, 4186.; c) K. Motoyama, H. Li, T. Koike, M. Hatakeyama, S. Yokojima, S. Nakamura, M. Akita, *Dalton Trans.*, **2011**, *40*, 10643; d) L. Kuroki, S. Takami, K. Yoza, M. Morimoto, M. Irie, *Photochem. Photobiol. Sci.*, **2010**, *9*, 221.
- 5 S. Kobatake, S. Takami, H. Muto, T. Ishikawa, M. Irie, *Nature*, **2007**, *446*, 778.
- 6 a) K. Matsuda, M. Irie, *Chem. Lett.*, **2000**, 16.; b) K. Matsuda, M. Irie, *J. Am. Chem. Soc.*, **2000**, *122*, 7195.; c) K. Matsuda, M. Irie, *J. Am. Chem. Soc.*, **2000**, *12*, 8309.
- 7 a) J. Park, D. Yuan, K. T. Pham, J. -R. Li, A. Yakovenko, H. -C. Zhou, *J. Am. Chem. Soc.*, **2012**, *134*, 99.; b) A. Modrow, D. Zargarani, R. Herges, N. Stock, *Dalton Trans.*, **2011**, *40*, 4217.; c) J. W. Brown, B. L. Henderson, M. D. Kiesz, A. C. Whalley, W. Morris, S. Grunder, H. Deng, H. Furukawa, J. I. Zink, J. F. Stoddart, O. M. Yaghi, *Chem. Sci.*, **2013**, *4*, 2858.; d) S. Bernt, M. Feyand, A. Modrow, J. Wack, J. Senker, N. Stock, *Eur. J. Inorg. Chem.*, **2011**, 5378.
- 8 a) K Matsuda, K. Takayama, M. Iri, *Chem. Commun.*, **2001**, 363.; b) K. Matsuda, K. Takayama, M. Irie, *Inorg. Chem.*, **2004**, *43*, 482.; c) K. Matsuda, Y. Shinkai, M. Irie, *Inorg. Chem.*, **2004**, *43*, 3774.; d) M. Munakata, J. Han, M. Maekawa, Y. Suenaga, T. Kuroda-Sowa, A. Nabei, H. Ebisu, *Inorg. Chim. Acta.*, **2007**, *360*, 2792.
- 9 S. K. Brayshaw, J.W. Knight, P.R. Raithby, T.L. Savarese, S. Schiffers, S. J. Teat, J. E. Warrena, M. R. Warrena, *J. Appl. Cryst.*, **2010**, *43*, 337.
- 10 a) M. Irie, T. Fukaminato, T. Sasaki, N. Tamai, T. Kawai, *Nature*, **2002**, *420*, 759.; b) K. Matsuda, M. Irie, *J. Am. Chem. Soc.*, **2000**, *122*, 7195.; c) K. Matsuda, M. Irie, *J. Am. Chem. Soc.* **2000**, *122*, 8309.; d) K. Matsuda, M. Irie, *J. Am. Chem. Soc.*, **2001**, *123*, 9896.

CHAPTER VI: PHOTOCROMIC COMPOUNDS

-
- 11 a) A. Fernandez-Acebes, J. -M. Lehn, *Adv. Mater.*, **1998**, *10*, 1519.; b) S. J. Lim, B. -K. An, S. D. Jung, M.-A. Chung, S. Y. Park, *Angew. Chem. Int. Ed.*, **2004**, *43*, 6346.; c) H. Tian, S. Yang, *Chem. Soc. Rev.*, **2004**, *33*, 85.
- 12 a) M. Irie, S. Kobatake, M. Horichi, *Science*, **2001**, *291*, 1769.; b) S. Takami, L. Kuroki, M. Irie, *J. Am. Chem. Soc.*, **2007**, *129*, 7319.; c) S. J. Chen, L. J. Chen, H. B. Yang, H. Tian, W. H. Zhu, *J. Am. Chem. Soc.*, **2012**, *134*, 13596.; d) H. Cahov, A. J. Schke, *Angew. Chem. Int. Ed.*, **2013**, *52*, 3186.
- 13 a) T. Fukaminato, T. Sasaki, T. Kawai, N. Tamai, M. Irie, *J. Am. Chem. Soc.* **2004**, *126*, 14843.; b) N. Tanifuji, M. Irie, K. Matsuda, *J. Am. Chem. Soc.*, **2005**, *127*, 13344.; c) S. Lim, J. Seo, S. Park, *J. Am. Chem. Soc.*, **2006**, *128*, 1454.
- 14 a) N. W. Ashcroft, N. D. Mermin, *Solid State Physics*; Holt, Rinehart & Winston: **1976**.; b) D. Das, T. Jacobs, L. J. Barbour, *Nature Mater.*, **2010**, *9*, 36.
- 15 a) D. Das, T. Jacobs, A. Pietraszko, L. J. Barbour, *Chem. Commun.*, **2011**, *47*, 6009.; b) A. D. Fortes, E. Suard, K. S. Knight, *Science*, **2011**, *331*, 742.
- 16 <http://www.theresonance.com/bruker-almanac-goes-digital/> accessed 13.09.14.
- 17 F. Luo, C. B. fan, M. B. Luo, Z. L. Wu, Y. Zhu, S. Z. Pu, W. -Y. Xu, G. -C. Guo, *Angew. Chem. Int. Ed.*, **2014**, *53*, 9298.
- 18 J. W. Brown, B. L. Henderson, M. D. Kiesz, A.C. Whalley, W. Morris, S. Grunder, H. Deng, H. Furukawa, J. I. Zink, J. F. Stoddartc, O. M. Yaghi, *Chem. Sci.*, **2013**, *4*, 2858.
- 19 Y. Zhu and W. Zhang, *Chem. Sci.*, **2014**, *5*, 4957.

Conclusions and future work

7.1 Summary and concluding remarks

The field of supramolecular chemistry is one of the few chemical disciplines wherein success requires the researcher to be a “Jack-of-all-trades”. Solid-state supramolecular chemists draw from physical, organic, inorganic, analytical, coordination chemistry and crystallography (amongst others) in order to navigate all aspects of this fascinating discipline. Unlike most other areas of chemistry where the growth of a crystal presents the final solution to some long sought question, supramolecular chemistry adopts the notion that the formation of a crystal is merely the beginning, with the capabilities of the material yet to be elucidated. As a result the rational design of MOFs is by no means an easy task and the work described in this thesis hopes to illustrate the enormous diversity available within the field of crystal engineering.

This dissertation has been subdivided into sections. Chapter III focuses on the synthesis of twenty-one new porous materials. These were grown using a selection of four previously described symmetrical pyridyl ligands in conjunction with four carboxylic acids (one of which is asymmetrical) and one of four divalent metal ions (namely zinc, cadmium, cobalt or manganese). Of these materials, all but one were novel at the time they were prepared but several have subsequently been published by other authors. Although TGA indicated that all of the materials could be activated, not all of these activations could be achieved with the retention of crystal singularity. Furthermore, not all of the frameworks could be obtained in sufficient bulk phase purity to perform gas sorption experiments. As a result, the only MOFs subjected to gas sorption experiments in Chapter III were **CP3'** and **CP5'** with **CP5'** showing the second largest guest sorption capabilities of all MOFs studied in this dissertation.

CHAPTER VII: CONCLUSIONS AND FUTURE WORK

In addition to TGA and sorption studies, SC-SC solvent exchange experiments were performed on **CP2** and **CP5**. The tetrazine based MOF **CP6** is highly sensitive to guest stimuli. The material could remain exposed to air with no crystal deterioration but upon exposure to any external stimulus, the crystals (not the framework) disintegrated. Exposure of this material to a mixture of xylenes induced a SC-SC transformation. The last portion of Chapter III focused on the formation of a previously published highly interpenetrated porous MOF (**CP7**) using the asymmetrical ligand **PYEB** in the hope of performing gas-cell sorption experiments. Unfortunately the published work could not be reproduced and two additional MOFs of a similar composition are presented instead.

Chapter IV focuses on two threefold interpenetrated honeycomb isostructural MOFs (**HC1** and **HC2**) obtained from the solvothermal reaction of **L1** and **OBA** with either zinc or cobalt nitrate and their ability to selectively sequester and store both liquid and vapour guest molecules. Crystals of **HC1** are capable of undergoing SC-SC guest exchange experiments with a selection of molecules. Selectivity testing showed **HC1** has a mild preference for *ortho*-xylene over the other xylene isomers. Gas sorption experiments revealed a clear preference for CO₂ (substantial absorbance with no hysteresis) above a selection of linear alkanes which were absorbed to a lesser extent and exhibited hysteresis. The pleochroic crystals of **HC2**, the cobalt analog of **HC1**, showed no selectivity toward any of the xylene isomers and gas sorption experiments revealed preferential selectivity toward, methane CO₂ and ethane. Owing to the different colours of the two crystal analogues, combining the components of both compounds resulted in the formation of trichroic solid solutions. The colour of these could be “fine-tuned” by varying the ratio of the two metals. EDX experiments revealed that regardless of the ratio employed, the material always contained more zinc than cobalt. This selectivity for zinc was found to be authentic when nickel (a metal with a much higher binding affinity when compared to either zinc or cobalt) was incorporated into the crystallisation conditions but not found in the crystal. To complete the study, a homoepitaxial crystal (**HC6**) was grown by immersing a **HC1** crystal in a solution of **HC2**. This materials ability to show such diversity *viz.* guest selectivity is a prime example of MOF versatility.

CHAPTER VII: CONCLUSIONS AND FUTURE WORK

Having obtained interesting results with the ligand **L1**, a modified version involving fluorine atoms located on the central phenyl ring was synthesised. This new ligand, **FL1**, was combined with **OBA** and zinc nitrate to form **SPC1a**, a twofold interpenetrated porous structure with solvent located in the crenelated triangular channels. Unlike its predecessor, this material appeared to be particularly susceptible to guest induced crank-handle motion. Mere activation as well as the SC-SC incorporation of guests such as acetonitrile, carbon dioxide, and trichloroacetonitrile elicited conformational changes (*anti* to *syn*). In particular, acetonitrile and trichloroacetonitrile induced anomalous changes as a result of guest-guest and host-guest interactions. Sorption experiments showed the material to be selective for CO₂ over a selection of linear alkanes.

Substitution of the **FL1** ligand for the **FL1·2HCl** (synthetic by-product) salt yielded an interdigitated MOF, **SPC1b**, wherein one of the two fluorinated ligands present in the ASU was only mono-coordinated, creating a material somewhat reminiscent of the MOF **HC1** from Chapter IV. When cadmium, a metal whose behaviour is often very similar to that of zinc, was incorporated in the presence of DMA, the 2D layered MOF **SPC2a** was formed with the **FL1** ligand present in the *anti* conformation, and having undergone partial [2 + 2] cycloaddition. The material was activated with a decrease in crystal quality, minor parameter changes but no alteration of the **FL1** ligand. UV irradiation of **SPC2a** showed increased cyclisation but the reaction had not proceeded to completion. SC-SC guest exchange experiments revealed MOF **SPC2a** to be less susceptible to crank-handle motion when compared to its zinc counterpart as not one of the included guest molecules induced conformational rotation from the *syn* to the *anti* conformer or *vice versa*. The use of a commercial mixture of xylenes did elicit several interesting results. Firstly, the material was found only to contain *meta*-xylene and the ratio of cyclised to non-cyclised conformer had increased. Exposure of the activated material to CO₂ and a series of linear alkanes resulted in an impressive uptake, with the material absorbing five molecules of CO₂ (highest uptake of all materials presented in this dissertation) and showed preferential selectivity toward CO₂ over the hydrocarbons with an interesting stepped sorption isotherm for ethane.

CHAPTER VII: CONCLUSIONS AND FUTURE WORK

By combining DMF with DMSO two isoskeletal structures (**SPC2b1** and **SPC2b2**). Both materials are isoskeletal to **SPC2a** but differ in guest nature, **FL1** conformation (*syn*) and **SPC2b** show no [2 + 2] addition. Furthermore, although isoskeletal and with the same **FL1** ligand conformation **SPC2b1** and **SPC2b2** differed in their paddlewheel construction and, as a result, in the solvent-accessible void space. In hindsight, Chapters IV and V may be considered parts of one larger idea in that they both focus on dynamic guest-host relationships.

Chapter VI involves new ligands and, in place of the standard stimulation techniques (temperature, pressure and guest inclusion), focuses on the response of these materials to light, both as separate compounds and as parts of larger MOFs. The chapter serves to further illustrate another means of engineering dynamism in solid-state materials. As previously mentioned, photochromic compounds have been known since the mid-1800s but it wasn't until the advancement of analytical instrumentation that these materials began to draw interest from the chemical community. In light of Irie's great success, two diarylethenes capable of undergoing symmetrical coordination were synthesised. Although the literature contains examples of the **DL1** ligand coordinated to various metals, no information regarding the photocyclisation capabilities of the ligand itself could be found. The results obtained from the examination of ligands **DL1** and **DL2** proved surprising.

Incorporation of a single heteroatom into what was previously a phenyl ring completely altered the electronic nature of the material to the point that, although ultraviolet light induced a dramatic colour change, no structural change occurred. The reactive carbon-carbon atom distance in **DL1** was found to range from 3.56 and 3.53 Å while it was found to be 3.64 Å in **DL2**. It is believed that the colour change was the result of the conversion of a limited quantity of available material and this was substantiated by solution NMR spectroscopy which showed only partial conversion. A series of five novel MOFs were crystallised and studied. The secondary carboxylic ligands used (terephthalic acid, 4,4'-biphenyl-dicarboxylic acid, 4,4'-oxybisbenzoic acid and 4,4'-azobenzene dicarboxylic acid) were selected as a means of systematically determining what type of ligand (short, long and rigid, flexible or one with inherent photocyclisation tendencies) would be most suited to maximizing light-induced dynamism.

CHAPTER VII: CONCLUSIONS AND FUTURE WORK

PCCP_1 is a porous two-fold interpenetrated MOF comprised of zinc, terephthalic acid and **DL1**. The distance between the two carbon atoms involved in ring closure is 3.49 Å. Upon irradiation with UV light, the material undergoes a dramatic change in colour (colourless to blue) as well as an obvious change in shape. Unfortunately no structure of the irradiated form could be determined because, although the crystal remained intact, irradiation induced a drop in diffraction quality. In spite of this, unit cell data recorded for a single crystal, pre-, during and post UV irradiation showed some interesting results. When placed under UV light, **PCCP_1** shows a swift and uniform decrease in cell parameters which is consistent with the notion of ring closure and framework contraction. When the same crystal is removed from the UV beam and rerecorded, although the material remains slightly coloured and with low diffraction quality, the parameters revert back to those of the original form. This may be the first sign of photocyclisation within a MOF. **PCCP_2** was constructed from zinc, 4,4'-biphenyl-dicarboxylic acid and **DL1**. This fourfold interpenetrated highly porous MOF was initially a very exciting discovery. The material could be activated with negligible unit cell parameter change, it showed an affinity for CO₂ (guest molecules were located in the structure after exposure to supercritical carbon dioxide) and the well-shaped rectangular crystals immediately turned a uniform blue colour upon exposure to UV light. The distance between carbon atoms associated with ring closure is 3.65 Å. It is important to note that the C-C distance may not be the only criterion for ring closure. Unfortunately, as with the ligands, despite numerous data collections for the irradiated form of **PCCP_2**, no ring closure was observed. PXRD experiments showed that prolonged irradiation does not increase photocyclisation, in fact it appears to induce cycloreversion. Substitution of the rigid biphenyl with **OBA** enabled the formation of **PCCP_3**. This two-fold interpenetrated porous material showed low temperature activation but could not be evacuated without loss of crystallinity. The distance between the two carbon atoms involved in ring closure in this solvate is 3.88 Å. UV irradiation once more induced a dramatic colour change but still no structural change was detected.

CHAPTER VII: CONCLUSIONS AND FUTURE WORK

Crystallisations were undertaken with **DL2** in the hope that the longer alkyl arm would facilitate greater motion and thus increase the likelihood of obtaining a ring closed structure. The first framework obtained was **PCCP_4**. This MOF is comprised of **DL2**, **OBA**, and zinc nitrate. The twofold interpenetrated structure contains DMF-filled channels and has a relative C-C distance of 3.71 Å. Activation was achieved with minor crystal deterioration but distinct changes in the unit cell parameters. This may be explained by the MOF being inherently dynamic and, upon guest expulsion, the components rearrange to form a more thermodynamically favourable seemingly non-porous material. More importantly, the activation process decreased the reactive C-C distance to 3.46 Å. As with all the other diarylethene frameworks, the activated crystals of **PCCP_4** were irradiated with UV light, which immediately induced a colour change (orange to green). Although the crystals had degraded quite substantially, the first solid state structure of a ring closed diarylethene molecule incorporated into a MOF was obtained. Upon cyclisation, the material underwent a further contraction as the C-C atom distance was reduced to 1.53 Å. Despite having shown that ring closure is possible, at least in the case of the **DL2** ligand, it remains unclear why this material underwent photocyclisation and the others did not.

To complete the study a final MOF, **PCCP_5** was synthesised using the ligand **DL1** with 4,4'-azobenzene-dicarboxylic acid and zinc nitrate hexahydrate. **PCCP_5** is fourfold interpenetrated with reactive carbon-carbon distances of 3.53 and 3.48 Å. Unlike all the previous examples, irradiation with UV light did not induce any visible colour change. Examination of the solid-state UV spectrum reveals the presence of a peak ascribed to the ring-closed conformer. Despite the short C-C atom distances observed in **PCCP_5** and the solid-state UV data, SCD studies revealed no ring closure.

Sequential analysis of both diarylethene ligands as well as the series of MOFs obtained from the progressive increase in size and flexibility of the secondary ligand has enabled the formulation of a list of requirements that may be necessary for photocyclisation. It is proposed that in order to attain the desired ring-closed conformer, a MOF must possess flexible components, a low level of interpenetration and a reactive C-C atom distance of no more than 3.5 Å.

CHAPTER VII: CONCLUSIONS AND FUTURE WORK

To conclude, crystal engineering is still in its infancy and the systematic study of crystals is the necessary foundation that will inevitably lead to future enlightenment and the design of target-specific materials. Leopold Ruzicka (Nobel prize in Chemistry, 1939) famously described a crystal as a *chemical cemetery*, implying that once precipitated from solution, the molecules cease to exhibit interesting behaviour. It is hoped that this work has helped to repudiate that notion.

7.2 Proposed future work

- (a) To continue rational MOF design with the organic ligands **L1-L4** with other metal salts.
- (b) Conduct breakthrough experiments on **HC1**, **HC2** and **HC6**.
- (c) To alter the electrostatic properties of the **L1** ligand by functionalising it with different halide substituents to ascertain what effect this would have on framework formation and function.
- (d) To perform computational studies on the **SPC1a** compounds to seek a clearer explanation regarding what drives crank-handle motion, with particular focus on the host-guest interactions between the **FL1** ligand and acetonitrile and trichloroacetonitrile.
- (e) To further probe the [2 + 2] cyclisation reactions observed in **SPC2a**.
- (f) To design diarylethene ligands with acid groups and determine what effect this has on the photochemistry of such materials.
- (g) Synthesis of more diarylethene MOFs that abide by the proposed guidelines for ring-closure. The study of such materials light-induced gas- and solvent-uptake and subsequent expulsion would be a most interesting area of focus with the formation of molecular switches a genuine possibility.